# Novel C-C Bond Formation Strategies for Access to Secondary and Tertiary Amides Enabled by New Synthetic Technologies

Jason D. Williams

Initiation of studies: October 2014


## Declaration

This thesis is the result of the author's original research. It has been composed by the author and has not been previously submitted for examination which has led to the award of a degree.



Signed: Date:

## Acknowledgements

I must begin by thanking Stuart Leach and William Kerr for their supervision throughout my PhD studies. Although the course of the project has taken a very different path from what Stuart originally imagined, it has certainly allowed me a great deal of freedom, to explore interesting new avenues. Stuart's positive input mixed in with constant challenges to my thought process have undoubtedly allowed me to develop as a researcher, and to build my confidence in driving the project forward. It has been a great privilege to work with you both.

The GSK/Strathclyde Collaborative PhD Programme has allowed me many fantastic opportunities, so I am grateful to both Harry Kelly and William Kerr for accepting me onto the programme in the first place. Furthermore, I would not have been able to capitalise on these opportunities were it not for a great deal of support from a whole host of people. I would like to thank, amongst many others: Lee Edwards, Blandine McKay, Sarah Hunter, Andy Payne, Colin Edge, Hakan Keles, Rose Bourdon, Tom Atherton, Andrea Malley, Dawn Peel and Terri Davidson, for helpful discussions and assistance in every aspect of chemistry, and non-science related matters!

The friendly atmosphere at GSK, tied in with a stimulating scientific environment has made it a real pleasure to come to work each morning and this is thanks to the many colleagues I have enjoyed working with during my time at GSK: within API chemistry, the Collaborative PhD Programme, and elsewhere on the Stevenage site. I also wish to extend these thanks to the members of the Kerr group at the University of Strathclyde, for helping me to enjoy being back in an academic lab, and feel at home in Glasgow for my short stay. Particularly, thank you to Dave Lindsay and Laura Paterson for the numerous occasions, over the past 4 years, on which they've been of great help in both chemistry-related and other areas.

Finally, I must thank my friends and family for their company and encouragement throughout my PhD. As is to be expected, there have been some difficult times, yet being able to relax with great friends from a number of different circles has helped keep things in perspective. Most of all, though, I can't underestimate the positive impact of having the trust, belief, and support of my family throughout the course of my studies, for which I am eternally grateful.

## Abstract

Amidation reactions represent a commonly used reaction within multiple industries, yet robust methods for their sustainable synthesis remain a significant challenge. The majority of current research into amide-forming transformations focuses on condensation of an amine with a carboxylic acid, *via* activation of the acid. However, the advent of modern synthetic technologies has brought about opportunities to discover new methodologies in this area, with the aim of achieving amide formation through alternative and efficient approaches. This thesis describes the development of two complementary amidation methods, which use new synthetic technologies to enable a less common disconnection, giving access to secondary and tertiary amides *via* C-C bond formation.

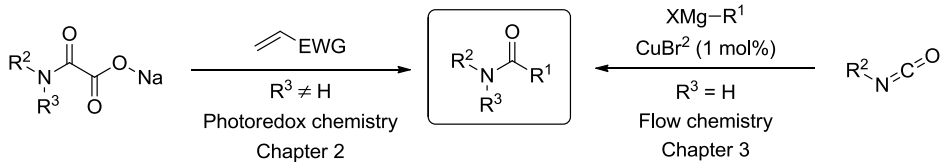


**Graphical abstract** - A summary of the transformations developed and discussed within this thesis.

Chapter 2 describes the use of photoredox catalysis, to develop a decarboxylative umpolung formation of tertiary amides. This proceeds by oxidation of sodium oxamate salts, followed by reaction of the resulting carbamoyl radical with electron-poor olefins. A variety of substrates have been found to be amenable to this protocol, and steps have been made towards exploring alternative solvent and photocatalyst systems, to attain a more sustainable system. Furthermore, DFT calculations have been used to explain and corroborate experimental results, in order to bolster reaction understanding, and maximise potential utility.

Chapter 3 describes the development of a flow chemistry methodology, which enables the synthesis of secondary amides, by the reaction of Grignard reagents with isocyanates. Initial investigations of this seemingly straightforward reaction revealed a major deleterious side reaction, which occurred in all but the most sterically hindered cases. It was found that this could be minimised through ensuring fast mixing of the two reagents, which then led towards the use of continuous flow chemistry. Further reaction investigation identified that inclusion of

a catalytic quantity of $CuBr_2$ reduced the extent of side product formation to an almost negligible level, to deliver an excellent yield of the desired product. After application to a wide range of substrates, kinetic data was obtained using quantum cascade laser infrared microscopy, which demonstrated a significant rate acceleration bestowed by the addition of the copper additive.

# Table of contents

## Abbreviations

**4CzIPN:** 1,2,3,4-Tetrakis(carbazol-9-yl)-5,6-dicyanobenzene

**API:** Active pharmaceutical ingredient

**Ac:** Acetyl

**Ar:** Aryl

**AT2:** Angiotensin 2

**ATR:** Attenuated total reflectance

**BCR-ABL:** Breakpoint cluster region-Abelson murine leukemia protein

**BHT:** Butylated hydroxytoluene (2,6-bis(1,1-dimethylethyl)-4-methylphenol)

**bpy:** 2,2'-Bipyridine

**bpz:** 2,2'-Bipyrazine

**C-PCM:** Conductor-like polarisable continuum model

**Cbz:** Carboxybenzyl

**CDI:** 1,1'-Carbonyldiimidazole

**CFL:** Compact fluorescent lamp

**CLR:** Controlled lab reactor

**COMU:** 1-[(1-(Cyano-2-ethoxy-2-oxoethylideneaminooxy)dimethylaminomorpholino-methylene)]methanaminium hexafluorophosphate

**conPET:** Consecutive photoinduced electron transfer

**CSTR:** Continuous stirred tank reactor

**Cy:** Cyclohexyl

**DABCO:** 1,4-Diazabicyclo[2.2.2]octane

**DATB:** 1,3-Dioxa-5-aza-2,4,6-triborinane

**DCM:** Dichloromethane

**dF(CF$_3$)ppy:** 2-(2,4-Difluorophenyl)-5-trifluoromethylpyridine

**DFT:** Density functional theory

**DMA:** *N*,*N*-Dimethylacetamide

**DMF:** *N*,*N*-Dimethylformamide

**DPPA:** Diphenylphosphoryl azide

**dtbbpy:** 4,4-Di-*tert*-butyl-2,2′-bipyridine

**EDCI:** 1-Ethyl-3-(3-dimethylaminopropyl)carbodiimide

**GC:** Gas chromatography

**GSK:** GlaxoSmithKline

**HAS:** Homolytic aromatic substitution

**HAT:** Hydrogen-atom transfer

**HMG-CoA:** 3-Hydroxy-3-methylglutaryl coenzyme A

**HOBt:** 1-Hydroxybenzotriazole

**HPLC:** High performance liquid chromatography

**HRMS:** High resolution mass spectroscopy

**IR:** Infrared

**IRC:** Intrinsic reaction coordinate

**LCMS:** Liquid chromatography mass spectroscopy

**LDA:** Lithium *N*,*N*-diisopropylamine

**MAP:** 4-Methoxyacetophenone

**MDAP:** Mass directed automated preparative HPLC

**NMP:** *N*-Methylpyrrolidinone

**NMR:** Nuclear magnetic resonance

**PCET:** Proton-coupled electron transfer

**PES:** Potential energy surface

**PET:** Photoinduced electron transfer

**PFA:** Perfluoroalkoxy

**Ph:** Phenyl

**phen:** Phenanthroline

**PTFE:** Polytetrafluoroethylene

**QCL:** Quantum cascade laser

**QM:** Quantum mechanical

**SCE:** Saturated calomel electrode

**SDHI:** Succinate dehydrogenase inhibitor

**SET:** Single electron transfer

**T3P:** 2,4,6-Tripropyl-1,3,5,2,4,6-trioxatriphosphorinane-2,4,6-trioxide

**TBME:** *tert*-Butylmethyl ether

**TBS:** *tert*-Butyldimethylsilyl

**TEMPO:** (2,2,6,6-Tetramethylpiperidin-1-yl)oxyl

**THF:** Tetrahydrofuran

**THP:** Tetrahydropyran

**TLC:** Thin layer chromatography

**TMEDA:** *N*,*N*,*N'*,*N'*-Tetramethylethylenediamine

**TMS:** Trimethylsilyl

**uB3LYP**: Unrestricted Becke3 Lee-Yang-Parr functional

**UV:** Ultraviolet

# Chapter 1. Introduction

## 1.1. The amide bond

Throughout organic chemistry the amide (or carboxamide) is an omnipresent functional group, occurring in biological systems as proteins, as synthetic polymeric materials, and also in natural products and fine chemicals. Specifically, drug-like small molecules created in laboratories worldwide often incorporate amides, for a myriad of biological, structural, and synthetic reasons. Within the pharmaceutical industry, the resultant APIs (active pharmaceutical ingredients) possessing amide functionality have led to, amongst many others: the best-selling drug of all time, Atorvastatin (**1**), used for lowering cholesterol; ground-breaking anticancer drug, Imatinib (**2**); and cardiovascular blockbuster, Valsartan (**3**) (**Figure 1**).

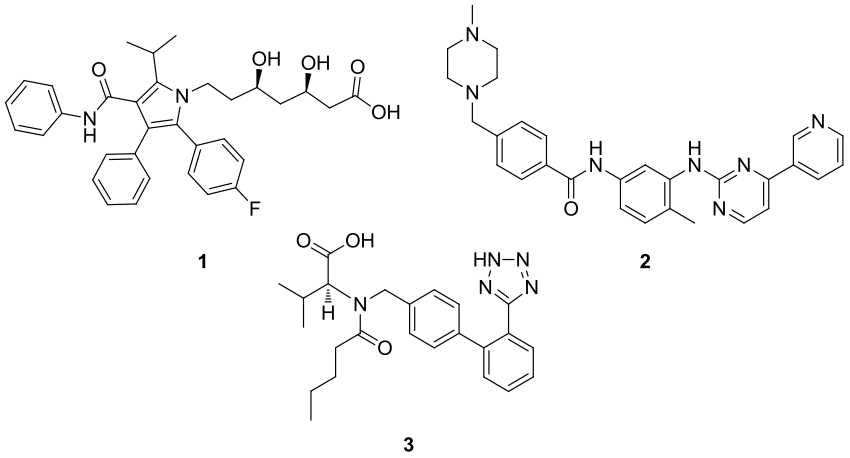


**Figure 1** - Drug molecules containing amides: HMG-CoA reductase inhibitor, Atorvastatin (**1**); BCR-ABL kinase inhibitor, Imatinib (**2**); and AT2 inhibitor, Valsartan (**3**).

In a survey of compounds in medicinal chemistry programmes, it was found that the mean number of amide bonds per "lead-like" compound was 0.67, with a maximum of 5 amide bonds in a single compound.[1] The frequency at which amides appear in this type of compound can be explained, in part, by the simplicity of "amide coupling" reactions, their wide-ranging functional group tolerance, and the well-developed coupling agents associated with their preparation.[2] Moreover, the common natural occurrence of the amide unit, alongside its dual hydrogen bond donor and acceptor properties,[3] result in a moiety with favourable characteristics in binding to biological targets.[4] Such wide applicability and preparative

accessibility drives the demand to quickly synthesise large libraries of amides, to be screened for biological activity.

## 1.2. General amidation strategies

Fundamentally, an amide bond can be disconnected in four main ways (**Scheme 1**). By far the most common of these disconnections corresponds to C-N bond formation (**Scheme 1a**), yet numerous alternative approaches have been well explored. Oxidation of amine functionalities to amides by C-O bond formation (**Scheme 1b**) has seen substantial developments in recent years, as has the aminocarbonylation approach (**Scheme 1c**) of combined C-C and C-N bond formation. A disconnection which has seen far less interest, though, is that of C-C bond formation (**Scheme 1d**) utilising an amine component prefunctionalised with a carbonyl group.

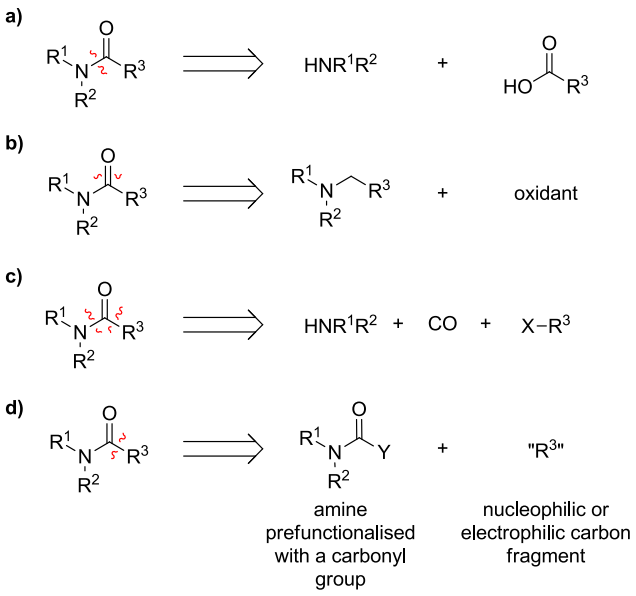


**Scheme 1** - General amide bond disconnections. **a)** C-N bond formation, **b)** C-O bond formation, **c)** C-O and C-N bond formation, and **d)** C-C bond formation.

### 1.2.1. C-N bond formation

Simplistically, it could be considered that an amide bond could be formed by a condensation reaction of an amine with a carboxylic acid. In reality, this reaction is less readily achieved, partly due to the relative acidity of the carboxylic acid, and basicity of the amine. The most

widely adopted solution to this issue is to activate the carboxylic acid, replacing its acidic –OH with a leaving group, which will readily be displaced by the desired amine. A plethora of activating strategies have been developed, using a range of coupling agents to form an activated intermediate, which is intercepted by an amine (**Scheme 2**).[5]

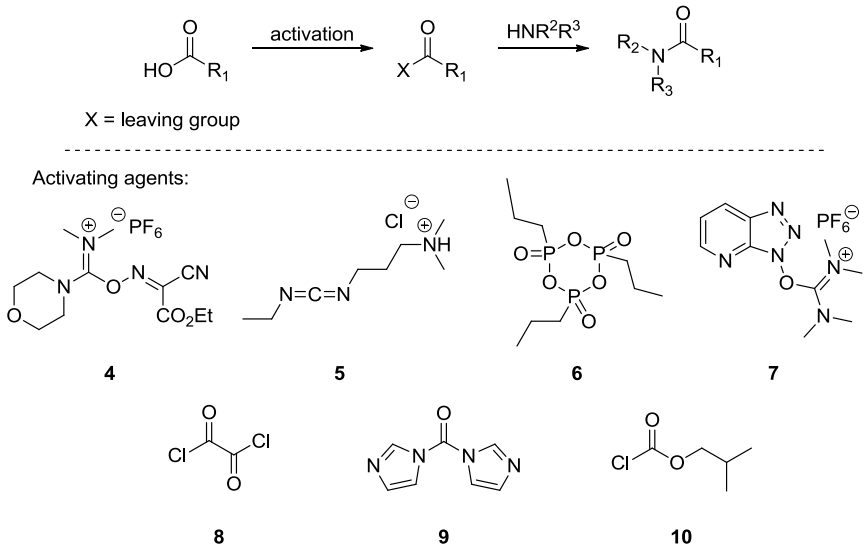


**Scheme 2** - General strategy of carboxylic acid activation, in amide bond formation. The structures of some commonly used coupling reagents are shown: COMU (**4**), EDCI hydrochloride (**5**), T3P (**6**), HATU (**7**), oxalyl chloride (**8**), CDI (**9**), and isobutyl chloroformate (**10**).

Although the most commonly used approach, the general method of activating a carboxylic acid is extremely wasteful. Activating agents are most widely used in stoichiometric quantities, generating considerable amounts of waste, to achieve what is essentially merely a condensation reaction. In addition to their large mass, most coupling agents have other drawbacks. EDCI, for example, usually employs an additive such as the high energy molecule HOBt.[6] Other issues can include: undesirable waste streams and by-products, expensive materials, toxic reagents or by-products, and the need for purification of the resulting amide.[7]

Possibly the most widely developed class of amidation catalysts, arylboronic acids have received significant attention.[8] Numerous catalysts have been examined,[9,10,11] yet 5-methoxy-2-iodophenylboronic acid (**16**) has been found to be arguably the most effective variant to date (**Scheme 3a**).[12,13] Recent studies have also identified borinanes, such as DATB (1,3-dioxa-5-aza-2,4,6-triborinane, **18**, **Scheme 3b**), as a new class of boron-based amidation catalyst.[14,15]

Whilst many examples of secondary amide formation have been showcased using these catalysts, tertiary amide formations using acyclic secondary amines remain a challenge. Moreover, general substrate scope often appears limited, particularly with less nucleophilic amines and anilines, limiting their application in API synthesis.[16]

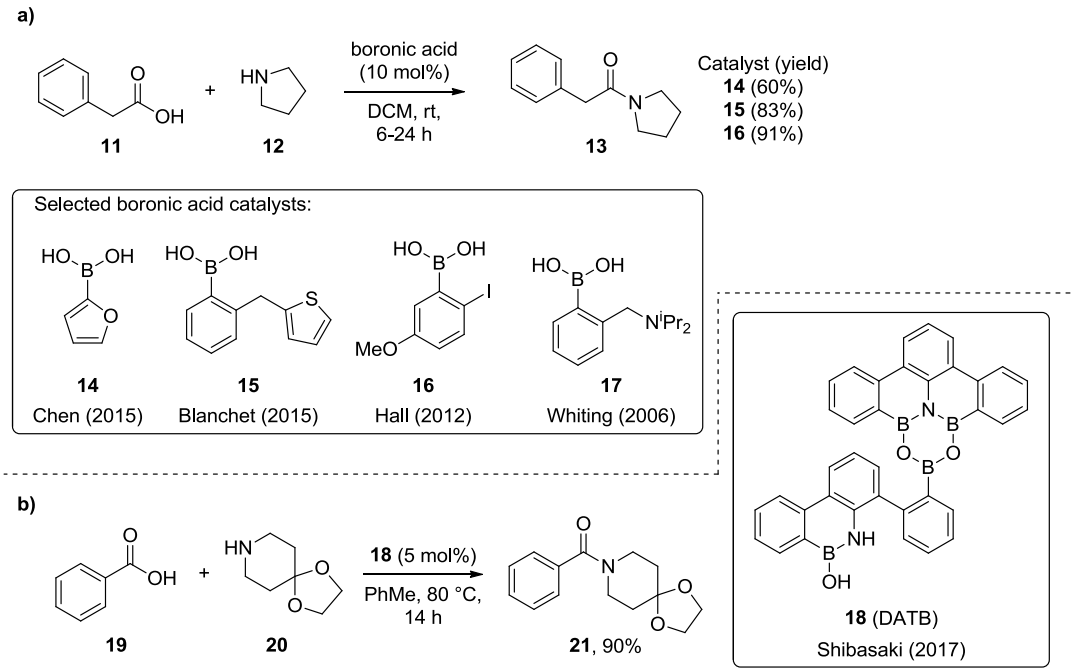


**Scheme 3** - Organoboron species as amidation catalysts. **a)** Performance of various arylboronic acid catalysts in the synthesis of **13**. **b)** DATB (**18**) catalysed synthesis of **21**.

A further reaction type, which falls into this category, is the dehydrogenative coupling of amines with alcohols (**Scheme 4**). The seminal paper in this field invoked the use of a ruthenium PNN pincer complex.[17] Since then, a great deal of effort has been made to expand upon the seemingly ideal reaction, through exploring mechanistic aspects,[18,19] catalyst systems,[20,21,22,23] and nucleophile/electrophile combinations.[24,25] Despite these advances, harsh reaction conditions are mandated, and it appears that reliable tertiary amide synthesis has yet to be achieved. Furthermore, the expensive ligand systems, and apparent lack of functional group tolerance reduce the potential applicability within more complex molecules.

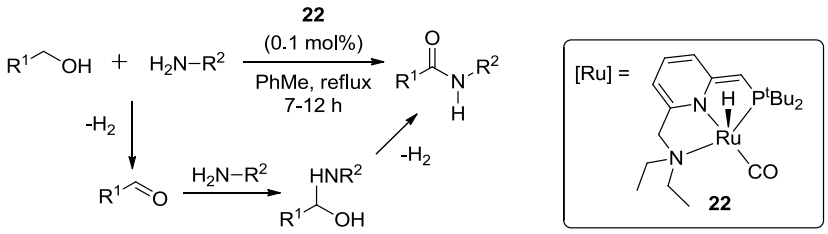


**Scheme 4** - Milstein's oxidative amide formation conditions, with a proposed mechanism, and Ru-PNN catalyst (**22**) structure.[17]

### 1.2.2. C-O bond formation

Derivatisation of an amine by the introduction of an α-amino carbonyl group, in an oxidative manner, can achieve an economical amidation, depending upon the oxidant used (**Scheme 5a**). Unfortunately, in the majority of cases, harsh conditions are required, often including an excess of hazardous oxidants, such as iodine (**Scheme 5b**),[26] peroxides,[27] or ruthenium oxides.[28] Catalytic systems have also been developed, in which this transformation is carried out using an oxidant generated from a benign source, such as water (**Scheme 5c**).[28] This procedure requires forcing conditions though, and very little functional group tolerance has been demonstrated. Whilst the general oxidative approach appears appealing, it is limited, in most cases, to cyclic amine starting materials.

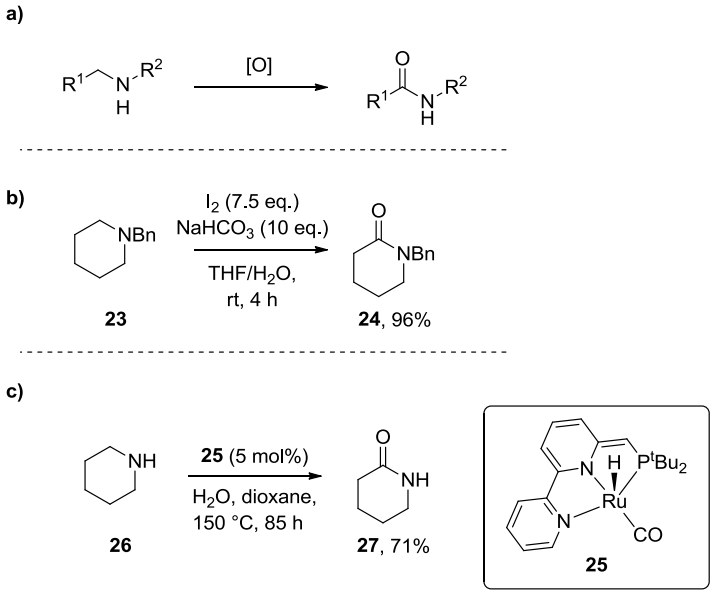


**Scheme 5** - **a)** General scheme, depicting the oxidation of an amine, to an amide. **b)** Oxidation of benzyl protected piperidine (**23**) using excess iodine.[26] **c)** Catalytic oxidant-free oxidation of a cyclic amine, to its corresponding lactam (**27**), using a ruthenium catalyst (**25**).[28]

### 1.2.3. C-C and C-N bond formation by aminocarbonylation

Utilisation of carbon monoxide (CO) as a carbonyl source has been well documented in recent years, through catalysed aminocarbonylation reactions with a carbon electrophile (**Scheme 6a**).[29,30] Although this constitutes an exceptionally efficient amidation method, there are three notable drawbacks to current methods: the requirement for forcing conditions and bespoke catalyst systems, alongside limited substrate applicability. Generally, palladium-catalysed aminocarbonylation reactions require high carbon monoxide pressure, high temperature, and long reaction times to achieve productive reaction. Moreover, the catalyst and ligand system is generally optimised for each reported protocol, or even in specific substrate cases. Finally, the currently available methods are limited to sp/sp$^2$ carbon electrophile substrates and, in most cases, primary or cyclic secondary amines. The problem of alkyl cross-couplings has been the subject of much research in recent years, but is far from solved.[31] Despite these general drawbacks, mild reaction conditions have been reported in recent years (**Scheme 6b**),[32] and aminocarbonylation represents a rapidly growing field.

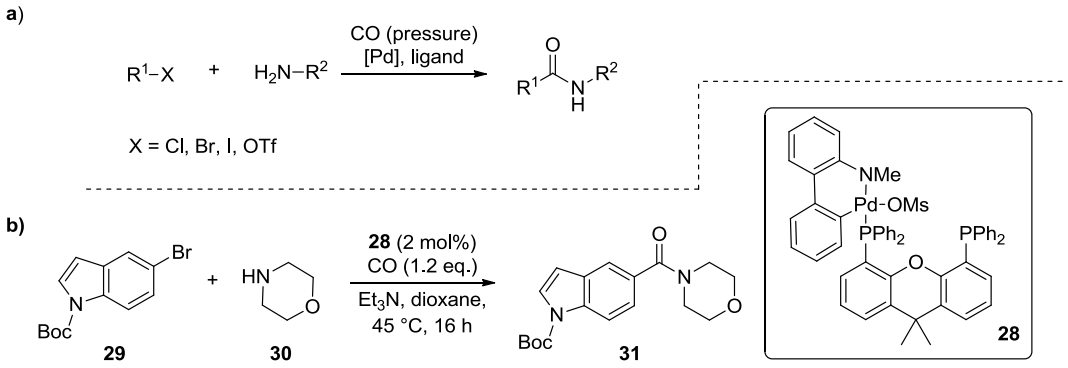


**Scheme 6** - **a)** General reaction scheme for the carbonylative coupling of a primary amine with an aryl (pseudo)halide. **b)** Mild aminocarbonylation of heteroaryl bromide (**29**) with morpholine (**30**), using a palladium Xantphos precatalyst (**28**).[32]

### 1.2.4. C-C bond formation

When compared with other strategies, the formation of a single C-C bond to form an amide product is comparatively rare. In theory, this could be considered in two complementary approaches: pairing a nucleophilic carbon with an electrophilic carbonyl-containing fragment (**Scheme 7a**) or, conversely, combining an electrophilic carbon with an umpolung[33] nucleophilic carbonyl-containing moiety (**Scheme 7b**).

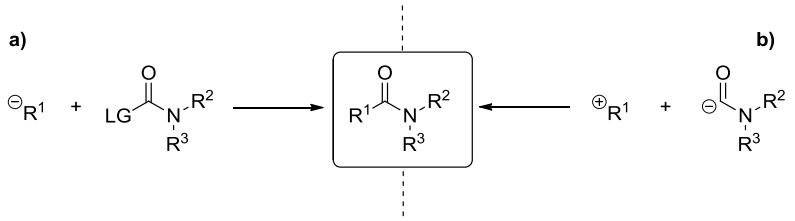


**Scheme 7** - General scheme depicting amidation by C-C bond formation, from the required synthons. **a)** nucleophilic carbon and electrophilic carbonyl unit, or **b)** electrophilic carbon and nucleophilic carbonyl unit.

The reaction of an electrophilic carbamoyl species with an organometallic species (**Scheme 7a**) seems a natural disconnection to make, when considering the analogous reactions of acid chlorides or Weinreb amides. However, the majority of these reactions make use of the less electrophilic carbamate species and, hence, require a Grignard reagent to furnish the desired tertiary amides.[34] Furthermore, the use of highly basic organometallic reagents has the implication that forming secondary amides using the same approach is far less straightforward, requiring a vast excess of nucleophile.[35] This approach will be reviewed in more detail below (see Chapter 3. Synthesis of secondary amides enabled by flow processing).

Nucleophilic carbamoyl species (**Scheme 7b**) have only rarely been utilised synthetically, in the form of either metalated carbamoyl anions, or as carbamoyl radicals. Recent work towards generating carbamoyl lithium species in flow have achieved synthetically useful nucleophilic functionalisation of this highly unstable species, through reductive lithiation,[36] or simply deprotonation.[37] Carbamoyl radicals have long been known,[38] but up until relatively recently have been invoked in very few synthetic methodologies. As with many radical species, their highly reactive nature has historically restricted their reactivity mainly to intramolecular reactions.[39,40] This approach will be reviewed in more detail in the following chapter (see Chapter 2. Synthesis of tertiary amides enabled by photoredox methods).

## 1.3. New synthetic technologies

Synthetic organic chemistry has recently benefitted from a wealth of new reactive pathways and previously unattainable transformations, due to the development and uptake of new synthetic technologies. These new technologies have begun to fundamentally alter the way in which organic synthesis is approached, by expanding towards a range of equipment and techniques, which were previously assumed to be the domain of specific experts, rather than widely usable synthetic tools. The cross-disciplinary nature of modern science has encouraged synthetic chemists to collaborate with biologists, physicists, and engineers, spawning synthetic biochemistry,[41] electrochemistry,[42] photoredox processes[43] and flow chemistry.[44] Whilst often beneficial in efficiency and sustainability, most importantly, these technologies can enable transformations and synthetic routes previously found to be inaccessible.

### 1.3.1. Photoredox chemistry

Despite being a well understood tool for many years,[45] synthetic organic photochemistry has undergone a recent renaissance. UV photochemistry has seen numerous applications within modern synthetic chemistry, particularly in the search for new medicinally-relevant 3-dimensional scaffolds,[46,47] including the development of larger scale reaction platforms.[48] However, visible light-mediated transformations have seen a far larger increase in interest. Visible light has numerous advantages over UV light, and most notable of these within synthetic applications is the remarkable improvement in tolerance of sensitive functional groups. The majority of organic compounds absorb lower wavelength UV radiation, but are essentially invisible to visible light wavelengths (>400 nm).[49]

Employing visible light allows the use of a photocatalyst, which absorbs the longer wavelengths used, then selectively activates the desired chemical substrate, by way of electron transfer,[49] or energy transfer.[50] The activated substrate can then undergo reaction, often *via* radical pathways, resulting in selective radical generation at a controlled rate, circumventing one of the fundamental barriers to performing classical synthetic radical chemistry.[51] Consequently, a myriad of transformations have been published to date, taking advantage of these mild radical generation methods, to perform selective and functional group-tolerant chemistry, which was not previously possible.[43]

In more detail, the generic outline for a simple single electron transfer photoredox reaction is shown below (**Figure 2**). This generally involves reductive (or oxidative) quenching of the excited state photocatalyst (**33**). The excited state quencher (**35**) will form a radical species (**36**) to undergo reaction, eventually forming a species of complementary redox reactivity to the initial quencher (**37**). This then interacts with the catalytic species (**34**), in order to regenerate the ground state catalyst (**32**), to be further excited by absorption of light, and propagate the catalytic cycle.

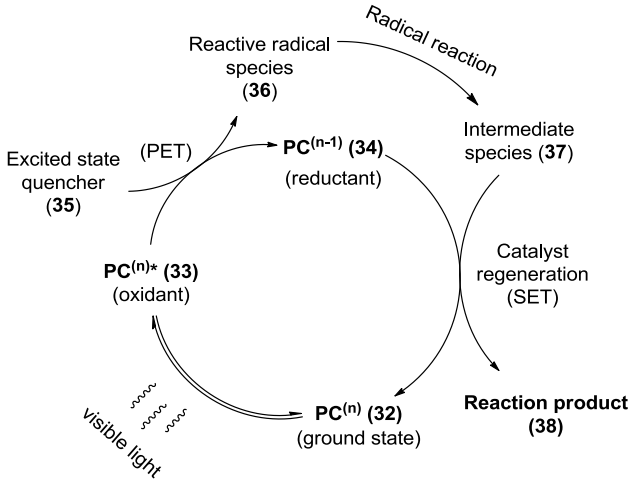


**Figure 2** - General photoredox catalytic cycle, demonstrated using a reductive quencher.

This basic idea of photoredox radical generation has been augmented in many ways since the concept's popularisation around a decade ago,[49] adding to the complexity and synthetic utility available. Some of these modifications include: inclusion of redox mediator additives, to expand the scope of possible chemistry;[52] introduction of a separate catalyst (often an organocatalyst, or a nickel- or palladium-based metal catalyst), to allow for radical-based cross-coupling reactions by dual catalysis;[53] and even the generation of more reactive photocatalyst species through consecutive photoinduced electron transfer processes (conPET).[54,55,56]

With the increased interest in photoredox transformations, an in-depth understanding of catalytic species has been accrued, in both organic[57] and metal-based[58,59] photocatalysts. The excited state oxidation and reduction potentials may be calculated through a combination of cyclic voltammetry, and UV/vis spectrophotometry. This consequently allows for an accurately informed choice of catalyst to match the substrate's redox potentials, which can also be found through the use of cyclic voltammetry.[60] Accordingly, there have been multiple instances of

catalyst optimisation for a specific transformation, through iterative installation of functional groups, to shift the redox window to the desired region.[61,62]

### 1.3.2. Flow chemistry

Flow chemistry, when applied to synthetic organic chemistry in the most fundamental sense, involves the reaction of material as it is pumped through a reactor vessel, whether this is a structured microreactor,[63] a continuous stirred tank reactor (CSTR),[64] or simply a length of tubing.[65] This idea has been employed in bulk chemical industries for some years, yet only recently has synthetic organic chemistry seen its benefits. It is likely that the reason for this significant lag period is due to the initial barrier to understanding and setting up a flow chemistry system, particularly for a process that is of low volume or is infrequently run. However, with advances in inline reaction monitoring,[66] optimisation of a flow chemistry process can be achieved on far shorter timescales. Moreover, increasing pressure upon the pharmaceutical and fine chemical industries to improve the sustainability of their manufacturing processes has assisted in driving this move towards continuous processing.

For most chemical reactions, the advantages of flow chemistry lie most significantly with the improved heat and mass transfer benefits,[67] or by the more precise control of reaction time.[68] Specifically, organometallic reactions benefit greatly from these improved characteristics, allowing temperature-sensitive reactions to be performed at higher temperatures,[69] and enabling transformations which are otherwise unproductive.[37] The lower reactive index within the flow reactor at any one point also has the implication of an improved safety profile, particularly for procedures in which a reactive intermediate is formed, and could accumulate.

Furthermore, processes performed in flow are amenable to further upscaling. Whilst the mixing and heat transfer characteristics of batch reactors vary greatly upon moving towards larger scales, this can be circumvented using continuous processing. Scaling up the flow reactor allows increased throughput, but will also change its characteristics; however, using elongated run times or "scaling out" (implementing multiple reactors in parallel) allow higher throughput, whilst maintaining the reaction characteristics. For these reasons, amongst others, reaction development using flow chemistry technology is becoming increasingly common within the pharmaceutical industry and, indeed, preparative laboratories elsewhere.[70]

## 1.4. Project aims

In a broad sense, the aim of this research programme is to explore and develop new strategies to access amides, through formation of a new C-C bond. As discussed within the introductory sections of this chapter, it is envisaged that new synthetic technologies will be utilised and further developed, in order to enable and improve transformations, which may have been previously reported but could not be carried out in a productive or widespread manner using the standard synthetic tools available at that time. These technologies will only be employed, though, when a genuine advantage is bestowed upon the developed protocols.

During method development, a focus will be maintained towards the future application of such methods within the manufacture of pharmaceutical and fine chemical products. Although there is a significant barrier to more widely developing and employing *new* amidation methodologies, due to the precedence and relative simplicity of current methods, it is envisaged that further development work would, indeed, result in an industrially-relevant process. Accordingly, efforts will be made, to maximise mass incorporation, to tackle one of the major issues with classical amide formation, using coupling reagents.[5] In addition, an overall consideration of scalability and manufacturability will be maintained, with a view to streamlining any future efforts, which might result in large scale application.

The methods developed herein, should cover a broad range of possible substrates, allowing for maximum possible inclusion in synthetic routes. The aim will also be to include primary, secondary and tertiary amides in the attainable broad product classes. Within this remit, a high degree of functional group tolerance is also necessary, to allow for use in the synthesis of highly functionalised small molecules, such as APIs or agrochemical products, in a manner not restricted to early synthetic steps.

# Chapter 2. Synthesis of tertiary amides enabled by photoredox methods

## 2.1. Introduction

As discussed previously (see 1.2.4. C-C bond formation), the combination of a carbamoyl nucleophile with a carbon-based electrophile represents an underexplored method of amide formation. Whilst recent reports of generation and reaction of carbamoyl anions show significant promise,[36,37] it is envisioned that the application of modern synthetic technologies will allow for advantageous reactivity, *via* carbamoyl radical species. More specifically, photoredox chemistry could act as a tool to enable gradual release of this radical species, for a clean and functional group-tolerant reaction protocol.

### 2.1.1. Carbamoyl radicals

Thus far, the most appealing strategy of photoredox amide bond-formation concerns the generation and onward reaction of carbamoyl radicals. Few synthetic applications of carbamoyl radicals have been reported when compared with other carbonyl-based radical species, perhaps in part due to a lack of mild and effective methods for their generation.[38] In order to employ this radical species in synthesis, it is necessary to consider the precedented protocols for its formation, alongside understanding of its behaviour in reactive systems. Aside from those described here, a host of other methods have been reported, yet are not seen as being synthetically relevant, due to limited applicability,[71] or the requirement for toxic or undesirable reagents.[72,73]

#### *2.1.1.1. Direct oxidation of formamides*

The most straightforward method of carbamoyl radical generation is simply through chemical oxidation of a formamide species.[38] However, formamides have very high oxidation potentials (for example: DMF = +2.26 V vs SCE, and 2-piperidinone = +2.58 V vs SCE),[60] therefore, exceedingly strong oxidising agents are required, which has a significant detrimental effect upon preparative applications. Furthermore, there are issues with regioselectivity, due to the possibility to form an α-amido alkyl radical.[74,75] The most commonly used oxidant in this reaction is Fenton's reagent,[76] a reactive system with many safety concerns related to its explosivity, particularly when employed on larger scale.[77] Direct formation of carbamoyl

radicals from formamides can also be achieved using UV irradiation, but these methods are not well developed, and require the amide to be present as the reaction solvent.[78,79] Accordingly, these approaches will not be considered further.

*2.1.1.2. Oxime oxalate amide precursors*

Through detailed study of oxime oxalate precursors, the generation of a variety of radical species has been achieved, and applied to synthetically useful transformations.[40] Of these precursor species, oxime oxalate amides (**42**) are of interest to this work, due to their decarboxylative fragmentation to form carbamoyl radical species (**45**).[80] Oxime oxalate amides are formed through reaction of an oxime with oxalyl chloride, followed by addition of an amine (**Scheme 8**).[81] These can then be fragmented by irradiation with a high pressure mercury lamp, in the presence of the photosensitiser, 4-methoxyacetophenone (MAP) (**43**). The resulting carbamoyl radicals then undergo a well-studied cyclisation[82] onto a strategically placed double bond, to form 4- and 5-membered lactams (**46**).

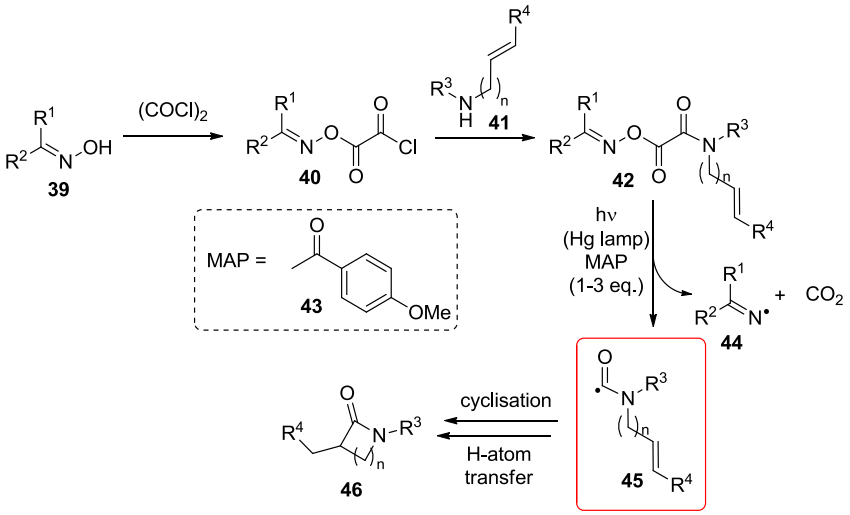


**Scheme 8** - Synthesis of oxime oxalate amides (**42**), followed by their photochemical decomposition, and concomitant cyclisation, to form lactam products (**46**).[81]

This approach to carbamoyl radical generation is limited in its application and, hence, has seen little activity since its seminal publication.[80] Due to the uncontrolled generation of carbamoyl radicals, and the high temperatures associated with the mercury lamp reaction setup, it is unlikely that an effective intermolecular reaction protocol could be developed. Furthermore,

the synthesis requires a sacrificial oxime, whose corresponding iminyl radical (**44**) is generated, and would also be expected to complicate any attempted intermolecular reactivity.

*2.1.1.3. Dithiocarbonyl-based precursors*

Inspired by the pioneering work of Zard, on the synthetic application of xanthates,[51] there have been multiple reports of dithiocarbonyl-based carbamoyl radical precursors in the past two decades,[39] consisting of carbamoylxanthate (**47**),[83] and carbamoyldithiocarbamate (**51**)[84] species. It has been found that carbamoylxanthates (**47**) are only synthetically tractable if the starting amine is sterically hindered (i.e. bears a *tert*-butyl group), thus limiting its synthetic utility (**Scheme 9a**).[85,86] Carbamoyldithiocarbamates (**51**), on the other hand, have been demonstrated to possess far more preparative flexibility, allowing a range of dithiocarbamate transfer radical cyclisation reactions (**Scheme 9b**), furnishing products which remain functionalised (**53**).[84]

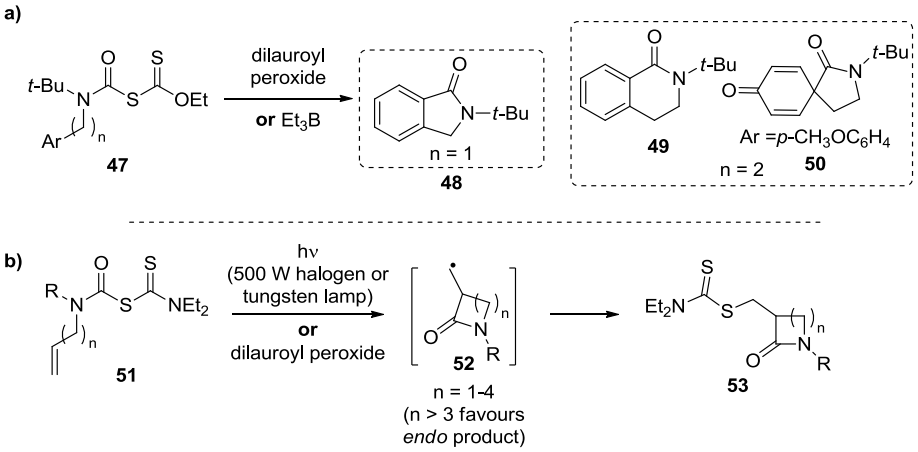


**Scheme 9** - **a)** Cyclisation reactions of carbamoylxanthates (**47**) to form bicyclic (**48**, **49**) or spirocyclic (**50**) amides. **b)** Group transfer radical cyclisation reactions of carbamoyldithiocarbamates (**51**).

## 2.1.2. Decarboxylative reactions

In the development of synthetic methodologies, the extrusion of carbon dioxide to mediate a functional transformation or bond forming reaction has been widely utilised in metal-catalysed coupling reactions in the past two decades (**Figure 3a)**.[87,88] This can likely be attributed to the widespread occurrence of carboxylic acids in naturally occurring and other readily available

molecules,[89,90] as well as their ease of synthesis. Additionally, a further attractive feature is the enthalpic driving force bestowed upon these reactions by the expulsion of a gaseous species. Most commonly, decarboxylative cross-coupling reaction pathways are copper- or palladium-catalysed, and result in C-C bond formation, in an analogous fashion to classical coupling reactions.[91] A small number of decarboxylative carbon-heteroatom bond-forming transformations have also been developed.[92,93,94]

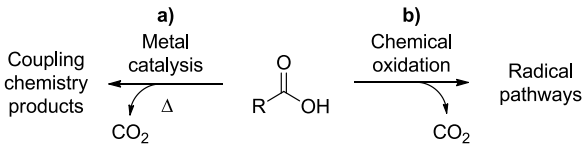


**Figure 3** - Decarboxylative functionalisation through metal catalysis or chemical oxidation.

Decarboxylation through interaction with a metal catalyst is not a facile process, and generally requires high temperatures of over 100 °C, limiting its practicability, and functional group tolerance. Accordingly, several decarboxylative C-C bond-forming methods have taken advantage of chemical oxidants, to access single electron reaction pathways (**Figure 3b)**. This is facilitated by a strongly oxidising species in stoichiometric quantities, such as potassium persulfate ($K_2S_2O_8$), and can be accelerated by carboxylate activation as a silver salt, as described by Minisci.[91] Redox-mediated decarboxylation has been employed to perform a number of transformations such as: azidation,[95] halogenation (the Hunsdiecker reaction),[96] alkynylation,[97] and even cycloadditions,[98] at far lower temperatures than those relying solely on a metal catalyst.

Direct reactions of nucleophilic acyl radicals, formed from oxidation of α-oxoacids, have been found to be limited in synthetic scope, and have shown poor selectivity (**Scheme 10a**).[99] However, the combination of a chemical oxidant with a transition metal catalyst has successfully given access to a range of transformations, particularly when implementing α-oxoacids as decarboxylation precursors, under Pd(II) catalysis (**Scheme 10b**).[100] The resulting methods allow a cross-coupling type functionalisation of carbonyl compounds. Whilst this was initially limited to ketone formation,[101,102] the general approach has since been extended to amides and esters.[103]

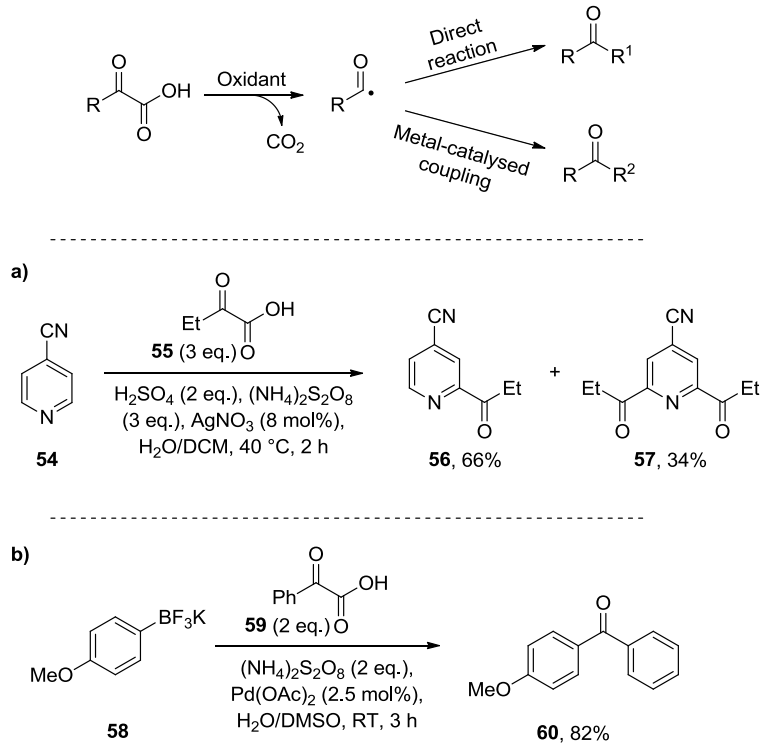


**Scheme 10** - Decarboxylation of α-oxoacids using a chemical oxidant, followed by either direct radical reaction, or metal-catalysed coupling, to form functionalised carbonyl compounds. **a)** Direct addition of acyl radicals to a heterocyclic substrate (**54**).[99] **b)** Palladium-catalysed coupling of acyl radicals with aryl tetrafluoroborate salts (**58**), to form benzophenone derivatives (**60**).[101]

Despite receiving substantial attention, both of these decarboxylation methods require harsh conditions, with respect to either high temperatures, or strong oxidants. Accordingly, the resulting substrate scope is severely limited, and applicability within a pharmaceutical setting is, by consequence, compromised.

Related to the decarboxylative processes discussed above, a recent interest in both visible light-mediated chemistry,[43] and electrochemistry[42] has popularised mild methods of radical formation, reinvigorating the use of radical chemistry within new synthetic organic methodology development. Whilst electrosynthesis undoubtedly has great potential, there are a substantial number of complexities involved, including but not limited to: choice of electrode material, optimisation of current and voltage, choice of divided or undivided reactors, and optimisation of electrolyte solution. Conversely, photoredox method development has a comparatively low accessibility barrier limited to, at first observation, the choice of photocatalyst, and light source.

### 2.1.3. Decarboxylative photoredox strategies

Many photoredox methodologies have taken advantage of $CO_2$-containing functionalities as radical precursors, due to their facile oxidation, in comparison to redox potentials attainable by modern photocatalysts.[104] The abundance of carboxylate groups in feedstock chemicals,[89,90] and their functional group compatibility, means that these serve as versatile radical precursors, to be engaged in a wide variety of transformations.[105] In analogue to non-photochemical methods, addition of an activating group, such as *N*-hydroxyphthalimide (to form species **62**),[106,107] can reverse the redox activity of a carboxylate (**61**)[108,109] or oxalate[110,111,112] species, turning it into an oxidative quencher, as opposed to its native reactivity as a reductive quencher (**Scheme 11**).

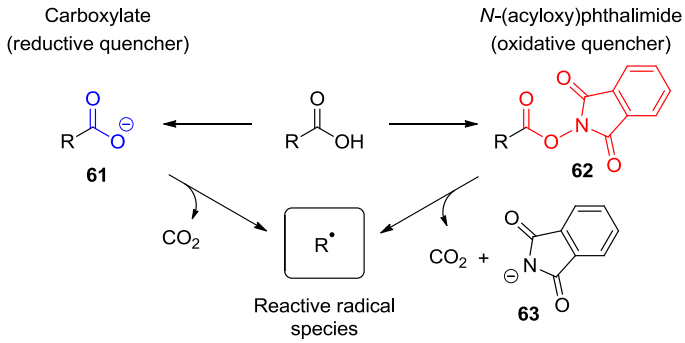


**Scheme 11** - General radical formation from carboxylic acid precursors, *via* oxidation of the carboxylate (**61**) (left), or reduction of the *N*-(acyloxy)phthalimide (**62**) (right).

This inversion of reactivity has been exploited even further, in the photoredox coupling reaction of an unactivated carboxylic acid (**64**) with an *N*-(acyloxy)phthalimide (**65**). Here, both oxidative and reductive decarboxylative transformations are carried out, to propagate the catalytic cycle, albeit with the addition of DABCO as a redox mediator (**Scheme 12**).[113] In the proposed mechanism, DABCO (**70**) is thought to act as a reductive quencher for the excited state photocatalyst (**68**). The reduced ruthenium species (**69**) then transfers an electron to the *N*-(acyloxy)phthalimide starting material (**65**), triggering decarboxylation, to provide an alkyl radical (**72**), which adds to the electron-deficient olefin (**73**). The radical addition product (**74**) can then be oxidised by DABCO radical cation (**71**), then undergoing decarboxylation to afford the desired product (**66**).

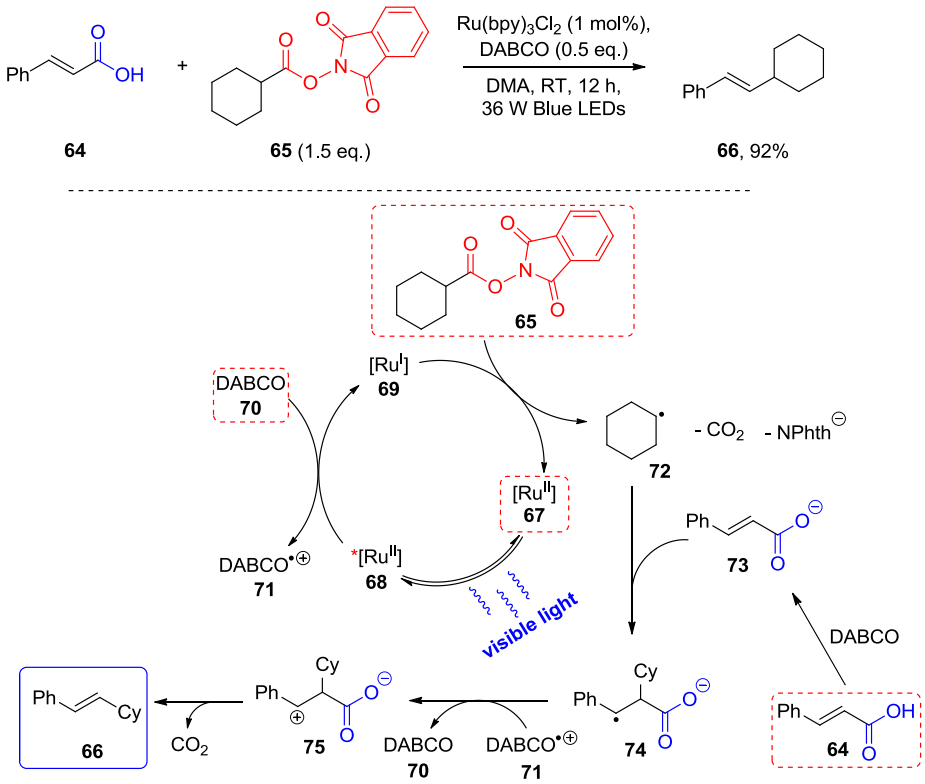


**Scheme 12** - Reaction scheme, and proposed catalytic cycle to describe the reductive and oxidative decarboxylation of two carbonyl species (**64** and **65**), combined in one reaction to furnish a functionalised styrene (**66**).[113] Red dashed boxes indicate starting material species.

### 2.1.4. Photoredox approaches to amide formation and functionalisation

*2.1.4.1. Amide functionalisation*

With respect to amide-forming and -functionalising reactions, photoredox approaches have been explored in recent years. These approaches, however, often proceed through the generation and further reaction of nitrogen-centred radicals.[114] More specifically, amidyl radicals are the most straightforward radical species from which to functionalise preformed amines. The first photoredox method for this transformation invoked a photochemically-promoted proton-coupled electron transfer (PCET),[115,116,117] from unfunctionalised secondary amides (**76**), followed by cyclisation, then reaction with an olefin radical acceptor (product **79**, **Scheme 13a**).[118] The transformation was then combined with a hydrogen atom transfer (HAT) catalyst, to form the corresponding unfunctionalized cyclic amide product (**80**, **Scheme 13b**).[119]

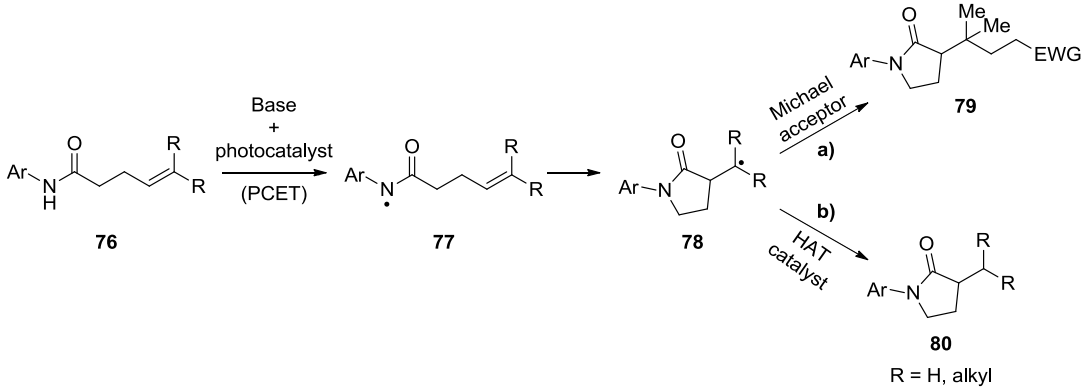


**Scheme 13** - Formation of amidyl radicals (**77**) through PCET, followed by cyclisation, then reaction with **a)** a Michael acceptor (product **79**),[118] or **b)** a HAT catalyst (product **80**).[119]

The group of Leonori have developed a complementary catalytic system, invoking tertiary amides, as specifically tuned redox-active derivatives (**81**, **85**, **90**, **Scheme 14**).[120] This system has been further applied to cyclisation onto alkenes or alkynes (**84**, **Scheme 14a**),[121] or in direct homolytic aromatic substitution (HAS) to furnish *N*-arylated amides (**89**, **Scheme 14b**). These conditions were adapted by Wang, to a system which cyclises onto a tethered indole, as exemplified in a natural product (**94**) synthesis (**Scheme 14c**).[122] These methods, however, require pre-functionalised reagents, which diminishes their mass-efficiency and reduces their applicability within a synthetic route. In this area, development has been focused more upon

amine and imine functionalisation, using analogous precursors,[123,124,125] rather than on formation of the amide bond itself.

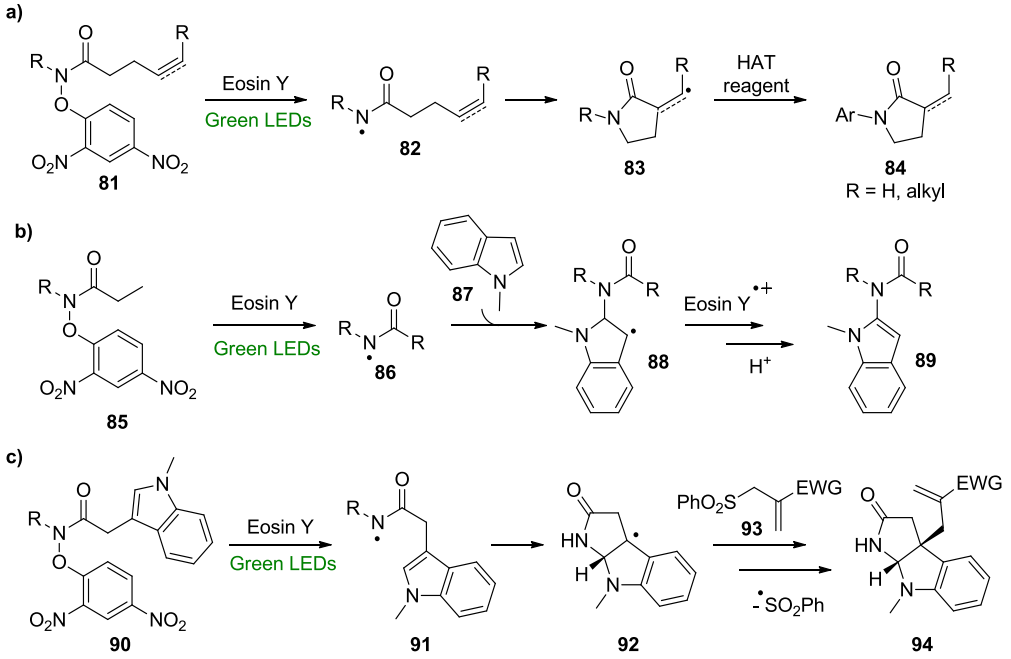


**Scheme 14** - Reactions of amidyl radicals, formed *via* reduction of *N*-OAr functionalised amides (**81**, **85**, **90**): **a)** in cyclisation, followed by HAT,[120,121] **b**) in direct arylation by HAS,[120] and **c)** in cyclisation-functionalisation using an indole core.[122]

Due to their improved stability, intermolecular reactions of imidyl radicals have been thoroughly investigated, by direct irradiation, or through use of a photocatalyst.[126] An example of this is the straightforward formation of aryl phthalimides (**96**), using *N*-(acyloxy)phthalimide (**95**) radical precursors (**Scheme 15a**).[127] These reactions, however, are limited to imide functionalisation, and so will not be discussed in further detail. Additionally, a nickel-photoredox dual catalytic methodology has been developed to form C-N bonds (**Scheme 15b**), but is limited to amines, with the exception of a single sulfonamide example.[128] Unlike traditional metal-catalysed C-N bond forming cross-coupling reactions,[129] there is no evidence of amide starting materials being compatible nucleophiles in this reaction.

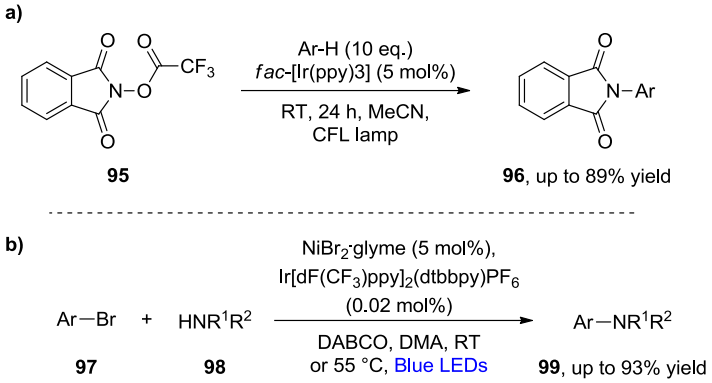


**Scheme 15 - a)** Photoredox generation and arylation of imidyl radicals from *N*-(acyloxy)phthalimides (**95**).[127] **b)** Nickel-photoredox dual catalytic arylation of amines (**98**) (and one example of a sulfonamide substrate).[130]

Another methodology that furnishes a functionalised amide invokes acyl azide (**100)** starting materials. The proposed mechanism of this reaction is thought to involve energy transfer from the $Ru(bpy)_3$ photocatalyst, liberating $N_2$ and forming a nitrene (**102**), which then reacts with various aromatic systems (**Scheme 16**). Unfortunately, this approach has synthetic drawbacks, as the acyl azide starting materials (**100**) are toxic and unstable. Moreover, five equivalents of the aromatic trapping agent are required for a synthetically useful yield to be obtained, due to the propensity for the nitrene intermediate (**102**) to form an isocyanate, through the Curtius rearrangement.[131]

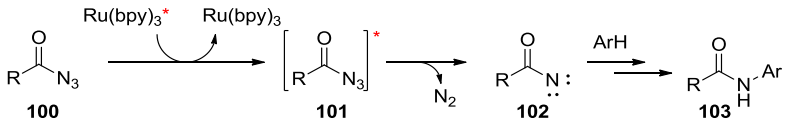


**Scheme 16** - Photosensitised reaction of acyl azides (**100**), to furnish arylated secondary amides (**103**), *via* a proposed nitrene intermediate (**102**).[131]

### *2.1.4.2. Amide bond-formation*

There has been substantially less focus upon photoredox reactions in which the amide moiety is actually formed (not taking into consideration protocols which employ photoredox functionalisation, followed by amidation *via* cyclisation onto an ester).[132] A C-N bond forming procedure has been reported, using α-keto acids (**104**) as precursors for acyl radicals, using a compact fluorescent lamp (CFL) as the light source. The radical species is thought to intercept

the amine starting material (**105**), in a redox cycle mediated by molecular oxygen (**Scheme 17**).[133]

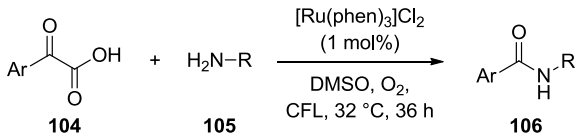


**Scheme 17** - Oxygen-mediated photoredox amidation of α -keto acids (**104**).[133]

All other examples of such amide synthesis are achieved in C-C bond forming reactions, and can be narrowed down to two reactive species: isocyanates, and oxamate derivatives. These two approaches show complementary reactivity, with isocyanates acting as electrophilic species, in direct addition or nickel catalysis, whilst oxamates form a nucleophilic carbamoyl radical.

In one isocyanate-based approach, direct radical addition to an isocyanate is thought to result in a nitrogen-centred radical (**110**), which will then undergo hydrogen atom transfer (HAT),[134] or reduction by the photocatalyst species (**Scheme 18**).[135] This transformation has also been demonstrated using triethylborane and air as stoichiometric reductant and oxidant.[136] The photoredox amidation method described, proceeds first through generation of an α-amino radical (**109**), by oxidation of *N*,*N*-dimethylaniline precursors (**107**). Therefore, this method is very limited in its scope, since extension to more electron-deficient anilines is not possible, due to their increased oxidation potential.

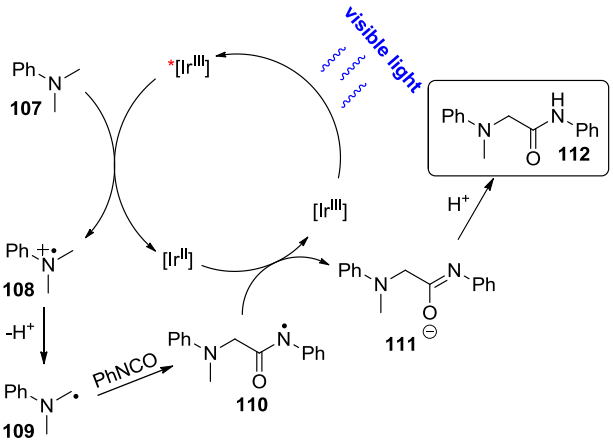


**Scheme 18** - Photoredox amidation through reaction of α-nitrogen radicals (**109**) with isocyanates.[135]

A recent nickel-photoredox dual catalysis amidation method has been published by the group of Molander, using alkylsilicates (**113**) as coupling partners (**Scheme 19**).[137] Here, it is proposed that the Ni(0) catalyst (**120**) undergoes oxidative addition into the isocyanate coupling partner (**119**), followed by radical addition, resulting in a Ni(III) species (**122**). Reductive elimination and protonation releases the amide product (**114**), and a Ni(I) species, which is reduced by the photoredox catalyst (**117**), to regenerate both ground state catalyst species (**115** and **120**). Despite being a theoretically elegant methodology, reaction yields are generally modest, and the protocol suffers from the requirement for atom-inefficient pre-functionalised silicate reagents,[138,139] alongside the use of toxic Ni(II) salts.[140]

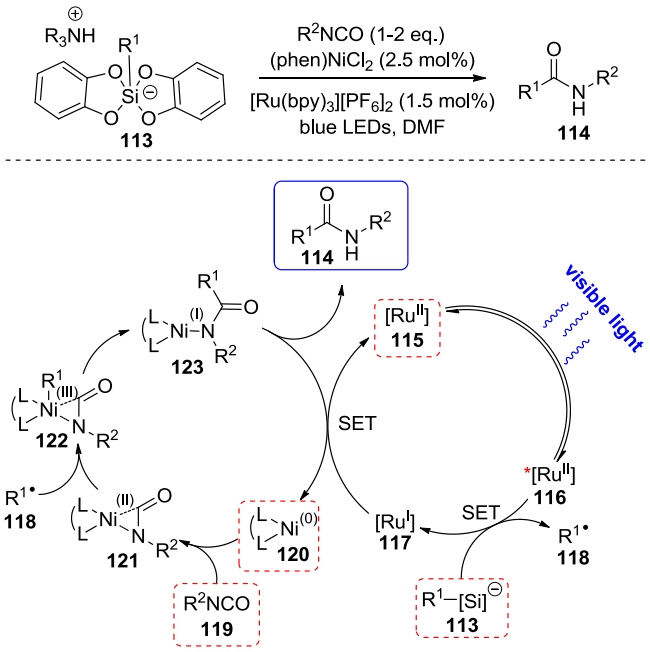


**Scheme 19** - Reaction scheme and proposed catalytic cycle of a nickel-photoredox dual catalytic amidation, from alkylsilicate precursors (**113**).[137] Red dashed boxes indicate starting material species.

Oxamate derivatives have seen application in a small number of photoredox methodologies in recent years. The oxamate species itself will act as a reductive quencher, by losing an electron to the photocatalyst, then decarboxylating to form the carbamoyl radical. Use of the latent oxamate as the potassium salt (**124**) has been demonstrated only within a palladium-photoredox dual catalytic system, in couplings with aryl halides (**125**, **Scheme 20**).[141] A range of substrates were tolerated, including several heteroaryl halides, with no requirement for heating the reaction. Unfortunately, the method could not be extended to (hetero)aryl chlorides. Moreover, successful reaction hinges upon the use of a specific ligand for palladium (NiXantphos, **127**),[142] alongside two equivalents of the oxamate starting material (**124**).

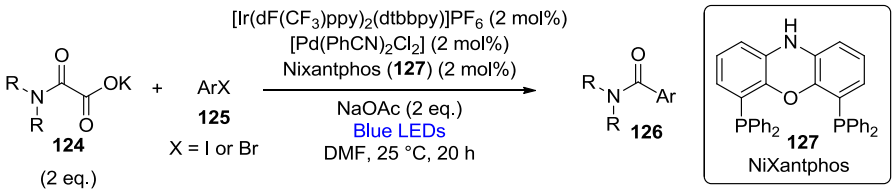


**Scheme 20** - Palladium-photoredox dual catalytic decarboxylative coupling of potassium oxamates (**124**), with (hetero)aryl iodides and bromides (**125**).[141]

A pair of recent publications describe the reaction of aromatic *N*-hydroxyphthalimido oxamides (**128**), in a decarboxylative homolytic aromatic substitution (HAS) protocol, furnishing derivatised dihydroquinolinone products (**133**, **Scheme 21**).[143,144] The proposed mechanism is initiated by a single electron transfer (SET) to the radical precursor (**128**). The carbamoyl radical (**129**) adds to an electron-deficient olefin, then the stabilised radical (**130**) cyclises by HAS, followed by regeneration of the ground state photocatalyst in a second SET event. Whilst this method represents a mild method of generating complexity, its scope is limited to formation of this specific heterocycle. Furthermore, the yields achieved are modest in most cases, and the overall transformation requires a prefunctionalised oxamate starting material, as the *N*-hydroxyphthalimide (**128**).

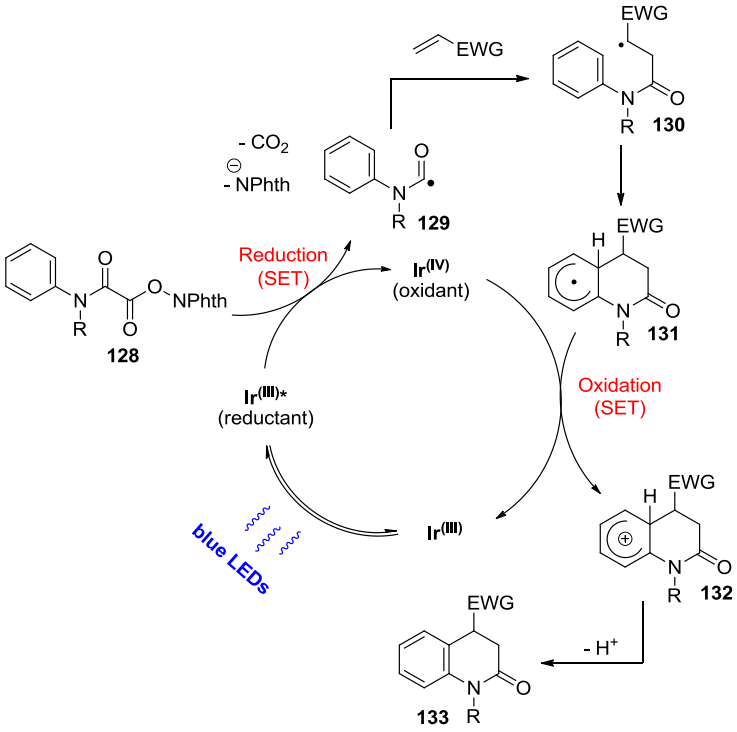


**Scheme 21** - Proposed reaction mechanism of decarboxylative HAS, from the *N*-hydroxyphthalimido oxamide (**128**).[143]

### 2.1.5. Mechanistic proposal and chapter aims

Upon consideration of current amidation methods, there is a substantial lack of precedence for the direct intermolecular reaction of carbamoyl radical species, following their mild generation by single electron transfer from a photocatalyst. In order to achieve a more mass-efficient

process, and to avoid the possibility of side-reactions with the phthalimide anion by-product, the oxamate (**134**) reaction pathway will be pursued, requiring an oxidatively active excited state photocatalyst. A proposed mechanistic pathway for this reaction is presented below (**Scheme 22**). The generated carbamoyl radical (**135**) will add to an electron-deficient olefin, forming a stabilised radical (**136**). This will then be reduced, regenerating the photocatalyst, and yielding an anion (**137**), which will furnish the product (**138**) upon protonation. Classical Michael acceptors are expected to be suitable reaction partners, as judged by their precedence in similar direct radical additions.[145,146]

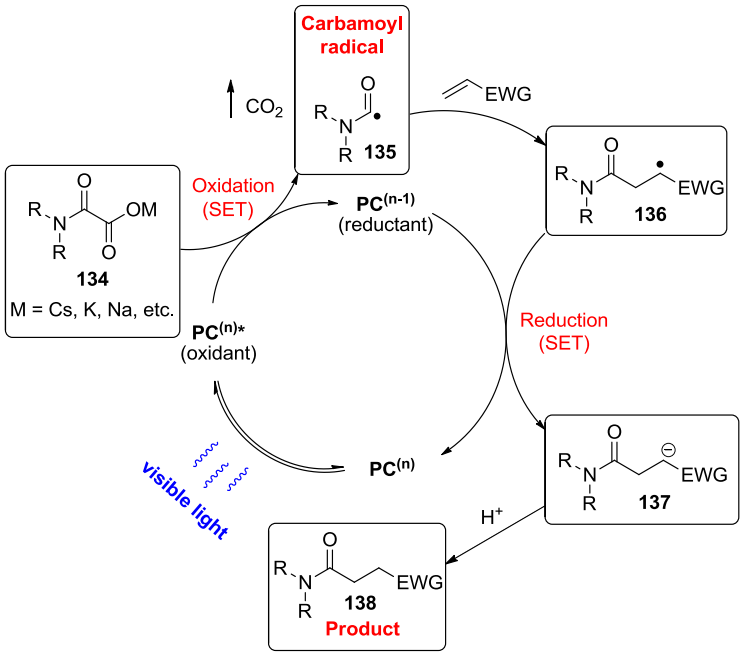


**Scheme 22** - Proposed catalytic cycle for decarboxylative amidation.

The developed protocol would ideally have the following features: no requirement for excess reagents, or for pre-activation of the oxamide starting material, room temperature reaction, and no requirement for strongly acidic, basic, or oxidising additives. It is desired that a range of electron-poor olefins, with diverse functionality, will be suitable reaction partners for the carbamoyl radical addition. Initially, alkyl oxamates without a free N-H will be examined, in order to avoid the precedented cyclisation reaction of anilinic carbamoyl radicals (see **Scheme 21**).[143]

This anilinic oxamate substrate class will also be explored, however, in order to extend the developed reactivity. In this respect, it would be desirable for the methodology to provide an alternative pathway to the previously disclosed cyclisation procedure using *N*-hydroxyphthalimido oxamides.[143,144] The existing methodology allows the preparation of cyclic amides in a straightforward manner, so development of a complementary transformation, furnishing the linear amide species (**138**), would be of synthetic benefit.

Ideally, the developed reaction protocol will be directly transferrable to continuous flow conditions, as this has been shown to be by far the most effective method to scale up photochemical reactions, for use in fine chemical production.[147] The identity of the metal counterion is expected to affect the efficiency of the initial oxidation, so will be examined early on in reaction development. Finally, density functional theory (DFT) calculations will also be carried out, to complement and support experimental results.

## 2.2. Results and discussion

### 2.2.1. Analysis of radical precursor species

Prior to initiating these synthetic studies, identification of a suitable precursor species for photoredox-based radical generation was required. As discussed previously, literature precedence was found for radical generation from both dithiocarbamate (**139**),[148,84] and oxamate (**134**)[141] functionalities (**Scheme 23a**). Both of these may be synthesised in a straightforward manner from amines (**140**): the dithiocarbamate by activation as the carbamoyl chloride (**141**), followed by displacement with a thiocarbamate; or the oxamate (**134**) by reaction with a chlorooxoacetate ester (**142**), followed by hydrolysis with a metal hydroxide or alkoxide (**Scheme 23b**).

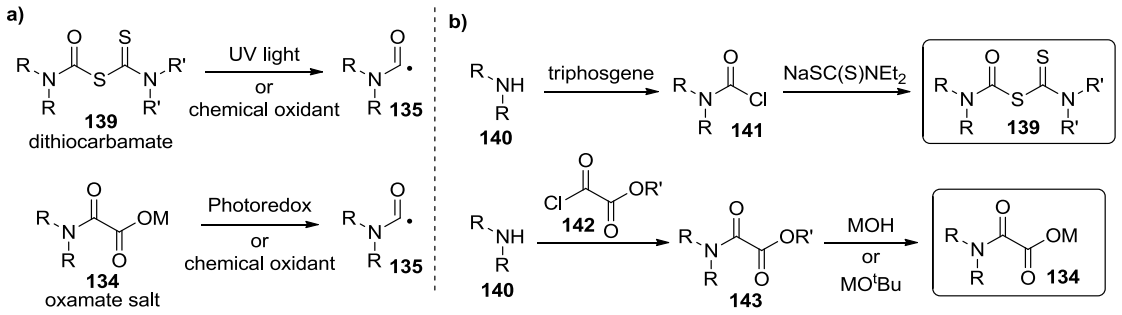


**Scheme 23 - a**) Carbamoyl radical (**135**) precursor species, and **b**) their synthesis from amine starting materials (**140**).

The suitability of these species for the desired transformation can be assessed simply by using cyclic voltammetry to estimate the oxidation potential required for electron transfer.[60] An aromatic and an aliphatic amine substrate of each species was synthesised in order to observe what effect conjugation with an aromatic system has upon the oxidation potential. Furthermore, two oxamate metal salts (cesium and potassium) were examined, to determine whether any major difference in oxidation potential is bestowed by the identity of the metal counterion (**Scheme 24**). Upon successful synthesis of these four compounds, each was analysed by cyclic voltammetry. The obtained cyclic voltammograms are shown below (**Table 1**).

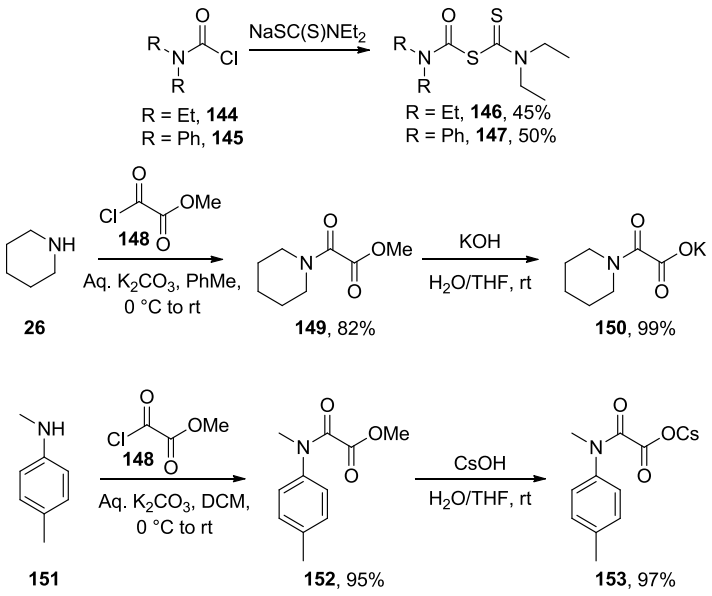


**Scheme 24** - Synthesis of dithiocarbamates (**146** and **147**) and oxamates (**150** and **153**), to be analysed by cyclic voltammetry.

All of the resulting voltammograms show an electron transfer event between +1.2 V and +1.5 V, giving oxidation potentials similar to those of metal oxalate species.[146] Notably, no back electron transfer was observed during the potential scan in the reverse direction (from +1.6 V back to 0 V). This is indicative of an instantaneous chemical transformation having taken place, and consequently, the redox active species is no longer present in solution.[60] This transformation is assumed to be a fragmentation in the case of the dithiocarbamate species, and decarboxylation in the case of the oxamate species, both resulting in the formation of carbamoyl radicals (**135**).

| | | |
|---|---|---|
| 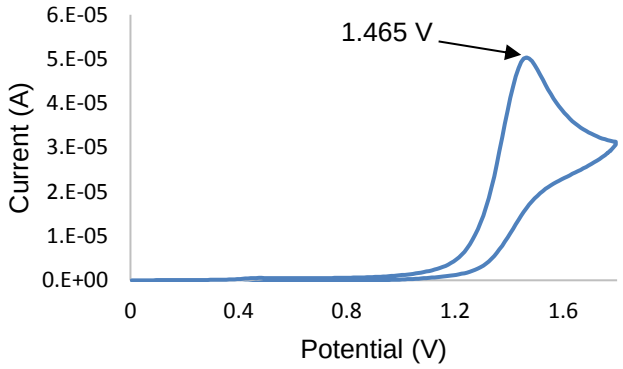 | 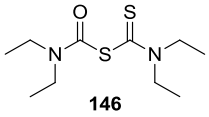 <br>146 | $E^{p}_{ox}$ = +1.43 V<br>(vs SCE† in MeCN) |
| 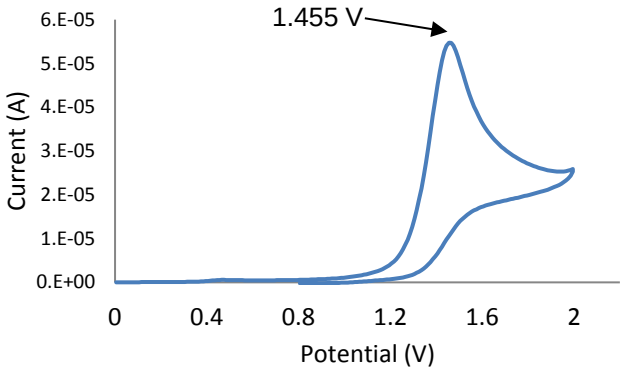 | 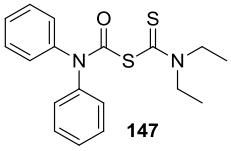 <br>147 | $E^{p}_{ox}$ = +1.42 V<br>(vs SCE† in MeCN) |
| 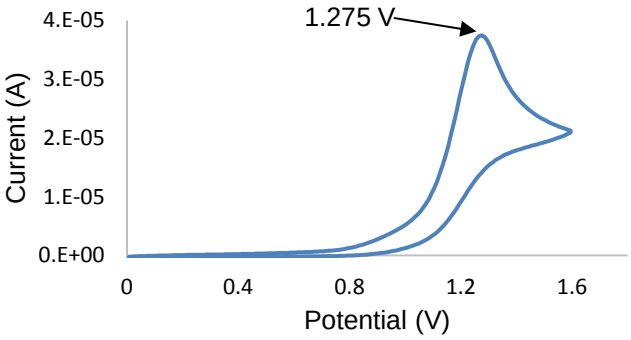 | 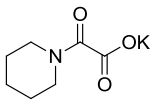 <br>150 | $E^{p}_{ox}$ = +1.24 V<br>(vs SCE† in DMF) |
| 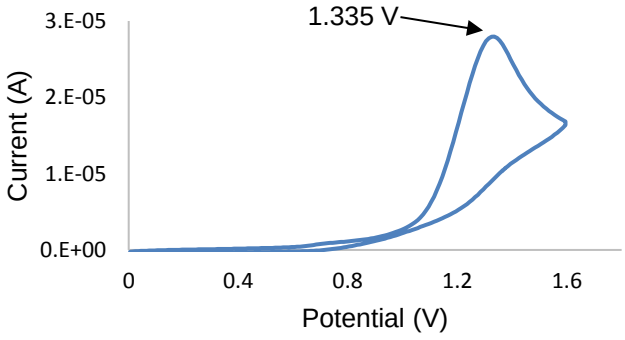 | 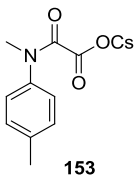 <br>153 | $E^{p}_{ox}$ = +1.30 V<br>(vs SCE† in DMF) |

**Table 1** - Cyclic voltammograms of selected radical precursor species, showing their structures and oxidation potentials. †The oxidation potentials were measured against the Ag/AgCl (3 M NaCl) reference electrode, then converted to values vs SCE, by subtracting 0.032 V.[149]

Whilst these results are not accurately comparable to those of similar compounds in the literature,[60] due to use of different electrodes and solvents, the observed oxidation potentials are accessible to a range of photoredox catalysts. Oxidation potentials well above these values may be reached by pyrylium salts, whose excited state oxidation potentials have been calculated to be up to +2.35 V (vs SCE[1]).[150] Alternatively, a multitude of organic and metal-based photocatalysts have been developed with excited state oxidation potentials closer to the radical precursors' oxidation potentials, which are more likely to be suitable for this reaction, with a view to ensuring smooth catalytic turnover, and functional group compatibility.[57,43]

Of the species examined, the oxamates appeared more suitable as a reactive starting material. This is owing to their slightly lower oxidation potentials, but more significantly, their comparative ease of synthesis. Whilst the dithiocarbamate species require the generation of a carbamoyl chloride intermediate, most commonly invoking highly toxic (di/tri)phosgene as a reagent, the oxamates can be synthesised using methyl chlorooxoacetate (**148**), which is less hazardous. Furthermore, from an atom economy perspective, oxamate precursors are the more desirable choice. Based on this choice, a trial reaction was carried out, directly utilising reaction conditions from a similar transformation, which employs a cesium oxamate (**154**) as a radical precursor (**Scheme 25**).[146] Pleasingly, this reaction gave a reasonable 62% isolated yield of the desired amide (**157**) upon first attempt.

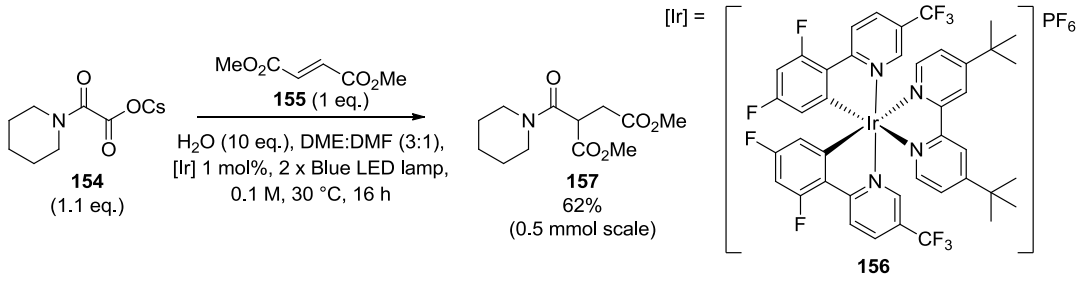


**Scheme 25** - Trial amidation reaction of cesium oxamate **154**, using literature conditions.[146]

[1] Oxidation potential converted from NHE to SCE, for ease of comparison, by subtracting 0.241 V.[149]

### 2.2.2. Reaction optimisation

*2.2.2.1. Equipment considerations*

Photochemical processes introduce an additional level of complexity, when compared with standard chemical reactions, due to the requirement for effective introduction and dispersion of light, for optimal reactivity. Despite the recent advancements in the field of photoredox chemistry, there has been a distinct lack of standardisation in the equipment used. Invoking the correct light source and reaction setup is vital to successful reaction in many cases, particularly where the rate of reaction appears to be "photon-limited", rather than limited by a fundamental reaction step.[151] From a process chemistry perspective, understanding and optimising the light source and reaction setup is of paramount importance for developing a robust transformation.

A major consideration to be made involves ensuring suitable overlap between the light source's spectral output, and the absorption spectrum of the photocatalyst. The iridium catalyst (**156**) was found to have an absorption maximum ($\lambda_{max}$) at 380 nm, which is in fact classified as UVA radiation.[147] It can be observed though, that the spectral output of the blue LED lamp used in this case (Kessil A160WE Tuna Blue) overlaps well (**Figure 4**). The small shoulder of UVA output at 385 nm could in fact be responsible for a significant portion of reaction observed, and should be carefully considered in future light source choices. Unfortunately, at the time of writing, there were no alternative powerful light sources available to us, of similar spectral output.

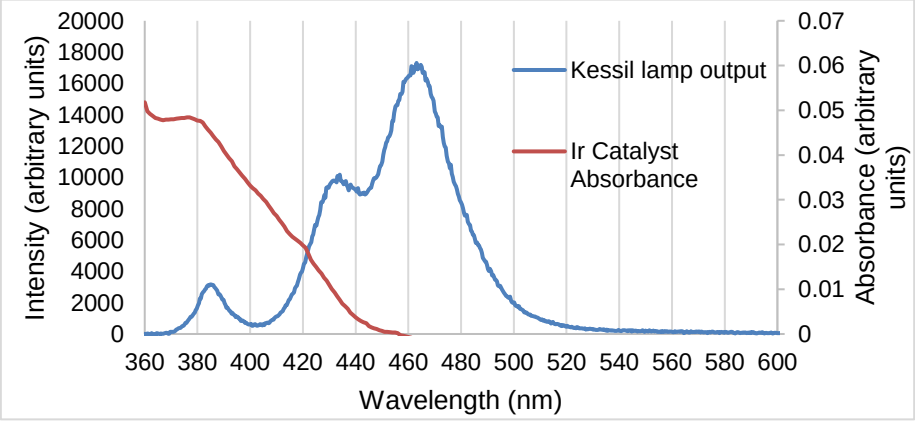


**Figure 4** - Graph showing the overlay of blue LED lamp output (blue), with iridium catalyst **156** absorbance (red).

In addition to the nature of the light source, varying the reaction scale is known to affect the performance of photochemical reactions, due to restricted light penetration throughout the reaction mixture. The severity of this restriction is surprising, and essentially rules out scaling up these transformations in batch mode. As can be calculated by the Beer-Lambert law,[152] and depending upon the given catalyst's solution concentration and molar extinction coefficient, in many cases light is estimated to penetrate less than 2 mm into a reaction vessel.[153,154,155] Accordingly, it must be considered, that smaller scale screening reactions will likely progress far faster than preparative scale reactions.

In order to standardise light exposure and reaction temperature, and for safety reasons, a 3D printed housing for the Kessil LED lamps was employed. This allowed reactions to be reproducibly carried out using either a single or dual lamp set up (**Figure 5**), with a choice of several discrete reaction vessels. The reactor housing contains a series of mirrors, enabling maximum light reflection towards the reaction vials. Furthermore, a fan blowing through the enclosure has been demonstrated to effectively remove heat generated by the lamp, maintaining a steady reaction temperature of around 30 °C. Further heating is not possible when using this equipment, as the reaction vials are not in contact with the hotplate, however, it is envisaged that suitable conditions could be found to perform the reactions at close to room temperature.

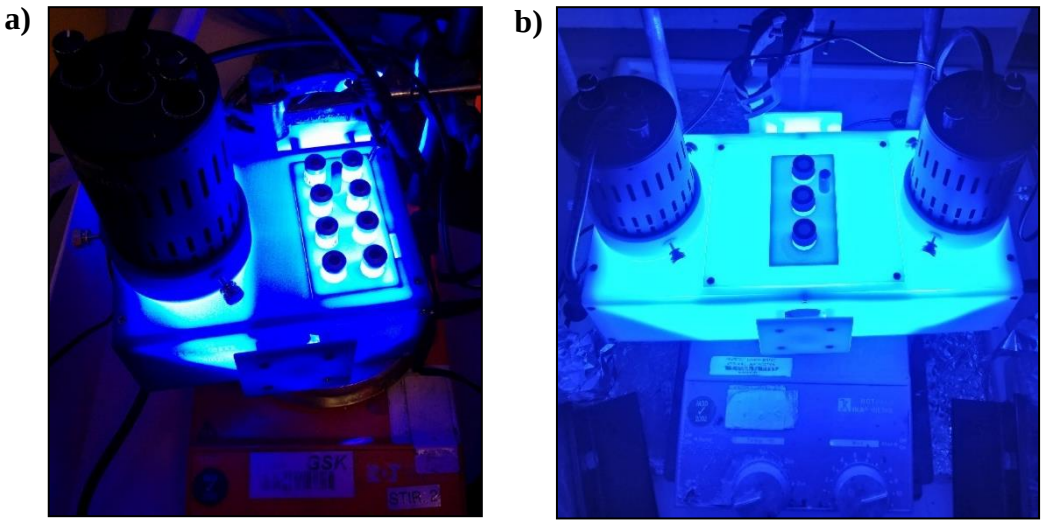


**Figure 5** - Reaction setup, showing reaction vials irradiated by Kessil lamps in a 3D-printed mirror box, mounted on a stirrer-hotplate. **a)** A single lamp irradiating 8 × 2 mL vials for screening reaction conditions. **b)** Two lamps irradiating 3 × 4 mL vials for preparative reactions.

*2.2.2.2. Oxamate salt selection*

Thus far, the oxamate starting material has been introduced to the reaction as the cesium salt (**154**), rather than the neutral species, due to the ease of synthesis and handling of the metal salt. This salt is crystalline, stable, and easily weighable, allowing a straightforward protocol. However, cesium is an undesirable counterion, due to its high mass and price, so identification of an alternative may be beneficial, provided there is no loss of reactivity. Consequently, a range of oxamate salts (**158**) were synthesised, by simply treating the oxamate methyl ester starting material (**149**) with different metal hydroxides (**Scheme 26**, reaction yields are displayed in **Table 2**). These progressed in near-quantitative yields, which is required to ensure the product's purity, since separating it from excess metal hydroxide would not be trivial.

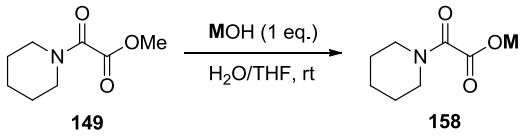


**149** **158**

**Scheme 26** - Synthesis of various oxamate salts (**158**) from a common oxamate methyl ester (**149**). Reaction yields for each salt are displayed below (**Table 2**).

Following their synthesis, each of these oxamate salts was subjected to the standard reaction conditions (**Table 2**). Surprisingly, it appeared that the more soluble salts actually saw poorer conversion. Of these salts, the tetrabutylammonium salt (**163**, entry 7) was the only substrate to provide an entirely homogeneous reaction mixture, yet gave far poorer conversion than any of the metal salts examined. Similarly, group 2 metal salts (**161** and **162**, entries 5 and 6) were expected to be more soluble in the organic solvent system, yet showed poorer conversion than the group 1 metal salts. Between the group 1 salts (**159**, **160**, **150**, and **154**, entries 1-4), there was little variance in product yield, with potassium, cesium, and sodium salts giving essentially the same performance. From a process chemistry perspective, sodium is the most favourable of these three, owing to its substantially lower cost[156] and mass.

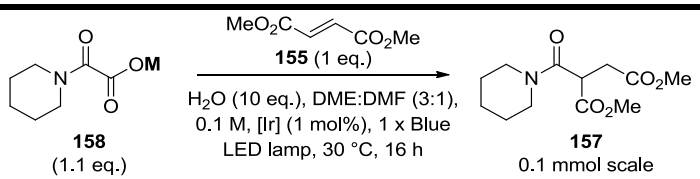


| Entry | Counterion (number, preparative yield) | Amide (157) yield (%)[a] | Olefin (155) remaining (%)[a] |
|---|---|---|---|
| **1** | Li (**159**, 94%) | **78** | 0 |
| 2 | Na (**160**, 99%) | **88** | 0 |
| 3 | K (**150**, 98%) | **87** | 0 |
| 4 | Cs (**154**, 94%) | **86** | 0 |
| 5 | 0.5 Ca (**161**, 94%) | **61** | 1 |
| 6 | 0.5 Ba (**162**, 96%) | **45** | 11 |
| 7 | $NBu_4$ (**163**, 99%) | **52** | 44 |

**Table 2** - Starting material salt preparative yields, and their performances in the amidation reaction. [a]Reaction yields determined by HPLC analysis, versus biphenyl as an internal standard.

The observation that less soluble oxamate salts appear to react less effectively is unwelcome, as it implies that operating this procedure under continuous flow conditions will not be trivial. Moreover, there is no straightforward explanation for the reaction to be slower under homogeneous conditions, aside from the implication that oxamate salt oxidation is, in fact, occurring at the solid-liquid interface. Additional understanding would require far more in-depth analysis of the solid form of these reagents, and the effect of particle size upon reaction rate. This is outside the scope of these studies, but would need to be considered if development of a larger scale process were to be attempted.

*2.2.2.3. Catalyst selection*

Following the decision to proceed with sodium oxamate salts, a range of theoretically suitable catalysts were screened, in order to determine which would be most suitable. Bearing in mind the oxidation potential of the oxamate radical precursor species, only catalysts with a calculated excited state oxidation potential of >+1.2 V (vs SCE) were considered (**Figure 6**). To detach any water sensitivity of these catalysts from the observed results, the reactions were run under anhydrous conditions. The results of this screen are summarised below (**Table 3**).

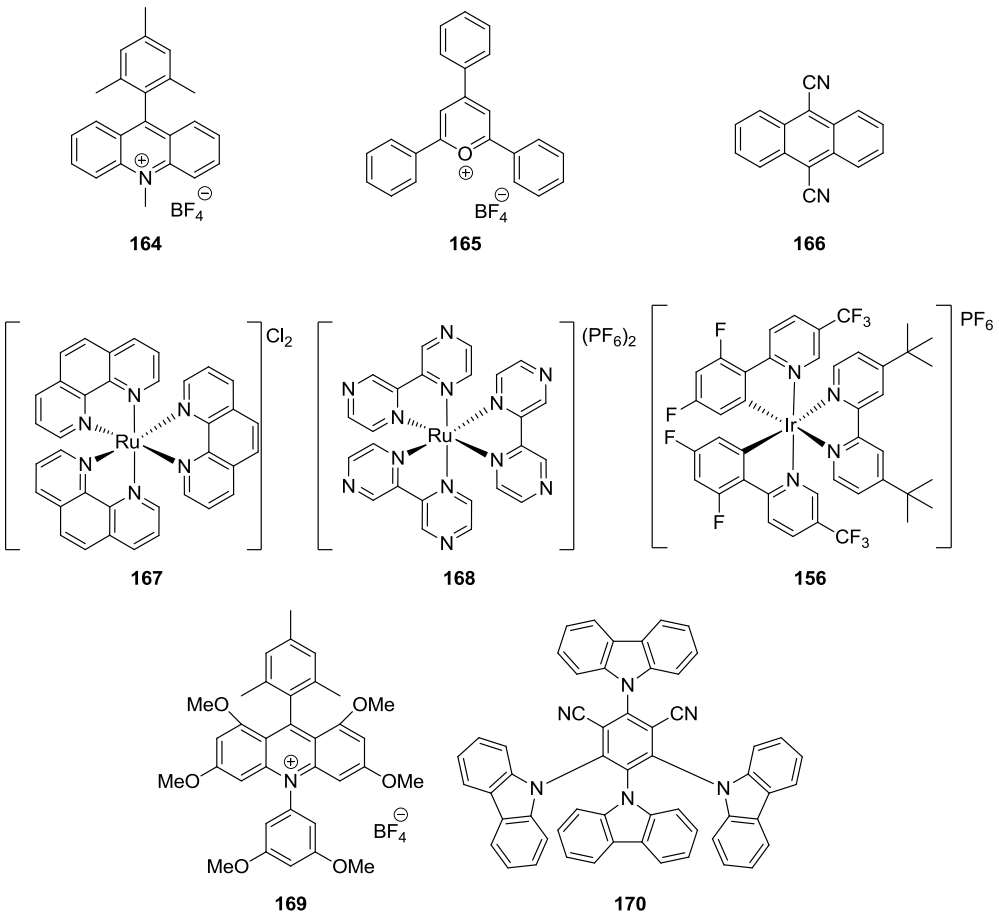


**Figure 6** - Structures of photocatalysts screened.

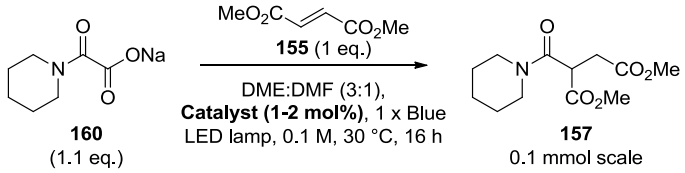


| Entry | Catalyst | Oxidation potential (V)[a] | Reduction potential (V)[a] | Amide (157) yield (%)[b] | Olefin (155) remaining (%)[b] |
|---|---|---|---|---|---|
| **1**[c] | Mesityl acridinium (**164**)[157] | +1.88 | −0.49 | **0** | 92 |
| **2**[c] | Triphenylpyrylium (**165**)[158] | +2.55 | −0.32 | **0** | 91 |
| **3**[d] | 9,10-Dicyanoathracene (**166**)[57] | +1.99 | −0.91 | **25** | 63 |
| **4**[d] | $Ru(phen)_3Cl_2$ (**167**)[58] | +0.82 | −1.36 | **3** | 96 |
| **5**[d] | $Ru(bpz)_3(PF_6)_2$ (**168**)[159] | +1.45 | −0.80 | **0** | 95 |
| **6**[d] | $Ir[dF(CF_3)ppy]_2(dtbbpy)PF_6$ (**156**)[146] | +1.21 | −1.37 | **37** | 46 |
| **7**[c] | Hexamethoxy mesitylacridinium (**169**)[61] | +1.65 | −0.82 | **31** | 53 |
| **8**[c] | 4CzIPN (**170**)[160] | +1.35 | −1.21 | **22** | 58 |

**Table 3** - Results of photocatalyst screen. [a]Redox potentials correspond to the relevant values (vs SCE) for this catalytic cycle (calculated oxidation potential of the excited state photocatalyst, and reduction potential required to regenerate the ground state species). [b]Yield determined by HPLC analysis, using biphenyl as an internal standard. [c]2 mol% catalyst loading was used for organocatalysts. [d]1 mol% catalyst loading was used for metal catalysts.

Due to the relatively high oxidation potential required to initiate reaction with the oxamate species, it was expected that catalysts with higher excited state oxidation potentials (e.g. mesityl acridinium **164**, entry 1, or pyrylium salt **165**, entry 2) would be more effective in this reaction. However, when considering the entire catalytic cycle, successful product formation also relies upon reduction of the radical product formed, following addition to the olefin, which requires finely balanced oxidation and reduction potentials. Furthermore, highly oxidising catalysts are more likely to be consumed through reaction with other oxidisable species present in the reaction, such as solvent (DMF has an oxidation potential of +2.26 V vs SCE),[60] or the olefin (**155**).

9,10-Dicyanoanthracene (**166**, entry 3) displayed some reactivity, which could be attributed to its higher reduction potential, allowing for successful catalytic turnover. Surprisingly, the seemingly well redox-balanced ruthenium (II) tris(bipyrazyl) catalyst (**168**, entry 5) gave no reaction, whilst the less strongly oxidising ruthenium (II) tris(phenanthroline) species (**167**, entry 4) yielded a very small quantity of the desired product. The previously used iridium species (**156**, entry 6) afforded a reasonable quantity of the amide product in a clean reaction, where the majority of mass balance (83%) was preserved between the starting material, and desired product. The bespoke acridinium salt (**169**, entry 7) gave a similar performance, which is unsurprising, bearing in mind its purpose as an organic replacement for the iridium catalyst (**156**).[61] Disappointingly, considering its successful implementation in reactions requiring similar oxidation potentials,[160,161,162,163,164] 4CzIPN (**170**, entry 8) afforded a lower yield of the desired amide (**157**).

Since the absence of water resulted in a poorer yield when using iridium catalyst (**156**) (37% yield in **Table 3** entry 6, versus 62% yield in **Scheme 25**), the most promising catalysts were examined once more, with the addition of 10 equivalents of water (**Table 4**). Unfortunately, no improvement was observed in the case of 9,10-dicyanoanthracene (**166**, entry 1), yet excellent assay yield was attained using the iridium and acridinium catalysts (**156**, entry 2 and **169**, entry 3). Increasing the acridinium catalyst loading was detrimental to reaction yield (entry 4), likely due to decreased light penetration. Finally, 4CzIPN (**170**, entry 5) unfortunately showed no improvement with the addition of water. The iridium catalyst (**156**) gave the best performance, so was studied further. Additionally, though, replacement of precious metals in organic synthesis is an important consideration,[57] so the acridinium photocatalyst (**169**) was also examined further (see section 2.2.3.4. Introduction of a metal-free photocatalyst).

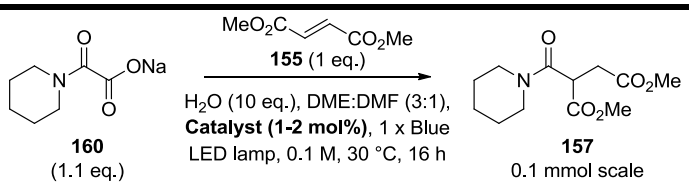


| Entry | Catalyst | Catalyst loading (mol %) | Amide (157) yield (%)[a] | Olefin (155) remaining (%)[a] |
|---|---|---|---|---|
| **1** | 9,10-dicyanoathracene (**166**) | 2 | **25** | 31 |
| **2** | $Ir[dF(CF_3)ppy]_2(dtbpy)PF_6$ (**156**) | 1 | **89** | 3 |
| **3** | Hexamethoxy mesitylacridinium (**169**) | 2 | **78** | 6 |
| **4** | Hexamethoxy mesitylacridinium (**169**) | 10 | **66** | 15 |
| **5** | 4CzIPN (**170**) | 2 | **23** | 44 |

**Table 4** - Further screening of successful catalysts, with the addition of water. [a]Yield determined by HPLC analysis, using biphenyl as an internal standard.

*2.2.2.4. Effect of water*

Having already observed that reaction performance is considerably poorer in the absence of water (**Table 3**, entry 6 versus **Table 4**, entry 2), a more detailed exploration of the effect of water was undertaken (**Table 5**). It had previously been expected that an increased aqueous fraction would enhance reaction performance, through improved solubility of the oxamate salt starting material. However, the resulting data proved to the contrary. After the initial increase in yield (entries 1 to 3), the addition of further water was detrimental to reaction performance (entries 4 to 7). Surprisingly, within an intermediate range, (entries 3 to 6), the decrease in product yield is linear, with excellent fit ($R^2 = 0.9998$).

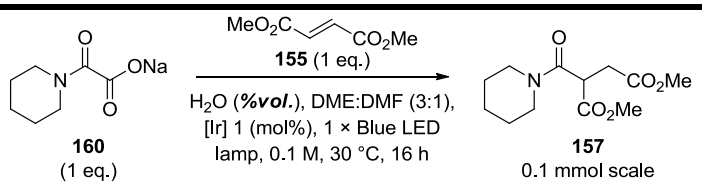


| Entry | Quantity of water (%volume of total solvent) | Amide (157) yield (%)[a] | Olefin (155) remaining (%)[a] |
|---|---|---|---|
| **1** | 0 | **37** | 46 |
| **2** | 0.9 | **73** | 18 |
| **3** | 1.8[b] | **82** | 7 |
| **4** | 10 | **71** | 0 |
| **5** | 20 | **56** | 10 |
| **6** | 50 | **8** | 4 |
| **7** | 75 | **0** | 16 |

**Table 5** - The effect of water on reaction performance. [a]Yield determined by HPLC analysis, using biphenyl as an internal standard. [b]1.8% is equal to 10 equivalents, as used in the optimal reaction conditions thus far.

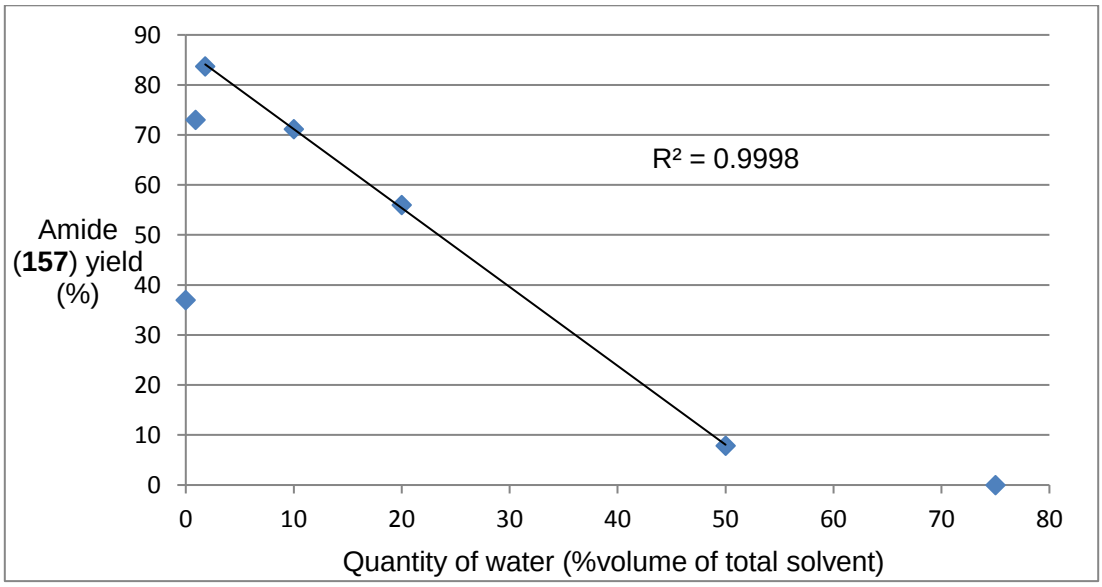


**Figure 7** - A graph to show the linear decrease in yield of amide (**157**), with increasing aqueous fraction. The data displayed is taken from **Table 5**, and the linear trendline is plotted using only entries 3 to 6.

These results could be explained by the requirement for a minimal quantity of water, to prevent agglomeration of oxamate (**160**) particles. Due to the heterogeneous nature of these reaction mixtures, surface area must be taken into account, and it is strongly implied that surface effects are at play, due to the poor performance of more soluble oxamate salts (see section 2.2.2.2.

Oxamate salt selection, **Table 2**). As the aqueous fraction is increased, the starting material becomes more soluble, which leads to poorer reaction performance, corroborating the idea that the reaction takes place at the oxamate surface.

*2.2.2.5. Solvent selection*

Following successful reactions using a solvent mixture of DME and DMF, an alternative solvent system was sought, due to the associated toxicity of both solvents,[165] and their restrictions within a manufacturing environment. Accordingly, a range of solvents was screened, covering different areas of chemical space, determined using a principal component analysis (PCA) solvent model (**Table 6**).[166,167] Perhaps unsurprisingly, the region of polar aprotic solvents (entries 2-7) performed the most favourably, compared to less polar solvents. Significantly, both DME (entry 2) and DMF (entry 3) exhibited poorer reactivity than the mixture of the two solvents (entry 1). Surprisingly, THF (entry 11) gave a moderate yield, despite containing the radical inhibitor, BHT (250 ppm). No improvement in yield was observed, when using inhibitor-free THF (entry 12), implying that BHT does not act as an effective radical quencher for this reaction, at least not in such low concentrations.

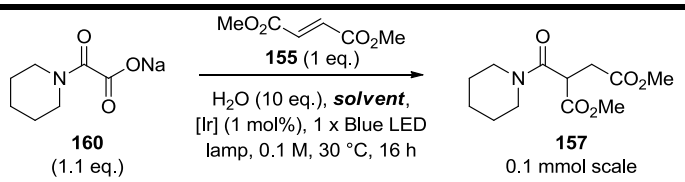


| Entry | **Solvent** | **Amide (157) yield (%)[a]** | **Olefin (155) remaining (%)[a]** |
|---|---|---|---|
| 1 | DME:DMF (3:1) | **89** | 3 |
| 2 | DME | **58** | 13 |
| 3 | DMF | **87** | 3 |
| 4 | DMSO | **32** | 33 |
| 5 | DMA | **68** | 16 |
| 6 | NMP | **66** | 22 |
| 7 | acetonitrile | **44** | 6 |
| 8 | heptane | **0** | 51 |
| 9 | TBME | **12** | 24 |
| 10 | toluene | **4** | 20 |
| 11 | THF[b] | **58** | 0 |
| 12 | THF | **54** | 3 |
| 13 | ethyl acetate | **41** | 12 |
| 14 | DCM | **22** | 18 |
| 15 | 2-methyl THF | **14** | 0 |
| 16 | TamiSolve®[c] | **74** | 0 |
| 17 | *N*-methyl formamide | **14** | 3 |
| 18 | propylene carbonate | **29** | 2 |
| 19 | acetone | **80** | 2 |
| 20 | methyl isobutyl ketone | **59** | 3 |
| 21 | methyl ethyl ketone | **73** | 5 |

**Table 6** - Results of reaction solvent screen. [a]Yield determined by HPLC analysis, using biphenyl as an internal standard. [b]Solvent contained BHT (250 ppm) as a radical inhibitor. [c]1-Butylpyrrolidin-2-one.

TamiSolve® (1-butylpyrrolidin-2-one, entry 16) was considered as a non-toxic alternative to other dipolar aprotic solvents.[168] Fairly good performance was observed, achieving a 74% assay yield. However, upon attempting to isolate the desired product from this reaction, it was found that removal of the solvent was challenging: a problem intensified by its high boiling

point (241 °C), and the relative similarity of its structure, to that of the desired product. Propylene carbonate (entry 18), another green alternative to dipolar aprotic solvents,[169] was unfortunately found to be relatively ineffective in this reaction. The only acceptable yield achieved with a less harmful solvent was with acetone (entry 19), so this will be explored in more detail, in parallel to the DME/DMF system (see section 2.2.3.3. Introduction of a non-toxic solvent).

An additional by-product was observed when acetone was used as solvent (entry 19), thought to be caused by radical or anionic attack of a reaction intermediate upon acetone. In attempt to disfavour this, an additional two ketone solvents, with increased steric bulk around the carbonyl, were examined (entry 20 and entry 21). Unfortunately, these both showed poorer reactivity, likely due to their decreased polarity, when compared with acetone.

*2.2.2.6. Reaction parameter optimisation*

Following on from the understanding obtained around water content, and selection of the optimal catalyst, oxamate salt, and solvent, it was necessary to ensure that the correct reaction concentration, stoichiometry, and catalyst loading was used. A small survey of reaction conditions was carried out to verify this (**Table 7**). It was found that a slight increase in oxamate (**160**) loading was beneficial (entry 2), which corroborates with the reaction mechanism, in which this species is the photocatalyst excited state quencher. Further improvement may be achieved by employing a greater excess of this reagent, but close to one-to-one stoichiometry is desirable for reasons of mass efficiency, and so 1.1 equivalents will be used in future reactions. A higher catalyst loading was found to be detrimental (entry 3), whilst a lower catalyst loading (entry 4) offered slight improvement. To allow for accurate catalyst weighing, 1 mol% was determined to be the most appropriate loading, however this could be lowered in larger scale applications. Both higher and lower reaction concentrations were found to be detrimental to reactivity (entries 5 and 6), due to the fine balance between light penetration and reaction kinetics.

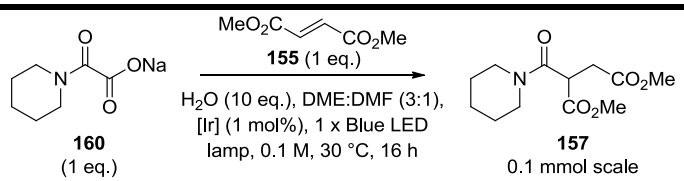


| Entry | Deviation from standard conditions | Amide (157) yield (%)[a] | Olefin (155) remaining (%)[a] |
|---|---|---|---|
| 1 | None | **82** | 7 |
| 2 | 1.1 eq. oxamate (**160**) | **89** | 3 |
| 3 | 2 mol% catalyst | **78** | 12 |
| 4 | 0.5 mol% catalyst | **85** | 7 |
| 5 | 0.2 M concentration | **53** | 36 |
| 6 | 0.05 M concentration | **77** | 0 |

**Table 7** - Results of parameter optimisation, and control experiments. [a]Yield determined by HPLC analysis, using biphenyl as an internal standard.

Control reactions were also performed, to corroborate the proposed reaction mechanism (see section 4.2.8. Control reactions for details). The reaction was, indeed, found to require a photocatalyst, and a light source, so must involve interaction of a starting material with the excited state photocatalyst. Furthermore, the reaction is entirely shut down by the inclusion of 2 equivalents of a radical inhibitor (TEMPO), implying that the reaction does proceed through a radical mechanism, as previously proposed (see section 2.1.5. Mechanistic proposal and chapter aims).

*2.2.2.7. Computational studies*

To improve the level of understanding around this reaction, density functional theory (DFT) calculations were performed in support of experiments within the laboratory. Use of this technique to reinforce and explain practical observations has become widespread in recent years, likely owing to improved understanding of the available methods, but also the increased availability of processors powerful enough to undertake such calculations.[170] Specifically, efforts have increasingly been made to support the growing number of synthetic photoredox methods currently being developed.[171,172]

Firstly, each structure in the proposed reaction pathway has been optimised, to form a potential energy surface (PES) (**Figure 8**). This contains all of the appropriate intermediate structures, and the available transition states, in order to establish that this pathway is theoretically possible, and there are no unreachable transition energies. Notably, the initial increase in energy between the ground state reagents (**171**), and the oxidised oxamate species (**172**) is easily attainable by the absorption of a photon of blue light, by the iridium photocatalyst (**156**).

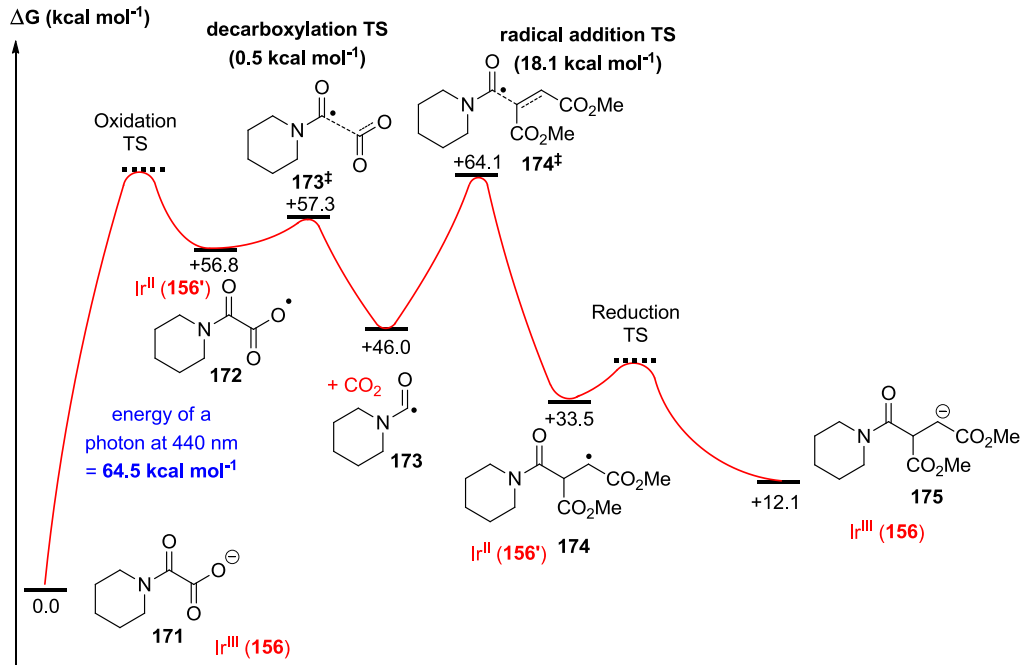


**Figure 8** - Potential energy surface of the studied reaction, with the appropriate relative energies appended.

From the oxamate radical species (**172**), decarboxylation has a negligible energy barrier (**173‡**), to form the far more thermodynamically favourable system, benefitting from a more stable carbamoyl radical (**173**), and the formation of an additional carbon-oxygen bond. This nucleophilic radical then attacks into the olefin, yielding the stabilised radical species (**174**). This transition state energy (**174‡**) of 18.1 kcal mol$^{-1}$ is higher than might be expected for a radical reaction, yet is well below 20 kcal mol$^{-1}$, which is widely approximated to be an instantaneous process at room temperature. Comparison of this transition state energy will be referred to for different substrates, in order to support the experimentally observed results. The radical addition product (**174**) is then reduced by the reduced state photocatalyst (**156'**), yielding the desired reaction product, upon protonation of the stabilised anion (**175**).

The relatively high transition state energy (**174**‡) is likely due to the poor nucleophilicity of the carbamoyl radical (**173**). The carbonyl group bestows stability when compared to a similar alkyl radical, and the nitrogen imparts further stability, by increasing delocalisation throughout the π system. The difference in reactivity between the carbamoyl radical (**173**) and its equivalent acyl radical (**178**) has been calculated computationally (**Figure 9**). The transition state energy difference of 3 kcal $mol^{-1}$ (**177**‡ vs **179**‡) will experimentally equate to a substantial rate difference in the two reaction processes, particularly as the reactive radical species is only present in low concentrations in the reaction mixture.

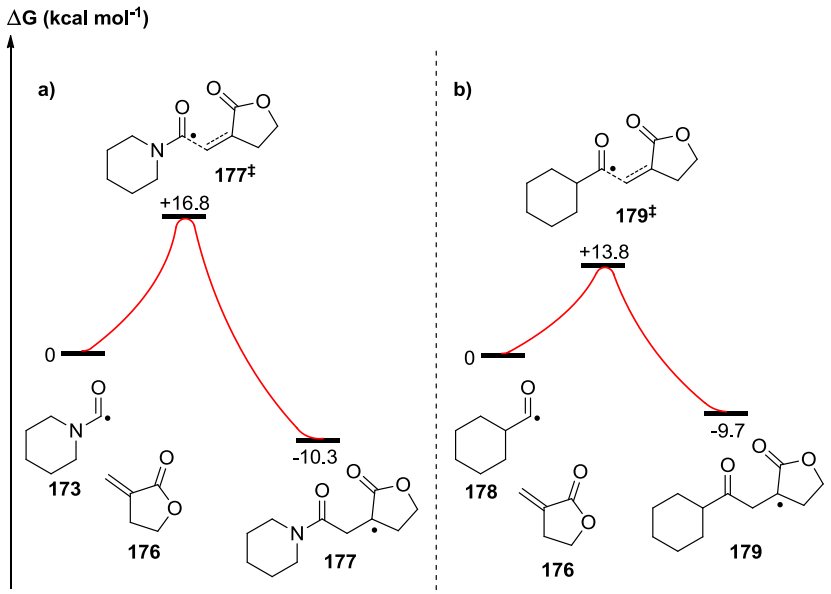


**Figure 9** - Computational comparison of transition state energies for addition to an electron-poor olefin, with **a)** carbamoyl radical (**173**) and **b)** acyl radical (**178**).

### 2.2.3. Application of reaction protocol

*2.2.3.1. Oxamate starting material synthesis*

To allow exploration of this reaction protocol's substrate tolerance within the amine-derived reaction partner, a range of sodium oxamate starting materials were prepared in two separate synthetic steps (**Scheme 27**). First, reaction of the secondary amine with methyl 2-chloro-2-oxoacetate (**148**) was performed under Schotten-Baumann conditions, affording pure products after a straightforward aqueous workup. The remaining mass balance of these reactions is assumed to be constituted of the water soluble oxamate, formed by *in situ* hydrolysis, and extracted during the aqueous washes. The isolated oxamate methyl esters were then dissolved in THF and treated with 1 M NaOH (1 eq.), to undergo hydrolysis, yielding a pure sample of the desired sodium salt after removal of solvent, or recrystallisation.

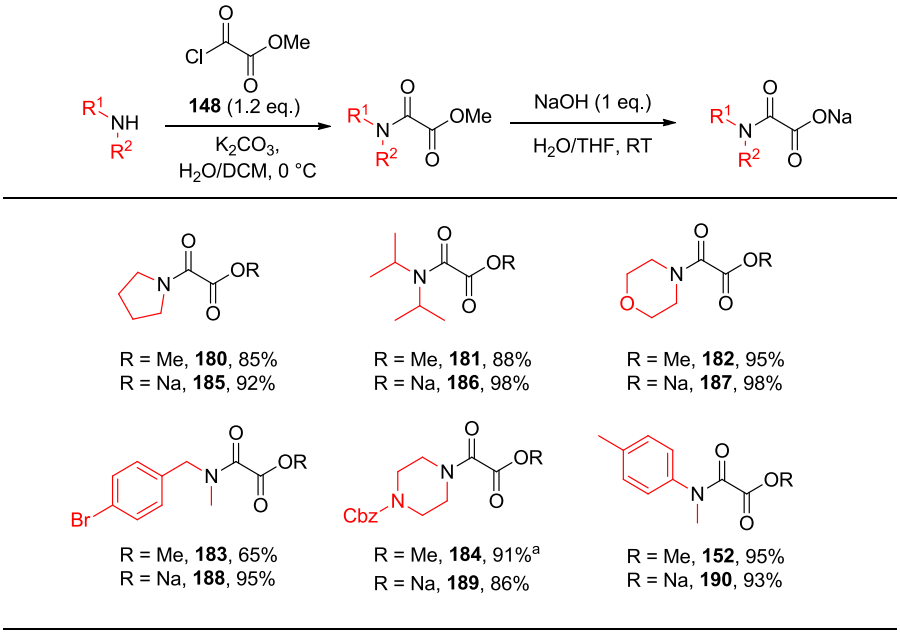


**Scheme 27** - Synthesis of oxamate salt starting materials, in two steps from the corresponding amine precursors. Isolated yields of both oxamate methyl esters, and oxamate sodium salts are shown. [a]Rather than the conditions shown, this reaction was carried out using $KHCO_3$ as a base, in a $H_2O$/PhH solvent system.

*2.2.3.2. Amidation substrate scope*

Using the developed conditions, the substrate scope was examined with respect to oxamate coupling partner (**Scheme 28a**). An excellent yield was achieved in the coupling of piperidinyl oxamate (**160**) with a 1,1-disubstituted olefin, 2-methylenebutyrolactone (product **191**). A

good yield was maintained when the protocol was applied to a significantly sterically hindered oxamate (product **192**). Importantly, the oxamate substrate tolerated the presence of both a benzylic position and an aryl bromide (product **193**), allowing for onward functionalisation by metal-catalysed cross-coupling reactions. A morpholine oxamate was well tolerated (product **194**), and a Cbz-protected piperidine also delivered a reasonable yield of its corresponding product (**195**).

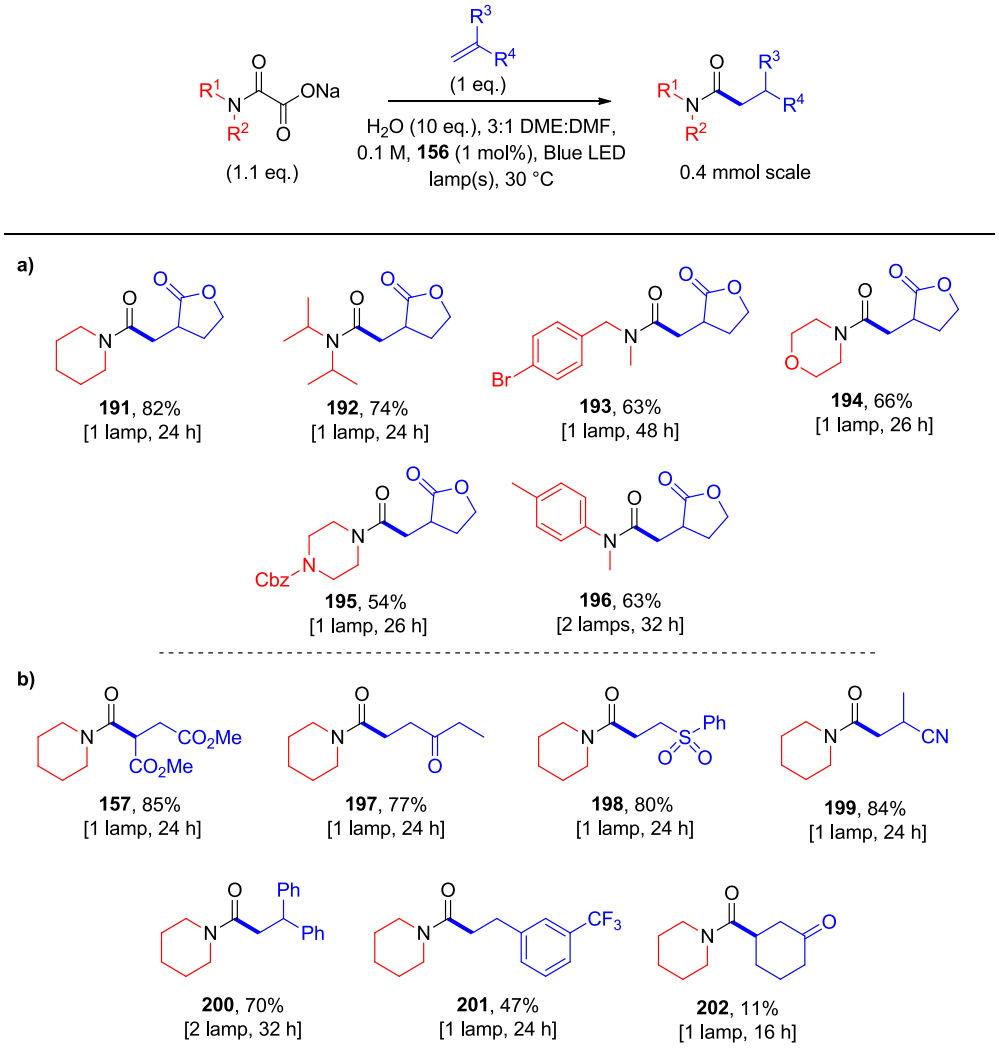


**Scheme 28** - Substrate scope of the developed reaction conditions, using iridium catalyst (**156**), in a DME/DMF solvent system. Yields shown are those of isolated compounds.

Moreover, the yield was maintained even when an aniline-derived oxamate was employed (product **196**). An increased light intensity was required, alongside an extended reaction period,

yet this is still a significant result, due to the higher oxidation potential of the aromatic oxamate (+1.30 V compared with +1.24 V, see section 2.2.1. Analysis of radical precursor species, **Table 1**). This reactivity is complementary to the cyclised products formed in the published *N*-hydroxyphthalimido oxamide protocol, discussed previously (see section 2.1.4.2. Amide bond-formation).[143,144] When considered computationally (**Figure 10**), the energy barrier to initiate homolytic aromatic substitution (**204**‡) is low, yet the intermediate radical species (**204**) is thermodynamically disfavoured. Accordingly, this catalytic system favours reduction of the more populated acyclic intermediate (**203**) instead of formation and oxidation of the HAS intermediate (**204**), forming the observed product (**196**) over the cyclic species (**205**).

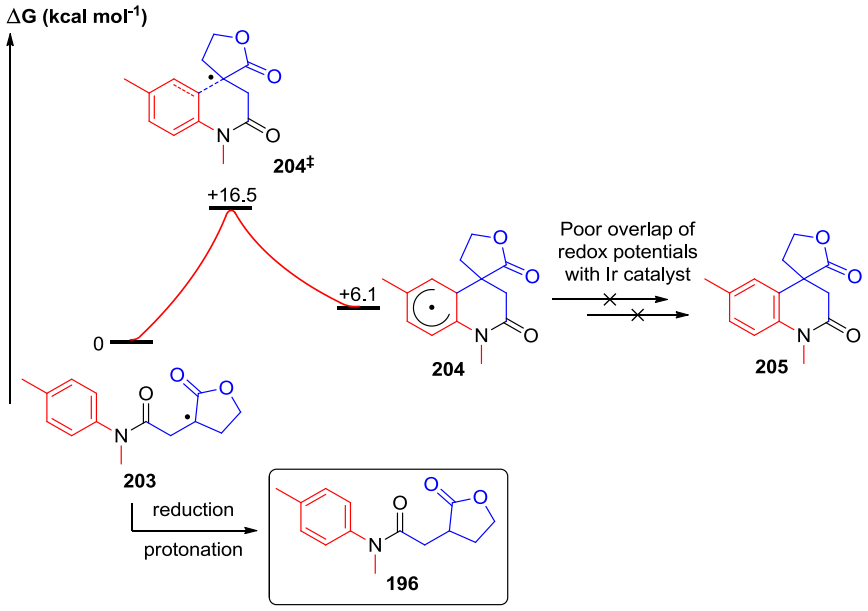


**Figure 10** - Computational consideration of homolytic aromatic substitution of radical intermediate (**203**), and formation of a cyclic (**205**) versus an acyclic (**196**) product.

The substrate tolerance was then examined with respect to olefin coupling partners (**Scheme 28b**), following a promising improvement upon the performance of the initially examined coupling partners (**157**, 85% yield, compared with 62%; see section 2.2.1. Analysis of radical precursor species, **Scheme 25**). The reaction protocol was amenable to various other Michael acceptors, exemplified by the excellent yields achieved in reactions to deliver ketone (**197**), sulfone (**198**), and nitrile (**199**) functionalised products. Furthermore, productive reaction was achieved with a common styrene radical trap (product **200**), prompting further examination of

styrene substrates. Some success was observed with an electron-deficient styrene (product **201**), but a relatively poor yield was obtained in this case, as a result of many low-level by-products being formed.

Aside from in the reaction of dimethyl fumarate (product **157**), substitution at both ends of the olefin coupling partner was not well tolerated, as exemplified by the sluggish reaction with cyclohexenone (product **202**). Additional steric hindrance results in a higher energy barrier to attack by the radical species, even in a relatively unhindered cyclic olefin such as this one. DFT calculations were performed (**Figure 11**), comparing the transition state energies of the attack of carbamoyl radical (**173**) upon a 1,1-disubstituted olefin (**176**), versus a 1,2-disubstituted olefin (**206**). As expected, attack on cyclohexenone (**206**) has an energy barrier (**177**‡ vs **207**‡) 3.4 kcal mol$^{-1}$ higher, which is significant, particularly considering the low concentration of carbamoyl radical (**173**) present at any point during the course of the reaction. It is expected that more reactive radical species may undergo this addition in a facile manner, or that a more efficient radical addition might be achieved at higher temperatures.

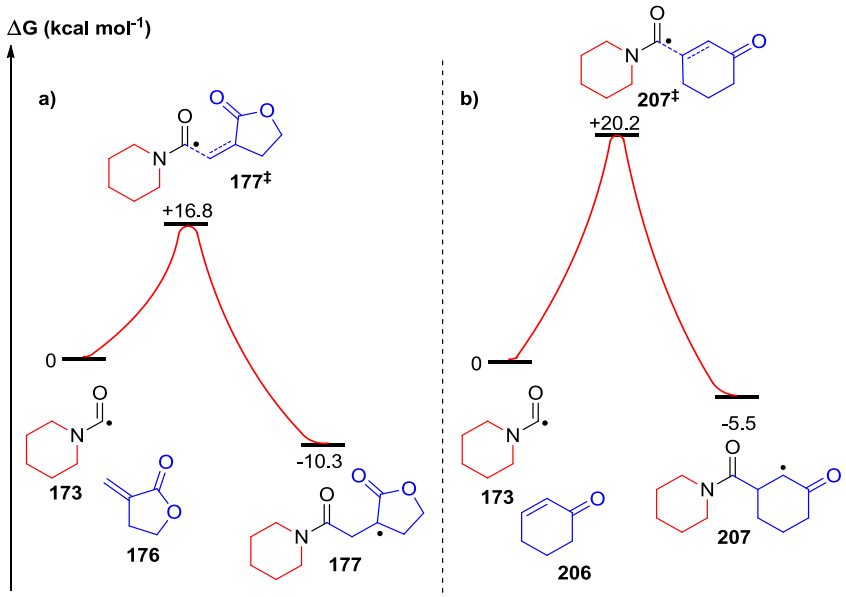


**Figure 11** - Computational comparison of transition state energies for addition to **a)** a 1,1-disubstituted olefin (**176**) and **b)** a 1,2-disubstituted olefin (**206**).

*2.2.3.3. Introduction of a non-toxic solvent*

As found previously (see 2.2.2.5. Solvent selection, **Table 6**), acetone represents the most effective of the examined solvents which could be considered to be more environmentally acceptable. To demonstrate that this substantially less toxic solvent system is still effective, the performance of a range of substrates was examined. In general, these reactions were far slower than their DME/DMF equivalent (see **Scheme 28**), and exhibited a greater extent of dual olefin addition, through either a radical or ionic pathway. The two pathways were compared through DFT calculations (**Figure 12**), the results of which strongly imply that the double addition pathway is ionic in nature. The radical reaction transition state (**208**‡) energy is significantly higher than that of the anionic transition state (**210**‡), and the reaction concentration of ionic intermediate (**209**) is predicated to be far higher than its shorter-lived radical equivalent (**177**).

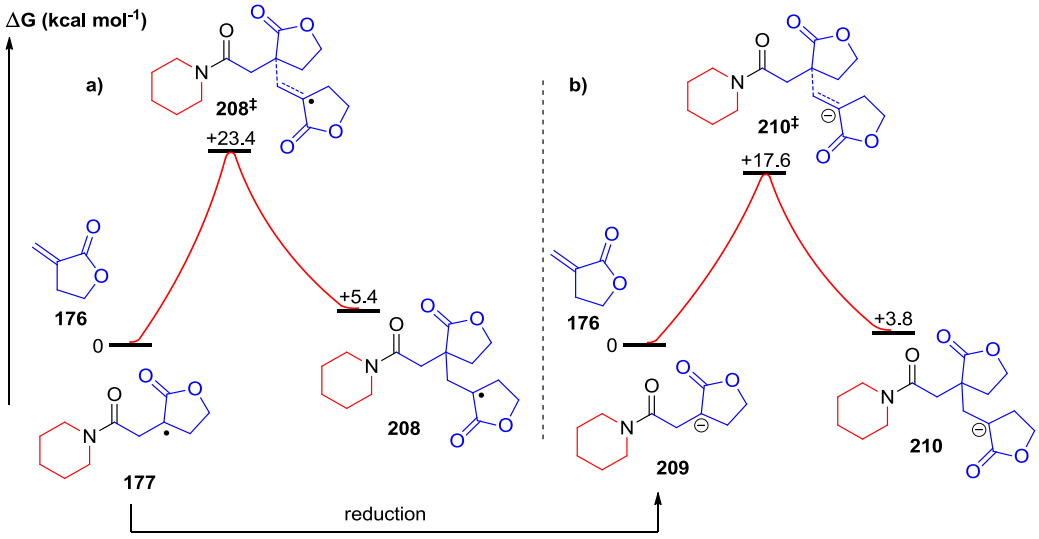


**Figure 12** - Computational comparison of **a)** radical versus **b)** anionic pathways for dual addition.

Upon examining the substrate scope in the alternative solvent system, the piperidinyl oxamate (product **191**), and diisopropyl oxamate (product **192**) displayed slightly diminished reaction yields. Pyrrolidinyl oxamate (product **211**) showed similar performance to these examples, and Cbz-protected piperazine oxamate (**195**) actually showed an improvement in yield from the previous conditions (**Scheme 28**). Unfortunately, under these alternative conditions, the aniline-derived oxamate reacted sluggishly, to afford a poor yield of its corresponding amide (**196**), even after a 48 hour reaction time.

The scope in olefin coupling partner was also examined, against the piperidinyl oxamate (**Scheme 29b**). Despite requiring a longer reaction time, an equivalent yield of nitrile containing amide (**199**) was achieved, when compared with the reaction using the original solvent system (see **Scheme 28**). A reaction by-product in this case was isolated (**199'**), in which an intermediate species reacted with the solvent, assumedly *via* the anionic intermediate species. Other olefin reaction partners generally displayed poorer reactivity using this solvent, such as the ketone coupling partner (product **197**), whose yield was lowered further due to the difficulty in separating its corresponding dual-addition by-product. Moderate yields were achieved in reactions with styrene and acrylamide partners (products **200** and **212**), with these also requiring the use of 2 lamps, due to far slower reaction.

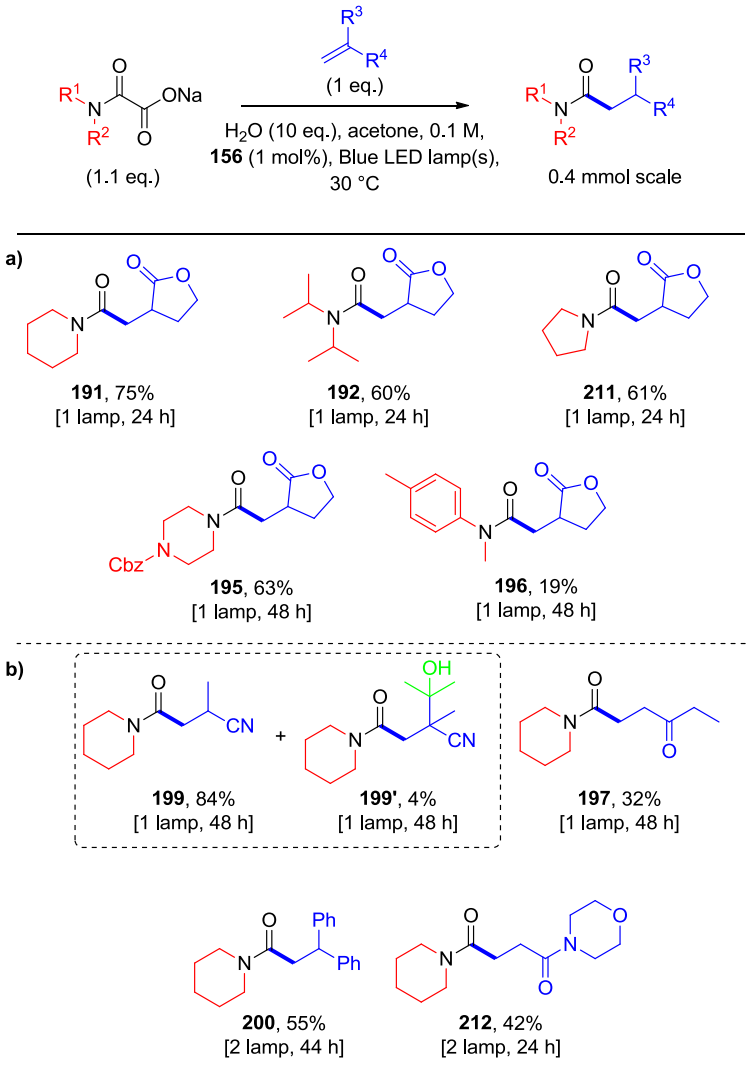


**Scheme 29** - Substrate scope of the developed reaction, using iridium catalyst (**156**), with acetone as reaction solvent. Yields shown are those of isolated compounds.

*2.2.3.4. Introduction of a metal-free photocatalyst*

Whilst this transformation utilises only mild conditions and a low catalyst loading, the use of an iridium photocatalyst remains less desirable. Depletion of precious metals is a key area of concern within industrial scale chemistry and, within this, iridium is particularly at risk.[173] Moreover, the use of iridium catalysis on large scales is not cost-effective, further decreasing the likelihood of its use in a production scale protocol. Accordingly, there have been many efforts to replace these broadly-applicable catalysts with metal-free alternatives.[57] In particular, Merck have undertaken a strategy of completing small-scale development work using an iridium catalyst, then developing a bespoke organic photocatalyst replacement, for use in process development. With some understanding of the required redox potentials, this has been demonstrated by systematic modification of the catalyst scaffold, in a similar manner to ligand development, with the corresponding metal catalysts.[61]

With respect to the amidation protocol developed here, hexamethoxy mesitylacridinium catalyst (**169**) has been demonstrated (see section 2.2.2.3. Catalyst selection) to be a suitable replacement for the complex and expensive iridium catalyst (**156**). Acridinium catalysts are classically very powerful oxidants,[157,174] yet the addition of methoxy groups has tempered this redox window, resulting in a milder oxidant, and stronger reductant. The catalyst was synthesised following the straightforward method developed within the Merck laboratories, involving a double Buchwald-Hartwig coupling, followed by Friedel-Crafts acylation-aromatisation (**Scheme 30**).[61]

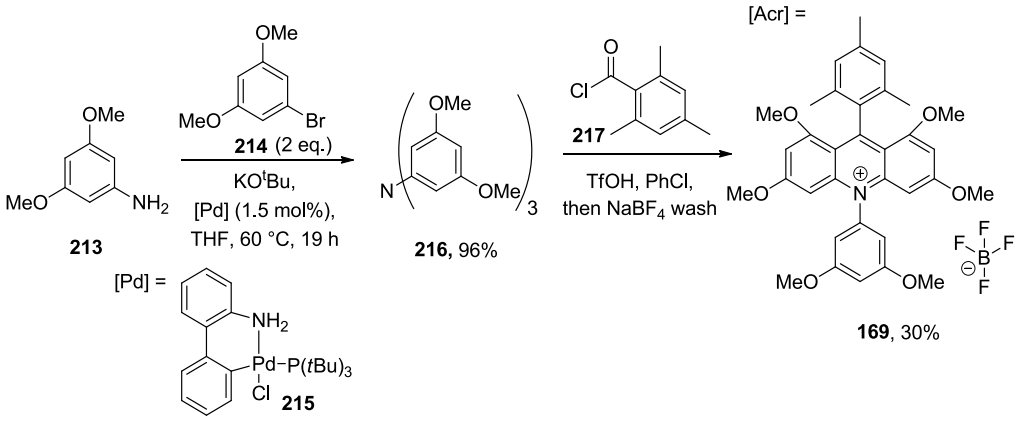


**Scheme 30** - Synthesis of hexamethoxy mesitylacridinium photocatalyst (**169**), using a literature procedure.[61]

As discussed previously (**Table 3** and **Table 4**), this catalyst was indeed productive under the standard reaction conditions. In attempt to further demonstrate its applicability within the amidation reaction protocol, additional substrates were examined (**Scheme 31**). Unfortunately, it was found that two of the four oxamate substrates examined did not undergo productive reaction (products **219** and **220**), despite observing some success with piperidine and morpholine oxamates (products **157** and **218**). Most significantly, 1,1-disubstituted olefin coupling partners were unreactive (products **199** and **191**), whilst the phenylsulfone coupling partner gave a modest yield (product **198**).

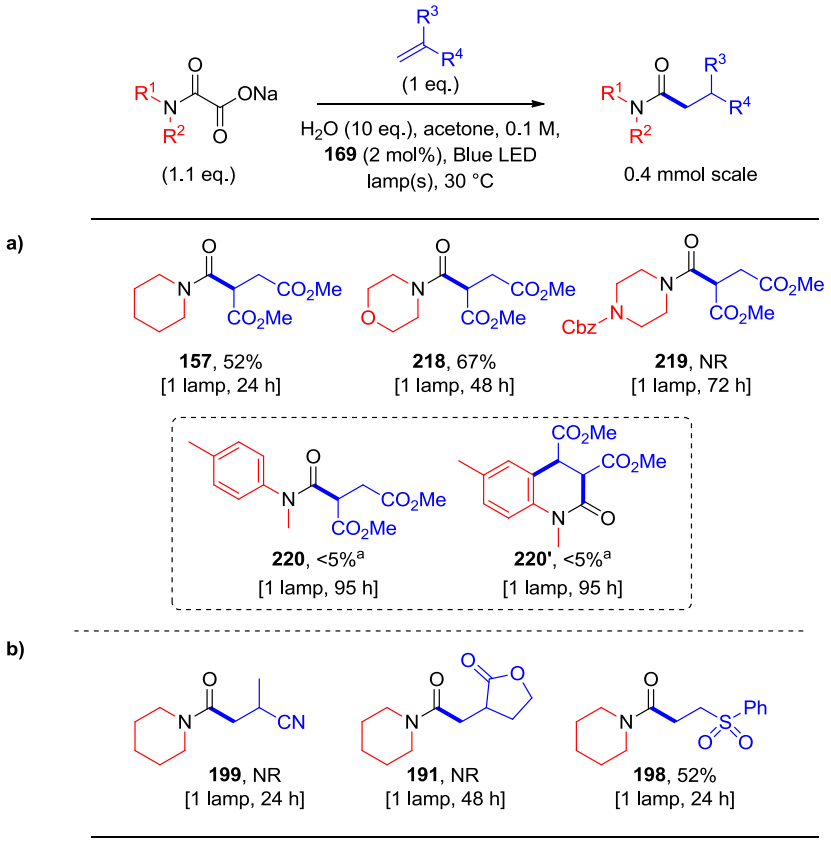


**Scheme 31** - Substrate scope using the hexamethoxy mesitylacridinium organic photocatalyst (**169**). Yields shown are those of isolated compounds. NR indicates that no (or negligible) reactivity was observed. [a]Product was not isolated, due to poor conversion by HPLC.

Although the organocatalyst (**169**) performed well with specific substrates, it was unfortunately found to be far less widely applicable, with non-productive reactions observed in many cases. This is thought to be due to the poorer redox window overlap in the reductive part of the catalytic cycle, where it has a reduction potential of only −0.82 V vs SCE (compared with

−1.37 V vs SCE[61] achieved by the iridium catalyst (**156**)). The initial substrate oxidation by the excited state photocatalyst is theoretically more facile (oxidation potential of +1.65 V vs SCE, compared with +1.21 V vs SCE), however the excited state has a far shorter lifetime (fluorescence lifetime of 12.3 ns, compared with 2300 ns), giving less opportunity for productive interactions in the reaction system: a problem regularly encountered by organic photocatalysts.[57] These hypotheses are summarised below, with respect to this transformation's proposed catalytic cycle (**Scheme 32**).

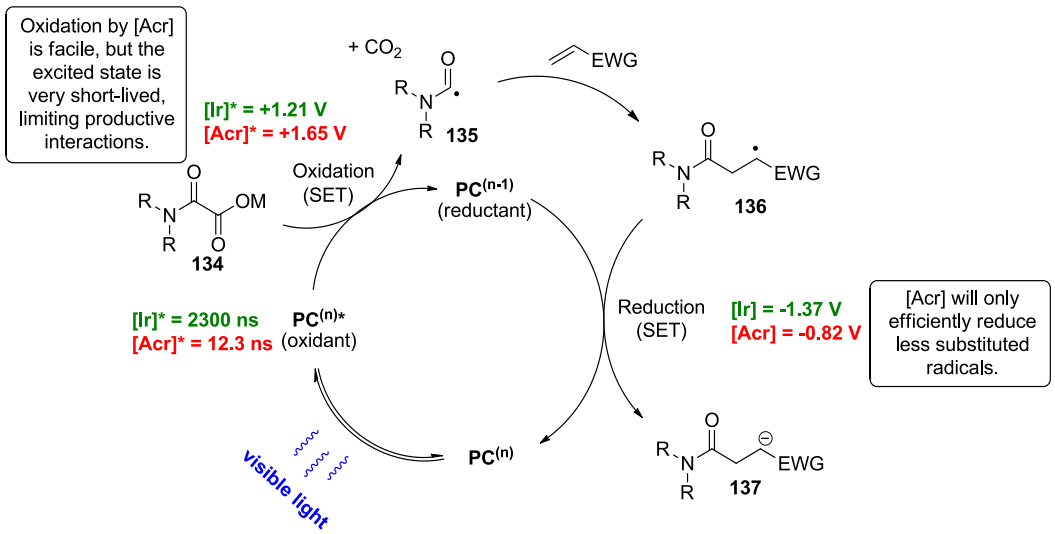


**Scheme 32** - Catalytic cycle highlighting the problems encountered in reactions using hexamethoxy mesitylacridinium photocatalyst (**169**).

It can be summarised that the use of an organic photocatalyst is possible in this instance, and effective for specific substrates. However, these findings support the strategy of organocatalyst optimisation for each substrate, which is entirely appropriate for a process development programme.[175] Therefore, this approach would be suggested for larger scale applications, which focus upon a single substrate.

## 2.3. Conclusions and future work

### 2.3.1. Conclusions

A novel amidation protocol has been successfully demonstrated for the formation of tertiary amides, through the coupling of metal oxamate salts with electron-deficient olefins. This represents an umpolung methodology, generating a nucleophilic carbonyl species in an atom-efficient manner, through photoredox-mediated oxidation-decarboxylation of the oxamate starting material. Styrene derivatives have been observed to be compatible with this method, alongside a range of classical Michael acceptors.

The initial reaction conditions have been adapted from prior publication of a related transformation,[146] and further developed, with the aim of achieving a robust and process-friendly reaction. The oxamate starting material was found to be equally reactive as a range of group 1 metal salts, with only lithium showing diminished performance. Consequently, the choice was made to employ sodium salts, to improve mass- and cost-efficiency. A low-cost 3D-printed lamp housing was used, in order to standardise reaction conditions and, in most cases, it was found that only one lamp was required for a suitable rate of reaction, whilst maintaining a clean reaction profile.

Importantly, significant insight into the mechanism and practical reaction aspects have been gained, such as the effect of water content and light intensity upon the reaction. DFT calculations have been used to support the mechanistic hypothesis, but also to compare substrate reactivity, and to corroborate the extent of by-product formation, and of cyclisation in specific cases. Accordingly, this has contributed to the overall reaction understanding, towards the establishment of a robust protocol.

A variety of electron-deficient olefins have been demonstrated to react effectively in this transformation, giving access to diversely functionalised amide products. Tolerance for the degree of substitution has been explored, and productive reaction in the presence of ketone, ester, amide, sulfone, and nitrile functional groups has been verified, as well as an aromatic bromide and a carbamate-protected nitrogen atom. The expansion to styrene coupling partners represents a considerable increase in the reaction's utility. Moreover, it has been demonstrated that this methodology can be successfully performed using organic photoredox catalysts, which could be optimised for the desired substrate, resulting in a more sustainable metal-free process.

### 2.3.2. Future work

*2.3.2.1. Further exploration of anilinic substrates*

Whilst it has been demonstrated that an anilinic oxamate species (**190**) forms the desired amide to a good extent, the previously precedented cyclisation *via* homolytic aromatic substitution (HAS) was also observed, to a minor extent.[143] Due to the delocalisation of the oxamate's π system within the aromatic ring, these substrates are less susceptible to oxidation, as observed in the preliminary cyclic voltammetry studies (+1.24 V for piperidine oxamate (**150**) vs +1.30 V for the toluidine oxamate (**153**), see section 2.2.1. Analysis of radical precursor species). Accordingly, two lamps were required to attain a reasonable rate of reaction using this oxamate, as SET is far less likely for each interaction with the excited state photocatalyst (**Scheme 33**).

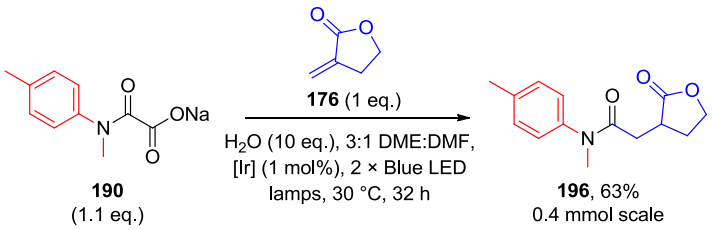


**Scheme 33** - Successful synthesis of a linear amide (**196**) from aniline-derived oxamate (**Scheme 28**).

In order to improve upon these reactions of aniline-derived oxamates, it may be advantageous to focus upon this class of substrates, and return to catalyst selection. More strongly oxidising photocatalysts may prove to be more suitable in allowing faster initiation of the catalytic cycle. Furthermore, it may be possible to include a chemical oxidant, with the goal of oxidising the HAS intermediate, allowing formation of the cyclised product (**205**) (**Scheme 34**). This would achieve complementary reactivity through the addition of a single additional reagent, further strengthening the impact of the developed method. It is anticipated that a mild stoichiometric oxidant would achieve this, since an oxidised state photocatalyst with an oxidation potential of just +0.77 V (vs SCE) successfully performed this elementary step.[143] Use of excess oxidant would also be expected to regenerate the ground state photocatalyst, ensuring that the catalytic cycle remains intact.

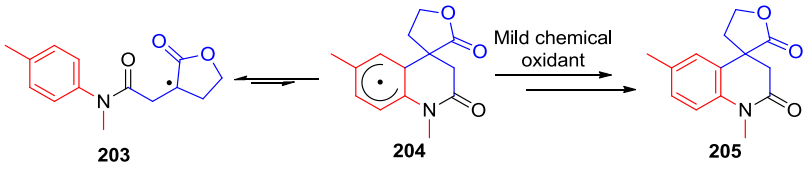


**Scheme 34** - Proposed synthesis of cyclic amide products (**205**) *via* cyclisation of the radical intermediate (**203**), generated in this synthesis.

*2.3.2.2. Improved reactor design*

As discussed previously (section 2.2.2.1. Equipment considerations), the rate of many modern photochemical methodologies is limited by the introduction of light to the system (i.e. a "photon-limited" kinetic regime).[151] Accordingly, reactions such as those discussed here can be vastly improved by increasing photon flux. Whilst this work was carried out within the laboratory, the "Tuna Blue" Kessil lamp was the only suitable choice of light source. However, since then, a versatile photochemical reactor has been developed within GlaxoSmithKline, in partnership with Pacer, for small scale screening, larger scale optimisation, and continuous processing (**Figure 13**). It is thought that the implementation of such a highly customisable reactor could impart significant improvements upon the developed reaction.

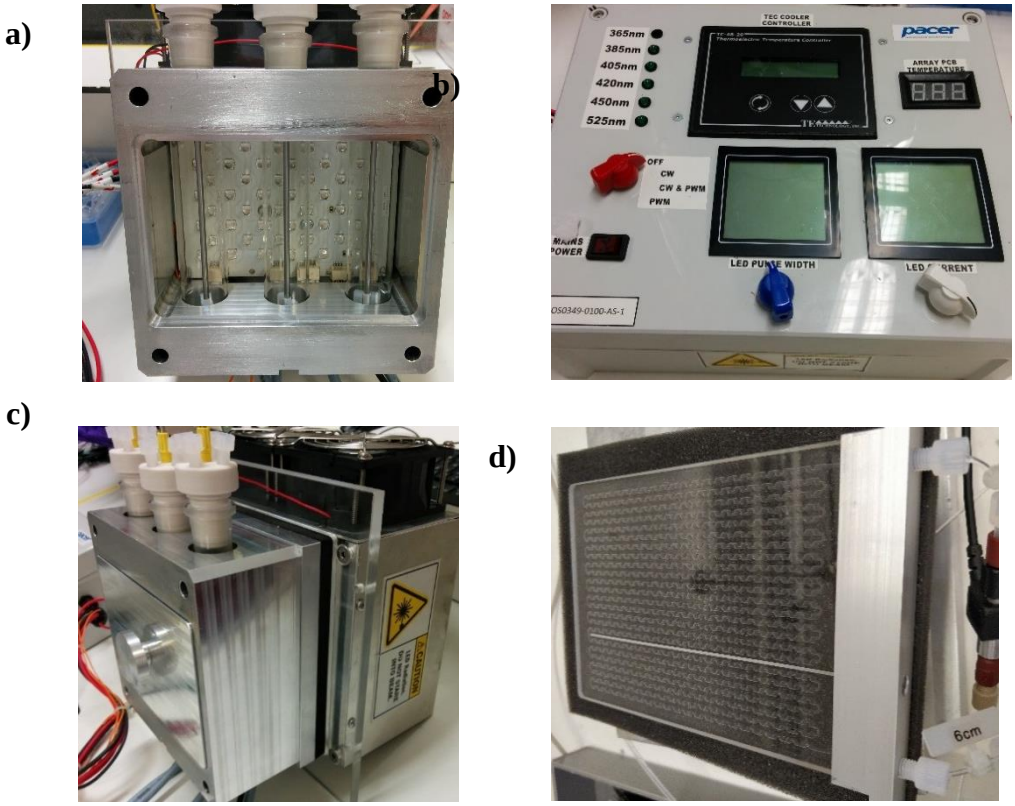


**Figure 13 - a)** Pacer photoreactor system with LED array exposed. **b)** Photoreactor control box, showcasing the highly customisable reactor system. **c)** Side on view of the photoreactor, showing the high capacity thermo-electric cooling unit. **d)** Glass flow reactor insert, for continuous processing.

The use of high power, narrow bandwidth LEDs is expected to achieve better spectral overlap with the catalyst, bestowing more efficient excitation, and a faster rate of reaction. Calibrated temperature control can also be applied to the system, with the potential for heating sluggish reactions, or cooling faster examples to obtain a cleaner reaction profile. Finally, a glass flow reactor has been integrated to the Pacer photoreactor, which ensures optimal irradiation of the reaction mixture through a shallow channel depth. Although a homogeneous reaction mixture could not be achieved thus far, there are several avenues which could be explored to enable continuous processing. For example, *in situ* formation of the oxamate salt could be pursued, using a *tert*-butoxide base to hydrolyse the methyl ester, as precedented in a prior publication.[141]

*2.3.2.3. Cyclisation-functionalisation*

As discussed previously, recent photoredox methods[120,121] have allowed cyclisation-functionalisation of amide functionalities. These cases require a precursor which is set up to undergo radical cyclisation, forming a 5-membered ring, with a relatively stable secondary or tertiary alkyl radical (2.1.4.1. Amide functionalisation, **Scheme 14**).[120,121] It could be envisioned that analogous reactivity could be achieved with oxamate radical precursors (**221**), as examined within this work. The resulting alkyl radical (**223**) could be reacted further in radical addition to an electron-deficient olefin (product **224**, **Scheme 35a**), or could undergo hydrogen atom transfer (HAT) in a stoichiometric or catalytic manner (product **225**, **Scheme 35b**).

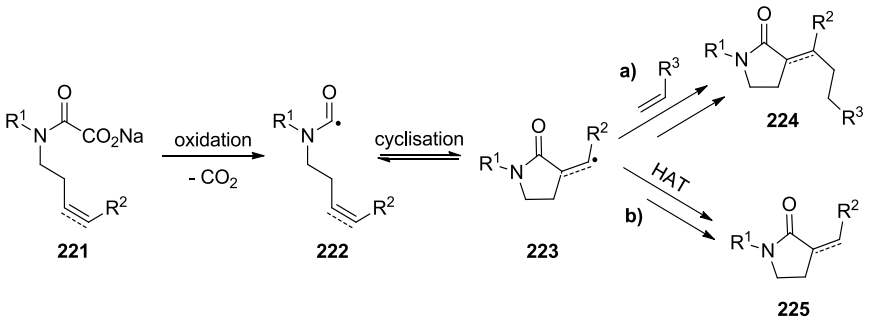


**Scheme 35** - Proposed cyclisation-functionalisation protocol of oxamate salts containing a strategically placed double or triple bond (**221**). Reaction of the alkyl radical with **a)** an olefin (product **224**), or **b**) a HAT reagent (product **225**).

Due to the stabilised nature of the carbamoyl radical, it is likely that the cyclisation step will be reversible. However, the more facile reaction of the resultant alkyl radical (**223**) could be expected to favour the desired reaction over direct reaction of the carbamoyl radical (**222**). Accordingly, the cyclised product (**224** or **225**) would likely be the major product. Expansion towards this methodology would allow the generation of molecular complexity in a single, efficient reaction step. A range of differentially functionalised oxamate starting materials could be reacted with various Michael acceptors and styrenes, to examine substrate compatibility, and generate a variety of pyrrolidinone products.

# Chapter 3. Synthesis of secondary amides enabled by flow processing

## 3.1. Introduction

As previously discussed (see 1.2.4. C-C bond formation), there is a lack of straightforward, efficient, and widely-applicable methods for synthesis of secondary amides from nucleophilic carbon synthon and an electrophilic carbamoyl source. Accordingly, this transformation will be explored in more detail, with a view to applying new synthetic technologies, where there is potential advantage. Isocyanates have been targeted as an easily synthesised and readily available starting material for secondary amide formation, particularly due to their absence of a free N-H, which improves compatibility with organometallic reagents.

### 3.1.1. Synthesis of isocyanates

Isocyanates (**230**) are most commonly synthesised using (di/tri)phosgene (**227**, **228**, **229**, **Scheme 36**),[176,177] resulting in a remarkably efficient method of introducing a carbonyl group, despite the use of a highly toxic reagent.[178] Consequently, for isocyanates which are synthesised on a large scale, where the necessary controls and precautions are in place for use of phosgene, isocyanates are a cheap and mass-efficient building block for the synthesis of a range of functionalities, but most commonly carbamates (**231**) and ureas (**232**).[179]

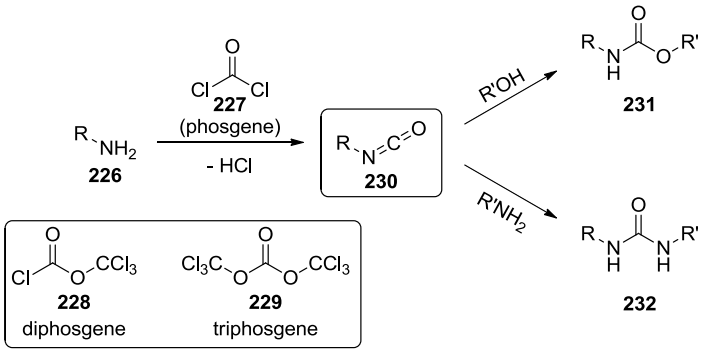


**Scheme 36** - Isocyanate (**230**) formation from primary amines (**226**) using phosgene (**227**), followed by derivatisation to the carbamate (**231**) or urea (**232**). The structures of the alternative reagents diphosgene (**228**) and triphosgene (**229**) are also shown.

Aside from this, there are several classical rearrangement methods, which furnish isocyanates. These are, the Curtius,[180] Schmidt,[181] Hofmann[182] and Lossen[182] rearrangements, which each begin from an amide with a nitrogen-bound leaving group, which is expelled upon the concerted formation of a new N-C π bond, and migration of the alkyl/aryl group (**Scheme 37**). The Curtius and Schmidt rearrangements begin with an acyl azide (**234**),[183,184] expelling nitrogen gas (**Scheme 37a**), and differ only in their methods of preparing this species. The Hofmann rearrangement utilises a halide leaving group under strongly basic conditions, where isolation of the isocyanate (**230**) is generally not possible prior to onward reaction (**Scheme 37b**).[185] Finally, the Lossen rearrangement begins with an *N*-hydroxy amide (**238**), which is further functionalised to act as a leaving group (**Scheme 37c**). Due to the absence of toxic reagents and forcing conditions, this is practically the most attractive method,[186] but requires synthesis of the *N*-hydroxy amide (**238**) starting material.

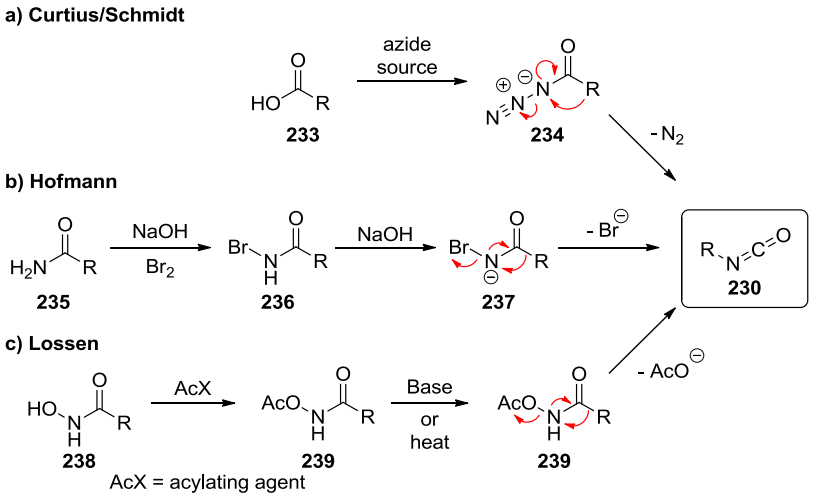


**Scheme 37** - Classical rearrangements in isocyanate synthesis. **a)** Curtius or Schmidt rearrangement of an acyl azide (**234**) **b)** Hofmann rearrangement of *N*-bromo amide (**236**) **c)** Lossen rearrangement of *N*-acetoxy amide (**239**).

### 3.1.2. Amide formation from isocyanates

*3.1.2.1. Direct attack of organometallics*

There are surprisingly few reports of amide formation from an isocyanate and stoichiometric organometallic species in the literature, given the theoretically simplistic nature of such a reaction. Perhaps the most generally applicable system, is that of Grignard reagents combining with isocyanates to form remarkably hindered secondary amides, as reported relatively recently by Bode,[187] avoiding any additives, or an excess of either reagent (**Scheme 38**). Although this method is restricted to the formation of secondary amides, incorporation of such hindered bonds in good yields is synthetically useful, and complementary to standard amide coupling methods.

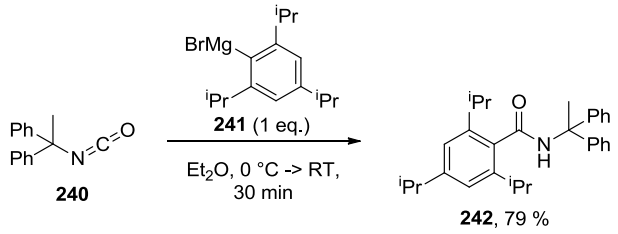


**Scheme 38** - Reaction of an isocyanate (**240**) and Grignard reagent (**241**) to form a sterically hindered secondary amide (**242**).[187]

Other examples of this reaction type are scarce, and are generally limited to systems containing a specific functional group, or are low yielding. Accordingly, a fairly comprehensive selection of these publications is summarised below (**Scheme 39**). Primary amides (**243**) have been synthesised through reaction of Grignard reagents with trimethylsilyl or chloroacetyl isocyanate, followed by reduction or hydrolysis.[188] Few substrates have been demonstrated in the report though, and the yield upon reaching the desired amide is generally below 50%. A separate publication describes the use of catalytic bis(cyclopentadienyl)titanium(IV) chloride with Grignard reagents, but is very limited in scope, and branched nucleophiles generate an isomeric product (**244**).[189]

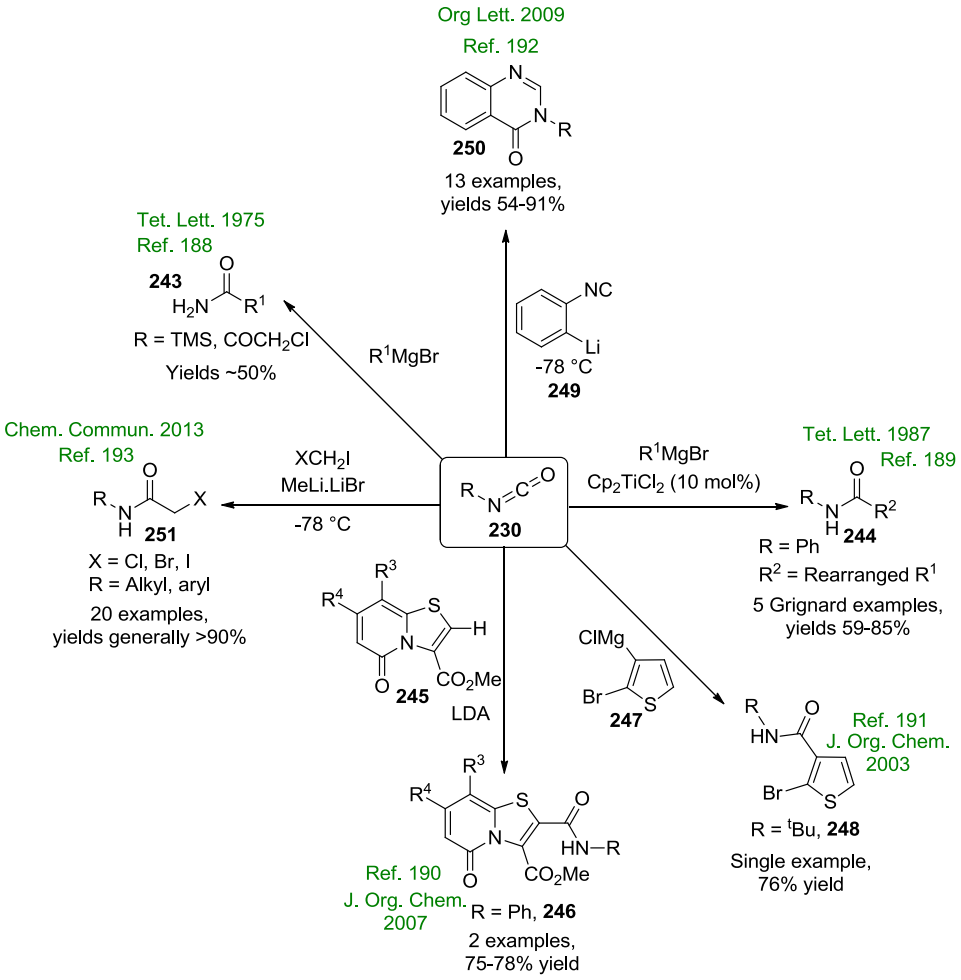


**Scheme 39** - Summary of literature stoichiometric organometallic reagents reacting with isocyanates to form amide bonds.

Other limited examples include the lithiation of a bicyclic heterocycle (**245**) using LDA, followed by quenching with phenyl isocyanate to obtain the amide (**246**) in reasonable yields.[190] A single example of forming a heteroaryl Grignard reagent (**247**) using EtMgCl, followed by reaction with *tert*-butyl isocyanate has also been demonstrated.[191] A more widely explored methodology uses lithiated isocyanides (**249**, formed *via* lithium-halogen exchange with the aryl bromide), in reactions with isocyanates, resulting in a cyclisation to form the corresponding 3*H*-quinazolin-4-ones (**250**) in good yields.[192] Introduction of a second electrophile at the 3-position can also be achieved in one pot.

Finally, a reaction of lithium carbenoids with isocyanates has been reported, furnishing an α-haloacetamide (**251**).[193] Whilst excellent yields are achieved with a variety of functionalised hindered and unhindered isocyanates, cryogenic temperatures are required to preserve

reactivity. Furthermore, the resulting α-halo (chloro in most cases) amides (**251**) are not likely to be useful products. Activation and displacement of the amide bond has been demonstrated, but not displacement of the halogen with a nucleophile, which would result in a more synthetically applicable product.

It could be envisioned that organozinc halides would be conveniently placed nucleophiles to attack an isocyanate, to form an amide. In the case of allyl- and propargylzinc halide species, this has precedence, although 3 equivalents of the organometallic are employed for a relatively long reaction time.[194] Yields of the desired amide (**253**) are low when using propargylzinc reagents, and the examples using allylzinc bromide are very atom inefficient, rendering this protocol of little use in the majority of scenarios. Alkyl- and benzylzinc halides, however, react by a different mechanism, furnishing the unexpected carbamate (**255**) product upon aqueous workup. Similarly, Reformatsky reagents result in a carbamate (**254**, **Scheme 40**).

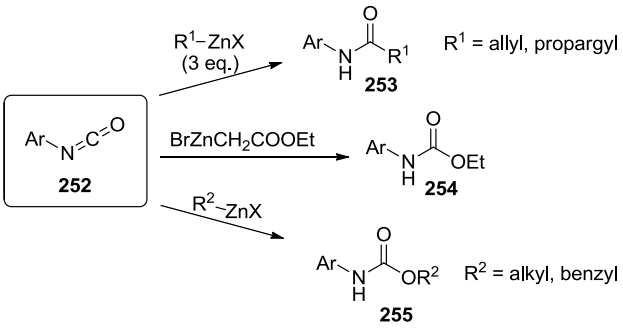


**Scheme 40** - Reaction of organozinc halides with isocyanates, resulting in amides (**253**) only in reactions with propargyl or allyl nucleophiles.

A further method of amide bond formation has been reported by Crich, in which a carboxylic acid acts as a nucleophile, forming an unstable adduct (**258**), which eliminates $CO_2$ upon decomposition to the amide (**Scheme 41**).[195] The addition of a base was deemed to be vital to the intermediate's decomposition, furnishing the desired amides under extremely mild conditions. The major drawbacks of this approach are the requirement for an electron-deficient isocyanate (generally aryl, with a *para* electron-withdrawing group), and the need to synthesise a carboxylic acid moiety (**256**), reducing overall efficiency.

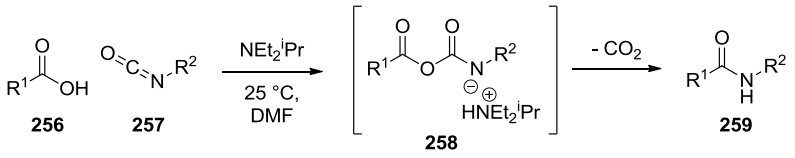


**Scheme 41** - Reaction of an isocyanate (**257**) and carboxylic acid (**256**) to form a secondary amide (**259**), *via* decomposition of an unstable intermediate (**258**).[195]

### *3.1.2.2. Metal-catalysed cross-coupling methods*

Another area which has received much attention in recent years, is the use of isocyanates (**260**) as electrophiles in metal-catalysed coupling reactions. Two main strategies have arisen from this approach; either C-H activation, or use of a boronic acid nucleophile (**Scheme 42**). Each strategy encounters similar problems, the most significant of which is the limitation to $sp^2$ coupling partners, likely due to the issue of β-hydride elimination, which is a common issue in coupling chemistry in general.[31]

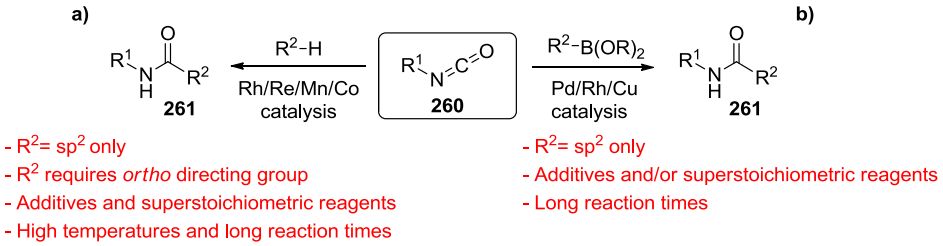


**Scheme 42** - Cross coupling strategies using isocyanates as electrophiles, along with their disadvantages.

Whilst C-H activation reactions (**Scheme 42a**) are often championed for their atom-efficiency, these procedures (using Rh,[196,197] Re,[198] Mn,[199] or Co[200,201] catalysts) require at least 1.5 equivalents of either reactant, alongside harsh conditions, extended reaction times (at least 70 °C for 16 hours),[200] and generally harmful solvents (such as DCE and 1,4-dioxane).[165] Furthermore, the use of a directing group is vital, in order to associate to the catalyst, facilitating breakage of the C-H bond, through a metallacyclic intermediate. Hence, substrate scope is limited to include only groups which do not interfere with the desired directing group through co-ordination of their own.

The classical Suzuki-type coupling of an organoboron species (**Scheme 42b**) has been less widely reported with isocyanate electrophiles (**260**). Catalyst systems using Pd,[202] Rh[203] and Cu[204] are known but, again, each has its disadvantages. The palladium-catalysed procedure suffers from poor yields and substrate scope in isocyanate, whilst the rhodium system requires 3 equivalents of boronic acid to achieve acceptable yields. Finally, the copper-catalysed variant calls for 20 mol% catalyst loading, the use of a highly toxic solvent (DMF),[165] and forcing conditions of 140 °C for 16 hours to achieve good yields in only select cases.

The final method of amidation using isocyanates to be discussed is that of reductive coupling with an organic halide (**263**),[205] or pseudohalide (tosylate or pivalate) (**262**).[206] The use of nickel catalysis, alongside stoichiometric manganese or zinc as a reductant, furnishes aryl or alkyl amides (**265**), depending upon the method followed (**Scheme 43**). Both variants suffer from the requirement for long reaction times and superstoichiometric isocyanate, alongside a problematic drop in yield once less sterically hindered isocyanates are employed. This approach is an elegant solution, and although currently lacking in scope may see major advances in the near future.

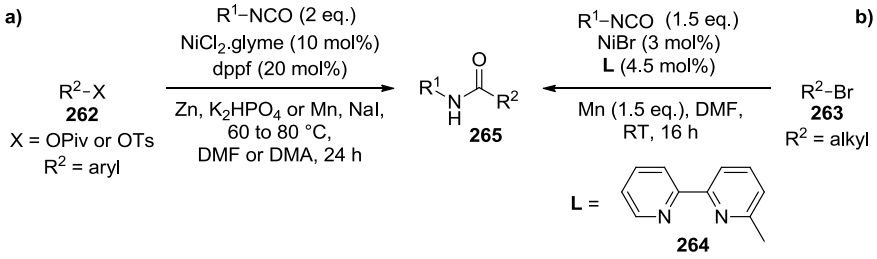


**Scheme 43** - Nickel-catalysed reductive amide formation, from **a)** phenol derived pseudohalides (**262**) or **b)** alkyl bromides (**263**).

A recent publication has also described the reaction of isocyanates with alkylsilicate species (**113**) to form amides, under nickel-photoredox dual catalysis conditions.[137] This methodology is discussed in more detail above (see section 2.1.4.2. Amide bond-formation).

### 3.1.3. Chapter aims

This chapter will describe progress in developing an effective amidation procedure utilising isocyanate starting materials. The main criteria for success are based on achieving a green[207,208] and scalable method, which would be advantageous in pharmaceutical or fine chemical production when compared with the current state of the art. In particular, mass efficiency will be pursued as far as possible, attempting to maintain a one-to-one reactant stoichiometry. Pivotal to the impact of this work, though, will be the avoidance of any stoichiometric activating agents, as this is the major drawback of current widely used amidation methods.

As summarised previously (section 3.1.2. Amide formation from isocyanates), the state of the art in amide formation from an isocyanate is lacking a widely applicable method, as all current protocols suffer from appreciable limitations. Whilst there is precedence for use of both $sp^2$ and $sp^3$ nucleophiles, the sole method which can tolerate both of these reactant classes has only been demonstrated effectively using sterically hindered isocyanate starting materials.[187] Consequently, a further target is the ability to incorporate $sp^2$ and $sp^3$ nucleophiles, whilst also tolerating a wide range of hindered *and* unhindered reactants.

Within this chapter, the use of Grignard reagents as nucleophiles will be examined. Good reactivity has been observed in some cases, yet no in depth studies of this seemingly fundamental reaction could be found within the literature. This has the implication that analysis of the transformation and its potential side reactions could lead to a better general understanding and an improved protocol.

## 3.2. Results and discussion

### 3.2.1. Reaction exploration in batch

*3.2.1.1. Initial trial reactions*

Despite literature precedence for facile reaction of Grignard reagents with isocyanates,[187] only sterically hindered reaction substrates were reported. Accordingly, our studies began by determining the course of reaction when less hindered substrates were used, in both the Grignard and isocyanate reaction partner. A hindered and unhindered isocyanate were reacted with a hindered and unhindered Grignard reagent, giving four possible reagent combinations. The results from these reactions are displayed below (**Table 8**). Both reactions of unhindered isocyanate (**266)** (entries 1 and 2) gave poor yields of the desired product, alongside a considerable quantity of an acylurea product. Conversely, both reactions using the sterically hindered *tert*-butyl isocyanate (**267**) (entries 3 and 4) gave an excellent yield of the desired product, where reaction with mesityl Grignard (**269**) (entry 4) matched the performance previously reported.[187]

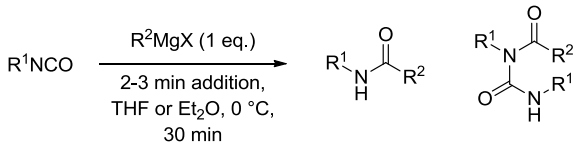


| Entry | $R^1NCO$ | $R^2MgX$ | Amide yield (%) | Acylurea yield (%)[a] |
|---|---|---|---|---|
| **1** | **266**, $R^1$ = Bn | **268**, $R^2$= $Ph(CH_2)_2$, X=Cl | **270**, 32[b] | **271**, 23[b] |
| **2** | **266**, $R^1$ = Bn | **269**, $R^2$=Mes, X=Br | **272**, 16[c] | **273**, 54[c] |
| **3** | **267**, $R^1$ = $^t$Bu | **268**, $R^2$=$Ph(CH_2)_2$, X=Cl | **274**, 90[c] | **275**, 0[c] |
| **4** | **267**, $R^1$ = $^t$Bu | **269**, $R^2$=Mes, X=Br | **276**, 85[c] | **277**, 0[c] |

**Table 8** - Initial studies, demonstrating poor reaction performance with unhindered isocyanate reaction partners. [a]Yield based on isocyanate starting material. [b]HPLC assay yield of products, versus anisole as an internal standard. [c]Isolated yield of product.

The acylurea formation was not reported in the literature and was, therefore unexpected. The formation of this by-product is assumed to occur simply through nucleophilic attack of the intermediate metalated species (**278**) through nitrogen, on another molecule of the electrophilic isocyanate (**Scheme 44**). Increased steric bulk around the amide nitrogen would significantly

reduce the rate of by-product (**271**) formation, rendering it negligible. This accounts for the results thus far, and agrees with the observation that steric hindrance within the Grignard reagent has no significant effect upon the extent of acylurea formation. Quantification of the steric bulk required to prevent acylurea formation could be achieved using the Taft equation, assigning steric parameters to isocyanate substituents.[209]

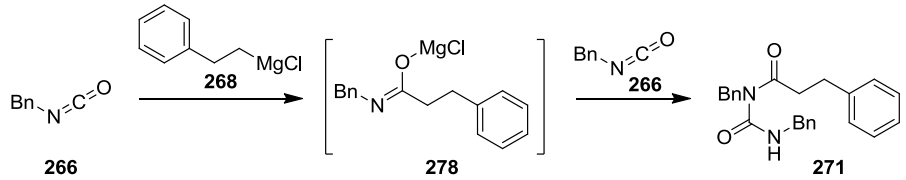


**Scheme 44** - Overreaction through amide nitrogen, forming acylurea by-product (**271**).

Theoretically, prevention of acylurea formation with less hindered substrates could be achieved by providing a reaction environment with no excess isocyanate available to react with the nucleophilic intermediate (**278**). Alternatively, altering the reaction temperature could favour the desired reaction outcome, over the undesired acylurea by-product (**271**) formation. The rate of addition was later found to be significant (see section 3.2.1.4. Importance of addition rate for further details), resulting in a marked improvement in yield, when compared to the initial reaction performance (as displayed in **Table 8**). However, to investigate the effect of other variables using the optimal fast addition procedure, a range of reaction conditions were examined (**Table 9**), looking at different temperatures (entries 1 to 5), addition regime (entry 6), and attempting to favour the undesired reaction by employing an excess of isocyanate (**266)** (entry 7).

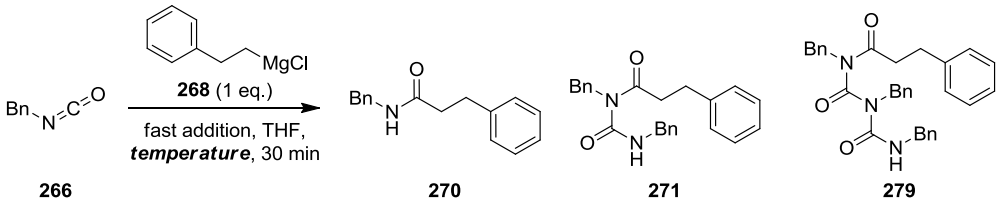


266 270 271 279

| Entry | Temperature (°C) | Deviation from standard conditions | Amide (270) yield (%)[a] | Acylurea (271) yield (%)[b] | "Trimer" (279) (HPLC %Area) |
|---|---|---|---|---|---|
| **1** | −78 | None | 79 | 8 | 2 |
| **2** | −50 | None | 73 | 5 | 1 |
| **3** | 0 | None | 73 | 9 | 1 |
| **4** | Room temp. | None | 69 | 9 | 1 |
| **5** | 40 | None | 59 | 9 | 1 |
| **6** | Room temp. | Inverse addition[c] | 9 | 28 | 13 |
| **7** | Room temp. | 2 eq. isocyanate (**266**)[d] | 21 | 34 | 15 |

**Table 9** - Various reaction conditions examined in attempt to disfavour acylurea formation. [a]HPLC yield, using anisole as an internal standard. [b]Acylurea (**271**) yield is calculated with respect to isocyanate (**266**) starting material. [c]Inverse addition refers to the isocyanate (**266**) being added to a solution of the Grignard reagent (**268**), keeping the Grignard reagent in excess at all times. [d]2 equivalents of isocyanate (**266**) were used, attempting to favour the formation of acylurea (**271**).

Altering the reaction temperature did not affect the acylurea (**271**) formation to any significant extent. The data does follow a trend of increasing amide product (**270**) yield with a decrease in temperature due to a cleaner reaction profile, but the quantity of acylurea product (**271**) formed remained roughly constant. Surprisingly, employing an inverse addition regime (entry 6) gave a far poorer result, with multiple other impurities seen by HPLC and, notably, an increased quantity of the proposed pseudo-trimeric by-product (**279**), identified by mass spectrometry. Furthermore, attempting to bias against the amide product (**270**, entry 7) still produced this species in a reasonable quantity (alongside a significant amount of the overreaction products, **271** and **279**), suggesting that no single product is entirely favoured in this reaction, and that the reaction kinetics are complex.

*3.2.1.2. Reaction calorimetry*

To further understand the difference in reactivity between a hindered and an unhindered isocyanate, reaction calorimetry was employed. This technique is vital prior to safely scaling up any chemistry, as it provides essential information around the reaction's heat profile, alongside potential insight into reaction mechanism. Accordingly, decisions regarding addition times, and heating/cooling periods rely upon data generated in these experiments, in order to prevent thermal runaway or any unexpected temperature variation.

First, the hindered *tert*-butyl isocyanate (**267**) was reacted with phenethylmagnesium chloride (**268**) (**Figure 14**). The resulting profile was smooth, with a steady heat output throughout the Grignard addition, peaking at 11 watts, meaning that the total adiabatic temperature rise of 33 °C is spread quite evenly throughout the 5 minute addition period. A peak like this is expected, due to the decrease in isocyanate concentration as it is consumed in productive reactions with the Grignard reagent. Additionally, a drop in heat output is seen immediately following the completion of Grignard addition, as expected for a fast reaction such as this. Quenching this reaction with ammonium chloride (over a 5 minute addition period) produced a peak heat output of 43 watts. The desired amide product (**274**) was isolated in an excellent 93% yield, with no significant by-products detected.

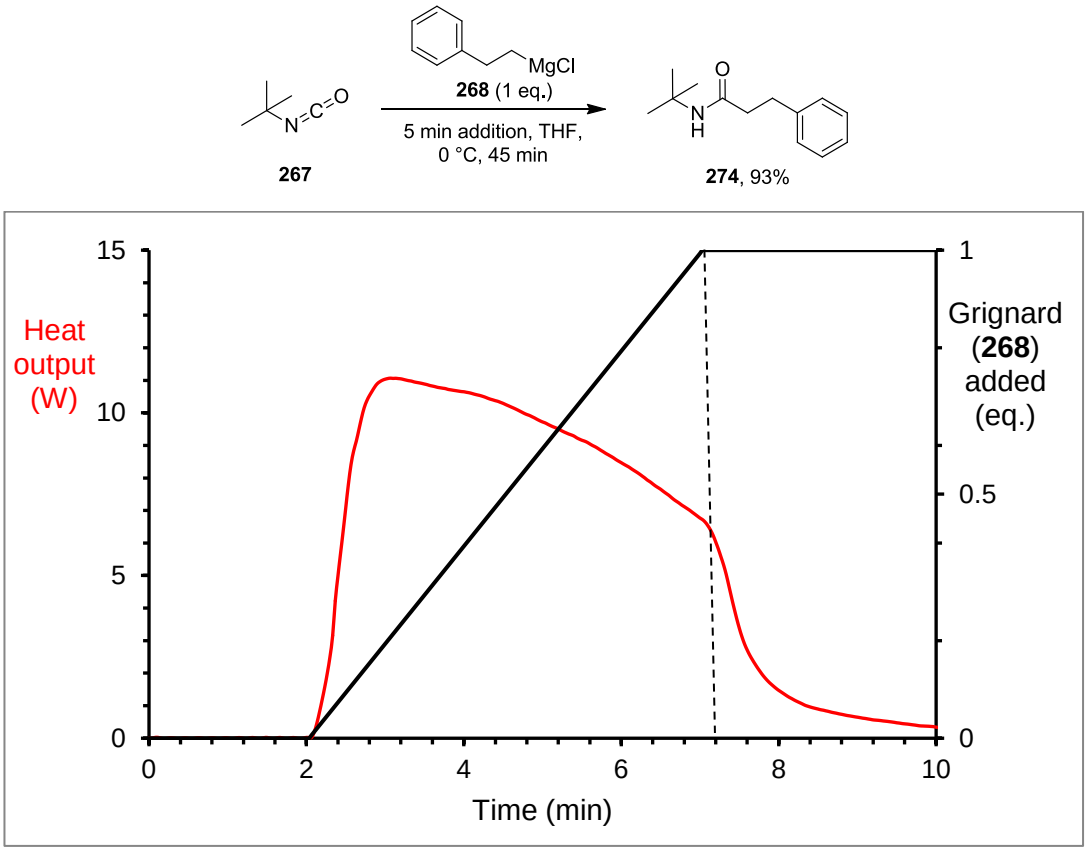


**Figure 14** - Heat flow profile throughout 5 minute addition period of Grignard reagent (**268**) to *tert*-butyl isocyanate (**267**).

Following this, the unhindered benzyl isocyanate (**266**) was examined (**Figure 15**). As expected, a simple heat evolution throughout the addition period was not observed. Instead, the heat output spiked sharply, peaking at almost 23 watts, around one minute in, then decreasing to zero by the third minute. The heat flow observed represents an adiabatic temperature rise of almost 28 °C, but in a very short time period. This can be explained by the desired reaction with isocyanate occurring quickly, followed by the magnesiated intermediate (**278**) attacking further isocyanate molecules, thus consuming all of the isocyanate reactant long before the completion of Grignard addition. Accordingly, a considerable quantity of Grignard reagent remained through to the ammonium chloride quench (addition controlled over 5 minutes), in which a violent exotherm was observed, with heat flow peaking at 75 watts. An 18% yield of the desired amide (**270**) was isolated, alongside 18% (with respect to isocyanate) of the acylurea by-product (**271**). Furthermore, the trimeric by-product (**279**) was also observed by HPLC (9%Area), but not isolated.

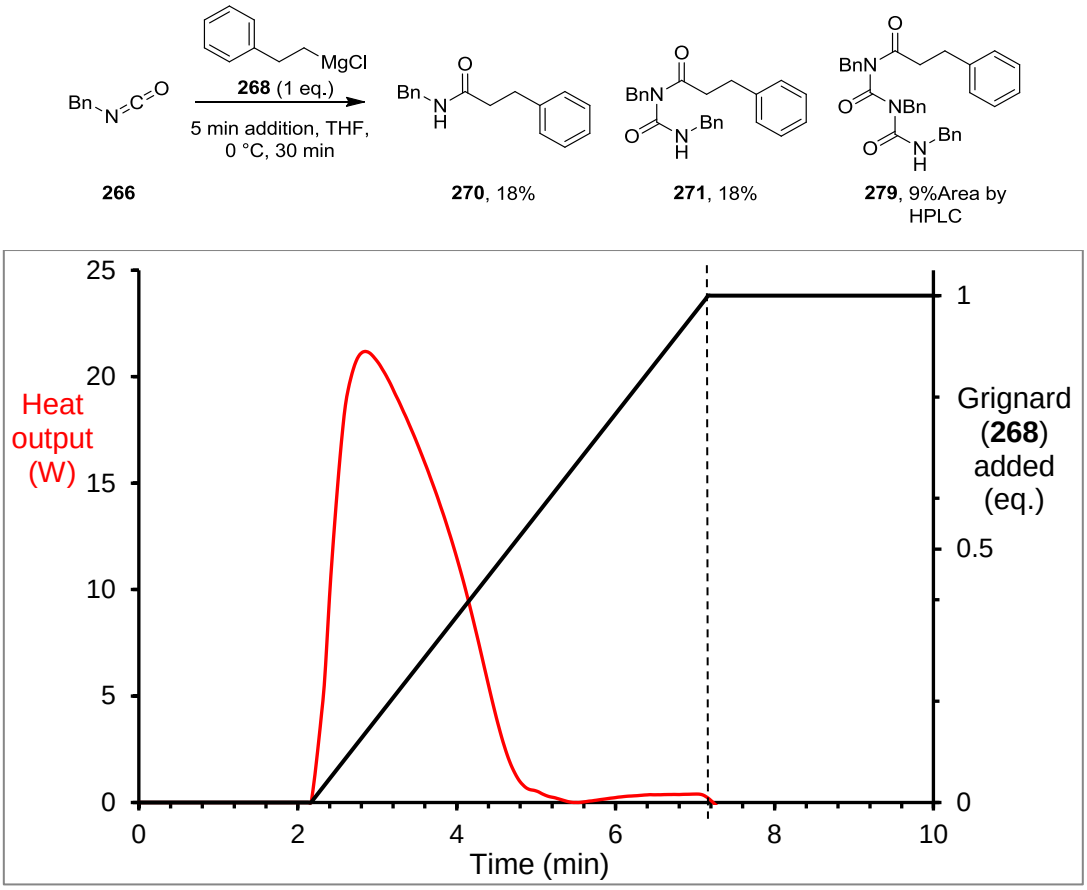


**Figure 15** - Heat flow profile throughout the 5 minute addition period of Grignard reagent (**268**) to benzyl isocyanate (**266**).

These two heat flow profiles demonstrate the significant differences between the reactions of hindered and unhindered isocyanates, and the importance of employing a compatible isocyanate for amidation by the Grignard reagent. If this reaction were to be scaled up, the sharp spike in heat output would prove problematic in the case of benzyl isocyanate (**266**), requiring an elongated addition period. Limitations on addition rate depend upon many factors, such as the reaction molarity, heat capacity of solvent, and temperature tolerance of the reaction itself. All of these factors would require consideration and adequate controls for safe operation. Additionally, the optimal fast addition, as discussed previously, would not be practically feasible on scale, due to the physical addition rate restriction, and that of controlling the exotherm.

*3.2.1.3. Reaction kinetics in batch*

To continue efforts towards optimising this reaction, it was deemed necessary to obtain further understanding of the reaction kinetics and, in particular, the relative rates of amide (**270**) and acylurea (**271**) formation, and at what point in the reaction the by-product begins to form. Complete consumption of Grignard reagent (**268**) was proposed to take place too quickly to monitor on a manual sampling timescale, and so an alternative method of analysis was sought. The presence of IR-active functional groups suggested that *in situ* IR analysis (ReactIR) would prove to be valuable, as has been demonstrated previously in monitoring fast transformations.[210] ReactIR has become a common process analytical technology (PAT) tool in the process development environment, due to the wealth of valuable reaction data and understanding attainable in a short time period.[211,212]

Reactions were run at three temperatures: room temperature, −50 °C and −78 °C, with single portion addition of Grignard reagent (**268**) (at 30 seconds on the graphical representations). IR signals corresponding to the isocyanate starting material (**266**), the metalated amide product (**278**), and acylurea by-product (**271**) were followed over time, giving rough reaction times (**Figure 16**). At room temperature, the reaction was complete within the time taken to perform a single scan (15 seconds). As expected, the reactions at lower temperatures were slower, giving a rough reaction time of 45 seconds at −50 °C and 90 seconds at −78 °C.

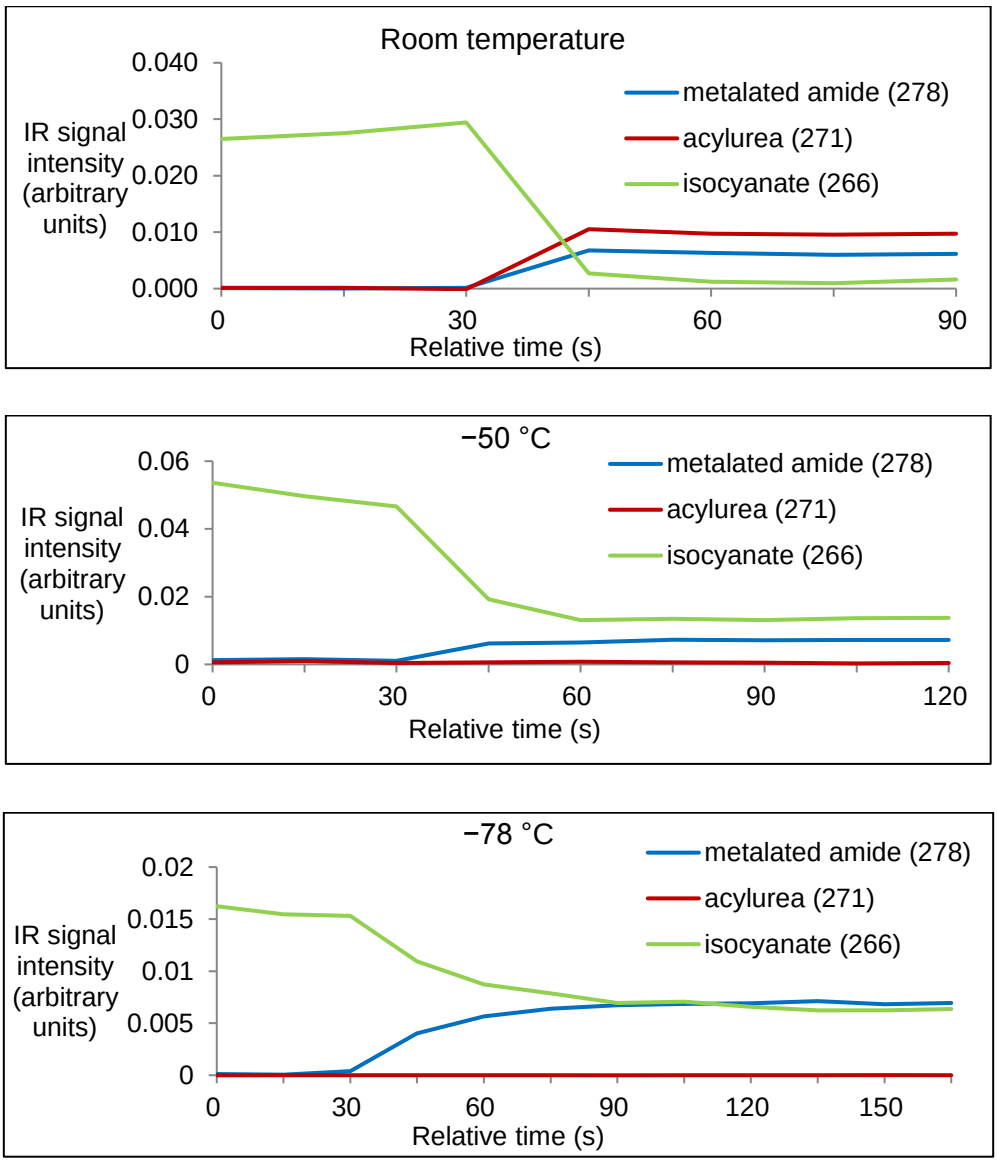


**Figure 16** - ReactIR data from batch reactions of isocyanate (**266**) at three temperatures. Data points were collected every 15 seconds. Reaction times were taken as the time between addition of Grignard reagent (**268**) at 30 seconds, and the system reaching a steady state. **Required reaction times: Room temperature = <15 s, −50 °C = 45 s, −78 °C = 90 s**

Although useful data was obtained in these experiments, there are significant limitations to its interpretation and implications. Perhaps most importantly, the addition of Grignard reagent (**268**) in each case resulted in a large exotherm of between 17 °C and 28 °C. As a consequence, reaction temperatures were higher than intended, leading to a faster rate of reaction. Furthermore, this rapid change in temperature can be responsible for peak intensities to change quite dramatically as an artefact of the equipment, which could explain why full consumption of starting material was not seen in the two lower temperature examples. Finally, the isocyanate

stretch is very close to the "diamond region": a blind spot at 2200-1900 $cm^{-1}$ caused by limited transmission through the IR probe's diamond optical window. Accordingly, this signal has a considerable amount of noise. This could be reduced by switching to a less chemically resistant silicon optical window, but this was unfortunately unavailable for use.

To give further insight to the reaction kinetics, two additional ReactIR experiments were conducted, utilising a portionwise addition of Grignard reagent (**268**) over 10 minutes (**Figure 17**). These results were much as expected, with the portions of Grignard reagent consumed almost instantaneously following their addition. At room temperature, a significant extent of acylurea (**271**) was formed, leading to the complete consumption of isocyanate (**266**) after addition of around 0.6 equivalents of Grignard reagent (at 450 seconds). The reaction at −50 °C showed a lesser extent of acylurea (**271**) formation, but more than in the previous ReactIR reaction at the same temperature (see **Figure 16**). This can be rationalised by the slow Grignard addition allowing time for the metalated amide intermediate (**278**) to react further.

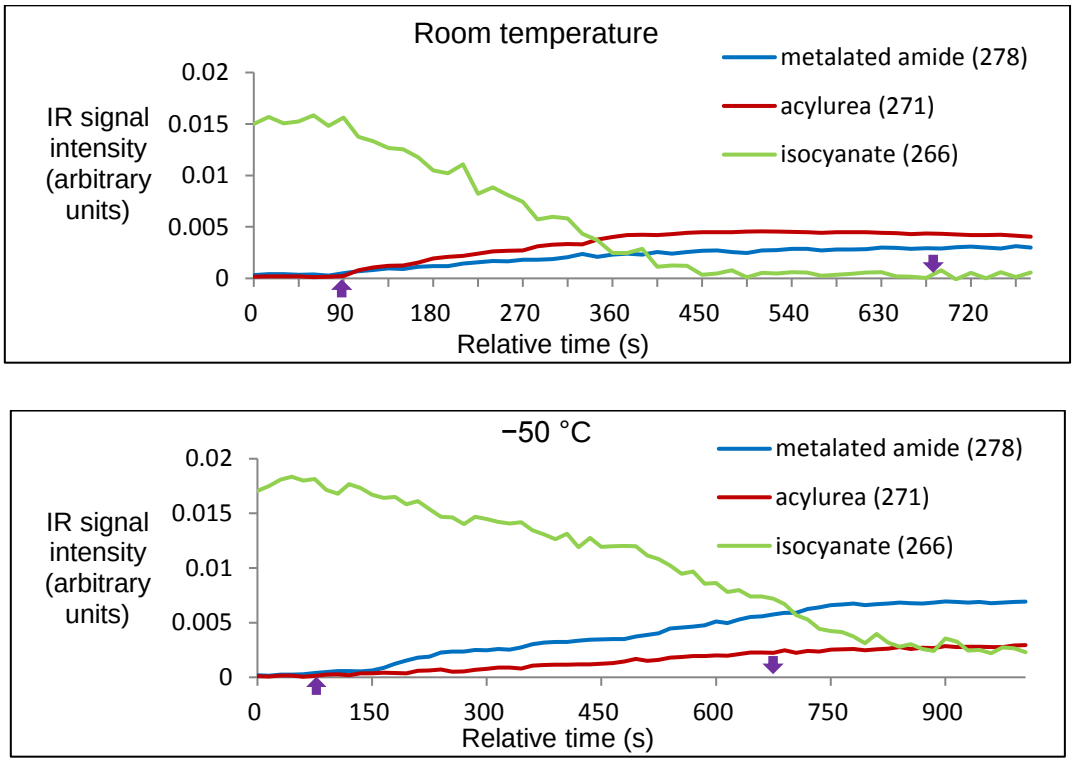


**Figure 17** - ReactIR data of slow Grignard reagent (**268**) addition to isocyanate (**266**) at two temperatures. Purple arrows indicate the beginning and end of Grignard reagent addition.

Thus far, attempts to understand the reaction kinetics in batch have revealed that complete reaction occurs in under 15 seconds at room temperature, but also that acylurea by-product (**271**) begins to form simultaneously with the desired amide product (**270**). Decreasing the reaction temperature has been observed to begin suppressing acylurea formation, but this is not a scalable solution. As reaction scale increases, the reaction mixture's surface area to volume ratio decreases rapidly, proving to be problematic for heat transfer, particularly for exothermic reactions such as this one. Furthermore, specialist equipment is required to perform low temperature reactions on a large scale, and the amount of energy required to maintain a vessel at this temperature is significant. The aim to conduct reactions at close to ambient temperature is stated in one of "The Twelve Principles of Green Chemistry", illustrating its importance.[207,208] Therefore, another solution must be pursued.

*3.2.1.4. Importance of addition rate*

So far, experiments implementing a slower or portionwise addition of the Grignard reagent have resulted in a lower yield of the desired amide. In order to gain better understanding of this reaction's dependence upon the rate of reagent mixing, a study was undertaken, varying the addition period from 0 (an "instantaneous" addition, achieved by adding the reagent by syringe as quickly as possible), to 30 minutes, using a syringe pump (**Figure 18**).

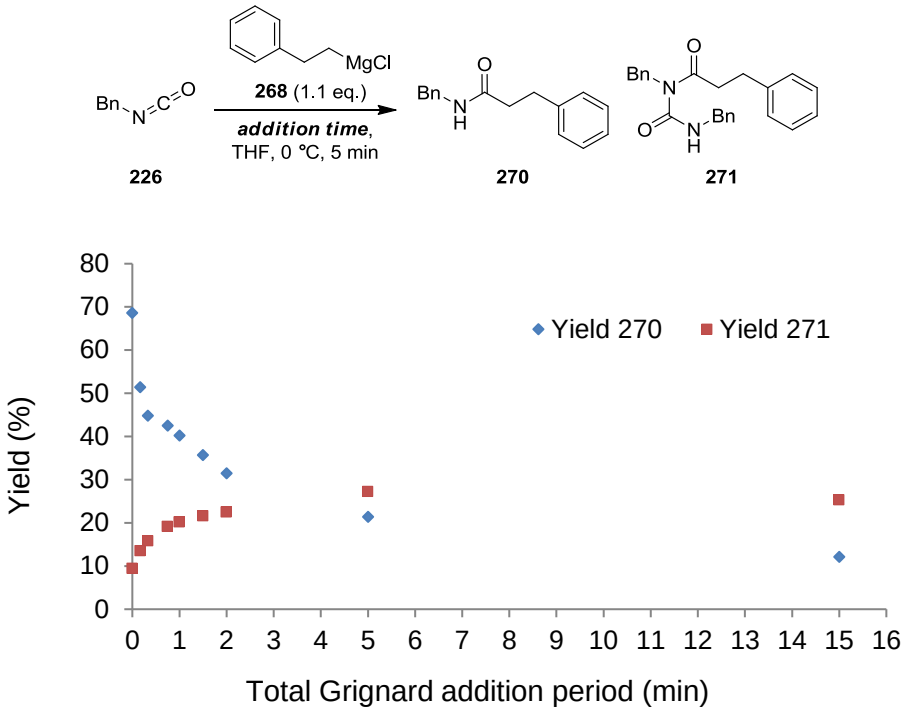


**Figure 18** - Influence of addition rate on yield of amide (**270**) and acylurea by-product (**271**), using the standard reaction studied so far. See section 4.3.5. Addition rate study, for results in a tabulated format.

Surprisingly, the results of this study clearly show that a fast addition of Grignard reagent (**268**) is vital for a productive amidation reaction. Whilst the fastest addition achieved an assay yield of 69% amide (**270**), with 9% acylurea (**271**), the yield of amide (**270**) suffered greatly when the addition period was elongated to 10 seconds. This seemingly small decrease in addition rate reduced the assay yield of amide (**270**) by 17% to just 51%; a result which was magnified further with slower additions. The longest addition time of 15 minutes gave a very poor amide (**270**) assay yield of just 12%, which would not be synthetically useful.

The implication of this result to the scalability of this amidation strategy is that a standard batch reaction would not be feasible. With increasing scale, the physical limitation to addition rate, and requirement for exotherm control (see section 3.2.1.2. Reaction calorimetry for further detail) will mean that it is impossible to keep the addition period within a productive region, as detailed in **Figure 18**. As a rough estimate at pilot plant (~30 kg) scale, around 30 minutes would be the minimum addition period for this reagent, without taking control of the exotherm into consideration.

Although this is seemingly a negative finding for scalability, it encourages the use of flow chemistry as an enabling technology. This will allow the required fast mixing of reagents to be carried out in an inherently scalable fashion, and should surpass the results acquired in small scale batch reactions. Use of fast flow rates, in combination with a sufficiently turbulent mixer should give the appropriate level of integration of the two reagent streams. The resulting reaction could theoretically be scaled to industrially useful quantities, whilst maintaining the same level of fast mixing.

### 3.2.2. Reaction exploration in flow

*3.2.2.1. Initial flow kinetic work*

In recent years, the use of continuous flow methodologies has increased exponentially in the fine chemical and pharmaceutical industries, owing mainly to its minimized risk when using hazardous reagents,[213] its improved control over fast reactions,[214] and access to a greater temperature range.[215] A solution to the issues observed in this amidation reaction is expected to be found in flow chemistry through improved mixing, in a scalable manner (**Figure 19**). In order to assess the suitability under flow conditions, the short reaction times found in batch using ReactIR were used as a basis for residence time estimates in flow. Due to the fast reaction kinetics, a high pump rate was necessitated, requiring large quantities of input material.

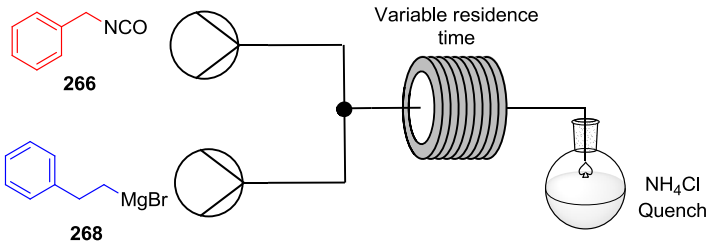


**Figure 19** - Simplified view of setup used for FlowIR kinetic studies. See **Figure 20**, below, for a more detailed diagram, including the equipment used.

To ensure that efforts in flow chemistry are well understood, a ReactIR flow cell setup[66] was used to determine conversion at differing residence times, achieved through varying the length of tubing leading to the ReactIR cell (**Figure 20**). After allowing a steady state composition to

be reached at each residence time, a percentage conversion was calculated. These percentages were used to graph conversion against reaction time (**Figure 21**). The resulting plot shows a fairly standard kinetic curve, with complete conversion seen by 5.25 seconds residence time.

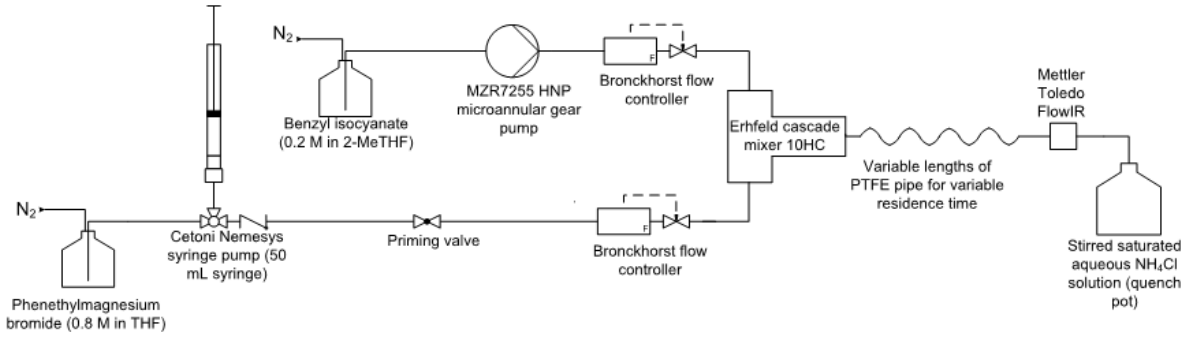


**Figure 20** - Engineering line diagram of flow ReactIR system for kinetic experiments.

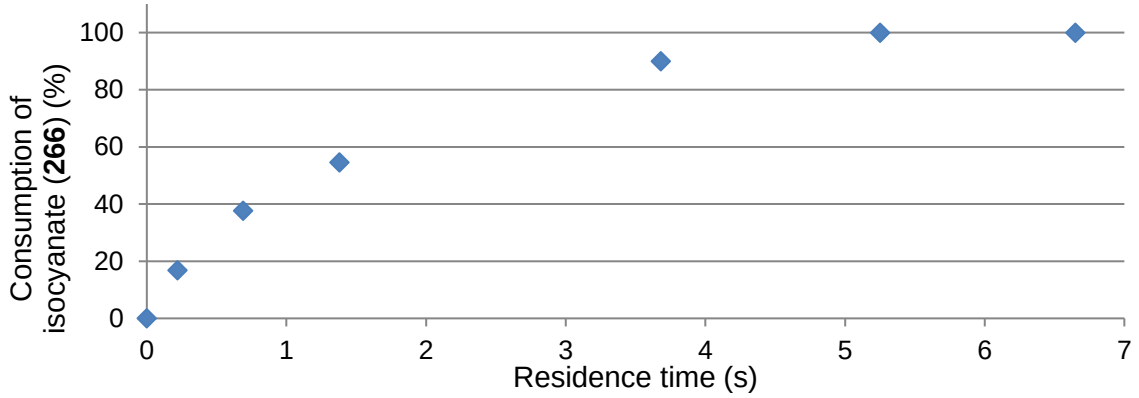


**Figure 21** - A graph of percentage isocyanate (**266**) conversion versus residence time, constructed from flow ReactIR experiments, using varying tubing lengths.

The flow ReactIR analysis suggests that the residence time could be reduced to a total of 5.25 seconds, and complete reaction would still be observed. However, at this residence time (as shown in **Figure 22**), the acylurea by-product was still produced, once constant reaction composition had been reached. Therefore, even at the shortest possible residence time, with a high-performance cascade mixer and fast flow rate giving what should be an excellent mixing profile, acylurea (**271**) formation is not completely suppressed. It was expected that a suitable

reactivity window between amide (**270**) and acylurea (**271**) may be reached by tuning the flow reaction parameters, particularly by lowering the temperature.

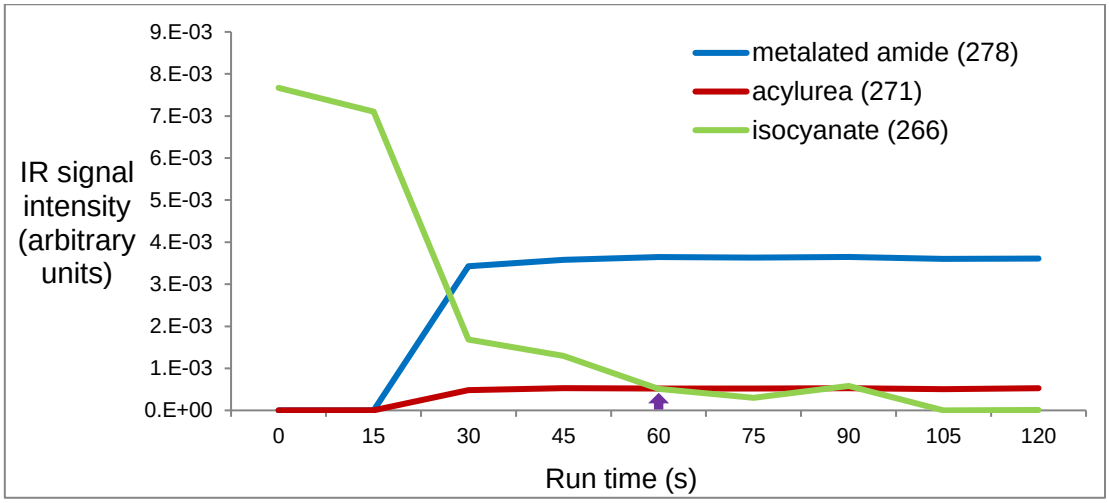


**Figure 22** - Flow ReactIR data measured by a probe placed after a length of tubing, equating to a 5.25 s residence time, continuously for two minutes "run time" (along the x axis). The arrow indicates an estimation of when a steady state was reached. Variation was seen in the isocyanate signal, due to its proximity to the IR diamond region.

*3.2.2.2. Reaction optimisation in flow*

In order to translate the results of the kinetic study to a more practically useful platform for further studies on reaction conditions, a Vapourtec R2-C+ pump module was employed, simply using PFA tubing with a T-piece mixer as the reaction vessel, and anisole as an internal standard for analysis. Attempts to replicate the incomplete reactions observed by flow ReactIR were unsuccessful, showing no real trends between the data. Further experimentation at varied residence times was problematic, due to solid formation blocking the tubing. After some investigation into the issue, the root cause was thought to be the delivery of inconsistent flow, and air being drawn into the pumps. Accordingly, an alternative reaction system was sought.

For reaction optimisation, continuous pumping was not required. Replacing the more complex system with a simple syringe pump was expected to give a more reproducible and robust reaction. The possibility of precipitation should also be minimised, as the system is closed with no possibility of drawing in air whilst pumping and, furthermore, any change in flow rate would be directly observable. Upon implementing a Harvard PHD dual syringe pump, smooth

delivery of reagents was seen, and the effects of varying reaction parameters could be investigated.

Initially, it was hypothesised that control of residence time would provide the desired decrease in acylurea formation; however, successful reaction is likely based upon effective mixing of the two reaction streams. This was tested in two reactions, where the flow rate was kept constant, but length of tubing changed in order to alter the residence time (**Table 10**). The reactions gave essentially the same result, despite a factor of two change in residence time. Having observed no further reaction of the Grignard reagent (**268**) with the amide product (**270**), this observation can be extrapolated to assume that residence time is not a key parameter, provided that it is sufficient for complete reaction. Once the reaction composition is set by the mixing of reagents, it will not be altered, regardless of the residence time allowed. A residence time of 10.6 seconds was chosen for the optimal reaction, as it is roughly double that of the required reaction time (see **Figure 21**), so should allow complete reaction when examining other (potentially less reactive) substrates.

| Entry | Combined flow rate (mL $min^{-1}$) | Residence time (s) | Starting material (266) yield (%)[a] | Amide (270) yield (%)[a] | Acylurea (271) yield (%)[a] |
|---|---|---|---|---|---|
| **1** | 12 | 6.1 | 0 | 90 | 8 |
| **2** | 12 | 12.3 | 0 | 91 | 8 |

**Table 10** - Results of the standard reaction with and without additional residence time after reaction completion. [a]Yields calculated by HPLC, using anisole as an internal standard. The results shown were obtained by averaging the assay yields of 5 samples, taken sequentially throughout an experimental run.

Having deduced that a change in residence time will not affect the reaction profile (provided the reaction has gone to completion), this variable can be kept constant, whilst others are examined. The reaction temperature was expected to have significant influence, and so was varied by submerging the reactor tubing in a jacketed CLR (controlled lab reactor) vessel, containing isopropanol (**Figure 23**). The reactions at 40 ºC and 0 °C, showed no significant difference against the result with no temperature bath (**Table 11**), but the reaction at 20 °C gave a slightly lower yield of the desired amide.

The reaction at −78 °C was carried out using a standard dry ice/isopropanol bath, as such low temperatures are not accessible with a standard jacketed vessel. Unsurprisingly, the 10.6 second residence time was not sufficient for complete reaction to take place at this temperature. However, the acylurea by-product (**271**) had already begun to form, despite almost half of the starting material remaining, demonstrating that this by-product formation cannot be avoided in flow reactions by using low temperature.

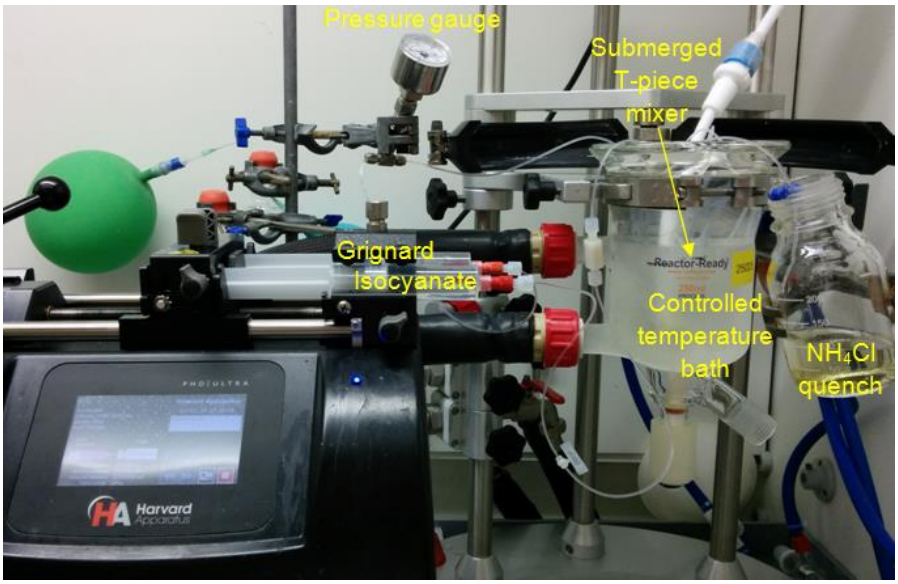


**Figure 23** - Reaction set up for examining the effect of different temperatures.

| Entry | Temperature (°C) | Starting material (266) remaining (%)[a] | Amide (270) yield (%)[a] | Acylurea (271) yield (%)[a] |
|---|---|---|---|---|
| **1** | 40 | 0 | 88 | 10 |
| **2** | 20 | 0 | 83 | 9 |
| **3** | 0 | 0 | 90 | 9 |
| **4** | Room temperature[b] | 0 | 90 | 8 |
| **5** | −78 | 45 | 50 | 1 |

**Table 11** - Results of the standard reaction at various temperatures. [a]Yields calculated by HPLC, using anisole as an internal standard. The results shown were obtained by averaging the assay yields of 5 samples, taken sequentially throughout an experimental run. [b]The result obtained at ”room temperature” was run without any controlled temperature bath.

A fundamental area in flow reaction engineering is the design and selection of the most suitable reactor. Altering mixing properties can have direct impact upon the reaction outcome, particularly in the case of fast reactions, such as this amidation. An alternative system was examined versus the T-piece with tubing used so far (**Figure 24**). This reactor features static mixing elements throughout, enhancing turbulence by generating eddies within the reactor pathway. The rate of mixing has been quantified in-house, using the Villermaux-Dushman reaction,[216] to give an estimated time required for complete mixing at the 10 mL $min^{-1}$ combined flow rate used (**Table 12**).

**Figure 24** - Photograph of Ehrfeld Flowplate® Process Plate whilst in use.

Surprisingly, the Flowplate did not provide any significant improvement when compared with the standard T-piece (**Table 12**). When considering the exponential effect of addition rate (**Figure 18**), it would be expected that increasing mixing speed by a factor of 10 would give a significantly more favourable reaction profile. However, the result of this experiment implies that any advantage given by faster mixing may have reached a limit, upon which it cannot reduce acylurea (**271**) formation any further. In practical terms, this suggests that the T-piece system is acceptable for use in subsequent reactions and, accordingly, its use was continued.

| Entry | Mixer | Mixing time at 10 mL $min^{-1}$ (combined flow)[a] | Starting material (266) remaining (%)[b] | Amide (270) yield (%)[b] | Acylurea (271) yield (%)[b] |
|---|---|---|---|---|---|
| **1** | T-piece | ~0.2 s | 0 | 90 | 8 |
| **2** | Ehrfeld Flowplate reactor | ~0.02 s | 0 | 89 | 5 |

**Table 12** - Results of the standard reaction, using an alternative mixer (Ehrfeld Flowplate). [a]Mixing times are approximate, and are taken from characterisation performed within GSK, using the Villermaux-Dushman reaction.[67] [b]Yields calculated by HPLC, using anisole as an internal standard. The results shown were obtained by averaging the assay yields of 5 samples, taken sequentially throughout an experimental run.

Subsequently, the effect of reaction concentration was examined (**Table 13**), finding 0.5 M to be optimal when compared with a higher and a lower concentration. The reaction at 0.25 M had not quite reached completion during this short residence time, which is perhaps unsurprising as this is expected to decrease the reaction rate by a factor of four (based on the assumption of bimolecular reaction kinetics). Whilst working at the maximum possible concentration would be beneficial in reducing solvent volumes, it also is expected to be more problematic as insolubility may lead to blockages within the small diameter of the flow reactor. 0.5 M is also a convenient concentration when considering substrate scope, due to commercial Grignard reagents generally being available as 1 M or 0.5 M solutions.

| Entry | Concentration (M) | Starting material (266) remaining (%)[a] | Amide (270) yield (%)[a] | Acylurea (271) yield (%)[a] |
|---|---|---|---|---|
| **1** | 0.25 | 2 | 78 | 9 |
| **2** | 0.50 | 0 | 86 | 7 |
| **3** | 0.75 | 0 | 80 | 8 |

**Table 13** - Results of the standard reaction at various concentrations. [a]Yields calculated by HPLC, using anisole as an internal standard. The results shown were obtained by averaging the assay yields of 5 samples, taken sequentially throughout an experimental run.

In order to ensure a robust reaction in spite of potential variation in input solutions, the effect of different stoichiometries, 0.1 equivalent either side of the standard conditions, was examined (**Table 14**). As expected, lowering the equivalents of Grignard reagent (**268**) had a negative

effect on the reaction result, however this was relatively minor, and not considered to be an issue. Conversely, an excess of Grignard reagent (**268**) gave a slightly improved performance. These results give confidence that the reaction successfully operates within the range of 0.9 - 1.1 equivalents of Grignard reagent (**268**), implying that unexpected variation from the desired one-to-one stoichiometry will be well tolerated. Although increasing the excess of Grignard reagent could be used to favourably alter the product ratio, this is not an elegant solution, and would be undesirable due to the resulting decrease in mass efficiency (see section 3.1.3. Chapter aims).

| Entry | Grignard equivalents | Starting material (266) remaining (%)[a] | Amide (270) yield (%)[a] | Acylurea (270) yield (%)[a] |
|---|---|---|---|---|
| **1** | 0.9 | 0 | 85 | 6 |
| **2** | 1.0 | 0 | 89 | 5 |
| **3** | 1.1 | 0 | 93 | 4 |

**Table 14** - Results of the standard reaction at slightly varied stoichiometries. [a]Yield calculated by HPLC, using anisole as an internal standard. The results shown were obtained by averaging the assay yields of 5 samples, taken sequentially throughout an experimental run.

It had been assumed previously, that keeping the Grignard reagent in excess throughout the reaction would achieve a higher yield of the desired amide. Accordingly, an alternative flow reactor was set up, in which the isocyanate stream is split, then introduced to the Grignard reagent in two separate portions (**Figure 25**, where T-pieces labelled A and B indicate mixing points of the two reagents). In keeping with the batch results for inverse addition experiments (see section 3.2.1.1. Initial trial reactions), this technique was surprisingly deleterious for the desired reaction. Only 18% assay yield of the desired amide product (**270**) was observed, alongside 29% of the acylurea by-product (**271**). The remaining mass balance was made up of the previously proposed pseudo-trimeric product (**279**) and a large number of unidentified impurities, which were previously only observed in trace quantities.

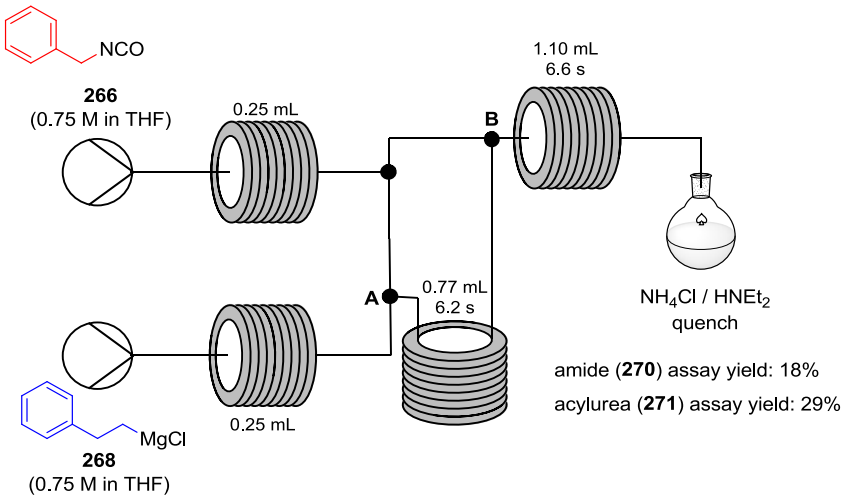


**Figure 25** - A schematic of the flow reactor set up for a reaction implementing double injection of isocyanate. Quoted assay yields are HPLC yields using anisole as an internal standard. The results shown were obtained by averaging the assay yields of 4 or 5 samples, taken sequentially throughout 3 separate experimental runs. Acylurea (**271**) yield is quoted with respect to isocyanate (**266**) starting material.

Thus far, no significant improvement has been achieved through reaction parameter optimisation in flow. Whilst the standard reaction setup (T-piece mixer, no temperature bath, 0.5 M solutions, 10.6 s residence time) has given assay yields within a range of 5% (from 86% to 91% throughout the experiments detailed within this section) this is not unreasonable, with various sources of error thought to contribute to this uncertainty. Importantly, each parameter was tested in a direct comparison against these reaction conditions, giving weight to the authenticity of the outcome.

### *3.2.2.3. Additive effects*

As it appeared that no further progress could be made through altering reaction conditions, an alternative approach was taken, turning to chemical additives instead. Consideration of the issue at hand provided three possible additive types to reduce the extent of side-reaction observed: **A**) an agent to reduce the Grignard reagent's degree of aggregation, increasing its nucleophilicity, and rate of attack at the isocyanate; **B**) a Lewis acidic additive to either activate the isocyanate, or to coordinate to the metalated amide intermediate (**278**), reducing its reactivity; or **C**) a sacrificial electrophile, which could react with the metalated intermediate, temporarily blocking it from attacking another isocyanate. With this in mind, a range of additives were screened in batch reactions, initially at 1 equivalent (**Table 15**).

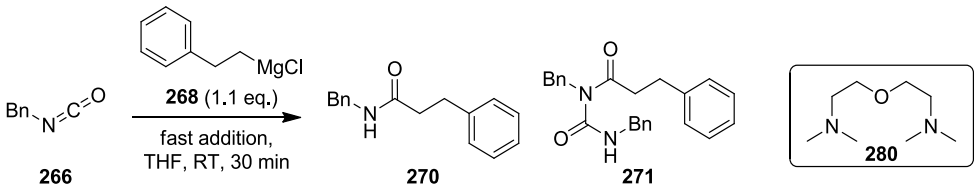


| Entry | Additive | Amide (270) yield (%)[a] | Acylurea (271) yield (%)[a] |
|---|---|---|---|
| **1** | None | 69 | 9 |
| **2** | TMSCl | 69 | 1 |
| **3** | TBSCl | 54 | 11 |
| **4** | LiCl | 24 | 32 |
| **5** | LiBr | 18 | 27 |
| **6** | $MgCl_2$ | 62 | 12 |
| **7** | TMEDA | 57 | 13 |
| **8** | NMP | 42 | 7 |
| **9** | CuI | 82 | 4 |
| **10** | bis[2-(*N*,*N*-dimethylamino)ethyl] ether (**280**) | 41 | 18 |

**Table 15** – Initial screen of additives, performed in batch. [a]Yields calculated by HPLC, using anisole as an internal standard.

Surprisingly, the anticipated disaggregating agents (LiCl,[217] LiBr, and $MgCl_2$; entries 4 to 6) seemed to encourage the overreaction pathway, perhaps due to disaggregation of the reactive intermediate (**278**). Bis[2-(*N*,*N*-dimethylamino)ethyl] ether (**280**, entry 10) was also found to increase the yield of acylurea by-product (**271**), which is perhaps unsurprising, as it has previously been demonstrated to reduce Grignard reagent reactivity through coordination.[218] Importantly though, several additives gave a marked decrease in the quantity of acylurea by-product (**271**), most notably TMSCl (entry 2) and CuI (entry 9). Accordingly, these additives were screened further, examining other copper salts, and by determining the effect of differing TMSCl loadings, using both fast and slow addition regimes (**Table 16** and **Table 17**).

| Entry | Additive | Quantity (eq.) | Amide (270) yield (%)[a] | Acylurea (271) yield (%)[a] |
|---|---|---|---|---|
| 1 | None | - | 69 | 9 |
| 2[b] | None | - | 21 | 27 |
| 3 | CuI | 1 | 82 | 4 |
| 4 | CuCl | 1 | 69 | 6 |
| 5 | CuBr | 1 | 71 | 3 |
| 6 | $Cu(OAc)_2$ | 1 | 25 | 19 |
| 7 | $Cu(acac)_2$ | 1 | 31 | 16 |
| 8 | $Cu(OTf)_2$ | 1 | 21 | 7 |
| 9 | $CuBr_2$ | 1 | 66 | 6 |
| 10 | CuI | 0.1 | 61 | 2 |
| 11[b] | CuI | 0.1 | 10 | 4 |
| 12 | CuCl | 0.1 | 70 | 6 |
| 13 | CuBr | 0.1 | 63 | 5 |
| 14 | $Cu(OAc)_2$ | 0.1 | 49 | 6 |
| 15 | $Cu(acac)_2$ | 0.1 | 64 | 9 |
| 16 | $Cu(OTf)_2$ | 0.1 | 65 | 5 |
| 17 | $CuBr_2$ | 0.1 | 78 | 2 |

**Table 16** – Further screening of copper salts as additives, at stoichiometric and substoichiometric loadings. [a]Yields calculated by HPLC, using anisole as an internal standard. [b]Grignard reagent was added evenly over 5 minutes, using a syringe pump.

From the variety of Cu (I) and Cu (II) salts screened, no clear trend was observed between the two oxidation states. The majority of experiments saw a decrease in acylurea by-product (**271**) (aside from stoichiometric $Cu(OAc)_2$ and $Cu(acac)_2$, entries 6 and 7), but also a decrease in the yield of amide (**270**). Most additives appeared to have superior effect at substoichiometric loadings (entries 10 to 17), aside from the initial hit (CuI, entries 3 and 10). The most promising result was that of $CuBr_2$ at a loading of 0.1 equivalents (entry 17), which reduced the acylurea by-product (**271**) to 2%, yet also reinforced the yield of desired product (**270**).

| Entry | Additive (eq.) | Addition regime | Amide (270) yield (%)[a] | Acylurea (271) yield (%)[a] |
|---|---|---|---|---|
| 1 | None | Fast | 69 | 9 |
| 2 | TMSCl (0.1) | Fast | 47 | 4 |
| 3 | TMSCl (0.5) | Fast | 74 | 3 |
| 4 | TMSCl (1.0) | Fast | 73 | 1 |
| 5 | TMSCl (2.0) | Fast | 58 | 2 |
| 6 | None | Slow[b] | 21 | 27 |
| 7 | TMSCl (0.1) | Slow[b] | 12 | 3 |
| 8 | TMSCl (0.5) | Slow[b] | 28 | 3 |
| 9 | TMSCl (1.0) | Slow[b] | 28 | 2 |
| 10 | TMSCl (2.0) | Slow[b] | 29 | 1 |

**Table 17** – Further screening, including altered quantities, and fast/slow addition regimes. [a]Yields calculated by HPLC, using anisole as an internal standard. [b]Grignard reagent was added evenly over 5 minutes, using a syringe pump.

The TMSCl experiments at a fast addition rate (**Table 17**, entries 2 to 5) showed that half an equivalent of the additive is likely to be sufficient to reduce the acylurea by-product (**271**) to an acceptable level, but also maintain a good level of amide product (**270**) (entry 3). Higher loadings of this electrophile are hypothesised to interfere with the Grignard reagent, reducing the amide (**270**) yield (entry 5). When considering a slower Grignard (**268**) addition (entries 6 to 10), a poorer yield was observed in every case if TMSCl was used, despite suppressing acylurea (**271**) formation. The reduced amount of overreaction in all cases suggests that this additive is working by reacting with the metalated intermediate (**278**) before being hydrolysed to yield the amide upon workup (**Scheme 45**). However, other unproductive reaction pathways are assumed to reduce the desired amide yield in many cases.

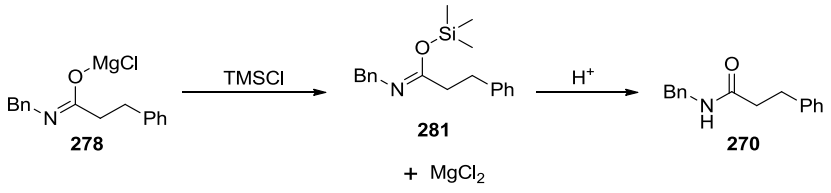


**Scheme 45** - Proposed mechanism for prevention of acylurea (**271**) formation by TMSCl, involving transient protection of the amide nitrogen (**281**).

The screens performed so far highlighted TMSCl and $CuBr_2$ as the most promising additives in batch. In order to transfer this to the flow chemistry system, further experiments were performed against an additive-free benchmark (**Table 18**). Gratifyingly, both additives were found to improve the yield of amide product (**270**), whilst decreasing the quantity of acylurea by-product (**271**) observed. $CuBr_2$ displayed slightly better performance (entry 3), and since lower than 10 mol% (0.1 eq.) loading had not been examined in batch, further experiments were conducted to verify the required quantity.

| Entry | Additive | Quantity (eq.) | Amide (270) yield (%)[a] | Acylurea (271) yield (%)[a] |
|---|---|---|---|---|
| 1 | None | - | 85 | 5 |
| 2 | TMSCl | 0.5 | 94 | 2 |
| 3 | $CuBr_2$ | 0.1 | 95 | 2 |
| 4 | $CuBr_2$ | 0.01 | 98 | 1 |
| 5 | $CuBr_2$ | 0.001 | 84 | 5 |
| 6 | $CuBr_2$ | 0.005 | 92 | 2 |

**Table 18** - Examination of additive effect and quantities in flow. [a]Yields calculated by HPLC, using anisole as an internal standard. The results shown were obtained by averaging the assay yields of 5 samples, taken sequentially throughout an experimental run.

Decreasing $CuBr_2$ loading to 1 mol% (0.01 eq., entry 4) gave an improved result, in terms of increased desired product (**270**) yield, and decreased acylurea by-product (**271**) yield. Further lowering this loading to 0.1 mol% (0.001 eq., entry 5), however, reverted back to a similar profile to that seen with no additive. An intermediate loading of 0.5 mol% (0.005 eq., entry 6) resulted in a moderate reaction profile, which was poorer than the previous best. Accordingly, 1 mol% was taken as the ideal additive loading, and an excellent yield of 96% was isolated using these conditions (**Scheme 46**).

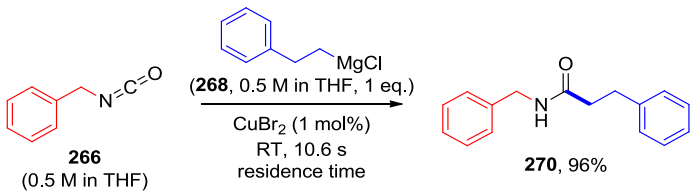


**Scheme 46** - Optimised reaction in flow with isolated yield. The desired product (**270**) was isolated from collecting a sample of 10 mL combined flow volume (2.5 mmol of both starting materials).

### 3.2.3. Further application of flow protocol

*3.2.3.1. Substrate scope with respect to isocyanate*

With the optimal conditions in hand, the substrate scope was examined, in both Grignard reagents and isocyanates. As this method's novelty lies mostly in the ability to use unhindered isocyanates, the range of isocyanates was looked at in more detail than the corresponding Grignard reagents. Accordingly, a range of aryl, benzyl and alkyl isocyanates were subjected to the standard reaction conditions, in order to assess functional group tolerance, and performance with each class of reactants (**Scheme 47**).

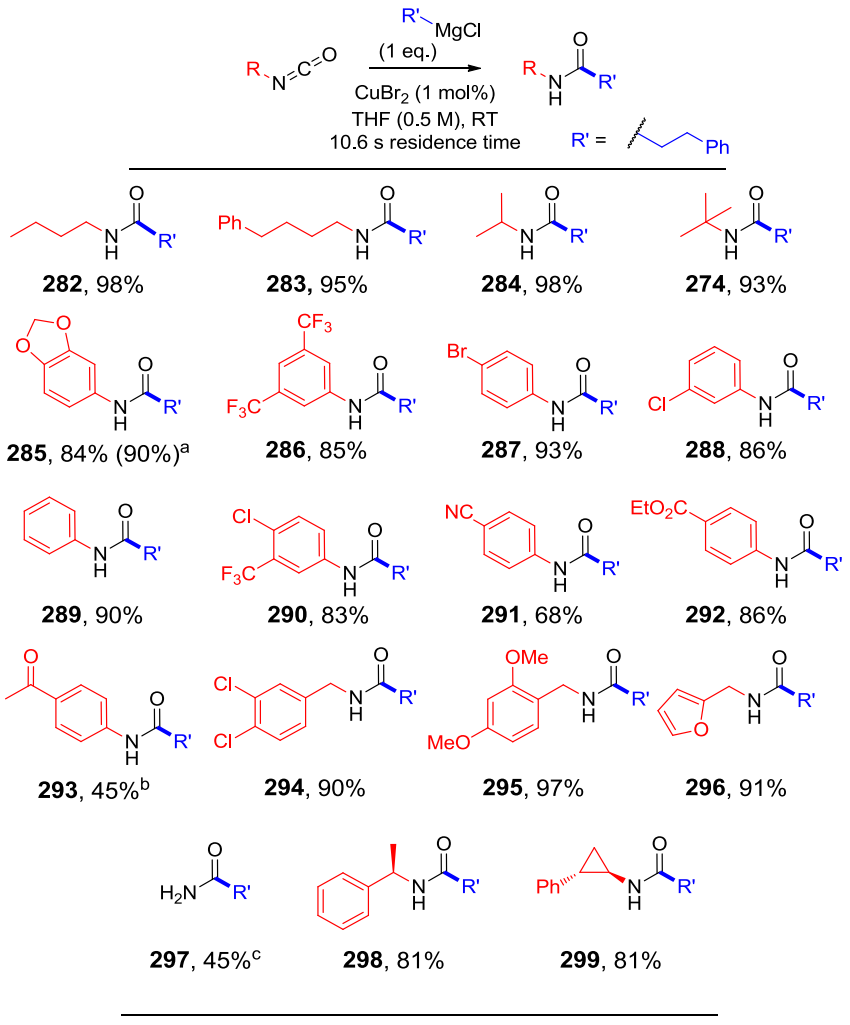


**Scheme 47** - Substrate scope of amidation, in isocyanate. [a]5 mol% $CuBr_2$ was used. [b]Reaction was performed at 0 °C. [c]The desired product formed from TMSNCO, which deprotected in the reaction quench.

Gratifyingly, the optimised conditions were found to give excellent results with the vast majority of isocyanates examined, including primary, secondary and tertiary alkyl (**282**, **284** and **274**), simple aryl (**289**), and substituted benzylic examples (**294** and **295**). Notably, this demonstrates the applicability of the reaction protocol to any level of steric bulk around the isocyanate, with a bulky example (**274** ) performing comparably with the previously published method.[187] Further results of note include: successful reaction in the presence of an ester group (**292**) without lowering the reaction temperature, and the coupling of a particularly electron-deficient aryl isocyanate (**286**), as this amide would be challenging to synthesise using standard amide coupling procedures.

Electronic variation on aryl rings was well tolerated in general, with similar yields achieved for unsubstituted (**289**), electron-rich (**285**) and electron-poor (**286** and **290**) aryl isocyanates. Furthermore, the successful inclusion of an aryl bromide or chloride substituent (**287** and **288**) provides a handle for further functionalisation in the product through transition metal-catalysed cross-coupling chemistry. An isocyanate containing an enolisable ketone (**293**) was reacted with some success, when using a lower reaction temperature. This implies that some extent of nucleophilic addition is occurring at a similar timescale to deprotonation α to the ketone, and furthermore, that the isocyanate is reacting as an electrophile preferably over the ketone. Finally, a primary amide (**297**) could be formed, albeit in a less favourable 45% yield, from the trimethylsilyl protected isocyanate. This drop in yield may be due to some extent of TMS deprotection *in situ,* causing problematic side reactions.

The methodology does not tolerate the processing of suspensions, hence is not suitable for insoluble starting materials. A selection of substituted aryl isocyanates (such as **300** and **301**, **Scheme 48**) were found to have no appreciable solubility in the standard THF reaction solvent. This was also observed with the pyridyl isocyanate (**302**), but a small screen of solvents found NMP to be sufficiently solubilising. This led to a flow reaction where the isocyanate (**302**) and $CuBr_2$ were dissolved in NMP, whilst the Grignard reagent stream remained in THF. The resulting reaction performed poorly, giving the isocyanate's symmetrical urea decomposition product (**303**). This could be, in part, due to ligation of $CuBr_2$ by NMP, or the poorer mixing profile as a consequence of using two different solvents.

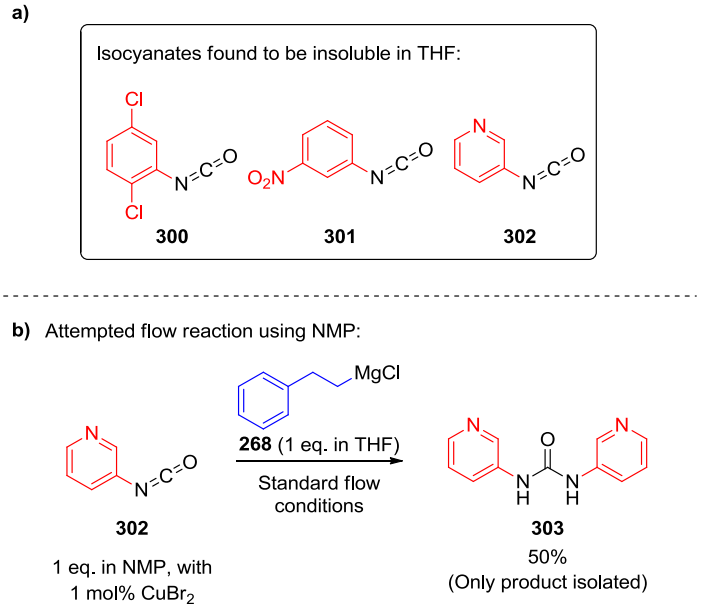


**Scheme 48 - a)** Isocyanate starting materials which were found to be insoluble in THF, hence unfit for the standard reaction protocol in flow. **b)** Result of flow reaction using NMP to solvate the heterocyclic isocyanate (**302**). The yield of urea product (**303**) was calculated based on isocyanate input material.

In order to examine a more drug-like motif, it was decided that a saturated nitrogen heterocycle would be suitable, due to their common occurrence in medicinal chemistry programmes.[219,220,221] Accordingly, the isocyanate (**305**) was synthesised by a Curtius rearrangement from the corresponding Cbz-protected carboxylic acid (**304**, **Scheme 49**). A poor yield of 38% was isolated, which was attributed to decomposition on the silica column during chromatography, since previous analysis had shown a relatively clean reaction profile. The quantity isolated was sufficient for subsequent reaction, but should synthesis of this isocyanate be required again, purification using alumina, or a fast manual column should be attempted. Upon subjecting this isocyanate to the previously developed flow conditions, the expected amide product (**306**) was isolated in 89% yield, demonstrating that this method can be applied to medicinally-relevant isocyanate components.

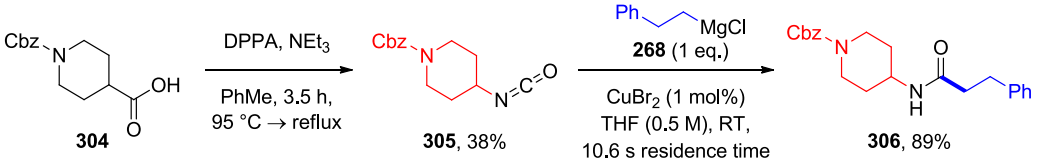


**Scheme 49** - Formation and flow reaction of saturated heterocyclic isocyanate (**305**).

*3.2.3.2. Substrate scope with respect to Grignard reagent*

The substrate scope was then examined with respect to the Grignard reagent (**Scheme 50**). Simple aryl (**307**), benzyl (**308**), and vinyl (**309**) reagents performed exceptionally, even where the magnesium bromide reagents were used. There was tolerance for a range of functional groups within the Grignard reagent. An aryl chloride remained intact (**311**), as well as a THP-protected phenol substrate (**312**) isolated as the protected product, and a bis(trimethylsilyl) protected aniline (**313**) whose protecting group was removed during a dilute acidic workup. Furthermore, a heteroaryl Grignard reagent reacted efficiently to give the thienyl amide product (**314**), adding to the possibilities for further functionalisation within the products of these reactions.

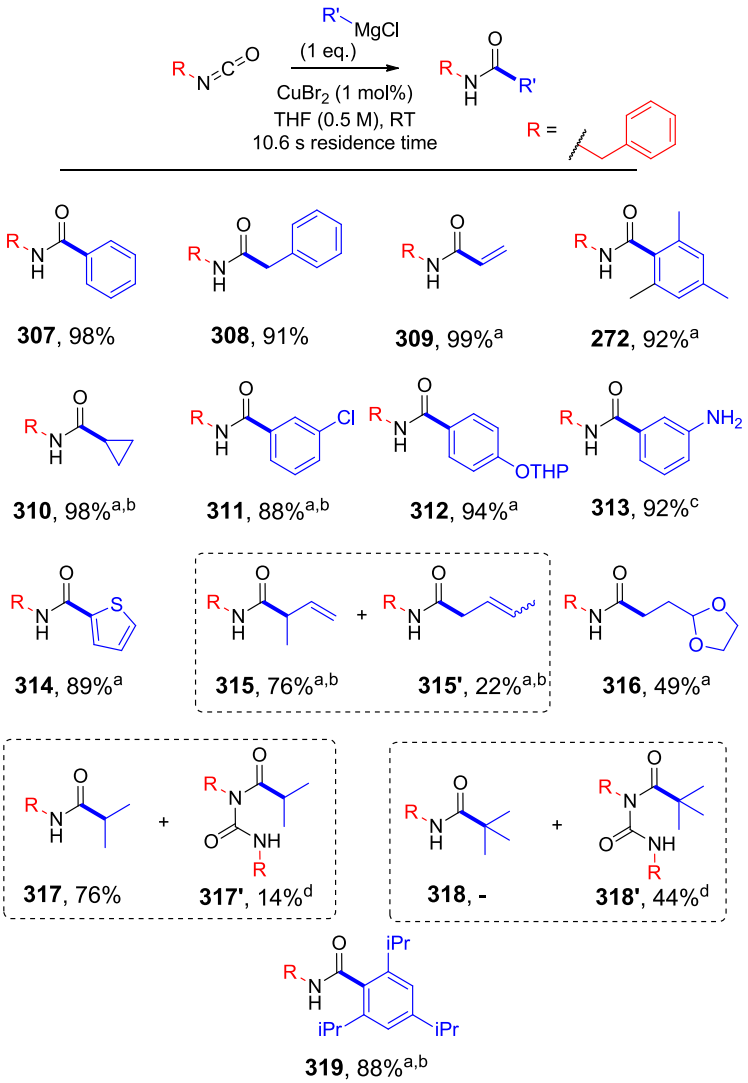


**Scheme 50** - Substrate scope of amidation, in Grignard reagent. [a]The MgBr Grignard reagent was used, in place of MgCl reagent. [b]This reaction was performed at 0.25 M concentration, due to Grignard availability. [c]The desired product was formed from $ArN(TMS)_2$, which deprotected in the reaction quench of dilute HCl. [d]Yield of acylurea by-products were calculated with respect to the isocyanate starting material.

Reaction with a substituted allyl Grignard reagent produced two regioisomeric products (**315** and **315'**). By far the most major of the two was the expected reaction through the secondary carbon (giving **315** in 76% yield), but attack through the less hindered end of the olefin was also observed (**315'**), giving an uneven mixture of *E*- and *Z*-isomers. A less productive Grignard reagent was an alkyl example containing a protected aldehyde functionality (**320**), which yielded 49% of its corresponding product (**316**). The lower yield of the desired amide (**316**) is thought to be caused by the reduced nucleophilicity of this specific Grignard reagent,

arising from stabilisation imbued by electron donation from oxygen to the metal centre (**Figure 26**).[222]

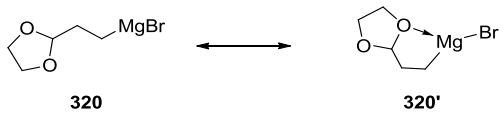


**Figure 26** - Intramolecular Lewis Acid/Base interaction, limiting nucleophilicity of the Grignard reagent (**320**).

Secondary (product **317**) and tertiary (product **318**) alkyl Grignards were examined, and found to be less effective. Reaction with isopropylmagnesium chloride gave an acceptable 76% yield, alongside a 14% yield of its corresponding acylurea by-product (**317'**). However, when the less nucleophilic *tert*-butylmagnesium chloride was employed, the desired amide product (**318**) could not be isolated from the crude mixture, found to be comprised mostly the expected acylurea by-product (**318'**) which was isolated in 44% yield. This was thought to be attributable to poor reactivity arising from steric hindrance. However, the significantly hindered 2,4,6-triisopropylphenyl product (**319**) was isolated in an excellent 88% yield, implying that the poor reactivity may be limited only to hindered *alkyl* Grignards. Cyclopropylmagnesium bromide gave its corresponding product (**310**) in almost quantitative yield, presumably as it is a significantly less hindered secondary alkyl group, when compared with isopropylmagnesium chloride.

Utilising a Grignard exchange protocol was expected to increase the scope of these reactions, allowing formation of an arylmagnesium halide reagent, followed by its reaction with an isocyanate in the developed flow methodology. Reagents for Grignard exchange reactions have been well studied, in particular by the group of Knochel, who pioneered LiCl as a disaggregating agent, displaying improved reactivity and functional group tolerance.[223,224,225] The reagent now known as "Turbo Grignard" (iPrMgCl.LiCl) has become one of the most readily used reagents in this field[217] and, accordingly, it should be straightforward to employ a previously demonstrated Grignard formation in batch, then introduce the metalated species to a flow reaction (**Scheme 51**).[226]

The commercially available functionalised pyrimidine (**321)** was brominated smoothly, providing the Grignard exchange precursor (**322**) in almost quantitative yield (**Scheme 51**).

The aryl Grignard reagent (**323**) was then generated successfully, with 99% of the protodehalogenated material (**321**) observed by HPLC. The Grignard reagent as a thin suspension caused no issues when pumped through the standard flow reactor. However, the desired amide product (**324**) was isolated in a poor 44% yield, after column chromatography, alongside 24% (with respect to isocyanate) of the expected acylurea by-product (**324'**), as well as 8% of the protonated arene (**321**).

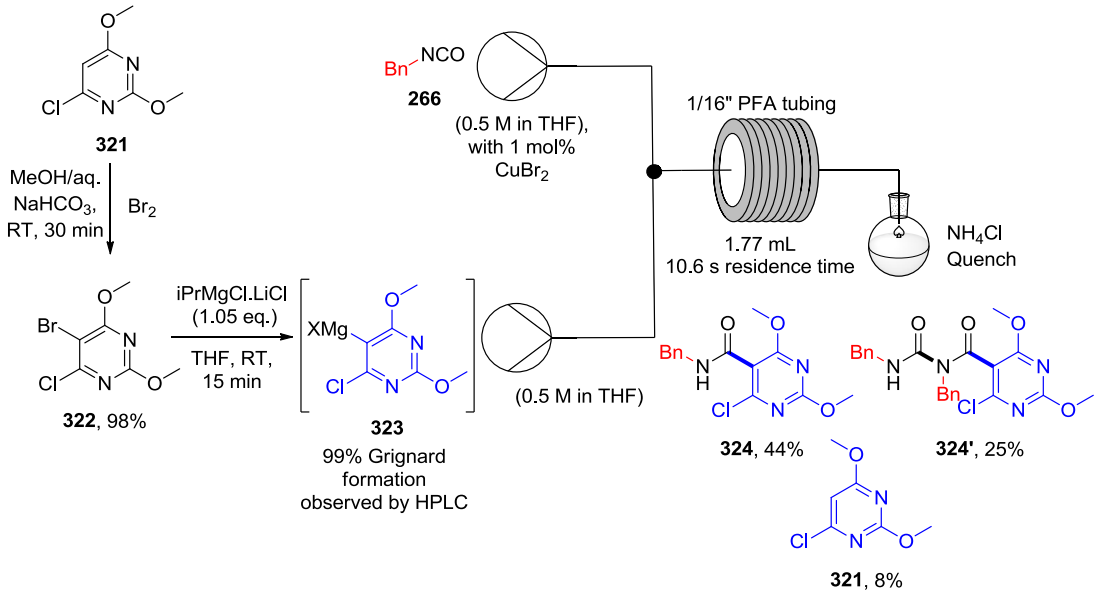


**Scheme 51** - Formation and reaction of heavily functionalised pyrimidine Grignard reagent (**323**).

The poor ratio of products was initially attributed to the inclusion of lithium chloride, which has previously been examined as an additive in batch, and vastly increased acylurea formation (**Table 15**, entry 4). Subsequently, the reaction was attempted using $^{i}$PrMgCl (without the LiCl adduct), displaying similar performance in the arylmagnesium (**323**) formation (94% conversion seen by HPLC, in under 2 minutes). Disappointingly though, the resulting flow reaction gave an even poorer ratio of products by HPLC, with additional impurities observed. The lack of success in this system is hypothesised to be simply due to the poor nucleophilicity of the electron-deficient and sterically hindered aromatic Grignard species, compared with other aryl Grignard reagents, examined previously.

*3.2.3.3. Larger scale application in flow*

Finally, although the developed methodology was assumed to be scalable due to the application of flow chemistry, it was desirable to demonstrate this scalability within the developed methodology. Accordingly, the standard syringe pump setup was equipped with the largest disposable syringes available (60 mL), filled with both reactants, and run continuously without fault for 12 minutes. It should be noted that due to the fast rate of reaction and flow rates used, this continuous run constitutes 68 residence times, which represents a significant successful demonstration within the scope of this work. An appreciably scaled-up quantity of the amide product (**270**, 6.6 g) was isolated, equating to 95% yield, following simply washing the crude solid with heptane (**Scheme 52**). This compares well with the 96% yield isolated on a smaller (2.5 mmol, 600 mg) scale, and the small loss of yield is assumed to be due to having collected all processed material rather than a sub-sample. Flow systems take a short time to achieve steady state, which was not accounted for in this larger scale demonstration.

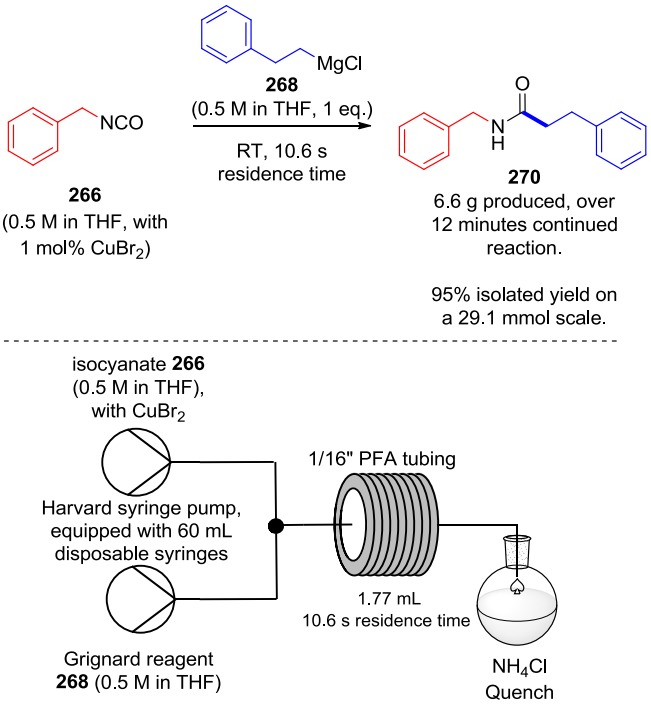


**Scheme 52** - Reaction scheme and schematic for larger scale amide (**270**) formation.

### 3.2.4. Determining the role of $CuBr_2$

*3.2.4.1. QCL-IR experimental setup*

Despite the successful application of this methodology to a range of substrates, the role of $CuBr_2$ within the reaction mechanism has not been determined thus far. Elucidation of such mechanistic information would be challenging by conventional techniques, due to the inherently fast kinetics of this reaction. Therefore, quantum cascade laser infrared microscopy (QCL-IR) was employed as an *in situ* analytical technique. This technique has been developed to obtain improved image resolution and accuracy by mid-IR imaging, rather than Fourier transform infrared (FT-IR), as used in most *in situ* IR spectroscopic techniques.[227,228] Moreover, the higher flux of a QCL-based IR source, compared to standard globular IR sources, allows improved penetration to a distance greater than 100 μm: the microreactor channel depth used in this configuration.

Proof of concept has been demonstrated previously for the use of QCL-IR with a microfluidic reactor, to obtain kinetic information regarding a fast organic reaction performed in flow.[229] Therein, semi-continuous quantification of reaction progress was recorded along a pathway, created by a PTFE gasket sandwiched between two $CaF_2$ disks (**Figure 27a**). This was achieved by continuous recording within a 2 mm × 2 mm window, at a resolution of 480 × 480 pixels (**Figure 27b**). Each of these 230,400 pixels yields an infrared spectrum, which can be converted to product concentrations by analysing known concentrations and setting up a calibration curve. The reaction pathway was specifically designed in order to ensure complete mixing of both input streams at a flow rate of 1 mL $min^{-1}$, by the end of the smaller serpentine channel, consisting of seven turns.

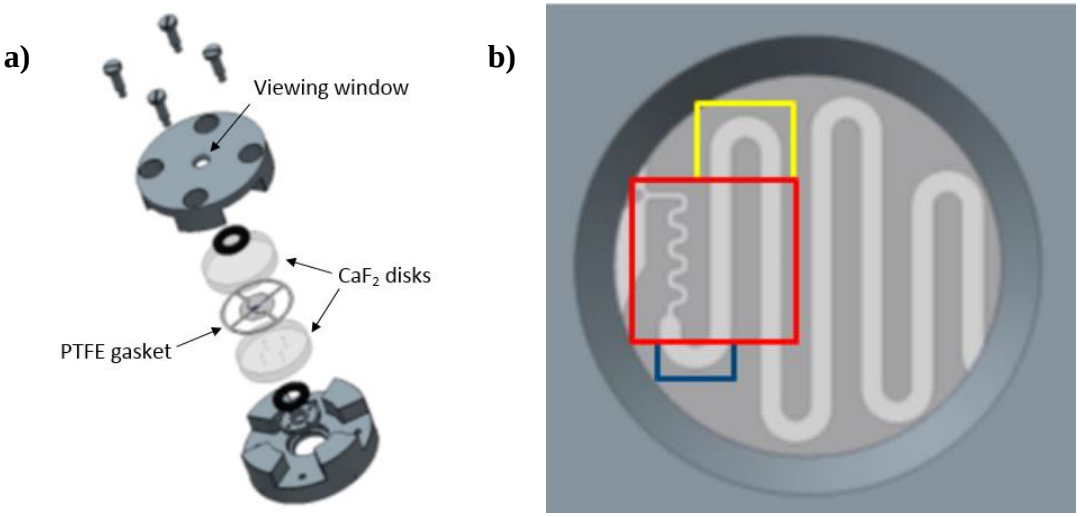


**Figure 27** - Schematics of the reaction pathway used for QCL-IR analysis. **a)** An exploded diagram of the microreactor setup. **b)** A schematic of the reaction pathway, showing the visible section (red) and the two parts of the reaction pathway which are not visible (blue and yellow). Diagrams reproduced from the referenced journal article, with the author's permission.[229]

Using the same reaction setup, the standard reaction (**Figure 28a**) was probed, under copper-free conditions (**Figure 28b**), then with 1 mol% $CuBr_2$ (**Figure 28c**). At first glance, there is an obvious qualitative increase in reaction rate when $CuBr_2$ is used. Perhaps even more interesting, though, is the observation of "hot spots" in only the reaction without $CuBr_2$ (circled in red, in **Figure 28b**). QCL-IR allows real-time detection of regions in which there is an increased concentration of the desired product. This corresponds to gumming, or even solid formation, issues which are known to be problematic in flow chemistry, particularly when using organometallic reagents.[65,230,231] It had initially been expected that small particles of undissolved $CuBr_2$ may act as aggregation points for solid formation, increasing the propensity for blockages. In fact, the opposite effect was observed.

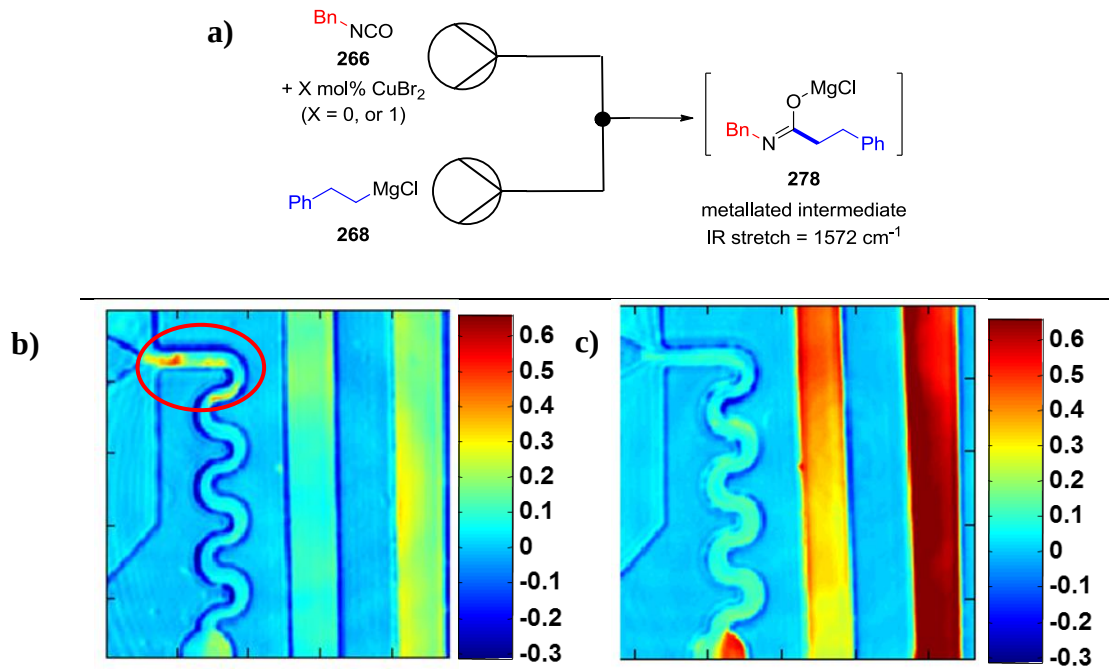


**Figure 28** - QCL-IR heat map traces from the standard reaction **a)**, detecting the metalated intermediate (**278**) in the following cases: **b)** without copper (hot spots, thought to correspond to gumming points, are circled in red) and **c)** with 1 mol% $CuBr_2$. These heat maps are coloured by absorption at 1572 $cm^{-1}$, in arbitrary absorption units.

In every run without a copper additive, hot spots of product formation were observed in the section immediately after the two streams met. These hot spots generally persisted throughout the entire run, implying solid formation which was not being cleared, or a perpetual gumming point. When considering the impact of these instances on a large-scale flow system, they would result in a non-uniform flow regime, giving pressure fluctuations, and potential blockage formation throughout the course of reaction. Conversely, the reaction using $CuBr_2$ was repeatedly shown to display none of these hot spots, conveying a considerable practical advantage. This is expected to be due to formation of more soluble mixed-metal aggregates of the intermediate species (**278**).

*3.2.4.2. Quantitative analysis using QCL-IR*

To allow quantitative analysis, conversion from arbitrary absorption units to concentration was required, using a calibration curve. As the metalated intermediate (**278**) was the quantifiable species, this could not be isolated and introduced into the reactor in known concentrations. Instead, it was expected that the reaction product could be instantaneously deprotonated using the Grignard reagent (**268**) as a base, forming the same metalated intermediate (**278**, **Scheme**

**53**). Pleasingly, complete deprotonation was observed by the end of the smaller volume serpentine mixing channel for most concentrations, and by the end of the total observable 14 ms residence time, for every concentration. The resulting absorption values at each known concentration were then used to plot a calibration curve (**Figure 29**), which demonstrated a good linear fit ($r^2$ = 0.9907).

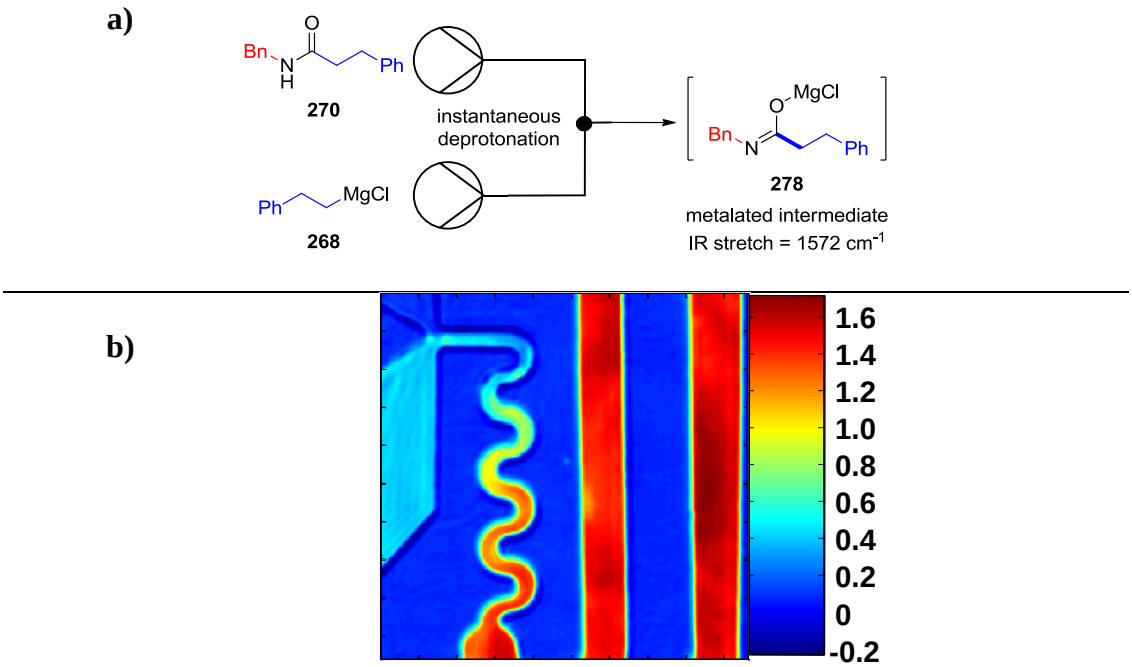


**Scheme 53** - **a)** Deprotonation of the reaction product to form the same metalated intermediate (**278**), for quantification, using a calibration curve. **b)** A sample heat map image of an instantaneous deprotonation, showing reaction progression within the serpentine mixing section, and complete reaction prior to the end of the channel.

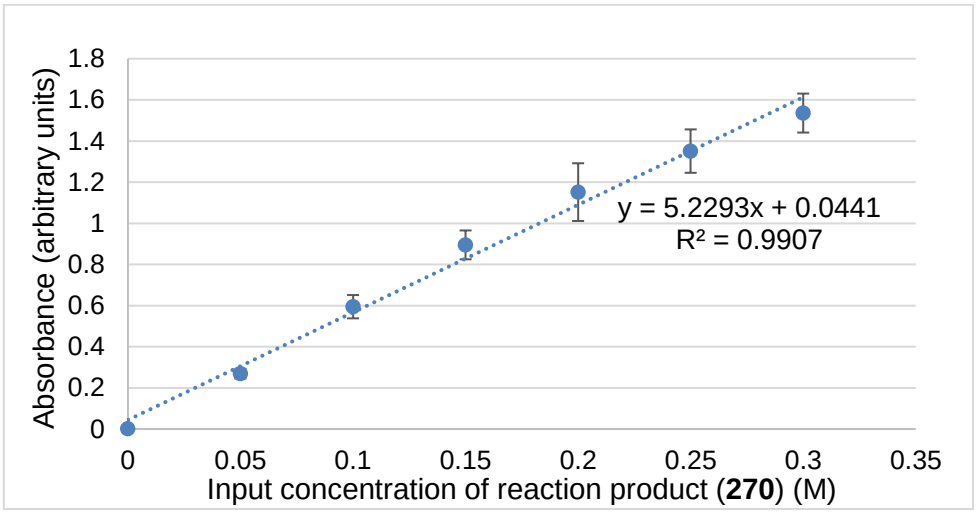


**Figure 29** - Calibration curve showing input concentration, versus absorbance observed by QCL-IR.

Following on from this, several combinations of reactant concentrations were examined, whilst ensuring to keep the concentration of Grignard (**268**) equivalent to, or in excess of isocyanate (**266**), to prevent formation of the undesired acylurea by-product (**271**). The most significant of these results showed the impact of $CuBr_2$ loading (**Figure 30**). It is clear that an increased $CuBr_2$ loading increases the rate of reaction, with only 16% of the desired product generated by the end of the reaction pathway in the copper-free reaction, compared with over 70% in the instance of a 3 mol% $CuBr_2$ loading.

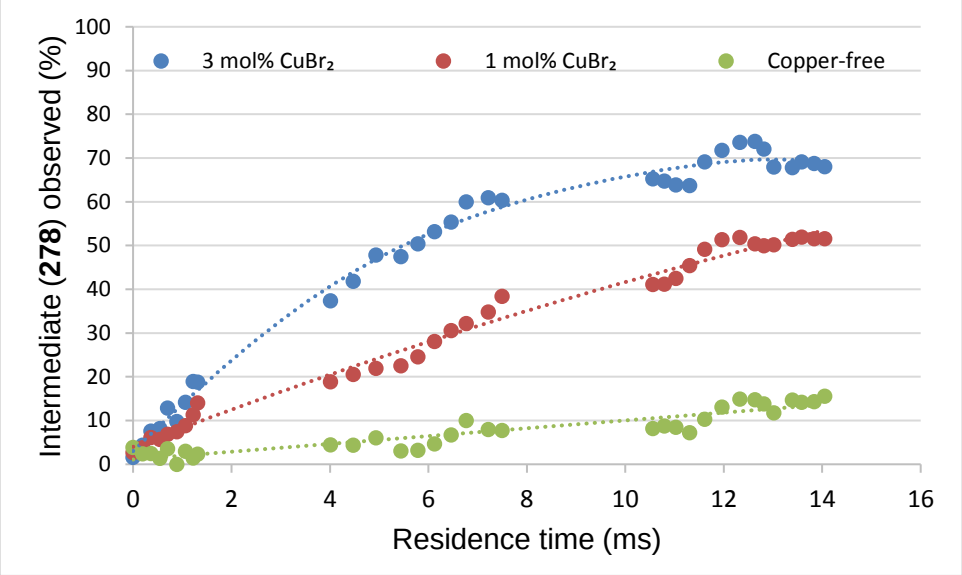


**Figure 30** - Impact of $CuBr_2$ loading upon the reaction rate, presenting product formation (using a calibration curve), versus time.

Unfortunately, varying the other reactant concentrations gave no significant insight into reaction mechanism. Analysis of this data, using kinetics software DynoChem,[232,233,234] and the analytical techniques Reaction Progress Kinetic Analysis (RPKA),[235,236] and Variable Time Normalisation Analysis (VTNA),[237,238] was thought to be limited by the linearity of the data obtained thus far. As the short residence time allowed only relatively low conversion in most cases, very little curvature in the kinetic profile was observed, so these techniques did not provide any insight to the rate equation.

Using the limited kinetic data, and literature precedence at hand, it has been possible to propose a tentative reaction mechanism. There are numerous reports of isocyanate formation through copper-[239,240] or palladium-catalysed[241,242] reaction with cyanate anion. Of particular interest in

this case, is the success of $CuBr_2$ in catalysing the reaction of potassium cyanate (**325**) with aryl boronic acids (**327**), forming the isocyanate (**330**), which is then quenched with an alcohol, yielding aryl carbamate species (**331**).[240] This publication invokes a mechanism (**Scheme 54**) in which the cyanate anion coordinates to copper (**326**), followed by a transmetalation of the organoboron species (to give intermediate **328**), then oxidation to a Cu(III) species (**329**), which reductively eliminates the isocyanate (**330**).

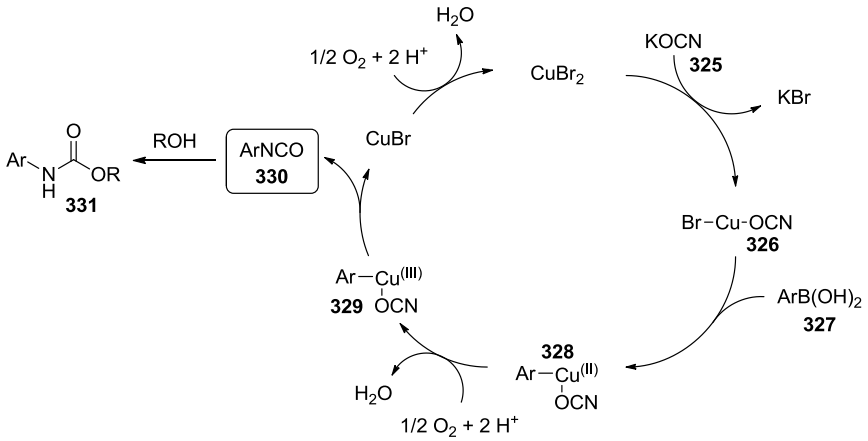


**Scheme 54** - Mechanism previously proposed for $CuBr_2$-catalysed isocyanate formation.[240]

Although the details of this catalytic cycle are not well explained, nor have any reported evidence to support them, the implication of catalytically active $CuBr_2$ in the proposed cycle is significant with respect to this work. The system developed here does not have the strongly binding cyanate anion, yet may operate through a looser coordination of the isocyanate to Cu(II) (species **332**), followed by a facile transmetalation event with the Grignard reagent (**268**), forming an alkylcopper species (**333**), which is set up to readily attack the isocyanate. Salt exchange of the imidate anion to the oxophilic MgCl would regenerate $CuBr_2$ (**Scheme 55**).

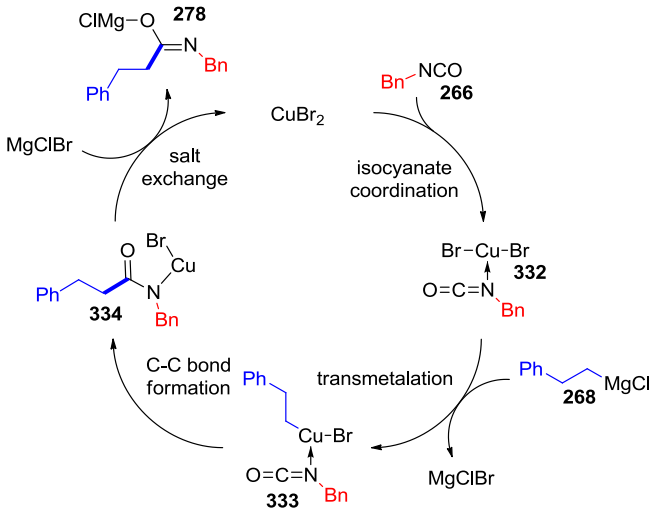


**Scheme 55** - Proposed mechanism of $CuBr_2$-catalysed reaction of Grignard reagents (**268**) with isocyanates (**266**).

Previously, a reaction was attempted in batch, where the Grignard reagent was mixed with 1 equivalent of $CuBr_2$, prior to its addition of the isocyanate solution. The resulting reaction profile was poor, suggesting that the reaction does not proceed through stoichiometric formation of a cuprate nucleophile. Furthermore, an attempt was made to generate the isocyanate-$CuBr_2$ complex (**332**), observing any shift in the isocyanate signal by IR spectroscopy. However, no significant change in the isocyanate stretch was observed, implying that any interaction here is relatively weak. This is not sufficient evidence to rule out the proposed mechanism though, and further work is required.

Despite the relatively low energy barrier to C-C bond formation in the uncatalysed reaction, it could be envisioned that a transmetalation event could proceed even more quickly. However, there is no experimental evidence to support this type of mechanism thus far. Moreover, the reaction could be progressing simply through Lewis acid activation of the isocyanate moiety. This could be disproved by examining the kinetic behaviour of the reaction under the influence of various Lewis acidic additives. Any further mechanistic work would benefit heavily from the continued use of the QCL-IR analytical platform.

## 3.3. Conclusions and future work

### 3.3.1. Conclusions

An effective amide forming protocol has been developed, through in-depth analysis of reaction kinetics, successfully tackling the acylurea by-product (**270**) formed when using current literature conditions. The implementation of flow chemistry has afforded excellent mixing of the two reactant solutions, which was found to be indispensable in the productive reaction of an unhindered isocyanate. Whilst a good yield was obtained using these standard flow conditions, targeted additive screening found $CuBr_2$ to further favour formation of the desired amide product (**270**), resulting in an excellent 96% isolated yield of the standard test reaction.

When examining further substrates, high yields were obtained in almost all cases, with no change to the optimised conditions. This method is particularly beneficial in successfully yielding amides which would prove troublesome in traditional amide coupling reactions, such as the coupling of a strongly electron-deficient aniline (**286**, **Scheme 47**). Furthermore, excellent functional group tolerance was observed considering the use of an organometallic reagent, allowing synthesis of products containing ester, amine, primary amide, aryl halide, and protected phenol functionalities (**292**, **313**, **297**, **310**, and **312**, **Scheme 47** and **Scheme 50**).

Exemplary mass efficiency was also achieved, with a 1:1 stoichiometry used in every case, and only 1 mol% of $CuBr_2$ additive, resulting in a very high mass incorporation. Importantly, $MgCl_2$ is the sole by-product, is non-toxic, and easily removed into the aqueous layer upon quench. Furthermore, these reactions are performed at ambient temperature, avoiding the need for cooling, as in similar protocols. These attributes align well with The Twelve Principles of Green Chemistry,[207] reinforcing the reported protocol's suitability as an industrially applicable amide bond forming method for use in fine chemical manufacture, particularly as flow chemistry conveys inherent scalability. This was illustrated in a 12-minute-long continuous reaction (**Scheme 52**), representing 68 residence times, which preserved the yield and reaction profile seen on smaller scale.

Finally, work towards understanding the role of $CuBr_2$ has shown that it substantially enhances the rate of reaction. This has been demonstrated by the use of *in situ* infrared kinetic monitoring, which has also revealed practical benefits of $CuBr_2$, in promoting homogeneity throughout the reaction. These insights will be valuable in future reaction optimisation and application, but also provide useful information on any engineering concerns for the scale-up of this reaction.

### 3.3.2. Future work

*3.3.2.1. In situ Grignard formation*

Further work on this methodology would likely include incorporating the Grignard reagent formation step into the continuous flow system (**Figure 31**). The formation of Grignard reagents in flow has been demonstrated in many cases by magnesium-halogen exchange using Turbo Grignard ($^{i}$PrMgCl.LiCl).[217] This exchange process has been previously studied using a flow ReactIR cell with both bromine and iodine leaving groups,[243] where aryl iodides are estimated to undergo exchange around $10^5$ times faster than the corresponding bromides.[244] Although there was some success achieved in pre-preparing the Grignard reagent in batch (**Scheme 51**), it is expected that more nucleophilic aryl substrates would perform more favourably in these reactions. Furthermore, adoption of Grignard generation in flow would allow the use of organometallic reagents bearing more sensitive functional groups (e.g. ester and nitrile groups), improving tolerance to these amidation reactions at a later stage of fine chemical synthesis.

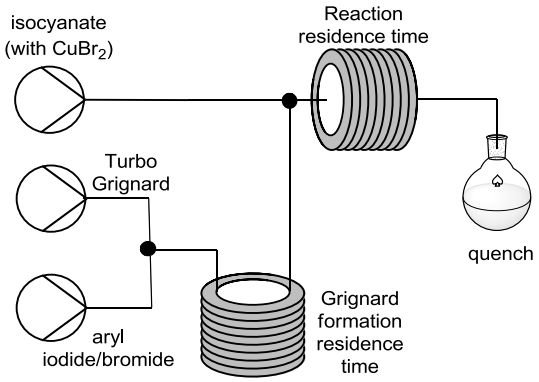


**Figure 31** - Schematic representation of the proposed Grignard formation and reaction in continuous flow.

It is expected that *in situ* metalation, prior to amidation, could also be achieved through deprotonation using a magnesium amide Turbo-Hauser base (for example, TMPMgCl.LiCl).[245,246] This may obviate pre-halogenating the aryl unit, to allow for complementary reactivity, and invoke the transformation as a late-stage functionalisation technique.[247] Furthermore, this protocol could be extended to organolithium reagents, formed by deprotonation or metal-halogen exchange, further expanding the possible substrate scope. It is unknown whether the $CuBr_2$-accelerated reaction would behave analogously to the

Grignard case, however a transmetalation to magnesium, forming the Grignard reagent, could be performed in a straightforward manner prior to reaction.[248,249]

*3.3.2.2. Synthesis of tertiary amides*

A valuable extension of this work would involve the formation of tertiary amides (**339**) directly. Whilst this was observed as an undesired side reaction in the work described here, it could theoretically be harnessed as a productive reaction pathway (**Scheme 56**). A major restriction of using isocyanates (**335**) in amidation is the limitation to secondary amide products. However, it could be envisioned that after reaction of the Grignard reagent (**336**) as a nucleophile, the resulting metalated species (**337**) could act as a deprotonated amide for further reaction with an electrophile (**338**). This strategy would allow for excellent mass efficiency in furnishing tertiary amide products (**339**).

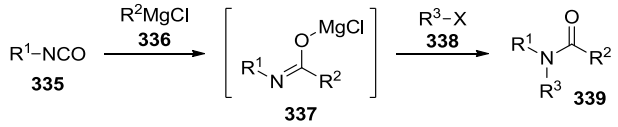


**Scheme 56** - Proposed formation of tertiary amides (**339**) as an extension of this methodology.

Successful development of a method for tertiary amide formation would vastly improve the applicability of this protocol. Should direct addition to a second electrophile be unfeasible, the metalated intermediate (**337**) could potentially act as a nucleophile in a copper-catalysed cross-coupling methodology, such as a Goldberg or Ullmann coupling,[250] or even a palladium-catalysed Buchwald-Hartwig coupling.[251] It is likely that simply quenching the intermediate (**337**) to give a telescoped transformation would be a viable strategy, yet making use of the pre-deprotonated moiety could yield some advantage in the coupling step.

*3.3.2.3. Further mechanistic work*

In order to further use kinetic analysis to examine the reaction mechanism, an additional set of reactions should be performed using QCL-IR. Ideally, these would look at the entire reaction profile, rather than just the linear regime, as in the set of experiments described above (see

section 3.2.4.2. Quantitative analysis using QCL-IR). This should be achieved by increasing the $CuBr_2$ loading to enhance reaction rate, but also reducing flow rate, to increase the visible residence time. The flow rates used above were selected in line with mixing calculations,[229] yet slower flow rates would allow a far better view of the overall reaction. More detailed kinetic analysis would allow definition of a rate equation, with orders in each reactant, which would likely improve any proposed reaction mechanism.

Furthermore, QCL-IR could be applied to numerous other unstudied reactions in flow, as a tool to obtain detailed kinetic information on fast processes, such as transmetalation events.[252,253] These *in situ* transmetalations are commonly used to form organozinc reagents for Negishi cross-couplings,[254] and cuprates for 1,4-addition reactions,[255] yet their rates of formation are not well-known, and are simply assumed to be fast. A suite of experiments determining the kinetics of these reactions, and the relatively unknown effect of additives could yield an improved understanding, lowering the barrier to employing these transformations in flow on a larger scale.

Finally, reactions found to behave capriciously in flow could be analysed using different additives, with the aim of preventing blockages. As discussed above, QCL-IR analysis revealed the unexpected influence of a small quantity of $CuBr_2$ on reaction homogeneity. Examining reaction additives in this way could reveal numerous compounds with previously unknown effects, which may decrease the detrimental effects and downtime caused by blockage formation in continuous processes.

*3.3.2.4. Application to industrially-relevant processes*

Although the developed methodology competes directly with a multitude of other efficient and functional group-tolerant amidation methods, the implementation of flow chemistry is likely to become truly advantageous when considering larger scale work. Within the pharmaceutical industry, throughput is less of a concern, due to the production of high value products, in relatively small quantities. Conversely, as lower value products are considered, for example in the fine chemical, agrochemical and even bulk chemical industries, throughput and cost of goods become increasingly important. Specifically, within the agrochemical industry, relatively simple carboxamide compounds represent a prominent class of succinate dehydrogenase inhibitor (SDHI) fungicides.[256]

With respect to starting material costs, isocyanate production from phosgene is an efficient and high-throughput reaction, resulting in a low-cost reagent. Moreover, the industrial manufacture of Grignard reagents also allows for a low-cost starting material, most simply, by reaction of an organohalide compound with metallic magnesium. These combined in a continuous flow system, with a low loading of base-metal additive, give a fast reaction, which should be straightforward to scale up. Consequently, it is envisioned that multi-ton quantities could be processed using this protocol, furnishing the desired amide, with very low material and operating costs. A selection of agrochemical products, which may be suitable for this methodology include the fungicides: boscalid (**340**)[257] (production volume over 1,000 tons per year),[258] bixafen (**341**),[259] fenfuram (**342**)[260] and flutolanil (**343**)[261] (**Scheme 57**).

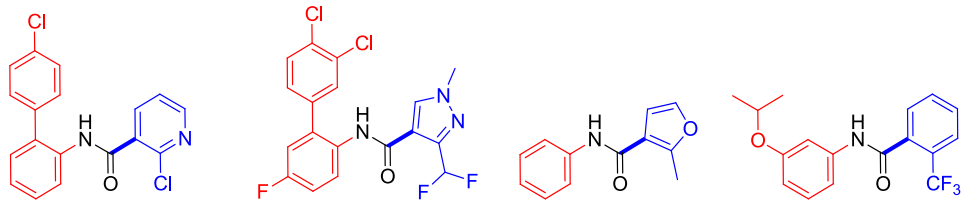


**Scheme 57** - Agrochemical products, to which this flow amidation methodology may be applicable and advantageous. The bond to be formed is highlighted.

*3.3.2.5. Telescoped isocyanate formation-amidation*

Whilst isocyanates can be synthesised in a cost-effective and mass efficient manner using phosgene (and its derivatives), further work into use of non-toxic reagents may improve their applicability as synthetic reagents. As mentioned previously (see section 3.2.4.2. Quantitative analysis using QCL-IR), recent publications have described telescoped copper-[239,240] and palladium-catalysed[241,242] carbamate and urea syntheses *via* an isocyanate intermediate (**346**), using an inorganic cyanate salt (**Scheme 58**). As readily available and stable crystalline solids, with comparatively benign toxicity profiles, these salts can be seen as convenient reagents for the installation of an isocyanate functionality.

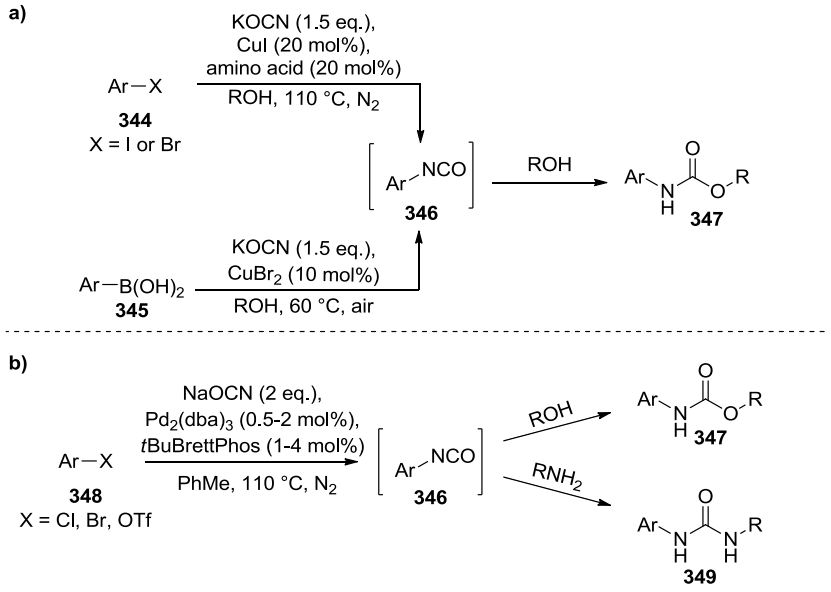


**Scheme 58** - Transition metal-catalysed carbamate (**347**) and urea (**349**) synthesis *via* an isocyanate (**346**). **a)** Copper-catalysed methods using potassium cyanate, from aryl halides (**344**),[239] or arylboronic acids (**345**).[240] **b)** Palladium-catalysed isocyanate formation-functionalisation, to furnish carbamates (**347**)[241] or ureas (**349**).[242]

All proposed mechanisms for these transformations suggest that the isocyanate moiety (**346**) is formally generated, then quenched by an external nucleophile. Isolation of the isocyanate itself is not generally achieved, so the driving force of the reaction may in fact be the isocyanate's onward reaction. However, it might be envisioned that the *in situ* generated isocyanate could be reacted to form an amide (**350**), in a reaction similar to that developed within this work. Further work into these methodologies could reveal a convenient and general amide synthesis. In particular the $CuBr_2$-catalysed[240] methodology should be pursued, as this species may promote both reaction steps (**Scheme 59**).

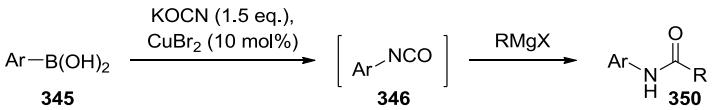


**Scheme 59** - Proposed $CuBr_2$-catalysed isocyanate (**346**) formation,[240] followed by amidation using the procedure developed within this work.

# Chapter 4. Experimental

## 4.1. General methods

### 4.1.1. Materials

All reactions specified as using dry solvents were carried out in oven-dried glassware under an atmosphere of dry $N_2$. Dry solvents were purchased in SureSeal bottles from Sigma Aldrich, and used without further purification. The THF used in these reactions contained BHT (250 ppm) as a stabilizer against peroxide formation. All commercial isocyanate starting materials were purified by Kugelrohr distillation under reduced pressure (at ~5-10 mbar) prior to use. All other chemicals were used without further purification.

### 4.1.2. Equipment and purification

**Purification by column chromatography**

Silica chromatography was performed on Biotage SP4, or Biotage Isolera, using Biotage SNAP or SNAP Ultra prepacked cartridges. UV response was monitored at 254 nm and 220 nm.

**Reaction Calorimetry**

Calorimetry experiments were carried out using a Mettler Toledo RC1 calorimetric system, equipped with a 100 mL vessel. Control of the system and analysis of the resulting data was carried out using Mettler Toledo iControl software.

**ReactIR**

Batch ReactIR experiments were conducted using a Mettler Toledo ReactIR iC10 system, with a 2 m × 9.5 mm AgX/DiComp fibre conduit probe. IR data was manipulated using Mettler Toledo iC IR software v4.3.

**Visible light photochemistry reaction setup**

All reactions were irradiated with either 1 or 2 × Kessil A160WE Tuna Blue 40 watt LED lamp(s)[262] (as specified in each individual experiment). Each lamp was set to 100% blue colour

and 100% intensity. The reactions were carried out in vials sealed with a screw cap, equipped with a rubber septum. HPLC (1.5 mL) vials were used for screening conditions, and 4 mL vials were used for preparative scale reactions. The vials were placed within the sample holders of a 3D printed internally mirrored housing, with an integrated cooling fan, purchased from Hepatochem.[263,264] The housing was situated on a stirrer-hotplate, to allow agitation of reaction mixtures. The temperature of reaction mixtures using this setup could not be regulated by the stirrer-hotplate, and was found to equilibrate at 30-32 °C. For a photo of both housings (for 1 and 2 × LED lamps), and the spectral output of the LED lamps, see section 2.2.2.1. Equipment considerations**.**

**General Flow Chemistry Considerations**

Reaction systems were set up using 1/16" PFA tubing, (1/16" refers to the outer diameter; the internal diameter is 1/32") with Swagelok T-pieces and connections. Prior to performing Grignard reactions, the system was flushed with dry THF, for at least 5 residence times. Any blockages arising from solid formation were cleared using a 0.1:1:1 solution of acetic acid:methanol:water.

**Flow IR**

FlowIR experiments were conducted using the set up shown in **Figure 20**. Grignard reagent was pumped using a Cetoni Nemesys syringe pump (with a 50 mL syringe), whilst isocyanate was pumped using an MZR7255 HNP microannular gear pump, both monitored by Bronckhorst flow controllers. An Ehrfeld cascade mixer 10HC was used to mix the two streams, and a Mettler Toledo FlowIR cell was used to acquire the IR traces. IR data was manipulated using Mettler Toledo iC IR software v4.3.

**Mass Directed Automated Preparative HPLC (MDAP)**

MDAP purifications were conducted on a Waters FractionLynx system comprising of a Waters 600 pump with extended pump heads, Waters 2700 autosampler, Waters 996 diode array, and Gilson 202 fraction collector. The high performance liquid chromatography (HPLC) separation was conducted on an X-select $C_{18}$ column (150 mm × 30 mm internal diameter, 5 μm packing diameter) at ambient temperature, utilising an appropriate solvent system and elution gradient

as determined by analytical LCMS (i.e. formic acid, ammonium bicarbonate, or trifluoroacetic acid modifier). Mass spectra were recorded on a Waters ZQ mass spectrometer using alternate-scan positive and negative electrospray ionisation ($ES^+$ and $ES^-$) with a scan range of 100 to 1500 atomic mass units, scan time of 0.50 s, and an inter-scan delay of 0.25 s. FractionLynx 4.1 software was used to analyse the results.

### 4.1.3. Analysis

**Nuclear Magnetic Resonance (NMR)**

NMR spectra were recorded using a Bruker AV400 instrument, and processed using ACD/SpecManager v12.5. Chemical shifts (δ) are reported in parts per million (ppm) relative to tetramethylsilane, and coupling constants (*J*) are reported in Hz. The following abbreviations are used for multiplicities: s = singlet; br. s = broad singlet; d = doublet; t = triplet; q = quartet; quin = quintet; spt = septet; m = multiplet; dd = doublet of doublets; and td = triplet of doublets. The prefix "app." (apparent) has been added, in cases where an alternative splitting pattern was expected, but a simplified version was observed. If not specifically stated, NMR experiments were run at 30 °C.

**High performance liquid chromatography (HPLC)**

**3 minute TFA method**

These data were recorded on an Agilent HPLC system, equipped with a Zorbax SB C18 column (50 mm × 2.0 mm internal diameter, 3.0 μm packing diameter) at 40 °C.

The solvents employed were:

A = Water + 0.05% *v/v* trifluoroacetic acid.

B = Acetonitrile + 0.05% *v/v* trifluoroacetic acid.

The gradient employed was as follows:

| Time (min) | Flow rate (mL $min^{-1}$) | % A | % B |
|---|---|---|---|
| 0 | 1 | 100 | 0 |
| 2.50 | 1 | 5 | 95 |
| 2.70 | 1 | 5 | 95 |
| 2.71 | 1 | 100 | 0 |

**8 minute TFA method**

These data were recorded on an Agilent HPLC system, equipped with a Phenomenex Luna C18 column (50 mm × 2.1 mm internal diameter, 3.0 μm packing diameter) at 40 °C.

The solvents employed were:

A = Water + 0.05% *v/v* trifluoroacetic acid.

B = Acetonitrile + 0.05% *v/v* trifluoroacetic acid.

The gradient employed was as follows:

| Time (min) | Flow rate (mL $min^{-1}$) | % A | % B |
|---|---|---|---|
| 0 | 1 | 100 | 0 |
| 8 | 1 | 5 | 95 |

**Low resolution liquid chromatography mass spectrometry (LCMS)**

**2 minute low pH method**

These data were recorded using a Waters Acquity UPLC, equipped with a CSH C18 column (50mm × 2.1mm internal diameter, 1.7μm packing diameter) at 40 °C.

The solvents employed were:

A = 0.1% v/v solution of formic acid in water

B = 0.1% v/v solution of formic acid in acetonitrile

The gradient employed was as follows:

| Time (min) | Flow rate (mL $min^{-1}$) | % A | % B |
|---|---|---|---|
| 0.1 | 1 | 97 | 3 |
| 1.5 | 1 | 5 | 95 |
| 1.9 | 1 | 5 | 95 |
| 2.0 | 1 | 97 | 3 |

The UV detection was an averaged signal from wavelength of 210 nm to 350 nm and mass spectra were recorded on a Waters ZQ mass spectrometer using alternate-scan positive and negative electrospray ionisation (ES).

**5 minute high pH method**

The analysis was conducted on a Waters Xbridge C18 column (50 mm × 4.6 mm internal diameter, 3.0 μm packing diameter) at 40 °C.

The solvents employed were:

A = 10 mM ammonium bicarbonate in water, adjusted to pH 10 with ammonia solution.

B = Acetonitrile.

The gradient employed was as follows:

| Time (min) | Flow rate (mL $min^{-1}$) | % A | % B |
|---|---|---|---|
| 0.1 | 1 | 97 | 3 |
| 1.5 | 1 | 5 | 95 |
| 1.9 | 1 | 5 | 95 |
| 2.0 | 1 | 97 | 3 |

The UV detection was an averaged signal from wavelength of 220 nm to 350 nm and mass spectra were recorded on a Waters ZQ mass spectrometer using positive and negative mode electrospray ionisation (ES +ve and ES -ve).

**8 minute TFA method**

The analysis was conducted on a Phenomenex C18 column (50 mm × 2.1 mm internal diameter, 3.0 μm packing diameter) at 40 °C.

The solvents employed were:

A = Water + 0.05% v/v trifluoroacetic acid.

B = Acetonitrile + 0.05% v/v trifluoroacetic acid.

The gradient employed was as follows:

| Time (min) | Flow rate (mL $min^{-1}$) | % A | % B |
|---|---|---|---|
| 0 | 1 | 100 | 0 |
| 8.0 | 1 | 5 | 95 |
| 8.5 | 1 | 5 | 95 |
| 8.6 | 1 | 100 | 0 |

The UV detection was an averaged signal from wavelength of 205 nm to 400 nm and mass spectra were recorded on a Waters ZQ mass spectrometer using positive mode electrospray ionisation (ES +ve).

**High resolution mass spectrometry (HRMS)**

These data were recorded using an LTQ Orbitrap purchased from Thermo Scientific, equipped with a Phenomenex Luna C18 column (50 mm × 2.1 mm internal diameter, 3.0 μm packing diameter) at 40 °C.

The solvents employed were:

A = Water + 0.05 % v/v trifluoroacetic acid

B = Acetonitrile + 0.05 % v/v trifluoroacetic acid

The gradient employed was as follows:

| Time (min) | Flow rate (mL $min^{-1}$) | % A | % B |
|---|---|---|---|
| 0 | 3 | 99 | 1 |
| 8 | 3 | 99 | 1 |
| 8.01 | 3 | 3 | 97 |
| 10 | 3 | 3 | 97 |

**Infrared spectroscopy (IR)**

IR spectra were recorded using a Perkin Elmer Spectrum One FT-IR spectrometer fitted with a Perkin Elmer Universal ATR (attenuated total reflectance) sampling accessory. Absorption frequencies are reported in reciprocal centimetres ($cm^{-1}$); only selected absorbances are reported.

**Melting point**

Melting points were measured on a Stuart automatic melting point apparatus, SMP40, or a Büchi Melting Point M-565.

**Ion Chromatography**

In order to confirm the identity of the oxamate metal salts prepared within this work, ion chromatography was carried out.

The analysis was conducted on a Dionex CS14 analytical column (250 mm × 4 mm internal diameter) with a CG14 (50 mm × 4 mm internal diameter) Guard column.

Flow rate: 1 mL $min^{-1}$
Mobile phase: 5% v/v aqueous acetonitrile solution, containing 10 mM methanesulfonic acid
Column temperature: 30 °C
Injection volume: 5 µL
Runtime: 15 min

Ion detection was achieved using a Dionex ICS3000 system, equipped with a conductivity detector, and Cation Self-Generating Suppressor (CSRS).

Only the cations lithium, sodium, potassium, and calcium were available for analysis, versus a calibration mix. In every case, the sample was found not to contain detectable levels (<0.0%) of the three other metal ions, which were not expected to be present.

### 4.1.4. General experimental procedures

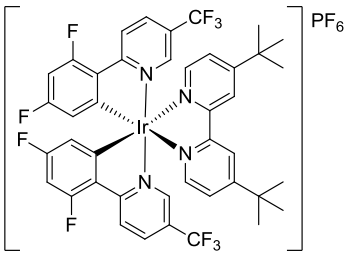


Iridium catalyst (**156**)

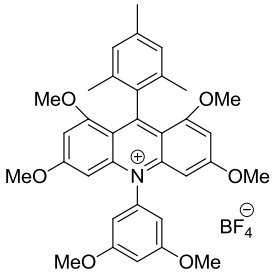


Acridinium catalyst (**169**)

**General method A, for the photoredox amidation of olefins by oxamate salts, using an iridium catalyst in DME/DMF solvent**

A 4 mL vial, equipped with a stirrer bar, was charged with ***iridium catalyst (156)*** (1 mol%, 4.5 mg, 0.004 mmol), ***olefin (if a solid)*** (0.4 mmol), and ***sodium oxamate salt*** (0.440 mmol). Under a flow of $N_2$, 3:1 DME:DMF (4 mL) was added then the vial was sealed with a screw cap septum. Water (72 µL, 4 mmol) and ***olefin (if a liquid)*** (0.4 mmol) were then added by piercing the septum. The reaction mixture was irradiated with ***1 or 2*** blue LED lamps, and stirred for ***reaction time***.

The reaction solvent was then removed *in vacuo*. The resulting residue was dissolved in DCM, and loaded onto a silica column for purification, as specified in each example.

**General method B, for the photoredox amidation of olefins by oxamate salts, using an iridium catalyst in acetone solvent**

A 4 mL vial, equipped with a stirrer bar, was charged with ***iridium catalyst (156)*** (1 mol%, 4.5 mg, 0.004 mmol), ***olefin (if a solid)*** (0.4 mmol), and ***sodium oxamate salt*** (0.440 mmol). Under a flow of $N_2$, $CO_2$-sparged acetone (4 mL) was added then the vial was sealed with a screw cap septum. Water (72 µL, 4 mmol) and ***olefin (if a liquid)*** (0.4 mmol) were then added by piercing the septum. The reaction mixture was irradiated with ***1 or 2*** blue LED lamps, and stirred for ***reaction time***.

The reaction mixture was transferred to a separating funnel where ethyl acetate (25 mL) was added followed by saturated brine solution (5 mL) and water (10 mL). The layers were separated and the aqueous layers extracted with further ethyl acetate (2 × 25 mL). The combined organic layers were dried over $MgSO_4$, filtered, and solvent removed *in vacuo*. The

resulting residue was dissolved in DCM and loaded onto a silica column for purification, as specified in each example.

**General method C, for the photoredox amidation of olefins by oxamate salts, using an acridinium catalyst in acetone solvent**

A 4 mL vial, equipped with a stirrer bar, was charged with ***acridinium catalyst (169)*** (2 mol%, 5.2 mg, 0.008 mmol), ***olefin (if a solid)*** (0.4 mmol), and ***sodium oxamate salt*** (0.440 mmol). Under a flow of $N_2$, $CO_2$-sparged acetone (4 mL) was added then the vial was sealed with a screw cap septum. Water (72 µL, 4 mmol) and ***olefin (if a liquid)*** (0.4 mmol) were then added by piercing the septum. The reaction mixture was irradiated with ***1 or 2*** blue LED lamps, and stirred for ***reaction time***.

The reaction mixture was transferred to a separating funnel where ethyl acetate (25 mL) was added followed by saturated brine solution (5 mL) and water (10 mL). The layers were separated and the aqueous layers extracted with further ethyl acetate (2 × 25 mL). The combined organic layers were dried over $MgSO_4$, filtered, and solvent removed *in vacuo*. The resulting residue was dissolved in DCM and loaded onto a silica column for purification, as specified in each example.

**General method D, for the flow amidation of isocyanates with Grignard reagents**

In round bottomed flasks, 0.5 M solutions of ***isocyanate*** (with 1 mol% $CuBr_2$) and ***Grignard reagent*** were made up in dry THF. The isocyanate solution was sonicated for 5 minutes, to ensure homogeneity as far as possible. Using a Harvard PHD Ultra syringe pump, equipped with 20 mL Normject disposable syringes, the solutions were mixed in a T-piece, at flow rates of 5 mL $min^{-1}$ each. After a 10.6 s residence time, the reaction flow was quenched into dilute ammonium chloride solution.

An equilibration period of 3 residence times was allowed, then samples of 1 mmol (4 mL combined flow volume) were collected into vials containing 10 mL of dilute ammonium chloride solution and diethylamine (~1 %vol). Ethyl acetate (10 mL) was added to each sample, alongside water (10 mL) and saturated brine (10 mL), and the layers separated. The aqueous layer was extracted with further ethyl acetate (25 mL). The combined organics were dried over

$MgSO_4$, and evaporated *in vacuo*. The crude product was then purified as specified in each example.

**General method E, for the flow amidation of isocyanates with Grignard reagents at a lower concentration**

In round bottomed flasks, 0.25 M solutions of ***isocyanate*** (with 1 mol% $CuBr_2$) and ***Grignard reagent*** were made up in dry THF. The isocyanate solution was sonicated for 5 minutes, to ensure homogeneity as far as possible. Using a Harvard PHD Ultra syringe pump, equipped with 20 mL Normject disposable syringes, the solutions were mixed in a T-piece, at flow rates of 5 mL $min^{-1}$ each. After a 10.6 s residence time, the reaction flow was quenched into dilute ammonium chloride solution.

An equilibration period of 3 residence times was allowed, then samples of 1 mmol (8 mL combined flow volume) were collected into vials containing 10 mL of dilute ammonium chloride solution and diethylamine (~1 %vol). Ethyl acetate (10 mL) was added to each sample, alongside water (10 mL) and saturated brine (10 mL), and the layers separated. The aqueous layer was extracted with further ethyl acetate (25 mL). The combined organics were dried over $MgSO_4$, and evaporated *in vacuo*. The crude product was then purified as specified in each example.

**General method 1 for the titration of Grignard reagents**[265]

To a solution of (1*S*,2*R*,5*S*)-2-isopropyl-5-methylcyclohexanol (313 mg, 2 mmol) and 1,10-phenanthroline (10 mg, 0.055 mmol) in dry THF (10 mL) at RT, was added ***Grignard reagent***, dropwise until a persistent violet colour was observed.

**General method 2 for the titration of Grignard reagents**[266]

To a solution of iodine (313 mg, 0.5 mmol) and LiCl (0.5 M in dry THF, 5 mL) at 0 °C, was added ***Grignard reagent***, dropwise until the solution's initial brown colour subsided, leaving a colourless solution.

## 4.2. Experimental data for Chapter 2

### 4.2.1 Calculation of HPLC assay yields

For the following transformation, molar absorbance ratios were obtained for starting material (**155**) and product (**157**), versus biphenyl, which was used as an internal standard (0.5 eq.) in these reactions.

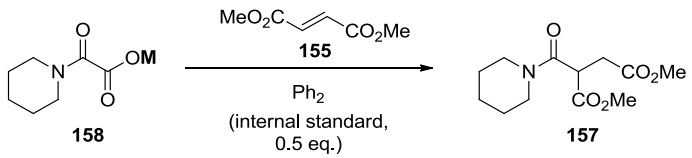


**Example calculation of molar absorbance ratio:**

$$k_x = \frac{\%_{is}}{\%_x} \times \frac{m_{is}}{m_x} \times \frac{M_{is}}{M_x}$$

Where:

% = %Area/Area from HPLC result, *m* = mass present in analysed sample, *M* = molecular mass

*x* = reaction component, *is* = internal standard

Product (**157**) (6.25 mg) = 11.004%A/A, biphenyl (10.51 mg) = 88.733%A/A

$$k_x = \frac{88.733}{11.004} \times \frac{6.25}{10.51} \times \frac{154.21}{257.28} = 2.874$$

An average of four samples gave the following results at each respective analytical wavelength:

**210 nm:**

Olefin (**155**), $k_x$ = 1.3063,

Product (**157**), $k_x$ = 2.8862

**220 nm**

Olefin (**155**), $k_x$ = 0.45068

Product (**157**), $k_x$ = 1.12

Assay yield = $k_x \times \frac{eq_{\cdot is}}{eq_{\cdot x}} \left(\frac{\%_x}{\%_{is}}\right) \times 100$

**Example HPLC trace and assay yield calculation:**

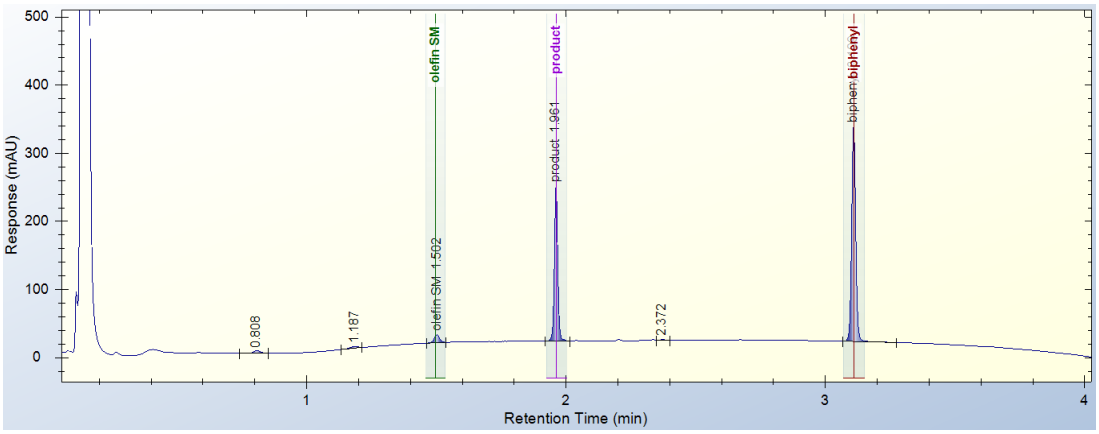


Olefin (**155**) = 2.932%A/A, product (**157**) = 35.486%A/A, biphenyl = 59.087%A/A

Olefin (**155**) assay yield = $1.3063 \times 0.5 \left(\frac{2.932}{59.087}\right) \times 100 = 3.24\%$

Product (**157**) assay yield = $2.8862 \times 0.5 \left(\frac{35.486}{59.087}\right) \times 100 = 86.67\%$

### 4.2.2. Analysis of radical precursors

***N*,*N*-Diethylcarbamoyl *N*,*N*-diethyldithiocarbamate**

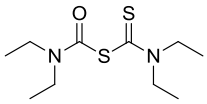

**146**

To a solution of diethylcarbamic chloride (0.127 mL, 1 mmol) in acetone (6 mL) was added sodium diethylcarbamodithioate (514 mg, 3 mmol) in one portion, and the reaction mixture was stirred at room temperature for 40 h. Water (25 mL) was added to the solution, followed by ethyl acetate (25 mL). The phases were separated, and the aqueous phase was extracted with further ethyl acetate (25 mL). The organic layers were combined, dried over $MgSO_4$, then filtered and evaporated *in vacuo*. The crude product was purified by chromatography on silica; elution gradient 0-25% ethyl acetate in heptane. The appropriate fractions were combined and evaporated *in vacuo* to afford the desired compound (**146**) (111 mg, 45% yield) as a yellow-green oil.

**IR $\nu_{max}$:** 2985, 2936, 1664, 1486, 1403, 1200 $cm^{-1}$

**$^1$H NMR (400 MHz, $CDCl_3$):** $\delta$ = 4.04 (q, *J*=7.1 Hz, 2H), 3.81 (q, *J*=7.1 Hz, 2H), 3.42 (br. s, 4H), 1.35 (t, *J*=7.1 Hz, 3H), 1.31 (t, *J*=7.1 Hz, 3H), 1.22 (br. s, 6H)

**$^{13}$C NMR (101 MHz, $CDCl_3$):** $\delta$ = 185.3, 161.1, 50.0, 48.8, 13.4, 11.1

**LCMS (2 min low pH):** $t_R$ = 1.04 min, $[M+H^+]$ 248.9 (100% purity)

**HRMS:** ($C_{10}H_{21}N_2OS_2$) $[M+H^+]$ requires: 249.1090, $[M+H^+]$ found: 249.1080

***N*,*N*-Diphenylcarbamoyl *N*,*N*-diethyldithiocarbamate**

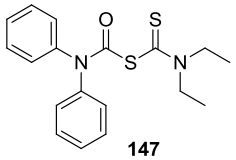

**147**

To a solution of diphenylcarbamic chloride (232 mg, 1 mmol) in acetone (6 mL) was added sodium diethylcarbamodithioate, trihydrate (676 mg, 3 mmol) in one portion. The resulting mixture was stirred at room temperature for 40 h. Water (25 mL) was added to the solution, followed by ethyl acetate (25 mL). The phases were separated, and the aqueous phase extracted with further ethyl acetate (25 mL). The organic layers were combined, dried over $MgSO_4$, filtered, and evaporated in vacuo, to afford the crude product. The crude product was recrystallised from acetone/heptane, using an evaporative recrystallisation, to afford the desired compound (**147**) (172 mg, 50% yield) as a pale yellow crystalline solid.

**Melting point:** 108.3-109.5 °C

**IR $\nu_{max}$:** 1690, 1591, 1488, 1420, 1268, 1142 $cm^{-1}$

**$^{1}$H NMR (400 MHz, DMSO-d$_6$):** δ = 7.53 - 7.31 (m, 10H), 3.92 (q, *J*=7.1 Hz, 2H), 3.76 (q, *J*=7.1 Hz, 2H), 1.17 (q, *J*=7.1 Hz, 6H)

**$^{13}$C NMR (101 MHz, DMSO-d$_6$):** δ = 183.2, 162.5, 141.1, 129.4, 128.0 (br. s), 50.0, 48.0, 13.2, 10.7

**LCMS (2 min low pH):** $t_R$ = 1.28 min, $[M+H^+]$ 248.9 (99.6% purity)

**HRMS:** ($C_{18}H_{21}N_2OS_2$) $[M+H^+]$ requires: 345.1090, $[M+H^+]$ found: 345.1083

**Methyl 2-oxo-2-(piperidin-1-yl)acetate**[267]

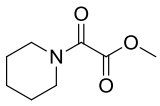

**149**

To a mixture of piperidine (4.94 mL, 50 mmol) and toluene (40 mL) was added potassium carbonate (20%w/w aq. solution, 8 mL). The biphasic mixture was cooled to 0 °C, and methyl 2-chloro-2-oxoacetate (5.52 mL, 60 mmol) added slowly over 20 minutes, then the reaction mixture was stirred for 1 h at room temperature. Ethyl acetate (25 mL) was added, followed by water (25 mL), then the layers separated. The aqueous layer was extracted with further ethyl acetate (25 mL), then the combined organics were dried over $MgSO_4$, filtered, and evaporated *in vacuo* to afford the desired product (**149**) (7.01 g, 82 % yield) as a colourless oil.

**IR $\nu_{max}$:** 2948, 2868, 1738, 1648, 1202 $cm^{-1}$

**$^1$H NMR (400 MHz, $CDCl_3$):** $\delta$ = 3.87 (s, 3H), 3.57 (app. dd, *J*=5.3, 5.7 Hz, 2H), 3.34 (app. dd, *J*=5.3, 5.7 Hz, 2H), 1.72 - 1.60 (m, 6H)

**$^{13}$C NMR (101 MHz, $CDCl_3$):** $\delta$ = 163.5, 159.9, 52.4, 47.2, 42.1, 26.1, 25.0, 24.2

**LCMS (2 min low pH):** $t_R$ = 0.65 min, $[M+H^+]$ 172.0 (100% purity)

**HRMS:** ($C_8H_{14}NO_3$) $[M+H^+]$ requires: 172.0968, $[M+H^+]$ found: 172.0963

**Potassium 2-oxo-2-(piperidin-1-yl)acetate**

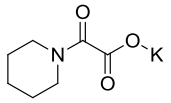

**150**

To a solution of methyl 2-oxo-2-(piperidin-1-yl)acetate (1.37 g, 8 mmol) in THF (8 mL) was added potassium hydroxide (1 M aq. solution, 8 mL, 8 mmol). The resulting solution was stirred vigorously at room temperature for 20 minutes. Solvent was removed *in vacuo*, to afford the desired product (**150**) (1.56 g, 99 % yield) as a white solid.

**LCMS (2 min low pH):** $t_R$ = 0.48 min, [M+H$^+$] 158.0 (100% purity)

Full product characterisation can be found below, on page 148.

**Methyl 2-(methyl(*p*-tolyl)amino)-2-oxoacetate**

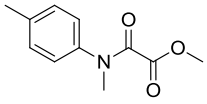

**152**

To a mixture of potassium carbonate (20%w/w aq. solution, 20 mL) and DCM (20 mL) was added *N*,4-dimethylaniline (2.53 mL, 20 mmol). The biphasic mixture was cooled to 0 °C, and methyl 2-chloro-2-oxoacetate (2.21 mL, 24 mmol) was added as a solution in DCM (20 mL), dropwise over 30 minutes. The reaction mixture was stirred for a further 2 h at 0 °C, then allowed to warm to room temperature. The organic layer was separated and the aqueous layer was extracted with further DCM (20 mL). The combined organics were washed with water (25 mL), then dried over $MgSO_4$, filtered, then solvent removed *in vacuo* to afford the desired product (**152**) (3.93 g, 95% yield) as a light orange oil, which crystallised on standing.

**Melting point:** 53.2-58.7 °C

**IR $\nu_{max}$:** 3051, 2956, 2928, 1739, 1666, 1514, 1227, 1112 $cm^{-1}$

**$^1$H NMR (400 MHz, DMSO-$d_6$):** δ = 7.24 (d, *J*=8.0 Hz, 2H), 7.21 - 7.15 (m, 2H), 3.50 (s, 3H), 3.23 (s, 3H), 2.31 (s, 3H)

**$^{13}$C NMR (101 MHz, DMSO-$d_6$):** δ = 163.1, 161.0, 138.4, 137.7, 130.0, 125.9, 52.1, 35.4, 20.5

**LCMS (2 min formic):** $t_R$ = 0.89 min, $[M+H^+]$ 208.1 (96.8% purity)

**HRMS:** ($C_{11}H_{14}NO_3$) $[M+H^+]$ requires: 208.0968, $[M+H^+]$ found: 208.0962

**Cesium 2-(methyl(*p*-tolyl)amino)-2-oxoacetate**

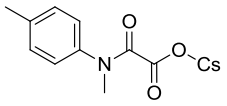


**153**

To a solution of methyl 2-oxo-2-(*p*-tolylamino)acetate (1.04 g, 5 mmol) in THF (5 mL) was added cesium hydroxide (1 M aq. solution, 5 mL). The resulting solution was stirred at room temperature for 5 minutes, then solvent was removed *in vacuo*. The resulting white solid was slurried in acetone (20 mL), then filtered and dried *in vacuo* to afford the desired product (**153**) (1.58 g, 97% yield) as a white solid.

**Melting point:** Decomposed at 232 °C

**IR $\nu_{max}$:** 1612, 1524, 1423, 1351, 1286 $cm^{-1}$

**$^{1}$H NMR (400 MHz, 77 °C, DMSO-d$_6$):** $\delta$ = 7.22 - 7.17 (m, 2H), 7.07 (d, *J*=8 Hz, 2H), 3.12 (s, 3H), 2.23 (s, 3H)

**$^{13}$C NMR (101 MHz, 77 °C, DMSO-d$_6$):** $\delta$ = 171.7, 167.6, 141.1, 134.0, 126.2, 125.2, 33.2 (br. s), 19.8

The *N*-Me carbon appears as a very broad signal, due to rotameric species, even when the data was collected at an elevated temperature.

**LCMS (2 min formic):** $t_R$ = 0.70 min, [M+H$^+$] 194.0 (99.9% purity)

**HRMS:** ($C_{10}H_{12}NO_3$) [M+H$^+$] requires: 194.0812, [M+H$^+$] found: 194.0818

**Cyclic voltammetry experiments**

Working electrode: Glassy carbon

Counter electrode: Pt wire

Reference electrode: Ag/AgCl/sat. KCl

Standardised against ferrocene result: $E_{1/2}$ = 0.44 V

Cyclic voltammetry was conducted using a three-electrode setup consisting of a platinum wire working electrode (d = 1.50 mm) and platinum gauze counter electrode. The reference electrode was a Ag/AgCl electrode (containing 3.0 M NaCl saturated with AgCl). Electrochemical measurements were carried out in a bespoke glass cell using a CHI1140C potentiostat (CH Instruments).

The analyte sample was dissolved in DMF or acetonitrile (with 0.1 M tetrabutylammonium hexafluorophosphate electrolyte), to make up 20 mL of a 0.01 M solution. The CV cell was filled with this solution, and degassed by bubbling nitrogen through the solution for 5 minutes. The nitrogen flow was ceased, and voltage scans were performed.

**Cesium 2-oxo-2-(piperidin-1-yl)acetate**

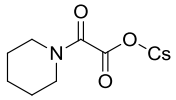


**154**

To a solution of methyl 2-oxo-2-(piperidin-1-yl)acetate (685 mg, 4 mmol) in THF (4 mL) was added cesium hydroxide (1 M aq. solution, 4 mL, 4 mmol). The resulting solution was stirred vigorously at room temperature for 20 minutes. Solvent was removed *in vacuo*, to afford the desired product (**154**) (1.10 g, 94% yield) as a white solid.

**Melting point:** Decomposed at 301 °C

**IR $\nu_{max}$:** 2934, 2854, 1589, 1455, 1378, 1248 $cm^{-1}$

**$^{1}$H NMR (400 MHz, DMSO-$d_6$):** δ = 3.27 (app. dd, *J*=5.4, 5.5 Hz, 2H), 3.22 (app. dd, *J*=5.4, 5.5 Hz, 2H), 1.60 - 1.51 (m, 2H), 1.45 - 1.33 (m, 4H)

**$^{13}$C NMR (101 MHz, DMSO-$d_6$):** δ = 169.6, 167.2, 46.0, 39.7, 26.0, 25.2, 24.4

**LCMS (2 min low pH):** $t_R$ = 0.50 min, $[M+H^+]$ 158.0 (100% purity)

**HRMS:** ($C_7H_{12}NO_3$) $[M+H^+]$ requires: 158.0812, $[M+H^+]$ found: 158.0808

**Dimethyl 2-(piperidine-1-carbonyl)succinate**

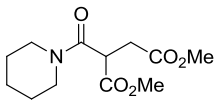

**157**

A 20 mL vial, equipped with a stirrer bar, was charged with cesium 2-oxo-2-(piperidin-1-yl)acetate (160 mg, 0.55 mmol), dimethyl fumarate (72 mg, 0.5 mmol) and $(Ir[dF(CF_3)ppy]_2(dtbpy))PF_6$ (5.6 mg, 0.005 mmol). The vial was sealed, then a 3:1 mixture of DME:DMF (5 mL) was added, followed by water (0.090 mL, 5 mmol). The reaction mixture was degassed by sparging with nitrogen for 30 minutes. The reaction mixture was then irradiated with 2 × Kessil "Tuna Blue" LED lamps, and stirred for 16 h. The reaction setup was cooled using a desk fan, and the temperature equilibrated at around 30 °C.

To the reaction mixture was added saturated brine solution (25 mL), and the organics were extracted sequentially with ethyl acetate (3 × 25 mL). The combined organics were dried over $MgSO_4$, filtered, and solvent removed *in vacuo*. The crude product was purified by chromatography on silica; elution gradient 0-25% ethyl acetate in heptane. The appropriate fractions were combined and evaporated *in vacuo*, to afford the desired product (**157**) (80 mg, 62% yield) as a yellow oil.

**LCMS (2 min low pH):** $t_R$ = 0.72 min, $[M+H^+]$ = 258.1 (95.6% purity)

Full characterisation can be found below, on page 182.

### 4.2.3. Oxamate salt selection

**Lithium 2-oxo-2-(piperidin-1-yl)acetate**

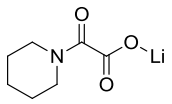

**159**

To a solution of methyl 2-oxo-2-(piperidin-1-yl)acetate (364 mg, 2.13 mmol) in THF (2 mL) was added lithium hydroxide (1 M aq. solution, 2.13 mL, 2.13 mmol). The resulting solution was stirred vigorously at room temperature for 5 minutes. TLC showed starting material remaining, so further lithium hydroxide (1 M aq. solution, 0.213 mL) was added, and the reaction was stirred for a further 5 minutes. Solvent was removed *in vacuo*, to afford desired product (**159**) (328 mg, 94% yield) as a white solid.

**Melting point:** Decomposed at 284 °C

**IR $\nu_{max}$:** 2937, 2850, 1651, 1618, 1450, 1394, 1262 $cm^{-1}$

**$^{1}$H NMR (400 MHz, DMSO-$d_6$):** $\delta$ = 3.32 - 3.24 (m, 4H), 1.60 - 1.52 (m, 2H), 1.46 - 1.35 (m, 4H)

**$^{13}$C NMR (101 MHz, DMSO-$d_6$):** $\delta$ = 169.1, 167.8, 46.1, 39.9, 26.0, 25.1, 24.3

**LCMS (2 min low pH):** $t_R$ = 0.52 min, $[M+H^+]$ 158.0 (100% purity)

**HRMS:** ($C_7H_{12}NO_3$) $[M+H^+]$ requires: 158.0812, $[M+H^+]$ found: 158.0808

**Ion Chromatography (Li):** Calculated cation mass (w/w): 4.3%, found: 4.1%

**Sodium 2-oxo-2-(piperidin-1-yl)acetate**[268]

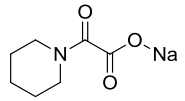


**160**

To a solution of methyl 2-oxo-2-(piperidin-1-yl)acetate (3.42 g, 20 mmol) in THF (20 mL) was added sodium hydroxide (1 M aq. solution, 20 mL, 20 mmol) in one portion. The resulting solution was stirred vigorously at room temperature for 5 minutes. Solvent was removed *in vacuo*, to afford the desired product (**160**) (3.56 g, 99% yield) as a white solid.

**Melting point:** Decomposed at 254 °C, literature value: 240 °C

**IR $\nu_{max}$:** 2937, 2859, 1598, 1444, 1387, 1255 $cm^{-1}$

**$^{1}$H NMR (400 MHz, DMSO-$d_6$):** $\delta$ = 3.34-3.25 (m, 4H), 1.61 - 1.52 (m, 2H), 1.47 - 1.36 (m, 4H)

**$^{13}$C NMR (101 MHz, DMSO-$d_6$):** $\delta$ = 169.4, 168.4, 46.6, 40.5, 26.5, 25.6, 24.8

**LCMS (8 min TFA):** $t_R$ = 0.64 min, $[M+H^+]$ 157.9 (100% purity)

**HRMS:** ($C_7H_{12}NO_3$) $[M+H^+]$ requires: 158.0812, $[M+H^+]$ found: 158.0807

**Ion Chromatography (Na):** Calculated cation mass (w/w): 12.8%, found: 11.3%

**Potassium 2-oxo-2-(piperidin-1-yl)acetate**

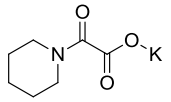

**150**

To a solution of methyl 2-oxo-2-(piperidin-1-yl)acetate (1.71 g, 10 mmol) in THF (20 mL) was added potassium hydroxide (1 M aq. solution, 10 mL, 10 mmol) in one portion. The resulting solution was stirred vigorously at room temperature for 5 minutes. Solvent was removed *in vacuo*, to afford the desired product (**150**) (1.91 g, 98% yield) as a white solid.

**Melting point:** Decomposed at 296 °C

**IR $\nu_{max}$:** 2932, 2853, 1602, 1441, 1363, 1254 $cm^{-1}$

**$^{1}$H NMR (400 MHz, DMSO-$d_6$):** $\delta$ = 3.27 (app. td, *J*=5.5, 10.9 Hz, 4H), 1.60 - 1.51 (m, 2H), 1.46 - 1.34 (m, 4H)

**$^{13}$C NMR (101 MHz, DMSO-$d_6$):** $\delta$ = 169.4, 167.5, 46.1 ($CH_2N$), 39.8, 26.0, 25.1, 24.3

**LCMS (2 min low pH):** $t_R$ = 0.53 min, $[M+H^+]$ 158.0 (100% purity)

**HRMS:** ($C_7H_{12}NO_3$) $[M+H^+]$ requires: 158.0812, $[M+H^+]$ found: 158.0811

**Ion Chromatography (K):** Calculated cation mass (w/w): 20.0%, found: 21.1%

**Cesium 2-oxo-2-(piperidin-1-yl)acetate**

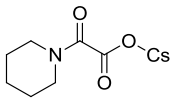

**154**

Synthesis description and full characterisation can be found above, on page 144.

**Calcium 2-oxo-2-(piperidin-1-yl)acetate**

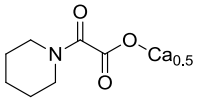

**161**

To a solution of methyl 2-oxo-2-(piperidin-1-yl)acetate (342 mg, 2 mmol) in THF (2 mL) was added calcium hydroxide (0.5 M aq. solution, 2 mL, 1 mmol), and water (2 mL). The resulting solution was stirred vigorously at room temperature for 4 h. Solvent was removed *in vacuo*, to afford the desired product (**161**) (334 mg, 94% yield) as a white solid.

**Melting point:** Decomposed at 276 °C

**IR $\nu_{max}$:** 2930, 2856, 1654, 1595, 1448, 1369, 1245 $cm^{-1}$

**$^{1}$H NMR (400 MHz, DMSO-$d_6$):** $\delta$ = 3.37 (app. dd, *J*=4.8, 4.6 Hz, 2H), 3.35 - 3.33 (m, 2H), 1.63 - 1.52 (m, 2H), 1.49 - 1.36 (m, 4H)

**$^{13}$C NMR (101 MHz, DMSO-$d_6$):** $\delta$ = 168.6, 167.9, 46.6, 40.8, 26.6, 25.7, 24.7

**LCMS (2 min low pH):** $t_R$ = 0.50 min, $[M+H^+]$ 158.0 (95.7% purity)

**HRMS:** ($C_7H_{12}NO_3$) $[M+H^+]$ requires: 158.0812, $[M+H^+]$ found: 158.0809

**Ion Chromatography (Ca):** Calculated cation mass (w/w): 11.4%, found: 9.9%

**Barium 2-oxo-2-(piperidin-1-yl)acetate**

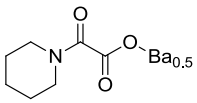


**162**

To a solution of methyl 2-oxo-2-(piperidin-1-yl)acetate (378 mg, 2.21 mmol) in THF (2 mL) was added barium hydroxide (0.5 M aq. solution, 2.22 mL, 1.11 mmol). The resulting solution was stirred vigorously at room temperature for 5 minutes. TLC showed starting material remaining, so further barium hydroxide (0.5 M aq. solution, 0.22 mL, 0.11 mmol) was added, and the reaction was stirred for a further 5 minutes. Solvent was removed *in vacuo*, to afford the desired product (**162**) (431 mg, 96% yield) as a white solid.

**Melting point:** Decomposed at 303 °C

**IR $\nu_{max}$:** 2935, 2868, 1592, 1445, 1345, 1249 $cm^{-1}$

**$^{1}$H NMR (400 MHz, DMSO-$d_6$):** $\delta$ = 3.46 - 3.24 (m, 4H), 1.63 - 1.53 (m, 2H), 1.51 - 1.37 (m, 4H)

**$^{13}$C NMR (101 MHz, DMSO-$d_6$):** $\delta$ = 168.3, 168.2, 46.2, 40.4, 26.1, 25.2, 24.2

**LCMS (2 min low pH):** $t_R$ = 0.52 min, $[M+H^+]$ 158.0 (96.7% purity)

**HRMS:** ($C_7H_{12}NO_3$) $[M+H^+]$ requires: 158.0812, $[M+H^+]$ found: 158.0808

**Tetrabutylammonium 2-oxo-2-(piperidin-1-yl)acetate**

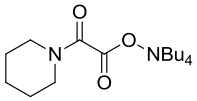

**163**

To a solution of methyl 2-oxo-2-(piperidin-1-yl)acetate (394 mg, 2.3 mmol) in THF (2 mL) was added tetrabutylammonium hydroxide (54-56% w/w in water, 1.09 mL, 2.3 mmol). The resulting solution was stirred vigorously at room temperature for 5 minutes. Solvent was removed *in vacuo*, to afford the desired product (**163**) (907 mg, 99% yield) as a waxy white solid.

**Melting point:** 53.7-54.8 °C

**IR $\nu_{max}$:** 2938, 2873, 1624, 1599, 1443, 1376, 1257 $cm^{-1}$

**$^{1}$H NMR (400 MHz, DMSO-$d_6$):** δ = 3.29 - 3.20 (m, 4H), 3.20 - 3.11 (m, 8H), 1.63 - 1.50 (m, 10H), 1.44 - 1.36 (m, 4H), 1.30 (tq, *J*=7.1, 7.4 Hz, 8H), 0.94 (t, *J*=7.4 Hz, 12H)

**$^{13}$C NMR (101 MHz, DMSO-$d_6$):** δ = 169.6, 167.0, 57.5 (t, *J*=2.5 Hz), 46.0, 39.6, 26.0, 25.1, 24.4, 23.0, 19.2, 13.5

**LCMS (2 min low pH):** $t_R$ = 0.87 min, $[M+H^+]$ 158.0 (100% purity)

**HRMS:** ($C_7H_{12}NO_3$) $[M+H^+]$ requires: 158.0812, $[M+H^+]$ found: 158.0810

**Dimethyl 2-(piperidine-1-carbonyl)succinate**

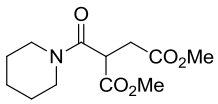

**157**

A 1.5 mL HPLC vial, equipped with a stirrer bar, was charged with $Ir[dF(CF_3)ppy]_2(dtbpy)PF_6$ (1.1 mg, 0.001 mmol), dimethyl fumarate (14.4 mg, 0.1 mmol), biphenyl (7.7 mg, 0.05 mmol) and ***oxamate salt (0.11 mmol)***. Under a flow of nitrogen, 3:1 DME:DMF (1 mL) was added, and the vial sealed. Water (0.018 mL, 1 mmol) was then added by piercing the cap. The reaction mixture was irradiated with 1 × blue LED lamp, and stirred for 16 h. After 16 h, the reaction mixture was sampled for analysis by HPLC (at 210 nm).

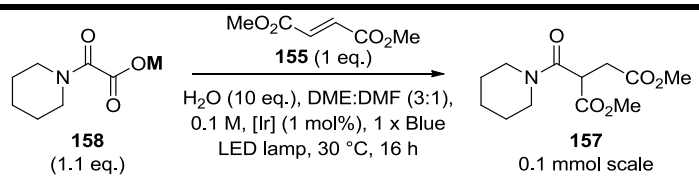


| Entry | Oxamate salt (mass used in reaction) | Dimethyl fumarate (155) (%Area) | Product (157) (%Area) | Biphenyl (%Area) |
|---|---|---|---|---|
| 1 | Li (**159**) (17.9 mg) | 0 | 30.9 | 55.5 |
| 2 | Na (**160**) (19.7 mg) | 0 | 34.4 | 54.7 |
| 3 | K (**150**) (21.5 mg) | 0 | 34.2 | 55.4 |
| 4 | Cs (**154**) (31.8 mg) | 0 | 35.2 | 57.2 |
| 5 | 0.5 Ca (**161**) (19.4 mg) | 1.1 | 21.6 | 49.4 |
| 6 | 0.5 Ba (**162**) (49.5 mg) | 8.2 | 16.0 | 49.3 |
| 7 | $NBu_4$ (**163**) (43.8 mg) | 27.8 | 15.2 | 41.3 |

### 4.2.4. Catalyst selection

Of the photocatalysts examined, the majority were commercially available, and were purchased from Sigma Aldrich, using the catalogue numbers listed below. A batch of catalyst **156** was also purchased from Strem Chemicals, due to stock shortages with the original supplier.

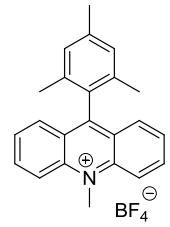


**164**
Sigma Aldrich (794171)

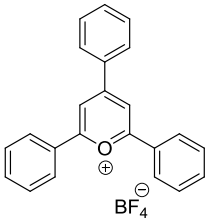


**165**
Sigma Aldrich (247367)

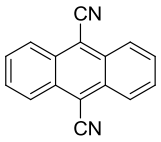


**166**
Sigma Aldrich (459852)

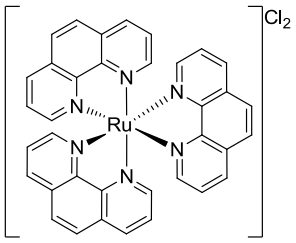


**167**
Sigma Aldrich (343714)

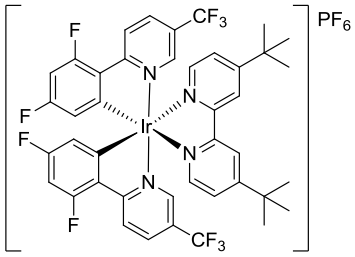


**156**
Sigma Aldrich (747793)
**or**
Strem (77-0425)

However, catalysts **168**, **169**, and **170** were unavailable, and so were prepared as follows.

**Tris(2,2'-bipyrazine)ruthenium(II) hexafluorophosphate**[269]

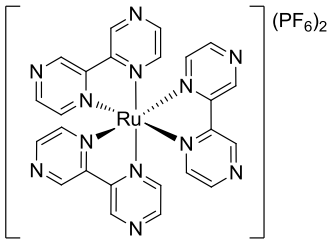


**168**

A 50 mL 3-necked flask was charged with ruthenium(III) chloride (0.21 g, 1 mmol), 2,2'-bipyrazine (631 mg, 4 mmol) and ethylene glycol (4 mL). The resulting black suspension was heated to 170 °C under nitrogen for 16 h, then was allowed to cool to room temperature. Potassium hexafluorophosphate (saturated aq. solution, 9 mL) was added in one portion, and the reaction mixture stirred at room temperature for 2 h. The reaction mixture was filtered through a sinter and washed with water (3 × 20 mL), before being eluted into a clean Büchner flask, using several portions of acetonitrile. The crude product was dry-loaded onto neutral alumina, and purified by gravity column chromatography, eluting with acetonitrile. The red/orange fractions were combined, concentrated, and dried *in vacuo* to afford the desired product (**168**) (171 mg, 20% yield) as a vibrant orange solid.

**Melting point:** 182.3-184.6 °C, literature value: 185 °C

**IR $\nu_{max}$:** 3107, 1588, 1410, 1159, 1074, 816, 751 $cm^{-1}$

**$^{1}$H NMR (400 MHz, DMSO-$d_6$):** δ = 10.12 (d, *J*=0.9 Hz, 6H), 8.71 (d, *J*=3.2 Hz, 6H), 7.99 (dd, *J*=0.9, 3.2 Hz, 6H)

**$^{13}$C NMR (101 MHz, DMSO-$d_6$):** δ = 150.3, 148.4, 146.9, 145.4

**$^{31}$P NMR (162MHz, DMSO-$d_6$):** δ = -144.19 (spt, *J*=712.1 Hz, 2P)

**LCMS:** Not detected by any of the methods available.

**Tris(3,5-dimethoxyphenyl)amine**[61]

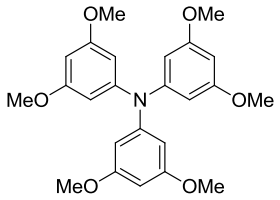


**216**

To a 100 mL 3-necked flask, equipped with a stirrer bar, was added 3,5-dimethoxyaniline (689 mg, 4.5 mmol), 1-bromo-3,5-dimethoxybenzene (1.95 g, 9 mmol), and chloro[(tri-*tert*-butylphosphine)-2-(2-aminobiphenyl)]palladium(II) (35 mg, 0.068 mmol). THF (23.8 mL) was added, and the resulting solution was sparged with nitrogen for 15 minutes. Sodium *tert*-butoxide (2 M in THF, 9.09 mL, 18.18 mmol) was added quickly, in one portion. The reaction mixture was heated to 60 °C, and stirred for 66 h, then allowed to cool to room temperature. The reaction mixture was transferred to a separating funnel, and water (40 mL) was added, followed by TBME (60 mL). The layers were separated, then the organics were washed with brine (2 × 25 mL), and the combined aqueous layers were back extracted with TBME (3 × 25 mL). The combined organics were dried over $MgSO_4$, filtered, and solvent removed *in vacuo* to afford the desired product (**216**) (1.85 g, 96% yield) as a light brown solid.

**Melting point:** 131-133 °C, literature value: Not reported

**IR $\nu_{max}$:** 3002, 2938, 2838, 1580, 1473, 1430, 1200, 1147, 1059 $cm^{-1}$

**$^1$H NMR (400 MHz, DMSO-$d_6$):** $\delta$ = 6.24 (t, *J*=2.2 Hz, 3H), 6.12 (d, *J*=2.2 Hz, 6H), 3.66 (s, 18H)

**$^{13}$C NMR (101 MHz, DMSO-$d_6$):** $\delta$ = 160.9, 148.4, 102.6, 95.2, 55.2

**LCMS (2 min low pH):** $t_R$ = 1.40 min, $[M+H^+]$ 426.1 (96.6% purity)

**HRMS:** ($C_{24}H_{28}NO_6$) $[M+H^+]$ requires: 426.1911, $[M+H^+]$ found: 426.1894

**10-(3,5-Dimethoxyphenyl)-9-mesityl-1,3,6,8-tetramethoxyacridin-10-ium tetrafluoroborate**[61]

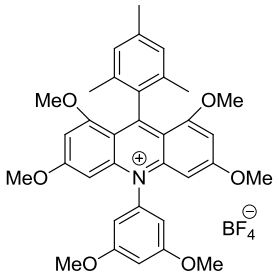


**169**

Tris(3,5-dimethoxyphenyl)amine (1.81 g, 4.25 mmol) and 2,4,6-trimethylbenzoyl chloride (1.49 mL, 8.93 mmol) were dissolved in chlorobenzene (14 mL). Trifluoromethanesulfonic acid (0.378 mL, 4.25 mmol) was added slowly, then the reaction mixture was heated to 80 °C and stirred for 21 hours. The reaction mixture was cooled to room temperature, and transferred to a separating funnel, then washed with $NaBF_4$ (0.2 M aq. solution, 3 × 10 mL) and water (2 × 30 mL). The layers were separated, and to the organic layer was added TBME (120 mL) slowly, over 15 minutes. Further TBME (150 mL) was added slowly, over 30 minutes, and the mixture was allowed to stir at room temperature for 1 hour. The solution was cooled to −5 °C in an ice/salt bath, and was stirred at this temperature for 2 h. The suspension was filtered, the solids were washed with further TBME (3 × 50 mL), and dried *in vacuo*. The liquors were evaporated *in vacuo* then the solid redissolved in chlorobenzene. The recrystallization procedure was repeated 3 times, and the crops of solid were combined to afford the desired product (**169**) (827 mg, 30% yield) as a bright orange solid.

Note: a significant quantity of desired product remained in the liquors, but the crystallisation procedure proved to be relatively ineffective in isolating the product.

**Melting point:** 221-224 °C, literature value: Not reported

**IR $\nu_{max}$:** 2944, 1602, 1575, 1471, 1418, 1264, 1205, 1160, 1048 $cm^{-1}$

**$^1$H NMR (400 MHz, $CDCl_3$):** δ = 6.91 (s, 2H), 6.84 (t, *J*=2.1 Hz, 1H), 6.61 (d, *J*=2.1 Hz, 2H), 6.51 (d, *J*=2.1 Hz, 2H), 6.19 (d, *J*=2.1 Hz, 2H), 3.93 (s, 6H), 3.86 (s, 6H), 3.49 (s, 6H), 2.38 (s, 3H), 1.84 (s, 6H)

**$^{13}$C NMR (101 MHz, $CDCl_3$):** δ = 168.3, 163.2, 162.3, 160.7, 144.8, 139.9, 137.6, 136.5, 132.1, 127.1, 113.4, 105.6, 102.9, 97.6, 92.8, 57.1, 56.5, 56.2, 21.1, 20.2

**LCMS (2 min low pH):** $t_R$ = 1.10 min, [M+H$^+$] 554.1 (96.0% purity)

**HRMS:** ($C_{34}H_{37}NO_6$) [M+H$^+$] requires: 554.2537, [M+H$^+$] found: 554.2520

**2,4,5,6-tetra(9H-carbazol-9-yl)isophthalonitrile**[160]

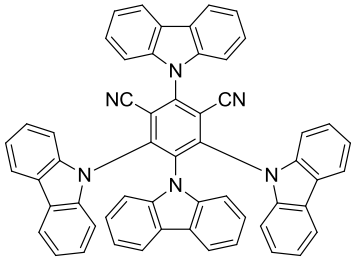


**170**

To a 250 mL 3-necked flask, equipped with a stirrer bar, was added 9H-carbazole (6.44 g, 38.5 mmol). The flask was vacuum purged and backfilled with nitrogen 3 times, then dry THF (77 mL) was added, and the temperature lowered to 0 °C using an ice bath. NaHMDS (1 M in THF, 36.8 mL, 36.8 mmol) was added by syringe. The resulting orange/brown solution was allowed to warm to room temperature, and stirred for 30 minutes. 2,4,5,6-Tetrafluoroisophthalonitrile (1.751 g, 8.75 mmol) was then added as a solid. The resulting dark green solution was heated to reflux, and stirred for 17 h under nitrogen. Additional THF (65 mL) was added, and the reaction mixture was stirred at reflux for a further 8 h. The reaction mixture was allowed to cool to room temperature, then the solids were filtered off, and washed with diethyl ether (350 mL). The Büchner flask was exchanged for a new one, and the yellow solid was then washed through the filter with chloroform (600 mL), in portions. The solvent was removed *in vacuo* to afford the desired product (**170**) (4.32 g, 63% yield) as a bright yellow solid.

**Melting point:** 377-379 °C, literature value: 354-356 °C

**IR $\nu_{max}$:** 3049, 2231, 1444, 1309, 1221, 1151, 1119 $cm^{-1}$

**$^{1}$H NMR (400 MHz, DMSO-$d_6$):** δ = 8.35 (d, *J*=8.0 Hz, 2H), 8.20 (d, *J*=8.0 Hz, 2H), 7.89 - 7.83 (m, 4H), 7.79 - 7.72 (m, 6H), 7.57 - 7.43 (m, 6H), 7.18 - 7.06 (m, 8H), 6.81 (t, *J*=8.0 Hz, 2H), 6.70 (t, *J*=8.0 Hz, 2H)

**$^{13}$C NMR (101 MHz, DMSO-$d_6$):** δ = 145.7, 144.9, 139.9, 138.6, 137.6, 136.5, 126.8, 125.4, 124.2, 123.6, 123.3, 122.8, 121.9, 121.3, 121.0, 120.5, 120.2, 119.4, 116.7, 112.3, 111.1, 111.0, 110.9

**LCMS (8 min TFA):** $t_R$ = 6.15 min, [M+$H^+$] 789.3 (92.8% purity)

**Dimethyl 2-(piperidine-1-carbonyl)succinate**

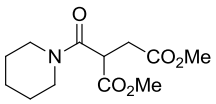

**157**

A 1.5 mL HPLC vial, equipped with a stirrer bar, was charged with ***catalyst*** (0.001 mmol or 0.002 mmol), dimethyl fumarate (14.4 mg, 0.1 mmol), biphenyl (7.7 mg, 0.05 mmol) and sodium 2-oxo-2-(piperidin-1-yl)acetate (17.9 mg, 0.1 mmol). Under a flow of nitrogen, 3:1 DME:DMF (1 mL) was added, and the vial sealed. The reaction mixture was irradiated with 1 × blue LED lamp, and stirred for 16 h. After 16 h, the reaction mixture was sampled for analysis by HPLC (at 210 nm).

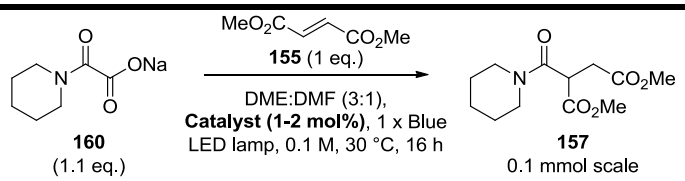


| Entry | Catalyst (mol%, number) | Dimethyl fumarate (155) (%Area) | Product (157) (%Area) | Biphenyl (%Area) |
|---|---|---|---|---|
| 1 | Mesityl acridinium (2%, **164**) | 41.9 | 0 | 29.7 |
| 2 | Triphenylpyrylium (2%, **165**) | 40.5 | 0 | 29.0 |
| 3 | 9,10-Dicyanoathracene (2%, **166**) | 40.8 | 7.3 | 42.1 |
| 4 | $Ru(phen)_3Cl_2$ (1%, **167**) | 50.5 | 0.7 | 34.4 |
| 5 | $Ru(bpz)_3(PF_6)_2$ (1%, **168**) | 59.3 | 0 | 40.74 |
| 6 | $Ir[dF(CF_3)ppy]_2(dtbbpy)PF_6$ (1%, **156**) | 6.5 | 33.2 | 58.7 |
| 7 | Hexamethoxy mesitylacridinium (2%, **169**) | 40.0 | 10.4 | 49.0 |
| 8[a] | 4CzIPN (2%, **170**) | 41.2 | 6.2 | 16.1 |

[a]This reaction was analysed by HPLC at 220 nm, using different molar absorbance ratios (see section 4.2.1 Calculation of HPLC assay yield).

**Dimethyl 2-(piperidine-1-carbonyl)succinate**

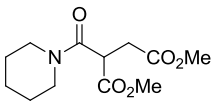

**157**

A 1.5 mL HPLC vial, equipped with a stirrer bar, was charged with ***catalyst*** (0.001 mmol, 0.002 mmol, or 0.010 mmol), dimethyl fumarate (14.4 mg, 0.1 mmol), biphenyl (7.7 mg, 0.05 mmol) and sodium 2-oxo-2-(piperidin-1-yl)acetate (17.9 mg, 0.1 mmol). Under a flow of nitrogen, 3:1 DME:DMF (1 mL) was added, and the vial sealed. Water (0.018 mL, 1 mmol) was then added by piercing the septum. The reaction mixture was irradiated with 1 × blue LED lamp, and stirred for 16 h. After 16 h, the reaction mixture was sampled for analysis by HPLC (at 210 nm).

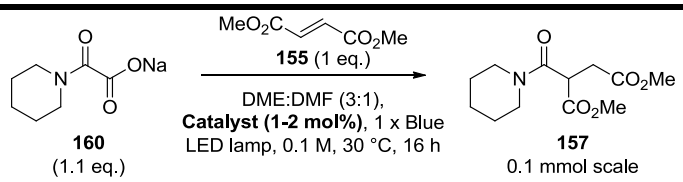


| Entry | Catalyst (mol%, number) | Dimethyl fumarate (155) (%Area) | Product (157) (%Area) | Biphenyl (%Area) |
|---|---|---|---|---|
| 1 | 9,10-Dicyanoathracene (2%, **166**) | 25.0 | 8.9 | 52.4 |
| 2 | $Ir[dF(CF_3)ppy]_2(dtbpy)PF_6$ (1%, **156**) | 8.6 | 34.2 | 55.5 |
| 3 | Hexamethoxy mesitylacridinium (2%, **169**) | 5.4 | 33.0 | 61.0 |
| 4 | Hexamethoxy mesitylacridinium (10%, **169**) | 13.0 | 25.0 | 54.9 |
| 5[a] | 4CzIPN (**170**) | 35.8 | 7.6 | 18.5 |

[a]This reaction was analysed by HPLC at 220 nm, using different molar absorbance ratios (see section 4.2.1 Calculation of HPLC assay yield).

### 4.2.5. Effect of water

**Dimethyl 2-(piperidine-1-carbonyl)succinate**

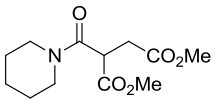

**157**

A 1.5 mL HPLC vial, equipped with a stirrer bar, was charged with $Ir[dF(CF_3)ppy]_2(dtbpy)PF_6$ (1.1 mg, 0.001 mmol), dimethyl fumarate (14.4 mg, 0.1 mmol), biphenyl (7.7 mg, 0.05 mmol) and sodium 2-oxo-2-(piperidin-1-yl)acetate (17.9 mg, 0.1 mmol). Under a flow of nitrogen, 3:1 DME:DMF (***see table for volume***) was added, and the vial sealed. Water (***see table for volume***) was then added by piercing the septum. The reaction mixture was irradiated with 1 × blue LED lamp, and stirred for 16 h. After 16 h, the reaction mixture was sampled for analysis by HPLC (at 210 nm).

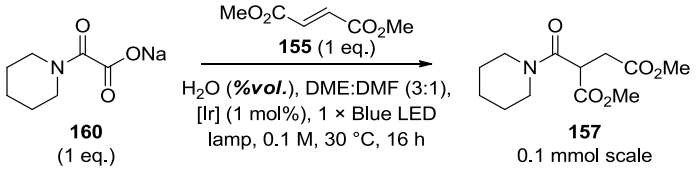


| Entry | Vol DME:DMF/$H_2O$ (mL/mL) [%vol $H_2O$] | Dimethyl fumarate (155) (%Area) | Product (157) (%Area) | Biphenyl (%Area) |
|---|---|---|---|---|
| 1 | 1/0 [0%] | 19.2 | 6.9 | 27.2 |
| 2 | 1/0.009 [0.9%] | 15.4 | 27.9 | 55.2 |
| 3 | 1/0.018 [1.8%][b] | 6.5 | 33.2 | 58.7 |
| 4 | 0.9/0.1 [10%] | 0 | 26.4 | 53.5 |
| 5 | 0.8/0.2 [20%] | 9.0 | 23.0 | 59.2 |
| 6 | 0.5/0.5 [50%] | 5.1 | 4.2 | 77.0 |
| 7 | 0.25/0.75 [75%] | 17.4 | 0 | 70.9 |

### 4.2.6. Solvent selection

**Dimethyl 2-(piperidine-1-carbonyl)succinate**

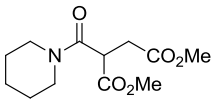


**157**

A 1.5 mL HPLC vial, equipped with a stirrer bar, was charged with $Ir[dF(CF_3)ppy]_2(dtbpy)PF_6$ (1.1 mg, 0.001 mmol), dimethyl fumarate (14.4 mg, 0.1 mmol), biphenyl (7.7 mg, 0.05 mmol) and sodium 2-oxo-2-(piperidin-1-yl)acetate (19.7 mg, 0.11 mmol). Under a flow of nitrogen, ***solvent*** (1 mL) was added, and the vial sealed. Water (0.018 mL, 1 mmol) was then added by piercing the septum. The reaction mixture was irradiated with 1 × blue LED lamp, and stirred for 16 h. After 16 h, the reaction mixture was sampled for analysis by HPLC (at 210 nm).

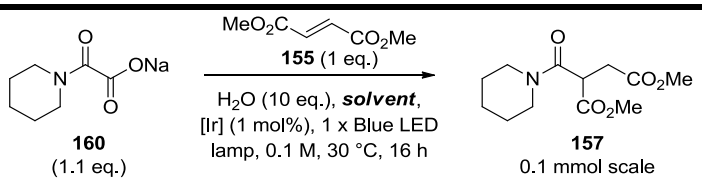


| Entry | Solvent | Dimethyl fumarate (155) (%Area) | Product (157) (%Area) | Biphenyl (%Area) |
|---|---|---|---|---|
| 1 | DME:DMF (3:1) | 2.2 | 34.2 | 55.5 |
| **2** | DME | 11.9 | 23.0 | 57.4 |
| **3** | DMF | 2.9 | 35.5 | 59.1 |
| **4** | DMSO | 10.8 | 3.6 | 83.8 |
| **5** | DMA | 13.4 | 25.3 | 53.7 |
| **6** | NMP | 17.8 | 23.7 | 52.1 |
| **7** | acetonitrile | 6.0 | 18.3 | 60.3 |
| **8** | heptane | 39.8 | 0 | 50.7 |
| **9** | TBME | 21.1 | 4.7 | 57.5 |
| **10** | toluene | 18.8 | 1.7 | 61.7 |
| **11** | THF[b] | 0 | 26.0 | 64.5 |
| **12** | THF | 2.6 | 24.2 | 64.9 |
| **13** | ethyl acetate | 9.1 | 14.2 | 50.3 |
| **14** | DCM | 15.6 | 9.0 | 58.2 |
| **15** | 2-methyl THF | 0 | 8.2 | 81.6 |
| **16** | TamiSolve®[c] | 0 | 27.3 | 53.3 |
| **17** | *N*-methyl formamide | 3.6 | 6.6 | 69.7 |
| **18** | propylene carbonate | 1.6 | 13.4 | 66.1 |
| **19** | acetone | 1.0 | 24.1 | 42.4 |
| **20** | methyl isobutyl ketone | 2.0 | 20.8 | 58.2 |
| **21** | methyl ethyl ketone | 4.0 | 27.3 | 52.3 |

### 4.2.7. Reaction parameter optimisation

**Dimethyl 2-(piperidine-1-carbonyl)succinate**

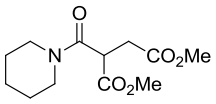

**157**

A 1.5 mL HPLC vial, equipped with a stirrer bar, was charged with $Ir[dF(CF_3)ppy]_2(dtbpy)PF_6$ (***1.1 mg, 0.001 mmol***), dimethyl fumarate (14.4 mg, 0.1 mmol), biphenyl (7.7 mg, 0.05 mmol) and sodium 2-oxo-2-(piperidin-1-yl)acetate (***17.9 mg, 0.1 mmol***). Under a flow of nitrogen, 3:1 DME:DMF (1 mL) was added, and the vial sealed. Water (0.018 mL, 1 mmol) was then added by piercing the septum. The reaction mixture was irradiated with 1 × blue LED lamp, and stirred for 16 h. After 16 h, the reaction mixture was sampled for analysis by HPLC (at 210 nm).

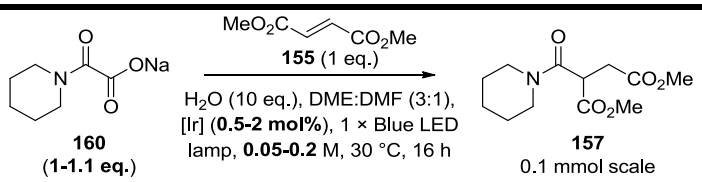


| Entry | Deviation from standard conditions (quantities listed above) | Dimethyl fumarate (155) (%Area) | Product (157) (%Area) | Biphenyl (%Area) |
|---|---|---|---|---|
| 1 | None | 6.5 | 33.2 | 58.7 |
| 2 | 1.1 eq. oxamate (**160**) | 2.2 | 34.2 | 55.5 |
| 3 | 2 mol% catalyst | 9.9 | 30.6 | 56.3 |
| 4 | 0.5 mol% catalyst | 6.4 | 34.0 | 57.9 |
| 5[a] | 0.2 M concentration | 28.2 | 18.6 | 50.5 |
| 6[b] | 0.05 M concentration | 0 | 34.1 | 64.3 |

[a]Concentration was altered by using the same volume of solvent, but doubling the starting material quantities. [b]Concentration was altered by using the same volume of solvent, but halving the starting material quantities.

### 4.2.8. Control reactions

**Reaction without catalyst**

A 4 mL vial, equipped with a stirrer bar, was charged with sodium 2-oxo-2-(piperidin-1-yl)acetate (78 mg, 0.44 mmol) and biphenyl (31 mg, 0.2 mmol). Under a flow of $N_2$, $CO_2$-sparged acetone (4mL) was added, then the vial was sealed with a screw cap septum. 3-Methylenedihydrofuran-2(3H)-one (0.035 mL, 0.4 mmol) and water (0.072 mL, 4 mmol) were then added by piercing the cap. The reaction mixture was irradiated with 1 blue LED lamp at 30 °C and stirred for 16 h. After 16 h, the reaction mixture was sampled for analysis by HPLC. The expected reaction product (**191**) was not observed to any extent.

**Reaction without light**

A 4 mL vial, equipped with a stirrer bar, was charged with $Ir[dF(CF_3)ppy]_2(dtbpy)PF_6$ (1.1 mg, 0.001 mmol), sodium 2-oxo-2-(piperidin-1-yl)acetate (78 mg, 0.44 mmol), and biphenyl (31 mg, 0.2 mmol). Under a flow of $N_2$, $CO_2$-sparged acetone (4mL) was added, then the vial was sealed with a screw cap septum. 3-Methylenedihydrofuran-2(3H)-one (0.035 mL, 0.4 mmol) and water (0.072 mL, 4 mmol) were then added by piercing the cap. The reaction mixture was wrapped in foil, and stirred in the reaction apparatus alongside irradiated reactions, at 30 °C for 24 h. After 24 h, the reaction mixture was sampled for analysis by HPLC. The expected reaction product (**191**) was not observed to any extent.

**With a radical inhibitor**

A 4 mL vial, equipped with a stirrer bar, was charged with $Ir[dF(CF_3)ppy]_2(dtbpy)PF_6$ (4.4 mg, 0.001 mmol), sodium 2-oxo-2-(piperidin-1-yl)acetate (78 mg, 0.44 mmol), TEMPO (124 mg, 0.8 mmol) and biphenyl (31 mg, 0.2 mmol). Under a flow of $N_2$, $CO_2$-sparged acetone (4mL) was added, then the vial was sealed with a screw cap septum. 3-Methylenedihydrofuran-2(3H)-one (0.035 mL, 0.4 mmol) and water (0.072 mL, 4 mmol) were then added by piercing the cap. The reaction mixture was irradiated with 1 blue LED lamp at 30 °C and stirred for 24 h. After 24 h, the reaction mixture was sampled for analysis by HPLC. The expected reaction product (**191**) was not observed to any extent.

### 4.2.9. Substrate scope

*4.2.9.1. Starting material synthesis*

**Methyl 2-oxo-2-(pyrrolidin-1-yl)acetate**[270]

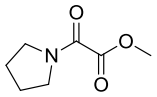

**180**

To a mixture of potassium carbonate (20%w/w aq. solution, 20 mL) and DCM (10 mL) was added pyrrolidine (1.67 mL, 20 mmol). The biphasic mixture was cooled to 0 °C, and methyl 2-chloro-2-oxoacetate (2.21 mL, 24 mmol) was added as a solution in DCM (10 mL), dropwise over 30 minutes. The reaction mixture was stirred at 0 °C for a further 1 h. The layers were separated, and the aqueous layer was extracted with DCM (3 × 10 mL). The combined organics were then washed with water (2 × 10 mL), dried over $MgSO_4$, filtered, and evaporated *in vacuo* to afford the desired product (**180**) (2.68 g, 85% yield) as a colourless oil.

**IR $\nu_{max}$:** 2958, 2884, 1736, 1649, 1456, 1425, 1243, 1223 $cm^{-1}$

**$^1$H NMR (400 MHz, $CDCl_3$):** δ = 3.87 (s, 3H), 3.65 (app. t, *J*=6.7 Hz, 2H), 3.54 (app. t, *J*=6.7 Hz, 2H), 2.01 - 1.87 (m, 4H)

**$^{13}$C NMR (101 MHz, $CDCl_3$):** δ = 162.6, 158.2, 52.6, 47.5, 46.3, 26.0, 23.9

Note: Signals were observed at 46.9 and 45.1, corresponding to pyrrolidine starting material (not visible by LC, due to lack of a chromophore). The oxamate salt prepared in the following step was washed with acetone, to remove this unreacted starting material.

**LCMS (8 min TFA):** $t_R$ = 1.08 min, $[M+H^+]$ 157.9 (99.6% purity)

**HRMS:** ($C_7H_{12}NO_3$) $[M+H^+]$ requires: 158.0812, $[M+H^+]$ found: 158.0808

**Sodium 2-oxo-2-(pyrrolidin-1-yl)acetate**

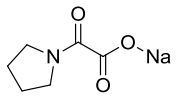

**185**

To a solution of methyl 2-oxo-2-(pyrrolidin-1-yl)acetate (786 mg, 5 mmol) in THF (4 mL) was added sodium hydroxide (1 M aq. solution, 5 mL, 5 mmol) in one portion. The resulting solution was stirred vigorously at room temperature for 5 minutes. Starting material remained, so further sodium hydroxide (1 M aq. solution, 0.25 mL, 0.25 mmol) was added, and the reaction mixture stirred at room temperature for a further 30 minutes. Solvent was removed *in vacuo*, and the resulting solid was washed with acetone (3 × 5 mL), then further dried *in vacuo* to afford the desired product (**185**) (759 mg, 92% yield) as a white solid.

**Melting point:** 240.6-242.9 °C

**IR $\nu_{max}$:** 2969, 2871, 1603, 1447 1366, 1339 $cm^{-1}$

**$^{1}$H NMR (400 MHz, DMSO-$d_6$):** δ = 3.43 (app. t, *J*=6.7 Hz, 2H), 3.20 (app. t, *J*=6.7 Hz, 2H), 1.82 - 1.70 (m, 4H)

**$^{13}$C NMR (101 MHz, DMSO-$d_6$):** δ = 168.7, 167.3, 46.3, 44.0, 25.5, 23.8

**LCMS (2 min low pH):** $t_R$ = 0.42 min, [M+$H^+$] 144.0 (98.4% purity)

**HRMS:** ($C_6H_{10}NO_3$) [M+$H^+$] requires: 144.0655, [M+$H^+$] found: 144.0652

**Ion Chromatography (Na):** Calculated cation mass (w/w): 13.9%, found: 13.4%

**Methyl 2-(diisopropylamino)-2-oxoacetate**[36]

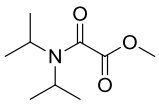

**181**

To a mixture of potassium carbonate (20%w/w aq. solution, 20 mL) and DCM (10 mL) was added diisopropylamine (2.8 mL, 20 mmol). The biphasic mixture was cooled to 0 °C, and methyl 2-chloro-2-oxoacetate (2.21 mL, 24 mmol) was added as a solution in DCM (10 mL), dropwise over 30 minutes. The reaction mixture was stirred at 0 °C for a further 1 h. The layers were separated, and the aqueous layer was extracted with DCM (3 × 10 mL). The combined organics were then washed with water (2 × 10 mL), dried over $MgSO_4$, filtered, and evaporated *in vacuo* to afford the desired product (**181**) (3.28 g, 88% yield) as a colourless oil, which solidified on standing.

**Melting point:** 36.2-38.2 °C, literature value: not reported

**IR $\nu_{max}$:** 2974, 2939, 1728, 1644, 1435, 1361, 1234, 1207 $cm^{-1}$

**$^1$H NMR (400 MHz, $CDCl_3$):** δ = 3.84 (s, 3H), 3.68 (spt, *J*=6.6 Hz, 1H), 3.52 (spt, *J*=6.7 Hz, 1H), 1.45 (d, *J*=6.6 Hz, 6H), 1.24 (d, *J*=6.6 Hz, 6H)

**$^{13}$C NMR (101 MHz, $CDCl_3$):** δ = 163.9, 161.4, 52.3, 50.7, 46.0, 20.7, 20.0

**LCMS (8 min TFA):** $t_R$ = 2.20 min, [M+H$^+$] 188.0 (100% purity)

**HRMS:** ($C_9H_{18}NO_3$) [M+H$^+$] requires: 188.1281, [M+H$^+$] found: 188.1274

**Sodium 2-(diisopropylamino)-2-oxoacetate**

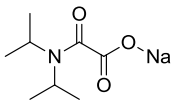


**186**

To a solution of methyl 2-(diisopropylamino)-2-oxoacetate (936 mg, 5 mmol) in THF (4 mL) was added sodium hydroxide (1 M aq. solution, 5 mL, 5 mmol) in one portion. The resulting solution was stirred vigorously at room temperature for 5 minutes. Solvent was removed *in vacuo* to afford the desired product (**186**) (956 mg, 98% yield) as a white solid.

**Melting point:** 281.4-283.8 °C

**IR $\nu_{max}$:** 2959, 1645, 1604,1481, 1305 1215, 1134 $cm^{-1}$

**$^{1}$H NMR (400 MHz, DMSO-$d_6$):** δ =3.94 (spt, *J*=6.7 Hz, 1H), 3.34 (spt, *J*=6.7 Hz, 1H), 1.30 (d, *J*=6.8 Hz, 6H), 1.07 (d, *J*=6.8 Hz, 6H)

**$^{13}$C NMR (101 MHz, DMSO-$d_6$):** δ = 171.0, 168.6, 48.6, 43.3, 20.6, 20.5

**LCMS (8 min TFA):** $t_R$ = 1.26 min, [M+$H^+$] 174.0 (100% purity)

**HRMS:** ($C_8H_{16}NO_3$) [M+$H^+$] requires: 174.1125, [M+$H^+$] found: 174.1121

**Ion Chromatography (Na):** Calculated cation mass (w/w): 11.8%, found: 9.5%

**Methyl 2-morpholino-2-oxoacetate**[270]

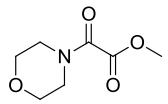

**182**

To a mixture of potassium carbonate (20%w/w aq. solution, 20 mL) and DCM (20 mL) was added morpholine (1.75 mL, 20 mmol). The biphasic mixture was cooled to 0 °C, and methyl 2-chloro-2-oxoacetate (2.21 mL, 24 mmol) was added as a solution in DCM (20 mL), dropwise over 30 minutes. The reaction mixture was stirred at 0 °C for a further 1 h. The layers were separated, and the aqueous layer was extracted with DCM (3 × 10 mL). The combined organics were then washed with water (2 × 10 mL), dried over $MgSO_4$, filtered, and evaporated *in vacuo* to afford the desired product (**182**) (3.29 g, 95% yield) as a colourless oil.

**IR $\nu_{max}$:** 2961, 2922, 2860, 1737, 1652, 1473, 1365, 1269, 1205 1031 $cm^{-1}$

**$^1$H NMR (400 MHz, $CDCl_3$):** $\delta$ = 3.90 (s, 3H), 3.78 - 3.71 (m, 4H), 3.70 - 3.65 (m, 2H), 3.50 (app. dd, *J*=4.6, 4.9 Hz, 2H)

**$^{13}$C NMR (101 MHz, $CDCl_3$):** $\delta$ = 162.6, 159.8, 66.7, 66.4, 52.8, 46.5, 41.9

**LCMS (2 min low pH):** $t_R$ = 0.42 min, $[M+H^+]$ 174.0 (100% purity)

**HRMS:** ($C_7H_{12}NO_4$) $[M+H^+]$ requires: 174.0761, $[M+H^+]$ found: 174.0755

**Sodium 2-morpholino-2-oxoacetate**[268]

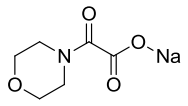


**187**

To a solution of methyl 2-morpholino-2-oxoacetate (1.80 g, 9.92 mmol) in THF (2 mL) was added sodium hydroxide (1 M aq. solution, 9.92 mL, 9.92 mmol). The resulting solution was stirred vigorously at room temperature for 5 minutes. Solvent was removed *in vacuo* to afford the desired product (**187**) (1.80 g, 98% yield) as a white solid.

**Melting point:** 268.0-271.5 °C, literature value: 248 °C

**IR $\nu_{max}$:** 1602, 1488, 1449, 1277, 1237, 1106 $cm^{-1}$

**$^{1}$H NMR (400 MHz, DMSO-$d_6$):** $\delta$ = 3.54 - 3.48 (m, 4H), 3.37 - 3.33 (m, 4H)

**$^{13}$C NMR (101 MHz, DMSO-$d_6$):** $\delta$ = 169.6, 166.8, 66.9, 66.5, 46.3, 40.4

**LCMS (2 min low pH):** $t_R$ = 0.37 min, $[M+H^+]$ 160.0 (99.0% purity)

**HRMS:** ($C_6H_{10}NO_4$) $[M+H^+]$ requires: 160.0604, $[M+H^+]$ found: 160.0601

**Methyl 2-((4-bromobenzyl)(methyl)amino)-2-oxoacetate**

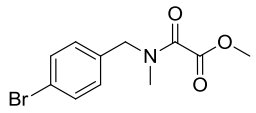

**183**

To a mixture of potassium carbonate (20%w/w aq. solution, 20 mL) and DCM (10 mL) was added 1-(4-bromophenyl)-*N*-methylmethanamine (4 mL, 20 mmol). The biphasic mixture was cooled to 0 °C, and methyl 2-chloro-2-oxoacetate (2.21 mL, 24 mmol) was added as a solution in DCM (10 mL), dropwise over 30 minutes. The reaction mixture was stirred at 0 °C for a further 1 h. The layers were separated, and the aqueous layer was extracted with DCM (3 × 10 mL). The combined organics were then washed with water (2 × 10 mL), dried over $MgSO_4$, filtered, and evaporated *in vacuo* to afford the desired product (**183**) (3.70 g, 65% yield) as a pale yellow oil.

**IR $\nu_{max}$:** 2955, 1738, 1655, 1488, 1405, 1237, 1201, 1095, $cm^{-1}$

**$^1$H NMR (400 MHz, $CDCl_3$):** δ = 7.53 - 7.46 (m, 4H), 7.20 - 7.13 (m, 4H), 4.55 (s, 2H), 4.40 (s, 2H), 3.90 (s, 3H), 3.88 (s, 3H), 2.91 (s, 3H), 2.87 (s, 3H)

Note: all peaks are duplicated due to the presence of two rotameric forms. A high temperature proton NMR displayed coalescence of these peaks, to some extent.

**$^1$H NMR (400 MHz, 121 °C, DMSO-$d_6$):** 7.56 (d, *J*=8.2 Hz, 2H), 7.24 (d, *J*=8.2 Hz, 2H), 4.53 (br. s, 2H), 3.83 (s, 3H), 3.00 - 2.77 (m, 3H)

**$^{13}$C NMR (101 MHz, $CDCl_3$):** δ = 163.2, 163.0, 161.7, 134.5, 134.1, 132.1, 132.0, 130.0, 129.3, 122.3, 122.0, 53.2, 52.8, 52.7, 49.5, 34.7, 31.8

Note: all peaks (aside from the ester carbonyl peak) are duplicated due to the presence of rotamers.

**LCMS (8 min TFA):** $t_R$ = 3.07 min, [($^{81}$Br)M+H$^+$] 287.9 (96.7% purity)

**HRMS:** ($C_{11}H_{13}[^{79}Br]NO_3$) [M+H$^+$] requires: 286.0073, [M+H$^+$] found: 286.0067

**Sodium 2-((4-bromobenzyl)(methyl)amino)-2-oxoacetate**

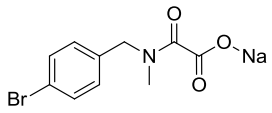


**188**

To a solution of methyl 2-((4-bromobenzyl)(methyl)amino)-2-oxoacetate (1.43 g, 5 mmol) in THF (20 mL) was added sodium hydroxide (1 M aq. solution, 5 mL, 5 mmol) in one portion. The resulting solution was stirred vigorously at room temperature for 30 minutes. Starting material was still present, so further NaOH (1 M aq. solution, 0.5 mL, 0.5 mmol) was added, and the reaction stirred at room temperature for a further 30 minutes. Solvent was removed *in vacuo*, then the resulting pale yellow solid was stirred with acetone (20 mL) at room temperature for 30 minutes, then filtered. The solids were washed with further acetone (2 × 5 mL) and dried *in vacuo* to afford the desired product (**188**) (1.40 g, 95% yield) as a white solid.

**Melting point:** 197.0-199.7 °C

**IR $\nu_{max}$:** 3280, 1599, 1484, 1367, 1236, 1102 $cm^{-1}$

**$^{1}$H NMR (400 MHz, DMSO-$d_6$):** $\delta$ = 7.55 - 7.52 (m, 2H), 7.52 - 7.49 (m, 2H), 7.43 - 7.36 (m, 2H), 7.20 - 7.14 (m, 2H), 4.38 (s, 2H), 4.36 (s, 2H), 2.78 (s, 3H), 2.53 (s, 3H)

All signals were duplicated, due to the presence of two rotameric forms.

**$^{13}$C NMR (101 MHz, DMSO-$d_6$):** $\delta$ = 171.1, 170.9, 167.5, 167.2, 137.4, 137.4, 131.2, 131.1, 130.5, 129.8, 120.3, 119.9, 51.9, 46.8, 34.3, 29.4

All signals were duplicated, due to the presence of two rotameric forms.

**LCMS (8 min TFA):** $t_R$ = 2.01 min, [($^{79}$Br)M+H$^+$] 271.8 (99.1% purity)

**HRMS:** ($C_{10}H_{11}[^{79}Br]NO_3$) [M+H$^+$] requires: 271.9917, [M+H$^+$] found: 271.9915

**Ion Chromatography (Na):** Calculated cation mass (w/w): 7.8%, found: 7.4%

**Benzyl 4-(2-methoxy-2-oxoacetyl)piperazine-1-carboxylate**

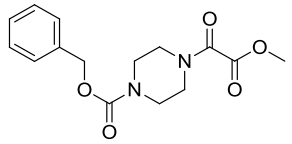

**184**

To a mixture of potassium hydrogen carbonate (20%w/w aq. solution, 5 mL) and toluene (5 mL) was added benzyl piperazine-1-carboxylate (0.964 mL, 5 mmol). The biphasic mixture was cooled to 0 °C, and methyl 2-chloro-2-oxoacetate (0.552 mL, 6 mmol) was added in one portion, then the reaction mixture was stirred for 2 hours at 0 °C. Ethyl acetate (25 mL) was added, followed by water (25 mL), then the layers were separated. The aqueous layer was extracted with further ethyl acetate (25 mL), then the combined organics were dried over $MgSO_4$, filtered, and evaporated *in vacuo* to afford the desired product (**184**) (1.40 g, 91% yield) as pale yellow gum.

**IR $\nu_{max}$:** 3028, 2869, 1727, 1693, 1655 1454, 1425, 1281, 1228, 1204, 1173 $cm^{-1}$

**$^1$H NMR (400 MHz, $CDCl_3$):** δ = 7.40 - 7.33 (m, 5H), 5.17 (s, 2H), 3.89 (s, 3H), 3.67 - 3.61 (m, 2H), 3.60 - 3.55 (m, 4H), 3.48 - 3.42 (m, 2H)

**$^{13}$C NMR (101 MHz, $CDCl_3$):** δ = 162.6, 159.9, 155.0, 136.2, 128.6, 128.3, 128.1, 67.7, 52.8, 45.9, 43.9, 43.3, 41.4

**LCMS (2 min low pH):** $t_R$ = 0.91 min, $[M+H^+]$ 307.0 (93.4% purity)

**HRMS:** ($C_{15}H_{19}N_2O_5$) $[M+H^+]$ requires: 307.1289, $[M+H^+]$ found: 307.1280

**Sodium 2-(4-((benzyloxy)carbonyl)piperazin-1-yl)-2-oxoacetate**

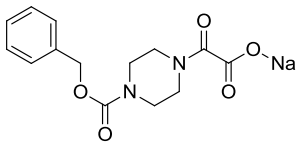


**189**

To a solution of benzyl 4-(2-methoxy-2-oxoacetyl)piperazine-1-carboxylate (628 mg, 2.05 mmol) in THF (2 mL) was added sodium hydroxide (1 M aq. solution, 2.05 mL, 2.05 mmol). The resulting solution was stirred vigorously at room temperature for 5 minutes. Acetone (25 mL) was added in one portion, and the reaction mixture stirred at room temperature for a further 30 minutes. The resulting precipitate was collected by filtration and dried *in vacuo* to afford the desired product (**189**) (556 mg, 86% yield) as a white solid.

**Melting point:** 243.8-245.7 °C

**IR $\nu_{max}$:** 1697, 1615, 1462, 1432, 1353, 1231, 1122, 1077, 1038 $cm^{-1}$

**$^{1}$H NMR (400 MHz, DMSO-$d_6$):** δ = 7.41 - 7.28 (m, 5H), 5.10 (s, 2H), 3.35 (br. s, 8H)

**$^{13}$C NMR (101 MHz, DMSO-$d_6$):** δ = 169.7, 167.4, 154.9, 137.3, 128.9, 128.3, 128.1, 66.8, 45.4, 44.4 (br. s), 43.8 (br. s), 39.65

**LCMS (2 min low pH):** $t_R$ = 0.83 min, $[M+H^+]$ 293.1 (100% purity)

**HRMS:** ($C_{14}H_{17}N_2O_5$) $[M+H^+]$ requires: 293.1132, $[M+H^+]$ found: 293.1126

**Ion Chromatography (Na):** Calculated cation mass (w/w): 7.3%, found: 7.6%

**Methyl 2-(methyl(*p*-tolyl)amino)-2-oxoacetate**

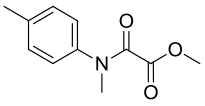


**152**

Synthesis description and full characterisation can be found above, on page 141.

**Sodium 2-(methyl(*p*-tolyl)amino)-2-oxoacetate**

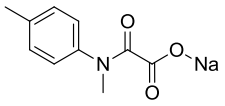


**190**

To a solution of methyl 2-(methyl(*p*-tolyl)amino)-2-oxoacetate (3.73 g, 18 mmol) in THF (18 mL) was added sodium hydroxide (1 M aq. solution, 18 mL, 18 mmol). The resulting solution was stirred vigorously at room temperature for 5 minutes. Acetone (500 mL) was added in one portion, and the mixture allowed to stir for 30 minutes. The solids were collected by filtration, and dried *in vacuo* to afford the desired product (**190**) (3.6 g, 93% yield) as a white solid.

**Melting point:** Decomposed at 258 °C

**IR $\nu_{max}$:** 1616, 1518, 1405, 1346, 1296 $cm^{-1}$

**$^{1}$H NMR (400 MHz, 77 °C, DMSO-$d_6$):** $\delta$ = 7.21 - 7.16 (m, 2H), 7.08 (d, *J*=8.1 Hz, 2H), 3.14 (s, 3H), 2.27 (s, 3H)

**$^{13}$C NMR (101 MHz, 77 °C, DMSO-$d_6$):** $\delta$ = 170.7, 167.1, 141.3, 134.2, 128.8, 124.9, 35.4 (br. s), 20.4

*N*-Me carbon appears as a very broad signal, due to rotameric species, even when data was collected at an elevated temperature.

**LCMS (2 min formic):** $t_R$ = 0.71 min, [M+H$^+$] 194.0 (99.6% purity)

**HRMS:** ($C_{10}H_{12}NO_3$) [M+H$^+$] requires: 194.0812, [M+H$^+$] found: 194.0809

**Ion Chromatography (Na):** Calculated cation mass (w/w): 10.7%, found: 9.8%

*4.2.9.2. Amidation substrate scope*

**3-(2-Oxo-2-(piperidin-1-yl)ethyl)dihydrofuran-2(3H)-one**

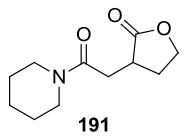

**191**

Prepared using **General method A**, **oxamate** sodium 2-oxo-2-(piperidin-1-yl)acetate (78 mg, 0.44 mmol) and **liquid olefin** 3-methylenedihydrofuran-2(3H)-one (0.035 mL, 0.4 mmol) were reacted under irradiation by 1 LED lamp, for 24 h.

The crude product was purified by chromatography on silica; elution gradient 0-100% ethyl acetate in heptane. The appropriate fractions were combined and evaporated *in vacuo* to afford the desired product (**191**) (69 mg, 82% yield) as a yellow solid.

**Melting point:** 56.0-58.9 °C

**IR $\nu_{max}$:** 2933, 2856, 1764, 1636, 1443, 1257, 1217, 1021 $cm^{-1}$

**$^{1}$H NMR (400 MHz, $CDCl_3$):** δ = 4.41 (ddd, *J*=2.1, 9.0, 9.2 Hz, 1H, $OCH_2$), 4.24 (ddd, *J*=6.8, 9.0, 10.2 Hz, 1H, $OCH_2$), 3.66 - 3.57 (m, 1H, $CH_2N$), 3.54 - 3.46 (m, 1H, $CH_2N$), 3.46 - 3.32 (m, 2H, $CH_2N$), 3.03 (t, *J*=3.0 Hz, 1H, CHC(O)O), 2.97 (dd, *J*=2.5, 16.7 Hz, 1H, $NC(O)CH_2$), 2.63 (dd, *J*=2.1, 10.2 Hz, 1H, $CHCH_2CH_2O$), 2.48 (dd, *J*=9.2, 16.7 Hz, 1H, $NC(O)CH_2$), 2.00 (ddd, *J*=2.1, 9.2, 10.2 Hz, 1H, $CHCH_2CH_2O$), 1.68 - 1.62 (m, 2H, $CH_2$), 1.61 - 1.52 (m, 4H, 2 × $CH_2$)

**$^{13}$C NMR (101 MHz, $CDCl_3$):** δ = 179.4 (C(O)O), 168.1 (NC(O)), 66.8 ($CH_2OC(O)$), 46.4 ($CH_2N$), 42.9 ($CH_2N$), 36.4 (CHC(O)O), 34.2 ($NC(O)CH_2$), 29.5 ($CHCH_2CH_2O$), 26.4 ($CH_2$), 25.5 ($CH_2$), 24.4 ($CH_2$)

**LCMS (2 min low pH):** $t_R$ = 0.59 min, $[M+H^+]$ 212.1 (97.7% purity)

**HRMS:** ($C_{11}H_{18}NO_3$) $[M+H^+]$ requires: 212.1281, $[M+H^+]$ found: 212.1275

***N*,*N*-Diisopropyl-2-(2-oxotetrahydrofuran-3-yl)acetamide**

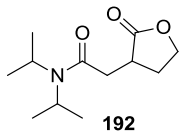

192

Prepared using **General method A**, **oxamate** sodium 2-(diisopropylamino)-2-oxoacetate (85 mg, 0.44 mmol) and **liquid olefin** 3-methylenedihydrofuran-2(3H)-one (0.035 mL, 0.4 mmol) were reacted under irradiation by 1 LED lamp, for 24 h.

The crude product was purified by chromatography on silica; elution gradient 0-100% ethyl acetate in heptane. The appropriate fractions were combined and evaporated *in vacuo*. The resulting solid was dissolved and pipetted away from the impure product, using portions of heptane (10 × 2 mL). These portions were combined and evaporated *in vacuo* to afford the desired product (**192**) (67 mg, 74% yield) as a yellow solid.

**Melting point:** 62.4-66.1 °C

**IR $\nu_{max}$:** 2999, 2968, 2929, 2874, 1764, 1634, 1442, 1371, 1024 $cm^{-1}$

**$^{1}$H NMR (400 MHz, $CDCl_3$):** δ = 4.40 (t, *J*=9.2 Hz, 1H), 4.27 - 4.17 (m, 1H), 3.96 (spt, *J*=6.5 Hz, 1H), 3.49 (br. s, 1H), 3.08 - 2.93 (m, 2H), 2.71 - 2.59 (m, 1H), 2.42 (app. dd, *J*=9.2, 16.4 Hz, 1H), 2.03 - 1.90 (m, 1H), 1.37 (d, *J*=6.5 Hz, 6H), 1.23 (d, *J*=6.5 Hz, 3H), 1.20 (d, *J*=6.5 Hz, 3H)

**$^{13}$C NMR (101 MHz, $CDCl_3$):** δ = 179.6, 168.4, 66.8, 48.3, 45.9, 36.5, 35.9, 29.7, 20.9, 20.8, 20.7, 20.6

**LCMS (2 min low pH):** $t_R$ = 0.79 min, $[M+H^+]$ 228.1 (95.3% purity)

**HRMS:** ($C_{12}H_{22}NO_3$) $[M+H^+]$ requires: 228.1594, $[M+H^+]$ found: 228.1583

***N*-(4-Bromobenzyl)-N-methyl-2-(2-oxotetrahydrofuran-3-yl)acetamide**

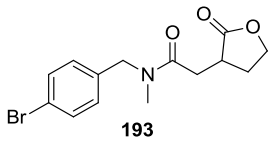


**193**

Prepared using **General method A**, **oxamate** sodium 2-((4-bromobenzyl)(methyl)amino)-2-oxoacetate (129 mg, 0.44 mmol) and **liquid olefin** 3-methylenedihydrofuran-2(3H)-one (0.035 mL, 0.4 mmol) were reacted under irradiation by 1 LED lamp, for 48 h.

The crude product was purified by chromatography on silica; elution gradient 0-100% ethyl acetate in heptane. The appropriate fractions were combined and evaporated *in vacuo*, to afford the desired product (**193**) (82 mg, 63% yield) as a pale yellow oil.

**IR $\nu_{max}$:** 2914, 1764, 1644, 1488, 1405, 1158, 1024 $cm^{-1}$

**$^{1}$H NMR (400 MHz, 121 °C, DMSO-$d_6$):** $\delta$ = 7.52 (d, *J*=8.3 Hz, 2H), 7.20 (d, *J*=8.3 Hz, 2H), 4.53 (s, 2H), 4.31 (ddd, *J*=2.9, 8.4, 8.8 Hz, 1H), 4.20 (dd, *J*=8.8, 16.4 Hz, 1H), 3.04 - 2.95 (m, 1H), 2.93 (s, 3H), 2.88 - 2.79 (m, 1H), 2.65 (app. dd, *J*=8.4, 16.4 Hz, 1H), 2.46 - 2.37 (m, 1H), 2.10 - 1.98 (m, 1H)

**$^{13}$C NMR (101 MHz, DMSO-$d_6$):** $\delta$ = 179.6, 179.5, 170.6, 170.5, 137.7, 137.3, 132.1, 131.8, 130.2, 129.2, 120.7, 120.5, 66.8, 66.7, 52.1, 50.0, 36.0, 36.0, 35.1, 34.0, 33.4, 33.1, 28.4, 28.3

All signals were duplicated, due to the presence of two rotameric forms.

**LCMS (2 min low pH):** $t_R$ = 0.92 min, [($^{81}$Br)M+H$^+$] 327.9 (93.4% purity)

**HRMS:** ($C_{14}H_{17}[^{79}Br]NO_3$) [M+H$^+$] requires: 326.0386, [M+H$^+$] found: 326.0379

**Dimethyl 2-(morpholine-4-carbonyl)succinate**

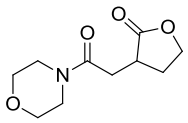

**194**

Prepared using **General method A**, **oxamate** sodium 2-morpholino-2-oxoacetate (80 mg, 0.44 mmol) and **liquid olefin** 3-methylenedihydrofuran-2(3H)-one (0.035 mL, 0.4 mmol) were reacted under irradiation by 1 LED lamp, for 26 h.

The crude product was purified by chromatography on silica; elution gradient 0-100% ethyl acetate in heptane. The appropriate fractions were combined and evaporated *in vacuo* to afford the desired product (**194**) (56 mg, 66% yield) as a yellow oil.

**IR $\nu_{max}$:** 2961, 2922, 2856, 1761, 1638, 1437, 1273, 1209, 1154, 1112 $cm^{-1}$

**$^{1}$H NMR (400 MHz, $CDCl_3$):** $\delta$ = 4.44 (dt, *J*=2.0, 9.2 Hz, 1H), 4.27 (ddd, *J*=6.6, 9.2, 10.7 Hz, 1H), 3.73 - 3.68 (m, 4H), 3.68 - 3.45 (m, 4H), 3.10 - 3.01 (m, 1H), 2.98 (app. dd, *J*=3.2, 16.9 Hz, 1H), 2.70 - 2.60 (m, 1H), 2.51 (dd, *J*=9.0, 16.9 Hz, 1H), 2.04 (dtd, *J*=9.0, 10.7, 12.4 Hz, 1H)

**$^{13}$C NMR (101 MHz, $CDCl_3$):** $\delta$ = 179.1, 168.6, 66.8, 66.5, 45.7, 42.1, 36.2, 33.9, 29.3

Note: only 1 × signal was observed for morpholine $\underline{C}H_2O$.

**LCMS (2 min low pH):** $t_R$ = 0.39 min, $[M+H^+]$ 214.1 (99.5% purity)

**HRMS:** ($C_{10}H_{16}NO_4$) $[M+H^+]$ requires: 214.1079, $[M+H^+]$ found: 214.1088

**Benzyl4-(2-(2-oxotetrahydrofuran-3-yl)acetyl)piperazine-1-carboxylate**

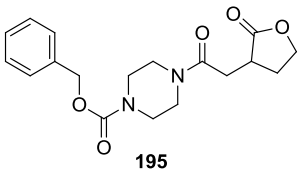

**195**

Prepared using **General method A**, **oxamate** sodium 2-(4-((benzyloxy)carbonyl)piperazin-1-yl)-2-oxoacetate (138 mg, 0.44 mmol) and **liquid olefin** 3-methylenedihydrofuran-2(3H)-one (0.035 mL, 0.4 mmol) were reacted under irradiation by 1 LED lamp, for 26 h.

The crude product was purified by chromatography on silica; elution gradient 0-100% ethyl acetate in heptane. The appropriate fractions were combined and evaporated *in vacuo* to afford the desired product (**195**) (75 mg, 54% yield) as a pale yellow oil.

**LCMS (2 min low pH):** $t_R$ = 0.83 min, [M+H$^+$] 347.0 (98.2% purity)

Full product characterisation can be found below, on page 191.

***N*-Methyl-2-(2-oxotetrahydrofuran-3-yl)-*N*-(*p*-tolyl)acetamide**

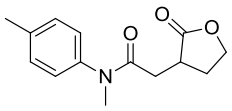

**196**

Prepared using **General method A**, **oxamate** sodium 2-(methyl(p-tolyl)amino)-2-oxoacetate (95 mg, 0.44 mmol) and **liquid olefin** 3-methylenedihydrofuran-2(3H)-one (0.035 mL, 0.4 mmol) were reacted under irradiation by 2 LED lamps, for 32 h.

The crude product was purified by chromatography on silica; elution gradient 0-100% ethyl acetate in heptane. The appropriate fractions were combined and evaporated *in vacuo* to afford the desired product (**196**) (63 mg, 63% yield) as a pale yellow solid.

**Melting point:** 65.3-67.4 °C

**IR $\nu_{max}$:** 2920, 1765, 1654, 1515, 1420, 1389, 1022 $cm^{-1}$

**$^{1}$H NMR (400 MHz, $CDCl_3$):** δ = 7.24 (d, *J*=8.1 Hz, 2H), 7.09 (d, *J*=8.1 Hz, 2H), 4.37 (ddd, *J*=2.0, 8.9, 9.2 Hz, 1H), 4.22 (dt, *J*=6.6, 9.2 Hz, 1H), 3.27 (s, 3H), 3.07 - 2.96 (m, 1H), 2.68 (app. dd, *J*=3.4, 17.0 Hz, 1H), 2.61 - 2.52 (m, 1H), 2.40 (s, 3H), 2.27 (app. dd, *J*=9.1, 17.0 Hz, 1H), 1.95 (s, 1H)

**$^{13}$C NMR (101 MHz, $CDCl_3$):** δ = 179.1, 170.2, 140.8, 138.2, 130.6, 127.1, 66.6, 37.4, 36.4, 35.1, 29.1, 21.1

**LCMS (2 min low pH):** $t_R$ = 0.83 min, $[M+H^+]$ 248.1 (98.1% purity)

**HRMS:** ($C_{14}H_{18}NO_3$) $[M+H^+]$ requires: 248.1281, $[M+H^+]$ found: 248.1273

**Dimethyl 2-(piperidine-1-carbonyl)succinate**

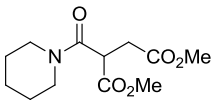


**157**

Prepared using **General method A**, **oxamate** sodium 2-oxo-2-(piperidin-1-yl)acetate (79 mg, 0.44 mmol) and **solid olefin** dimethyl fumarate (58 mg, 0.4 mmol) were reacted under irradiation by 1 LED lamp, for 24 h.

The crude product was purified by chromatography on silica; elution gradient 0-100% ethyl acetate in heptane. The appropriate fractions were combined and evaporated *in vacuo* to afford the desired product (**157**) (87 mg, 85% yield) as a yellow oil.

**IR $\nu_{max}$:** 2920, 1765, 1654, 1515, 1389, 1156, 1123, 1022, $cm^{-1}$

**$^{1}$H NMR (400 MHz, $CDCl_3$):** δ = 4.18 (dd, *J*=6.4, 7.9 Hz, 1H), 3.75 (s, 3H), 3.71 (s, 3H), 3.64 - 3.54 (m, 4H), 3.06 (dd, *J*=7.9, 17.2 Hz, 1H), 2.97 (dd, *J*=6.4, 17.2 Hz, 1H), 1.74 - 1.62 (m, 4H), 1.61 - 1.54 (m, 2H)

**$^{13}$C NMR (101 MHz, $CDCl_3$):** δ = 172.0, 169.4, 165.6, 116.3, 52.6, 51.9, 47.4, 44.2, 43.6, 33.4, 26.2, 25.5, 24.4

**LCMS (2 min low pH):** $t_R$ = 0.72 min, $[M+H^+]$ 258.1 (99.3% purity)

**HRMS:** ($C_{12}H_{20}NO_5$) $[M+H^+]$ requires: 258.1336, $[M+H^+]$ found: 258.1332

**1-(Piperidin-1-yl)hexane-1,4-dione**

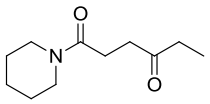

**197**

Prepared using **General method A**, **oxamate** sodium 2-oxo-2-(piperidin-1-yl)acetate (79 mg, 0.44 mmol) and **liquid olefin** pent-1-en-3-one (0.040 mL, 0.4 mmol) were reacted under irradiation by 1 LED lamp, for 24 h.

The crude product was purified by chromatography on silica; elution gradient 0-100% ethyl acetate in heptane. The appropriate fractions were combined and evaporated *in vacuo* to afford the desired product (**197**) (60 mg, 77% yield) as a yellow oil.

**IR $\nu_{max}$:** 2936, 2856, 1713, 1636, 1440, 1413, 1368, 1218, 1114 $cm^{-1}$

**$^{1}$H NMR (400 MHz, $CDCl_3$):** $\delta$ = 3.53 (app. dd, *J*=5.2, 5.4 Hz, 2H), 3.44 (app. dd, *J*=5.2, 5.4 Hz, 2H), 2.75 (t, *J*=6.6 Hz, 2H), 2.61 (t, *J*=6.6 Hz, 2H), 2.54 (q, *J*=7.4 Hz, 2H), 1.69 - 1.49 (m, 6H), 1.08 (t, *J*=7.4 Hz, 3H)

**$^{13}$C NMR (101 MHz, $CDCl_3$):** $\delta$ = 210.8, 169.8, 46.4, 42.9, 36.9, 36.2, 27.0, 26.4, 25.5, 24.6, 7.8

**LCMS (2 min low pH):** $t_R$ = 0.70 min, $[M+H^+]$ 198.1 (97.3% purity)

**HRMS:** ($C_{11}H_{20}NO_2$) $[M+H^+]$ requires: 198.1489, $[M+H^+]$ found: 198.1478

**3-(Phenylsulfonyl)-1-(piperidin-1-yl)propan-1-one**

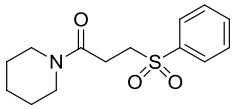

198

Prepared using **General method A**, **oxamate** sodium 2-oxo-2-(piperidin-1-yl)acetate (79 mg, 0.44 mmol) and **solid olefin** (vinylsulfonyl)benzene (67 mg, 0.4 mmol) were reacted under irradiation by 1 LED lamp, for 24 h.

The crude product was purified by chromatography on silica; elution gradient 0-100% ethyl acetate in heptane. The appropriate fractions were combined and evaporated *in vacuo* to afford the desired product (**198**) (91 mg, 80% yield) as a yellow oil.

**IR $\nu_{max}$:** 2936, 2857, 1638, 1446, 1307, 1284, 1254, 1150, $cm^{-1}$

**$^{1}$H NMR (400MHz, $CDCl_3$):** $\delta$ = 7.97 - 7.92 (m, 2H), 7.71 - 7.66 (m, 1H), 7.63 - 7.57 (m, 2H), 3.54 - 3.46 (m, 4H), 3.40 (app. dd, *J*=5.2, 5.4 Hz, 2H), 2.89 - 2.79 (m, 2H), 1.70 - 1.64 (m, 2H), 1.62 - 1.56 (m, 2H), 1.56 - 1.49 (m, 2H)

**$^{13}$C NMR (101MHz, $CDCl_3$):** $\delta$ = 166.8, 139.2, 133.8, 129.3, 128.0, 52.2, 46.5, 43.1, 26.3, 26.0, 25.4, 24.4

**LCMS (2 min low pH):** $t_R$ = 0.82 min, $[M+H^+]$ 282.1 (93.7% purity)

**HRMS:** ($C_{14}H_{20}NO_3S$) $[M+H^+]$ requires: 282.1158, $[M+H^+]$ found: 282.1150

**2-Methyl-4-oxo-4-(piperidin-1-yl)butanenitrile**

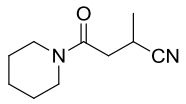


**199**

Prepared using **General method A**, **oxamate** sodium 2-oxo-2-(piperidin-1-yl)acetate (79 mg, 0.44 mmol) and **liquid olefin** methacrylonitrile (0.034 mL, 0.4 mmol) were reacted under irradiation by 1 LED lamp, for 24 h.

The crude product was purified by chromatography on silica; elution gradient 0-100% ethyl acetate in heptane. The appropriate fractions were combined and evaporated *in vacuo* to afford the desired product (**199**) (60 mg, 84% yield) as a yellow oil.

**IR $\nu_{max}$:** 2937, 2857, 2241, 1636, 1444, 1227 $cm^{-1}$

**$^{1}$H NMR (400 MHz, $CDCl_3$):** $\delta$ = 3.65 - 3.51 (m, 2H), 3.44 - 3.34 (m, 2H), 3.26 (dqd, *J*=6.6, 7.1, 7.3 Hz, 1H), 2.75 (dd, *J*=6.6, 16.1 Hz, 1H), 2.50 (dd, *J*=7.3, 16.1 Hz, 1H), 1.70 - 1.64 (m, 2H), 1.63 - 1.53 (m, 4H), 1.39 (d, *J*=7.1 Hz, 3H)

**$^{13}$C NMR (101 MHz, $CDCl_3$):** $\delta$ = 166.6, 123.0, 46.5, 43.0, 37.2, 26.4, 25.5, 24.4, 21.9, 18.1

**LCMS (2 min low pH):** $t_R$ = 0.67 min, $[M+H^+]$ 181.0 (98.5% purity)

**HRMS:** ($C_{10}H_{17}N_2O$) $[M+H^+]$ requires: 181.1335, $[M+H^+]$ found: 181.1326

**3,3-Diphenyl-1-(piperidin-1-yl)propan-1-one**[271]

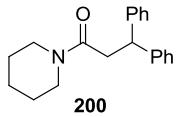


**200**

Prepared using **General method A**, **oxamate** sodium 2-oxo-2-(piperidin-1-yl)acetate (79 mg, 0.44 mmol) and **liquid olefin** ethene-1,1-diyldibenzene (0.071 mL, 0.4 mmol) were reacted under irradiation by 2 LED lamps, for 32 h.

The crude product was purified by chromatography on silica; elution gradient 0-100% ethyl acetate in heptane. The appropriate fractions were combined and evaporated *in vacuo* to afford the desired product (**200**) (82 mg, 70% yield) as a pale yellow solid.

**Melting point:** 134-136 °C, literature value: 122-124 °C

**IR $\nu_{max}$:** 2945, 2855, 1618, 1451 $cm^{-1}$

**$^{1}$H NMR (400 MHz, $CDCl_3$):** $\delta$ = 7.32 - 7.25 (m, 8H), 7.23 - 7.17 (m, 2H), 4.70 (t, *J*=7.5 Hz, 1H), 3.50 (app. dd, *J*=5.5, 5.7 Hz, 2H), 3.32 (app. dd, *J*=5.5, 5.7 Hz, 2H), 3.07 (d, *J*=7.5 Hz, 2H), 1.60 - 1.53 (m, 2H), 1.49 - 1.41 (m, 2H), 1.38 - 1.30 (m, 2H)

**$^{13}$C NMR (101 MHz, $CDCl_3$):** $\delta$ = 169.4, 144.4, 128.5, 127.9, 126.3, 47.4, 46.8, 42.8, 38.9, 26.3, 25.5, 24.5

**LCMS (2 min low pH):** $t_R$ = 1.20 min, $[M+H^+]$ 294.1 (99.6% purity)

**HRMS:** ($C_{20}H_{24}NO$) $[M+H^+]$ requires: 294.1852, $[M+H^+]$ found: 294.1838

**1-(Piperidin-1-yl)-3-(3-(trifluoromethyl)phenyl)propan-1-one**

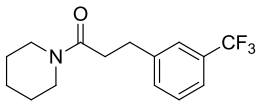

**201**

Prepared using **General method A**, **oxamate** sodium 2-oxo-2-(piperidin-1-yl)acetate (79 mg, 0.44 mmol) and **liquid olefin** 1-(trifluoromethyl)-3-vinylbenzene (0.059 mL, 0.4 mmol) were reacted under irradiation by 1 LED lamp, for 24 h.

The crude product was purified by chromatography on silica; elution gradient 0-100% ethyl acetate in heptane. The appropriate fractions were combined and evaporated *in vacuo* to afford the desired product (**201**) (54 mg, 47% yield) as a yellow oil.

**IR $\nu_{max}$:** 2938, 2858, 1639, 1444, 1328, 1161, 1121, 1074 $cm^{-1}$

**$^{1}$H NMR (400 MHz, $CDCl_3$):** δ = 7.52 - 7.38 (m, 4H,), 3.58 (dd, *J*=5.5, 5.7 Hz, 2H), 3.36 (dd, *J*=5.5, 5.7 Hz, 2H), 3.06 (dd, *J*=7.3, 7.9 Hz, 2H), 2.65 (dd, *J*=7.3, 7.9 Hz, 2H), 1.68 - 1.63 (m, 2H), 1.59 - 1.44 (m, 4H)

**$^{13}$C NMR (101 MHz, $CDCl_3$):** δ = 169.8, 142.5, 132.1, 130.7 (q, *J*=32.0 Hz,), 125.1 (q, *J*=3.3 Hz), 123.0 (q, *J*=3.8 Hz), 124.2 (q, *J*=272.4 Hz), 116.4, 46.6, 42.8, 34.6, 31.3, 26.4, 25.5, 24.5

**$^{19}$F NMR (377 MHz, $CDCl_3$):** δ = −62.56 (s, 3F)

**LCMS (2 min low pH):** $t_R$ = 1.16 min, $[M+H^+]$ 286.1 (96.7% purity)

**HRMS:** ($C_{15}H_{19}F_3NO$) $[M+H^+]$ requires: 286.1413, $[M+H^+]$ found: 286.1398

**3-(Piperidine-1-carbonyl)cyclohexan-1-one**

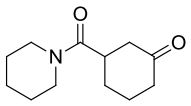

**202**

A 20 mL vial, equipped with a stirrer bar, was charged with iridium catalyst (**156**) (2.2 mg, 0.002 mmol), and sodium 2-oxo-2-(piperidin-1-yl)acetate (36 mg, 0.2 mmol). Under a flow of nitrogen, 3:1 DME:DMF (1 mL) was added, then the vial was sealed. Water (0.036 mL, 2 mmol) was added to the vial, followed by cyclohex-2-en-1-one (0.019 mL, 0.2 mmol). The reaction mixture was irradiated with 1 blue LED lamp, and stirred at 30 °C for 16 h. The reaction mixture was transferred to a separating funnel, then LiCl (saturated aq. solution, 25 mL) was added, and the aqueous layer was extracted with TBME (3 × 25 mL), then further TBME (5 × 10 mL). The combined organics were dried over $MgSO_4$, filtered, and evaporated *in vacuo*. The resulting residue was dissolved in DMSO, and purified by MDAP (formic acid method). The appropriate fractions were combined and evaporated *in vacuo* to afford the desired product (**202**) (4.8 mg, 11% yield) as a white solid.

**Melting point:** Not obtained, due to lack of material.

**IR $\nu_{max}$:** 2943, 2858, 1718, 1637, 1445, 1268, 1220 $cm^{-1}$

**$^1$H NMR (400 MHz, $CDCl_3$):** δ = 3.56 (app. dd, *J*=5.2, 5.7 Hz, 2H), 3.42 (app. dd, *J*=5.2, 5.7 Hz, 2H), 3.10 - 2.98 (m, 1H), 2.71 (app. dd, *J*=11.1, 14.4 Hz, 1H), 2.41 - 2.31 (m, 3H), 2.16 - 2.06 (m, 1H), 1.93 - 1.86 (m, 2H), 1.79 - 1.64 (m, 3H), 1.61 - 1.52 (m, 4H)

**$^{13}$C NMR (101 MHz, $CDCl_3$):** δ = 210.6, 171.4, 46.6, 44.1, 43.1, 41.0, 40.3, 28.0, 26.9, 25.6, 24.8, 24.6

**LCMS (2 min low pH):** $t_R$ = 0.67 min, $[M+H^+]$ 210.1 (100% purity)

**HRMS:** ($C_{12}H_{20}NO_2$) $[M+H^+]$ requires: 210.1489, $[M+H^+]$ found: 210.1483

*4.2.9.3. Reactions using acetone as solvent*

**3-(2-Oxo-2-(piperidin-1-yl)ethyl)dihydrofuran-2(3H)-one**

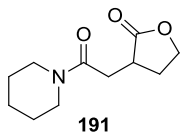

**191**

Prepared using **General method B**, **oxamate** sodium 2-oxo-2-(piperidin-1-yl)acetate (79 mg, 0.44 mmol) and **liquid olefin** 3-methylenedihydrofuran-2(3H)-one (0.035 mL, 0.4 mmol) were reacted under irradiation by 1 LED lamp, for 24 h.

The crude product was purified by chromatography on silica; elution gradient 0-100% ethyl acetate in heptane. The appropriate fractions were combined and evaporated *in vacuo* to afford the desired product (**191**) (63 mg, 75% yield) as a yellow solid.

**LCMS (2 min low pH):** $t_R$ = 0.59 min, [M+H$^+$] 212.1 (95.8% purity)

Full product characterisation can be found above, on page 176.

**3-(2-Oxo-2-(pyrrolidin-1-yl)ethyl)dihydrofuran-2(3H)-one**

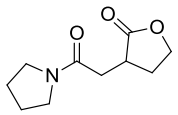

**211**

Prepared using **General method B**, **oxamate** sodium 2-oxo-2-(pyrrolidin-1-yl)acetate (72 mg, 0.44 mmol) and **liquid olefin** 3-methylenedihydrofuran-2(3H)-one (0.035 mL, 0.4 mmol) were reacted under irradiation by 1 LED lamp, for 24 h.

The crude product was purified by chromatography on silica; elution gradient 0-100% ethyl acetate in heptane. The appropriate fractions were combined and evaporated *in vacuo* to afford the desired product (**211**) (47 mg, 61% yield) as a pale yellow oil.

**IR $\nu_{max}$:** 2973, 2878, 1760, 1622, 1444, 1207, 1153, 1020 $cm^{-1}$

**$^{1}$H NMR (400 MHz, $CDCl_3$):** δ = 4.41 (app. ddd, *J*=2.1, 9.0, 9.1 Hz, 1H), 4.24 (app. ddd, *J*=6.7, 9.0, 10.3 Hz, 1H), 3.47 (app. t, *J*=6.9 Hz, 2H), 3.45 - 3.37 (m, 2H), 3.04 (dtd, *J*=3.3, 9.0, 11.0 Hz, 1H), 2.90 (dd, *J*=3.2, 16.9 Hz, 1H), 2.63 (app. dddd, *J*=2.0, 6.8, 9.0, 12.6 Hz, 1H), 2.45 (app. dd, *J*=9.1, 16.9 Hz, 1H), 2.04 (dtd, *J*=9.0, 10.7, 12.5 Hz, 1H), 2.00 - 1.93 (m, 2H), 1.92 - 1.82 (m, 2H)

**$^{13}$C NMR (101 MHz, $CDCl_3$):** δ = 179.4, 168.4, 66.8, 46.5, 45.8, 36.1, 35.4, 29.3, 26.1, 24.4

**LCMS (8 min TFA):** $t_R$ = 1.03 min, $[M+H^+]$ 198.1 (96.6% purity)

**HRMS:** ($C_{10}H_{16}NO_3$) $[M+H^+]$ requires: 198.1125, $[M+H^+]$ found: 198.1119

**Benzyl4-(2-(2-oxotetrahydrofuran-3-yl)acetyl)piperazine-1-carboxylate**

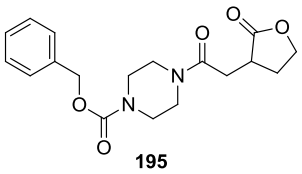

**195**

Prepared using **General method B**, **oxamate** sodium 2-(4-((benzyloxy)carbonyl)piperazin-1-yl)-2-oxoacetate (138 mg, 0.44 mmol) and **liquid olefin** 3-methylenedihydrofuran-2(3H)-one (0.035 mL, 0.4 mmol) were reacted under irradiation by 1 LED lamp, for 48 h.

The crude product was purified by chromatography on silica; elution gradient 24-100% ethyl acetate in heptane. The appropriate fractions were combined and evaporated *in vacuo* to afford the desired product (**195**) (87 mg, 63% yield) as a pale yellow oil.

**IR $\nu_{max}$:** 2911, 1762, 1695, 1641, 1456, 1421, 1285, 1218, 1022 $cm^{-1}$

**$^{1}$H NMR (400 MHz, $CDCl_3$):** δ = 7.42 - 7.30 (m, 5H), 5.15 (s, 2H), 4.42 (ddd, *J*=2.0, 9.2, 9.4 Hz, 1H), 4.25 (ddd, *J*=6.7, 9.2, 10.3 Hz, 1H), 3.72 - 3.39 (m, 8H), 3.04 (ddd, *J*=2.0, 3.2, 10.3 Hz, 1H), 2.97 (dd, *J*=3.2, 16.6 Hz, 1H), 2.67 - 2.57 (m, 1H), 2.51 (dd, *J*=8.7, 16.6 Hz, 1H), 2.08 - 1.94 (m, 1H)

**$^{13}$C NMR (101 MHz, $CDCl_3$):** δ = 179.1, 168.7, 155.1, 136.3, 128.6, 128.3, 128.1, 67.6, 66.8, 45.1, 43.7, 41.5, 36.2, 34.1, 29.3

**LCMS (2 min low pH):** $t_R$ = 0.83 min, $[M+H^+]$ 347.0 (93.2% purity)

**HRMS:** ($C_{18}H_{23}N_2O_5$) $[M+H^+]$ requires: 347.1602, $[M+H^+]$ found: 347.1593

***N*,*N*-Diisopropyl-2-(2-oxotetrahydrofuran-3-yl)acetamide**

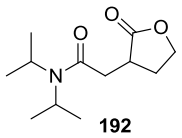

**192**

Prepared using **General method B**, **oxamate** sodium 2-(diisopropylamino)-2-oxoacetate (85 mg, 0.44 mmol) and **liquid olefin** 3-methylenedihydrofuran-2(3H)-one (0.035 mL, 0.4 mmol) were reacted under irradiation by 1 LED lamp, for 24 h.

The crude product was purified by chromatography on silica; elution gradient 10-100% ethyl acetate in heptane. The appropriate fractions were combined and evaporated *in vacuo*. The resulting solid was dissolved and pipetted away from the impure product, using portions of heptane (10 × 2 mL). These portions were combined and evaporated *in vacuo* to afford the desired product (**192**) (54 mg, 60% yield) as a pale yellow solid.

**LCMS (2 min low pH):** $t_R$ = 0.79 min, [M+H$^+$] 228.1 (97.8% purity)

Full characterisation can be found above, on page 177.

***N*-Methyl-2-(2-oxotetrahydrofuran-3-yl)-*N*-(*p*-tolyl)acetamide**

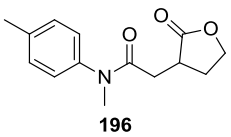

**196**

Prepared using **General method B**, **oxamate** sodium 2-(methyl(*p*-tolyl)amino)-2-oxoacetate (95 mg, 0.44 mmol) and **liquid olefin** 3-methylenedihydrofuran-2(3H)-one (0.035 mL, 0.4 mmol) were reacted under irradiation by 1 LED lamp, for 48 h.

The crude product was purified by chromatography on silica; elution gradient 12-100% ethyl acetate in heptane. The appropriate fractions were combined and evaporated *in vacuo* to afford the desired product (**196**) (18 mg, 19% yield) as a pale yellow solid.

**LCMS (2 min low pH):** $t_R$ = 0.83 min, [M+H$^+$] 248.1 (98.9% purity)

Full characterisation can be found above, on page 181.

**2-Methyl-4-oxo-4-(piperidin-1-yl)butanenitrile**

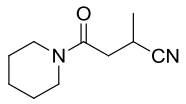


**199**

Prepared using **General method B**, **oxamate** sodium 2-oxo-2-(piperidin-1-yl)acetate (79 mg, 0.44 mmol) and **liquid olefin** methacrylonitrile (0.034 mL, 0.4 mmol) were reacted under irradiation by 1 LED lamp, for 48 h.

The crude product was purified by chromatography on silica; elution gradient 0-100% ethyl acetate in heptane. The appropriate fractions were combined and evaporated *in vacuo* to afford the desired product (**199**) (60 mg, 84% yield) as a yellow oil.

**LCMS (2 min low pH):** $t_R$ = 0.67 min, [M+H$^+$] 181.0 (94.4% purity)

Full characterisation can be found above, on page 185.

Also isolated:

**3-Hydroxy-2,3-dimethyl-2-(2-oxo-2-(piperidin-1-yl)ethyl)butanenitrile**

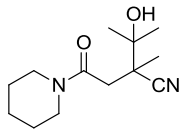


**199'**

(**199'**) (4 mg, 4% yield) as a yellow oil.

**IR $\nu_{max}$:** 3416, 2985, 2940, 2859, 2232, 1619, 1446, 1378, 1253 cm$^{-1}$

**$^1$H NMR (400 MHz, $CDCl_3$):** δ = 4.21 - 4.15 (m, 1H, OH), 3.66 - 3.54 (m, 2H, $CH_2N$), 3.49 (app. dd, *J*=5.2, 4.8 Hz, 2H, $CH_2N$), 3.00 (d, *J*=15.4 Hz, 1H, $NC(O)CH_2$), 2.64 (d, *J*=15.4 Hz, 1H, $NC(O)CH_2$), 1.68 - 1.62 (m, 4H, 2 × $CH_2$), 1.61 - 1.54 (m, 2H, $CH_2$), 1.50 (s, 3H, $CH_3CCN$), 1.45 (s, 3H, $C\underline{H}_3COH$), 1.34 (s, 3H, $C\underline{H}_3COH$)

**$^{13}$C NMR (101 MHz, $CDCl_3$):** δ = 167.9 (NC(O)), 123.3 (CN), 73.0 (COH), 47.7 ($CH_2N$), 44.7 ($\underline{C}CN$), 43.17 ($CH_2N$), 37.7 ($NC(O)\underline{C}H_2$), 27.0 ($\underline{C}H_3COH$), 26.5 ($CH_2\underline{C}H_2CH_2$), 25.5 ($CH_2\underline{C}H_2CH_2$), 25.0 ($\underline{C}H_3COH$), 24.3 ($CH_2\underline{C}H_2CH_2$), 20.9 ($CNC\underline{C}H_3$)

**LCMS (2 min low pH):** $t_R$ = 0.66 min, [M+H$^+$] 239.1 (92.7% purity)

**HRMS:** ($C_{13}H_{23}N_2O_2$) [M+H$^+$] requires: 239.1754, [M+H$^+$] found: 239.1751

**1-(Piperidin-1-yl)hexane-1,4-dione**

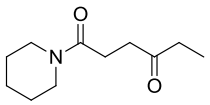

197

Prepared using **General method B**, **oxamate** sodium 2-oxo-2-(piperidin-1-yl)acetate (79 mg, 0.44 mmol) and **liquid olefin** pent-1-en-3-one (0.04 mL, 0.4 mmol) were reacted under irradiation by 1 LED lamp, for 48 h.

The crude product was purified by MDAP (formic acid method). The appropriate fractions were combined and evaporated *in vacuo* to afford the desired product (**197**) (25 mg, 32% yield) as a colourless oil.

**LCMS (2 min low pH):** $t_R$ = 0.70 min, [M+H$^+$] 198.1 (100% purity)

Full characterisation can be found above, on page 183.

**3,3-Diphenyl-1-(piperidin-1-yl)propan-1-one**

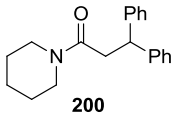

200

Prepared using **General method B**, **oxamate** sodium 2-oxo-2-(piperidin-1-yl)acetate (79 mg, 0.44 mmol) and **liquid olefin** ethene-1,1-diyldibenzene (0.071 mL, 0.4 mmol) were reacted under irradiation by 2 LED lamps, for 44 h.

The crude product was purified by chromatography on silica; elution gradient 0-100% ethyl acetate in heptane. The appropriate fractions were combined and evaporated *in vacuo* to afford the desired product (**200**) (64 mg, 55% yield) as a pale yellow solid.

**LCMS (2 min low pH):** $t_R$ = 1.20 min, [M+H$^+$] 294.1 (96.6% purity)

Full characterisation can be found above, on page 194.

**1-Morpholino-4-(piperidin-1-yl)butane-1,4-dione**

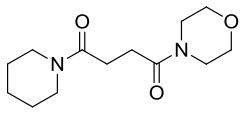

**212**

Prepared using **General method B**, **oxamate** sodium 2-oxo-2-(piperidin-1-yl)acetate (79 mg, 0.44 mmol) and **liquid olefin** 1-morpholinoprop-2-en-1-one (0.050 mL, 0.4 mmol) were reacted under irradiation by 2 LED lamps, for 24 h.

The crude product was purified by chromatography on silica; elution gradient 0-5% methanol in DCM. The appropriate fractions were combined and evaporated *in vacuo* to afford the desired product (**212**) (43 mg, 42% yield) as a yellow solid.

**Melting point:** 70.3-74.2 °C

**IR $\nu_{max}$:** 2931, 2855, 1627, 1435, 1357, 1276, 1210, 1110 $cm^{-1}$

**$^{1}$H NMR (400 MHz, $CDCl_3$):** δ = 3.71 - 3.64 (m, 4H), 3.64 - 3.59 (m, 2H), 3.58 - 3.51 (m, 4H), 3.46 (app. dd, *J*=5.3, 5.7 Hz, 2H), 2.70 (dd, *J*=4.2, 10.4 Hz, 2H), 2.65 (dd, *J*=4.2, 10.4 Hz, 2H), 1.68 - 1.49 (m, 6H)

**$^{13}$C NMR (101 MHz, $CDCl_3$):** δ = 170.9, 170.0, 66.9, 66.6, 46.4, 45.9, 42.9, 42.1, 28.1, 28.0, 26.4, 25.6, 24.6

**LCMS (2 min low pH):** $t_R$ = 0.56 min, $[M+H^+]$ 255.1 (99.7% purity)

**HRMS:** ($C_{13}H_{23}N_2O_3$) $[M+H^+]$ requires: 255.1703, $[M+H^+]$ found: 255.1700

*4.2.9.4. Reactions using a metal-free photocatalyst*

**Dimethyl 2-(piperidine-1-carbonyl)succinate**

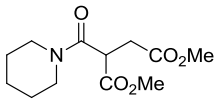


**157**

Prepared using **General method C**, **oxamate** sodium 2-oxo-2-(piperidin-1-yl)acetate (79 mg, 0.44 mmol) and **solid olefin** dimethyl fumarate (58 mg, 0.4 mmol) were reacted under irradiation by 1 LED lamp, for 24 h.

The crude product was purified by chromatography on silica; elution gradient 0-50% ethyl acetate in heptane. The appropriate fractions were combined and evaporated *in vacuo* to afford the desired product (**157**) (54 mg, 52% yield) as a colourless oil.

**LCMS (2 min low pH):** $t_R$ = 0.72 min, [M+H$^+$] 258.1 (99.5% purity)

Full characterisation can be found above, on page 182.

**Dimethyl 2-(morpholine-4-carbonyl)succinate**

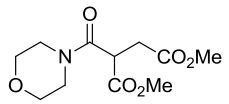


**218**

Prepared using **General method C**, **oxamate** sodium 2-morpholino-2-oxoacetate (80 mg, 0.44 mmol) and **solid olefin** dimethyl fumarate (58 mg, 0.4 mmol) were reacted under irradiation by 1 LED lamp, for 48 h.

The crude product was purified by chromatography on silica; elution gradient 0-100% ethyl acetate in heptane. The appropriate fractions were combined and evaporated *in vacuo* to afford the desired product (**218**) (70 mg, 67% yield) as a colourless oil.

**IR $\nu_{max}$:** 2957, 2858, 1731, 1642, 1435, 1364, 1265, 1161, 1112 $cm^{-1}$

**$^{1}$H NMR (400 MHz, $CDCl_3$):** δ = 4.12 (dd, *J*=5.7, 8.4 Hz, 1H, NC(O)CH), 3.74 (s, 3H, $OCH_3$), 3.69 (s, 3H, $OCH_3$), 3.81 - 3.53 (m, 8H, 2 × $OCH_2$, 2 × $CH_2N$), 3.08 (dd, *J*=8.4, 17.6 Hz, 1H, $CH_2C(O)O$), 2.97 (dd, *J*=5.7, 17.6 Hz, 1H, $CH_2C(O)O$)

**$^{13}$C NMR (101 MHz, $CDCl_3$):** δ = 172.1 ($CH_2\underline{C}(O)O$), 169.0 ($CH\underline{C}(O)O$), 166.2 ($N\underline{C}(O)CH$), 66.8 ($O\underline{C}H_2$), 66.6 ($O\underline{C}H_2$), 52.9 ($C(O)O\underline{C}H_3$), 52.1 ($C(O)O\underline{C}H_3$), 46.8 ($\underline{C}H_2N$), 44.0 ($\underline{C}H_2N$), 42.9 ($NC(O)\underline{C}H$), 33.25 ($\underline{C}H_2C(O)O$)

**LCMS (8 min TFA):** $t_R$ = 1.11 min, [M+H$^+$] 255.1 (98.2% purity)

**HRMS:** ($C_{11}H_{18}NO_6$) [M+H$^+$] requires: 260.1129, [M+H$^+$] found: 260.1122

**Dimethyl 2-(4-((benzyloxy)carbonyl)piperazine-1-carbonyl)succinate**

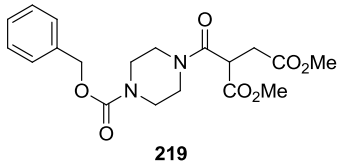

**219**

Prepared using **General method C**, **oxamate** sodium 2-(4-((benzyloxy)carbonyl)piperazin-1-yl)-2-oxoacetate (139 mg, 0.44 mmol) and **solid olefin** dimethyl fumarate (58 mg, 0.4 mmol) were reacted under irradiation by 1 LED lamp, for 72 h.

The reaction was not worked up, as poor conversion was observed by HPLC, with a substantial quantity of both starting materials.

**LCMS (2 min low pH):** $t_R$ = 0.91 min, [M+H$^+$] 393.1 (58%Area/Area by HPLC)

**Dimethyl 2-(methyl(*p*-tolyl)carbamoyl)succinate**

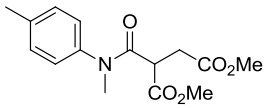

**220**

Prepared using **General method C**, **oxamate** sodium 2-(methyl(*p*-tolyl)amino)-2-oxoacetate (95 mg, 0.44 mmol) and **solid olefin** dimethyl fumarate (58 mg, 0.4 mmol) were reacted under irradiation by 1 LED lamp, for 95 h.

The reaction was not worked up, as poor conversion was observed by HPLC, alongside both starting materials remaining.

**LCMS (2 min low pH):** $t_R$ = 0.93 min, [M+H$^+$] 294.0 (3.5%Area/Area by HPLC)

Also observed:

**Dimethyl 1,6-dimethyl-2-oxo-1,2,3,4-tetrahydroquinoline-3,4-dicarboxylate**

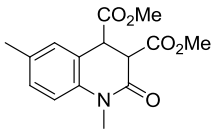

**220'**

**LCMS (2 min low pH):** $t_R$ = 0.89 min, [M+H$^+$] 292.0 (4.5%Area/Area by HPLC)

**2-Methyl-4-oxo-4-(piperidin-1-yl)butanenitrile**

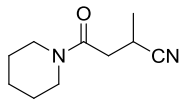


199

Prepared using **General method C**, **oxamate** sodium 2-oxo-2-(piperidin-1-yl)acetate (79 mg, 0.44 mmol) and **liquid olefin** methacrylonitrile (0.034 mL, 0.4 mmol) were reacted under irradiation by 1 LED lamp, for 24 h.

The reaction was not worked up, as the desired product was not observed by HPLC or LCMS, both starting materials remained.

**3-(2-Oxo-2-(piperidin-1-yl)ethyl)dihydrofuran-2(3H)-one**

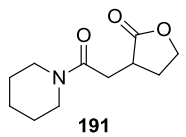


191

Prepared using **General method C**, **oxamate** sodium 2-oxo-2-(piperidin-1-yl)acetate (79 mg, 0.44 mmol) and **liquid olefin** 3-methylenedihydrofuran-2(3H)-one (0.035 mL, 0.4 mmol) were reacted under irradiation by 1 LED lamp, for 48 h.

The reaction was not worked up, as poor conversion was observed by HPLC, and both starting materials remained.

**LCMS (8 min TFA):** $t_R$ = 1.43 min, [M+H$^+$] 212.0 (51.5%Area/Area by HPLC)

**3-(Phenylsulfonyl)-1-(piperidin-1-yl)propan-1-one**

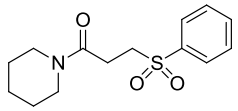

**198**

Prepared using **General method C**, **oxamate** sodium 2-oxo-2-(piperidin-1-yl)acetate (79 mg, 0.44 mmol) and **solid olefin** (vinylsulfonyl)benzene (67 mg, 0.4 mmol) were reacted under irradiation by 1 LED lamp, for 24 h.

The crude product was purified by chromatography on silica; elution gradient 0-50% ethyl acetate in heptane. The appropriate fractions were combined and evaporated *in vacuo* to afford the desired product (**198**) (59 mg, 52% yield) as a yellow oil.

**LCMS (2 min low pH):** $t_R$ = 0.82 min, [M+H$^+$] 282.1 (99.6% purity)

Full characterisation can be found above, on page 184.

### 4.2.10. Computational methods

All density functional theory (DFT) calculations[272] were carried out using the Gaussian09 software package,[273] using the uB3LYP functional, with a 6-31+G(d,p) basis set on all atoms.[274] Photocatalyst structures were optimised using LANL2DZ pseudopotential on iridium,[275] with a 6-31+G(d,p) basis set on all other atoms. Solvation was modelled implicitly, using a conductor-like polarisable continuum model (C-PCM)[276] with acetone assigned as the solvent. All structures were found as energy minima, with frequency calculations performed, to verify zero imaginary frequencies. Transition states also underwent frequency calculations, and were found to have a single imaginary frequency. They were then further confirmed as local maxima, by running intrinsic reaction coordinate (IRC) calculations.[277] Potential energy surfaces are plotted using the calculated Gibbs free energy values. GaussView 5.0.9 was used for the visualisation of structures. Details of optimised structures and transition states are contained within the appendix.

## 4.3. Experimental data for Chapter 3

### 4.3.1 Calculation of HPLC assay yields

For the following transformation, molar absorbance ratios were obtained for amide product (**270**) and acylurea by-product (**271**) versus anisole, which was used as an internal standard (0.5 eq.) in these reactions, in both batch and flow.

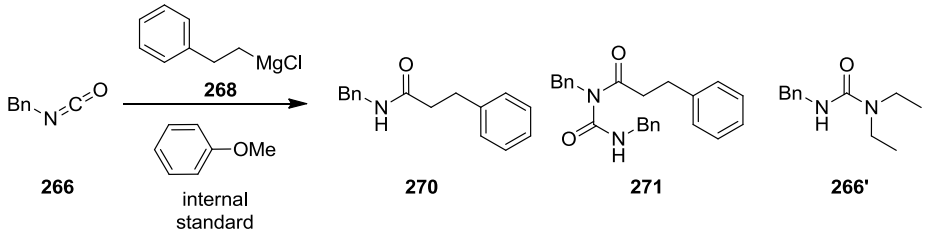


**Example calculation of molar absorbance ratio:**

$$k_x = \frac{\%_{is}}{\%_x} \times \frac{m_{is}}{m_x} \times \frac{M_{is}}{M_x}$$

Where:

% = %Area/Area from HPLC result, *m* = mass present in analysed sample, *M* = molecular mass

*x* = reaction component, *is* = internal standard

Amide product (**270**) (18.9 mg) = 32.782%A/A, anisole (14.93 mg) = 21.855%A/A

$$k_x = \frac{20.978}{35.156} \times \frac{14.93}{19.82} \times \frac{108.138}{239.312} = 0.35169$$

An average of four samples gave the following results at each respective analytical wavelength:

**210 nm:**

Starting material (as diethylurea, **266'**), $k_x$ = 0.42522

Amide product (**270**), $k_x$ = 0.35059

Acylurea by-product (**271**), $k_x$ = 0.18092

Assay yield = $k_x \times \frac{eq_{\cdot is}}{eq_{\cdot x}} \left(\frac{\%_x}{\%_{is}}\right) \times 100$

**Example HPLC trace and assay yield calculation:**

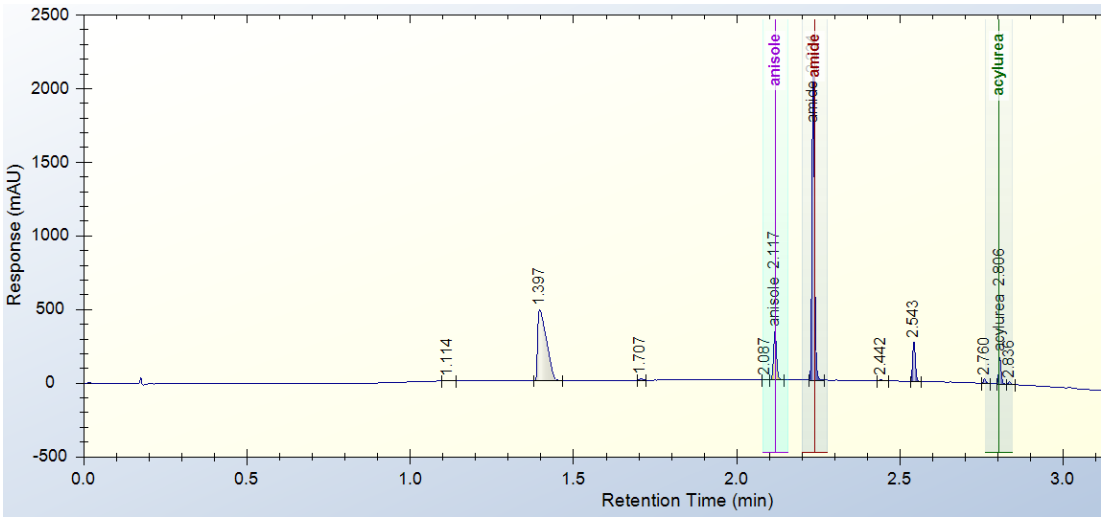


Amide (**270**) = 68.525%A/A, acylurea (**271**) = 5.758%A/A, anisole = 13.510%A/A

Amide (**270**) assay yield = $0.35059 \times 0.5 \left(\frac{68.525}{13.510}\right) \times 100 = 88.913\%$

Acylurea (**271**) assay yield = $0.18092 \times 0.5 \left(\frac{5.758}{13.510}\right) \times 100 = 7.711\%$

### 4.3.2. Initial scoping experiments

These reactions were performed following the general method previously reported by Bode.[187]

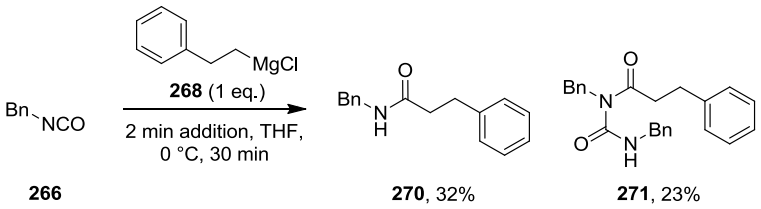


To a solution of (isocyanatomethyl)benzene (0.124 mL, 1 mmol) and anisole (0.055 mL, 0.5 mmol) in dry THF (4 mL) at 0 °C, was added phenethylmagnesium chloride (0.88 M in THF, 1.14 mL, 1 mmol), *via* syringe pump, over 2 minutes. The reaction was allowed to warm to room temperature and was stirred for 30 minutes. Saturated ammonium chloride solution (10 mL) was added in one portion, followed by water (4 mL) and ethyl acetate (10 mL). Due to difficulty in separating the two products, the organic phase was separated and was sampled for HPLC analysis, giving the following result:

| **Anisole (%Area)** | **Amide (270) (%Area)** | **Acylurea (271) (%Area)** |
|---|---|---|
| 15.8 | 28.4 | 19.6 |

***N*-Benzyl-*N*-(benzylcarbamoyl)-3-phenylpropanamide**

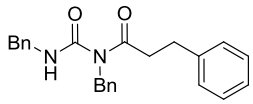

**271**

**IR $\nu_{max}$:** 3283, 3063, 3029, 1698, 1660, 1520, 1496, 1390, 1169, 1148 $cm^{-1}$

**$^1$H NMR (400 MHz, $CDCl_3$):** δ = 9.72 (br. s, 1H), 7.36 - 7.21 (m, 11H), 7.14 (d, *J*=7.1 Hz, 2H), 7.04 (d, *J*=7.1 Hz, 2H), 5.05 (s, 2H), 4.55 (d, *J*=5.6 Hz, 2H), 2.87 (t, *J*=7.1 Hz, 2H), 2.78 (t, *J*=7.1 Hz, 2H)

**$^{13}$C NMR (101 MHz, $CDCl_3$):** δ = 176.8, 155.2, 140.2, 138.3, 137.4, 128.9, 128.7, 128.6, 128.3, 127.6, 127.42, 127.36, 126.3, 126.0, 47.2, 44.8, 38.0, 30.6

**LCMS (5 min high pH):** $t_R$ = 3.50 min, $[M+H^+]$ = 373.2 (90.6% purity)

**HRMS:** ($C_{24}H_{25}N_2O_2$) $[M+H^+]$ requires 373.1911, found $[M+H^+]$ 373.1916

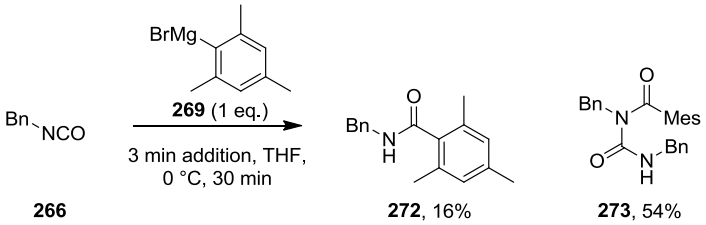


**266** **272**, 16% **273**, 54%

To a solution of (isocyanatomethyl)benzene (0.124 mL, 1 mmol) in dry THF (4 mL) at 0 °C, was added mesitylmagnesium bromide (0.85 M in THF, 1.18 mL, 1 mmol), dropwise over 3 minutes, *via* syringe pump. The reaction was allowed to warm to room temperature and stirred for 30 minutes. Saturated ammonium chloride solution (10 mL) was added, followed by ethyl acetate (25 mL). The organic phase was washed with brine (10 mL), dried over $MgSO_4$, filtered, and concentrated *in vacuo* to afford a white solid. The crude product was purified by chromatography on silica; elution gradient 12-100% ethyl acetate in heptane. The appropriate fractions were combined and evaporated *in vacuo* to afford the desired amide product (**272**) (41 mg, 16% yield) as a white crystalline solid, and the acylurea by-product (**273**) (101 mg, 54% yield) as a colourless gum.

***N*-Benzyl-2,4,6-trimethylbenzamide** [278]

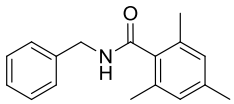

**272**

**Melting point:** 135-137 °C, literature value: 137.5-138.5 °C

**IR $\nu_{max}$:** 3277, 1629, 1609, 1542, 1303, 1236 $cm^{-1}$

**$^1$H NMR (400 MHz, DMSO-$d_6$):** δ = 8.73 (t, *J*=6.1 Hz, 1H), 7.37 - 7.31 (m, 4H), 7.25 (dq, *J*=2.8, 5.9 Hz, 1H), 6.84 (s, 2H), 4.42 (d, *J*=6.1 Hz, 2H), 2.22 (s, 3H), 2.15 (s, 6H)

**$^{13}$C NMR (101 MHz, DMSO-$d_6$):** δ = 169.2, 139.6, 137.0, 135.7, 133.5, 128.2, 127.7, 127.5, 126.8, 42.3, 20.6, 18.8

**LCMS (5 min high pH):** $t_R$ = 2.85 min, [M+$H^+$] 254.2 (98.2% purity)

**HRMS:** ($C_{17}H_{20}NO$) [M+$H^+$] requires: 254.1539, [M+$H^+$] found: 254.1531

***N*-Benzyl-*N*-(benzylcarbamoyl)-2,4,6-trimethylbenzamide**

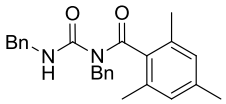

**273**

**IR $\nu_{max}$:** 3285, 1701, 1649 $cm^{-1}$

**$^1$H NMR (400 MHz, $CDCl_3$):** δ = 9.87 (t, *J*=5.7 Hz, 1H), 7.39 - 7.34 (m, 4H), 7.31 - 7.29 (m, 1H), 7.20 - 7.14 (m, 3H), 6.87 - 6.83 (m, 2H), 6.79 (s, 2H), 4.78 (s, 2H), 4.64 (d, *J*=5.7 Hz, 2H), 2.29 (s, 3H), 1.91 (s, 6H)

**$^{13}$C NMR (101 MHz, $CDCl_3$):** δ = 176.1, 155.4, 139.1, 138.3, 137.4, 133.6, 133.4, 128.7, 128.4, 128.2, 127.9, 127.6, 127.4, 127.4, 48.9, 44.8, 21.2, 18.8

**LCMS (5 min high pH):** $t_R$ = 3.73 min, [M+$H^+$] = 387.3 (91.7% purity)

**HRMS:** ($C_{25}H_{27}N_2O_2$) [M+$H^+$] requires 387.2067, found [M+$H^+$] 387.2068

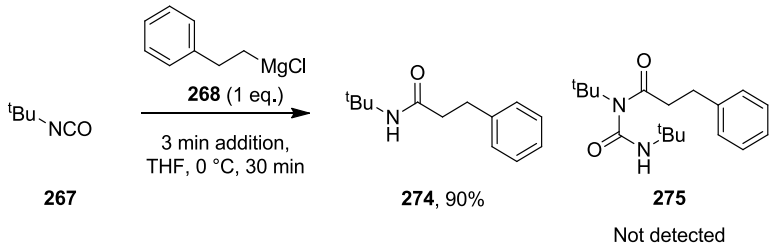


**267** **274**, 90% **275** Not detected

To a solution of 2-isocyanato-2-methylpropane (0.114 mL, 1 mmol) in dry THF (4 mL) at 0 °C, was added phenethylmagnesium chloride (0.88 M in THF, 1.14 mL, 1 mmol), dropwise over 3 minutes, *via* syringe pump. The reaction was allowed to warm to room temperature and stirred for 30 minutes. Saturated ammonium chloride solution (10 mL) was added, followed by ethyl acetate (25 mL). The organic phase was washed with brine (10 mL), dried over $MgSO_4$, filtered, and concentrated *in vacuo*. The crude product was washed with cold heptane (5 mL) and dried *in vacuo* to afford the desired amide (**274**) (185 mg, 90% yield) as a white crystalline solid.

***N*-(*tert*-Butyl)-3-phenylpropanamide**[279]

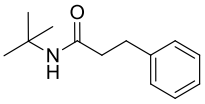


**274**

**Melting point:** 88-89 °C, literature value: 88-89 °C

**IR $\nu_{max}$:** 3313, 2969, 1640, 1547, 1454, 1391, 1359, 1226 $cm^{-1}$

**$^1$H NMR (400 MHz, DMSO-$d_6$)** δ = 7.38 (br. s, 1H), 7.29 - 7.23 (m, 2H), 7.22 - 7.14 (m, 3H), 2.77 (t, *J*=7.7 Hz, 2H), 2.30 (t, *J*=7.7 Hz, 2H), 1.21 (s, 9H)

**$^{13}$C NMR (101 MHz, DMSO-$d_6$):** δ = 170.8, 141.5, 128.22, 128.15, 125.8, 49.8, 37.7, 31.2, 28.5

**LCMS (5 min high pH):** $t_R$ = 3.31 min, $[M+H^+]$ = 206.2 (100% purity)

**HRMS:** ($C_{13}H_{20}NO$) $[M+H^+]$ requires: 206.1539, $[M+H^+]$ found: 206.1535

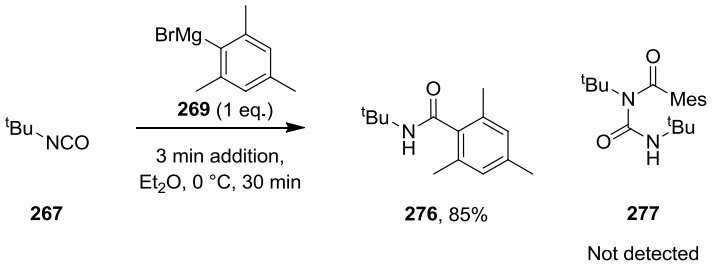


To a solution of 2-isocyanato-2-methylpropane (0.228 mL, 2 mmol) in $Et_2O$ (8 mL) at 0 °C, was added mesitylmagnesium bromide (0.94 M in $Et_2O$, 2.13 mL, 2 mmol), dropwise over 3 minutes. The reaction was allowed to warm to room temperature and stirred for 30 minutes. Saturated ammonium chloride solution (10 mL) was added slowly, followed by ethyl acetate (25 mL). The organic phase was washed with brine (10 mL), dried over $MgSO_4$, filtered, and concentrated *in vacuo*. The crude product was washed with heptane (5 mL) and dried *in vacuo* to afford the desired amide (**276**) (372 mg, 85% yield) as a white crystalline solid.

***N*-(*tert*-Butyl)-2,4,6-trimethylbenzamide**[187]

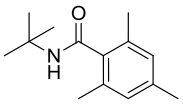

**276**

**Melting point:** 139.2-139.8 °C, literature value: 143 °C

**IR $\nu_{max}$:** 3239, 1630 $cm^{-1}$

**$^1$H NMR (400 MHz, $CDCl_3$):** δ = 6.82 (s, 2H), 5.43 (br. s, 1H), 2.30 (s, 6H), 2.26 (s, 3H), 1.45 (s, 9H)

**$^{13}$C NMR (101 MHz, $CDCl_3$):** δ = 169.7, 138.1, 136.0, 133.9, 128.1, 51.7, 28.9, 21.0, 18.9

**LCMS (5 min high pH):** $t_R$ = 2.68 min, $[M+H^+]$ = 220.2 (95.3% purity)

**HRMS:** ($C_{14}H_{22}NO$) $[M+H^+]$ requires 220.1696, found $[M+H^+]$ 220.1695

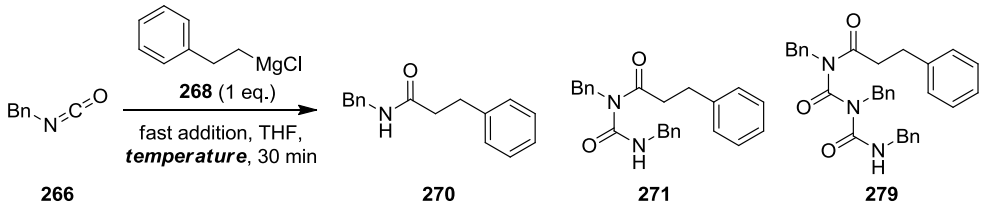


266 270 271 279

| Entry | Temp. (°C) | Deviation from standard conditions | Anisole (%Area) | Amide (270) (%Area) | Acylurea (271) (%Area) | "Trimer" (279) (%Area) |
|---|---|---|---|---|---|---|
| **1** | −78 | None | 13.6 | 60.9 | 5.7 | 1.7 |
| **2** | −50 | None | 15.8 | 66.2 | 4.5 | 0.5 |
| **3** | 0 | None | 13.0 | 54.2 | 6.3 | 0.5 |
| **4** | Room temp. | None | 12.6 | 49.2 | 6.5 | 1 |
| **5** | 40 | None | 16.2 | 54.6 | 8.4 | 1.5 |
| **6** | Room temp. | Inverse addition | 14.7 | 7.7 | 22.8 | 12.8 |
| **7** | Room temp. | 2 eq. isocyanate (**266**) | 9.6 | 23.6 | 36.7 | 15.3 |

**Entries 1-5**

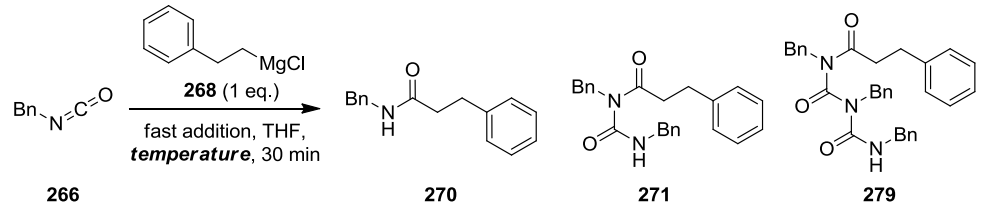


266 270 271 279

To a solution of (isocyanatomethyl)benzene (0.124 mL, 1 mmol) and anisole (0.055 mL, 0.5 mmol) in dry THF (4 mL) at ***temperature***, was added phenethylmagnesium chloride (0.88 M in THF, 1.14 mL, 1 mmol), rapidly *via* syringe. The reaction was stirred at ***temperature*** for 30 minutes. Saturated ammonium chloride solution (2 mL) was added in one portion, followed by saturated brine solution (4 mL) and ethyl acetate (4 mL). The organic phase was separated and was sampled for HPLC analysis, giving the assay yields of **270** and **271** displayed in the main text. As the trimeric product (**279**) has not been isolated, an HPLC %Area is quoted in place of an assay yield.

**Entry 6**

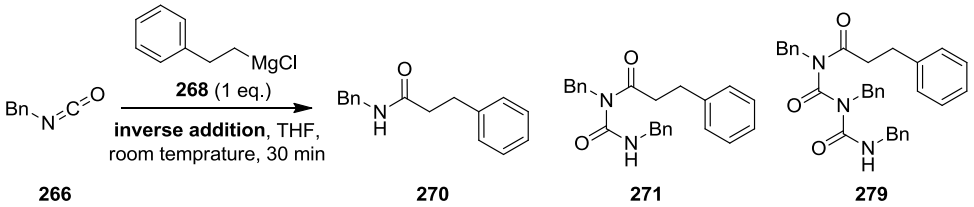


To a solution of phenethylmagnesium chloride (0.88 M in THF, 1.14 mL, 1 mmol) and anisole (0.055 mL, 0.5 mmol) in dry THF (4 mL) at room temperature, was added, (isocyanatomethyl)benzene (0.124 mL, 1 mmol) rapidly *via* syringe. The reaction was stirred at room temperature for 30 minutes. Saturated ammonium chloride solution (2 mL) was added in one portion, followed by saturated brine solution (4 mL) and ethyl acetate (4 mL). The organic phase was separated and was sampled for HPLC analysis, giving the assay yields of **270** and **271** displayed in the main text. As the trimeric product (**279**) has not been isolated, an HPLC %Area is quoted in place of an assay yield.

**Entry 7**

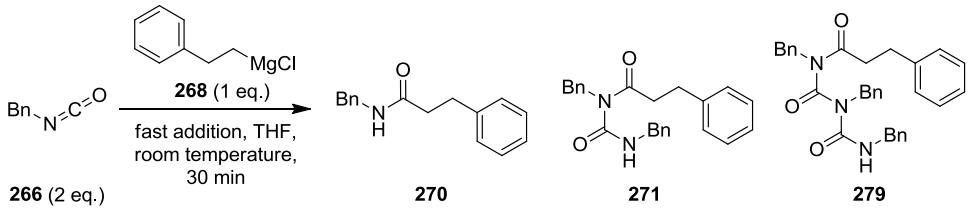


To a solution of (isocyanatomethyl)benzene (0.248 mL, 2 mmol) and anisole (0.055 mL, 0.5 mmol) in dry THF (4 mL) at ***temperature***, was added phenethylmagnesium chloride (0.88 M in THF, 1.14 mL, 1 mmol), rapidly *via* syringe. The reaction was stirred at ***temperature*** for 30 minutes. Saturated ammonium chloride solution (2 mL) was added in one portion, followed by saturated brine solution (4 mL) and ethyl acetate (4 mL). The organic phase was separated and was sampled for HPLC analysis, giving the assay yields of **270** and **271** displayed in the main text. As the trimeric product (**279**) has not been isolated, an HPLC %Area is quoted in place of an assay yield.

### 4.3.3. Calorimetry experiments

***N*-(*tert*-Butyl)-3-phenylpropanamide**

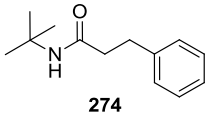

**274**

To a solution of 2-isocyanato-2-methylpropane (1.386 mL, 12.14 mmol) in dry tetrahydrofuran (THF) (48 mL) at 0 °C, was added phenethylmagnesium chloride (0.85 M in THF, 14.28 mL, 12.14 mmol), dropwise over 5 minutes *via* syringe pump (a 32.62 °C temperature rise was recorded, with a maximum heat flow of 11.07 W), and the reaction was stirred for 45 minutes at 0 °C.

Ammonium chloride (saturated aq. solution, 10 mL) was then added dropwise over 5 minutes *via* syringe pump (a 23.55 °C temperature rise was recorded, with a maximum heat flow of 42.97 W), and the reaction stirred for a further 45 minutes at 0 °C. Ethyl acetate (100 mL) was added followed by brine (25 mL). The organics were separated and dried over $MgSO_4$, then filtered, and concentrated *in vacuo*. The crude product was recrystallised from heptane, to afford the desired product (**274**) (2.32 g, 93% yield) as a white solid.

**LCMS (5 min high pH):** $t_R$ = 3.30 min, $[M+H^+]$ = 206.2 (95.9% purity)

Full characterisation can be found above, on page 207.

***N*-Benzyl-3-phenylpropanamide**

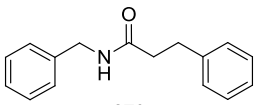

**270**

To a solution of (isocyanatomethyl)benzene (1.5 mL, 12.14 mmol) in dry THF (48 mL) at 0 °C, was added phenethylmagnesium chloride (0.85 M in THF, 14.3 mL, 12.14 mmol), dropwise over 5 minutes *via* syringe pump (a 27.89 °C temperature rise was recorded, with a maximum heat flow of 22.76 W), and the reaction was stirred for 30 minutes at 0 °C.
Ammonium chloride (saturated aq. solution, 10 mL) was added dropwise over 5 minutes *via* syringe pump (a 24.66 °C temperature rise was recorded, with a maximum heat flow of 74.65 W). Ethyl acetate (50 mL) was added and the layers separated. The organic layers were washed with brine (10 mL), dried over $MgSO_4$, filtered, and concentrated *in vacuo*. The crude product was purified by chromatography on silica; elution gradient 0-100% ethyl acetate in heptane. The appropriate fractions were combined and evaporated *in vacuo* to afford the desired product (**270**) (518 mg, 18% yield) as a white crystalline solid.
**LCMS (5 min high pH):** $t_R$ = 2.64 min, $[M+H^+]$ = 240.2 (97.0% purity)
Full characterisation can be found below, on page 234.

Also isolated:
***N*-benzyl-*N*-(benzylcarbamoyl)-3-phenylpropanamide**

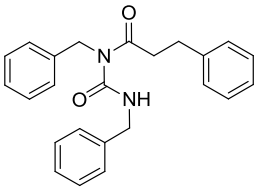

**271**

The acylurea by-product (**271**) (408 mg, 18% yield) as a colourless oil.
**LCMS (5 min high pH):** $t_R$ = 3.55 min, $[M+H^+]$ = 373.3 (95.6% purity)
Full characterisation can be found above, on page 205.

The trimeric by-product (**279**) was also observed by HPLC (8.9 %Area), but could not be isolated.

### 4.3.4. ReactIR in batch

***N*-Benzyl-3-phenylpropanamide**

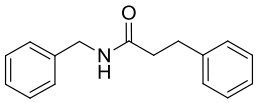

**270**

A ReactIR probe was set up, and a reference spectrum of dry 2-MeTHF was acquired.
To a solution of (isocyanatomethyl)benzene (0.25 mL, 2 mmol) in dry 2-MeTHF (8 mL) was added phenethylmagnesium chloride (0.85 M in THF, 2.35 mL, 2 mmol) in one portion at room temperature. The reaction was stirred for 1 h, then the ReactIR probe was removed, and the reaction was quenched with saturated ammonium chloride solution (10 mL).
The reaction had gone to completion before a single IR scan was acquired (15 seconds).

***N*-Benzyl-3-phenylpropanamide**

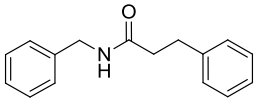

**270**

A ReactIR probe was set up, and a reference spectrum of dry 2-MeTHF was acquired.
To a solution of (isocyanatomethyl)benzene (0.25 mL, 2 mmol) in dry 2-MeTHF (8 mL) was added phenethylmagnesium chloride (0.85 M in THF, 2.35 mL, 2 mmol) in one portion at −50 °C. The reaction was stirred for 1 h at −50 °C, then the ReactIR probe was removed, and the reaction was quenched with saturated ammonium chloride solution (10 mL).
The reaction had gone to completion in around 45 seconds.

***N*-Benzyl-3-phenylpropanamide**

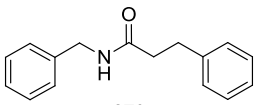

**270**

A ReactIR probe was set up, and a reference spectrum of dry 2-MeTHF was acquired.
To a solution of (isocyanatomethyl)benzene (0.25 mL, 2 mmol) in dry 2-MeTHF (8 mL) was added phenethylmagnesium chloride (0.85 M in THF, 2.35 mL, 2 mmol) in one portion at −78 °C. The reaction was stirred for 1 h at −78 °C, then the ReactIR probe was removed, and the reaction was quenched with saturated ammonium chloride solution (10 mL).
The reaction had gone to completion in around 90 seconds.

***N*-Benzyl-3-phenylpropanamide**

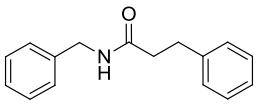

**270**

A ReactIR probe was set up, and a reference spectrum of dry 2-MeTHF was acquired.
To a solution of (isocyanatomethyl)benzene (0.25 mL, 2 mmol) in dry 2-MeTHF (8 mL) was added phenethylmagnesium chloride (0.85 M in THF, 2.35 mL, 2 mmol), in portions of 0.235 mL per minute, for 10 minutes at room temperature. The reaction was stirred for a further 10 minutes at room temperature, then the ReactIR probe was removed, and the reaction was quenched with saturated ammonium chloride solution (10 mL).
Fast consumption of the Grignard reagent throughout its addition was observed. After around 0.6 equivalents of Grignard reagent had been added, no further reaction was seen, as all of the starting material had been consumed in the formation of the acylurea and further overreaction by-products.

***N*-Benzyl-3-phenylpropanamide**

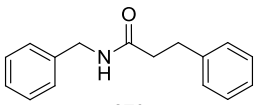

**270**

A ReactIR probe was set up, and a reference spectrum of dry 2-MeTHF was acquired.
To a solution of (isocyanatomethyl)benzene (0.25 mL, 2 mmol) in dry 2-MeTHF (8 mL) was added phenethylmagnesium chloride (0.85 M in THF, 2.35 mL, 2 mmol), in portions of 0.235 mL per minute, for 10 minutes at −50 °C. The reaction was stirred for a further 10 minutes at −50 °C, then the ReactIR probe was removed, and the reaction was quenched with saturated ammonium chloride solution (10 mL).
A reasonably fast rate of consumption of the Grignard reagent throughout its addition was observed. A small amount of overreaction product was observed throughout the reaction, and reaction had not reached completion before 1 equivalent of Grignard reagent had been added.

### 4.3.5. Addition rate study

***N*-Benzyl-3-phenylpropanamide**

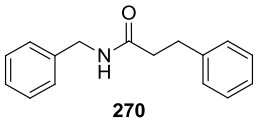

**270**

To a solution of (isocyanatomethyl)benzene (0.124 mL, 1 mmol) and anisole (0.055 mL, 0.5 mmol) in dry THF (4 mL) at 0 °C, was added phenethylmagnesium chloride (0.85 M in THF, 1.29 mL, 1.1 mmol), *via* syringe pump, over ***addition time*** (see table, below). The reaction was stirred for a further 5 minutes at 0 °C. Saturated ammonium chloride solution (2 mL) was added in one portion, followed by saturated brine solution (4 mL) and ethyl acetate (4 mL). The organic layer was sampled for HPLC analysis, with assay yields calculated against the internal standard (anisole).

| Reaction Number | Addition time (sec) | Addition time (min) | Anisole (%Area) | Amide (270) (%Area) | Acylurea (271) (%Area) |
|---|---|---|---|---|---|
| 1 | 1800 | 30 | 18.9 | 9.8 | 23.5 |
| 2 | 900 | 15 | 17.3 | 12.0 | 24.1 |
| 3 | 300 | 5 | 15.6 | 19.0 | 23.4 |
| 4 | 120 | 2 | 15.8 | 28.4 | 19.6 |
| 5 | 90 | 1.5 | 15.2 | 31.0 | 18.2 |
| 6 | 60 | 1 | 15.3 | 35.1 | 17.1 |
| 7 | 45 | 0.75 | 15.6 | 37.8 | 16.4 |
| 8 | 30 | 0.5 | 14.5 | 43.3 | 14.3 |
| 9 | 20 | 0.333 | 16.4 | 41.9 | 14.3 |
| 10 | 10 | 0.1667 | 16.2 | 47.6 | 12.1 |
| 11 | 0 | 0 | 12.6 | 49.2 | 6.5 |

Note: Reaction number 1 was not included in the graph in the main text, to allow clearer representation of the data at shorter addition periods. Reaction number 8 was not included in the graph in the main text, due to its outlying amide yield. Addition time of 0 (entry 11) was achieved by manually adding the Grignard reagent *via* syringe as quickly as possible.

### 4.3.6. FlowIR experiment

**Phenethylmagnesium bromide**

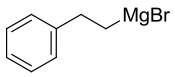


**351**

Magnesium shavings (5.83 g, 240 mmol) were added to an oven-dried 3-necked flask, and stirred dry under vacuum at 100 °C for 16 hours. A dropping funnel was fitted, and dry THF (120 mL) was added to the flask. The dropping funnel was charged with a solution of (2-bromoethyl)benzene (27.3 mL, 200 mmol) in dry THF (80 mL). A small amount of the solution was added to the flask, and the contents were stirred and heated to reflux until reaction commenced. After subsidence of the initial reaction, the remaining bromide solution was added dropwise, at a rate such that the mixture refluxed gently. Once all of the bromide had been added, the reaction mixture was stirred at reflux for a further 1 h, and then allowed to cool to room temperature. The Grignard solution was transferred to a dry flask, using oven-dried PTFE tubing, with a gas dispersion head as an in-line filter.

The resulting Grignard reagent (**351**) was titrated twice using **General method 1**, and was found to be of 0.80 M concentration.

***N*-Benzyl-3-phenylpropanamide**

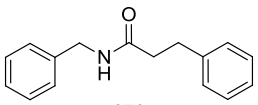

**270**

In order to establish the required residence time for the reaction of isocyanate (**266**) with Grignard reagent (**268**) in flow, a kinetic study was carried out, using a flow ReactIR cell. Flow IR experiments were conducted using the set up shown in **Figure 20**. Grignard reagent was pumped using a Cetoni Nemesys syringe pump (fitted with a 50 mL syringe), whilst isocyanate was pumped using an MZR7255 HNP microannular gear pump, both monitored by Bronckhorst flow controllers. An Ehrfeld cascade mixer 10HC was used to mix the two streams, and a Mettler Toledo FlowIR gave the IR traces. IR measurements were collected every 15 seconds. IR data was processed using Mettler Toledo iC IR software v4.3.

(Isocyanatomethyl)benzene (0.25 M in dry 2-MeTHF) and phenethylmagnesium bromide (0.8 M in dry THF) were pumped into the Ehrfield cascade mixer at flow rates of 32 mL $min^{-1}$ and 10 mL $min^{-1}$, respectively, for a sustained ***run time***, to allow equilibration of the reaction mixture. After a ***varied residence time*** (determined by length of of 1/8" PTFE tubing), the mixture was passed through a Mettler Toledo FlowIR cell. After a further 0.7 s residence time (0.54 m of 1/16" PFA tubing), the flow was quenched into a pot of saturated ammonium chloride solution (250 mL). The conversion values used in the graphical representation (**Figure 21**) were calculated for each time point, by division of equilibrium isocyanate peak height by initial isocyanate peak height. The conversion value at 1.38 s is based on a system that may have not reached equilibrium, so may potentially be erroneous.

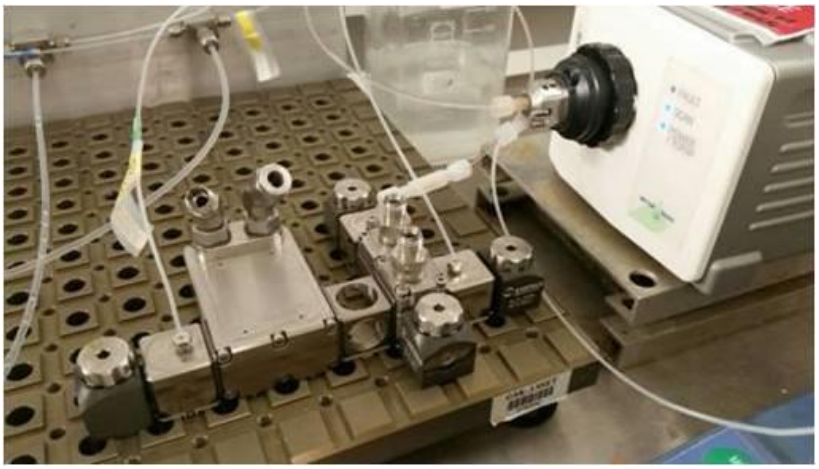

**Figure 32 -** Photograph of the flow React IR equipment set up.

### 4.3.7. Optimisation in flow

***N*-Benzyl-3-phenylpropanamide**

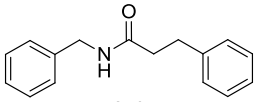

**270**

In an oven-dried round bottomed flask, a solution of (isocyanatomethyl)benzene (0.5 M) and anisole (0.25 M) was made up in dry THF, under nitrogen. In a separate oven-dried round bottomed flask, a solution of phenethylmagnesium chloride (0.5 M) was made up in dry THF, using a commercial bottle of the Grignard reagent (found to be 0.85 M concentration by **General method 1**).

Using a Harvard PHD Ultra syringe pump, equipped with 20 mL Normject disposable syringes, the solutions were mixed in a T-piece, at flow rates of 6 mL $min^{-1}$ each. After ***residence time*** (determined by using different lengths of tubing), the reaction flow was quenched into dilute ammonium chloride solution.

An equilibration period of 3 residence times was allowed, then five samples were collected into vials containing 10 mL of dilute ammonium chloride solution and diethylamine (~1 %vol). Ethyl acetate (10 mL) was added to each sample, and the organic layer was sampled for HPLC analysis, with assay yields calculated against the internal standard (anisole). The values displayed in the main text were taken as the average yields of these five samples.

| Residence time (s) | Sample | Anisole (%Area) | Amide (270) (%Area) | Acylurea (271) (%Area) |
|---|---|---|---|---|
| 6.13 | 1 | 12.3 | 62.6 | 7.9 |
| | 2 | 8.6 | 46.1 | 6.8 |
| | 3 | 11.9 | 63.2 | 7.7 |
| | 4 | 11.1 | 57.9 | 6.2 |
| | 5 | 11.3 | 58.2 | 7.8 |
| 12.25 | 1 | 12.3 | 64.7 | 7.7 |
| | 2 | 11.7 | 65.2 | 7.5 |
| | 3 | 10.9 | 58.9 | 8.0 |
| | 4 | 12.7 | 63.2 | 8.5 |
| | 5 | 11.4 | 58.9 | 8.5 |

***N*-Benzyl-3-phenylpropanamide**

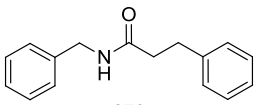

**270**

In an oven-dried round bottomed flask, a solution of (isocyanatomethyl)benzene (0.5 M) and anisole (0.25 M) was made up in dry THF, under nitrogen. In a separate oven-dried round bottomed flask, a solution of phenethylmagnesium chloride (0.5 M) was made up in dry THF under nitrogen, using a commercial bottle of the Grignard reagent (found to be 0.85 M concentration by **General method 1**).

Using a Harvard PHD Ultra syringe pump, equipped with 20 mL Normject disposable syringes, the solutions were each flowed a through 0.5 m "pre-cooling loop" (immersed in a temperature bath as detailed below), then mixed in a T-piece, at flow rates of 5 mL $min^{-1}$ each. After 10.6 s residence time (in tubing also immersed in the temperature bath), the reaction flow was quenched into dilute ammonium chloride solution.

An equilibration period of 3 residence times was allowed, then five samples were collected into vials containing 5 mL of dilute ammonium chloride solution and diethylamine (~1 %vol). Ethyl acetate (5 mL) was added to each sample, and the organic layer was sampled for HPLC analysis, with assay yields calculated against the internal standard (anisole). The values displayed in the main text were taken as the average yields of these five samples.

| Temperature (°C) | Sample | Anisole (%Area) | Starting material (266) (%Area) | Amide (270) (%Area) | Acylurea (271) (%Area) |
|---|---|---|---|---|---|
| 40 | 1 | 13.3 | 0 | 66.8 | 7.6 |
| | 2 | 13.3 | 0 | 65.9 | 7.4 |
| | 3 | 13.4 | 0 | 66.7 | 7.3 |
| | 4 | 13.1 | 0 | 68.0 | 7.3 |
| | 5 | 13.2 | 0 | 67.3 | 7.2 |
| 20 | 1 | 13.5 | 0 | 66.3 | 6.7 |
| | 2 | 13.7 | 0 | 66.2 | 7.0 |
| | 3 | 14.1 | 0 | 65.2 | 7.0 |
| | 4 | 13.8 | 0 | 65.7 | 7.0 |
| | 5 | 14.4 | 0 | 64.3 | 7.6 |
| 0 | 1 | 13.0 | 0.3 | 68.6 | 6.7 |
| | 2 | 13.4 | 0.3 | 67.7 | 6.7 |
| | 3 | 13.3 | 0.3 | 67.9 | 6.6 |
| | 4 | 13.6 | 0.3 | 67.5 | 6.8 |
| | 5 | 12.9 | 0.3 | 68.6 | 6.7 |
| −78 | 1 | 12.5 | 26.6 | 34.8 | 0.8 |
| | 2 | 12.6 | 27.6 | 34.2 | 0.8 |
| | 3 | 12.6 | 26.4 | 35.5 | 0.9 |
| | 4 | 12.5 | 25.3 | 35.5 | 0.8 |
| | 5 | 12.4 | 25.5 | 36.9 | 0.9 |
| No bath | 1 | 13.4 | 0 | 68.2 | 5.9 |
| | 2 | 13.5 | 0 | 68.8 | 5.8 |
| | 3 | 13.5 | 0 | 68.5 | 5.8 |
| | 4 | 13.3 | 0 | 69.0 | 5.8 |
| | 5 | 13.4 | 0 | 68.6 | 5.7 |

***N*-Benzyl-3-phenylpropanamide**

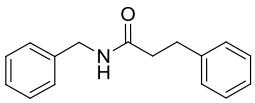

**270**

In an oven-dried round bottomed flask, a solution of (isocyanatomethyl)benzene (0.5 M) and anisole (0.25 M) was made up in dry THF, under nitrogen. In a separate oven-dried round bottomed flask, a solution of phenethylmagnesium chloride (0.5 M) was made up in dry THF under nitrogen, using a commercial bottle of the Grignard reagent (found to be 0.85 M concentration by **General method 1**).

Using a Harvard PHD Ultra syringe pump, equipped with 20 mL Normject disposable syringes, the solutions were mixed in an **Ehrfeld Flowplate® Process Plate TG (large)** (1.2 mL total volume), at flow rates of 5 mL $min^{-1}$ each. After 7.2 s residence time within the mixer, the reaction flow was quenched into dilute ammonium chloride solution.

An equilibration period of 3 residence times was allowed, then five samples were collected into vials containing 5 mL of dilute ammonium chloride solution and diethylamine (~1 %vol). Ethyl acetate (5 mL) was added to each sample, and the organic layer was sampled for HPLC analysis, with assay yields calculated against the internal standard (anisole). The values displayed in the main text were taken as the average yields of these five samples.

| Mixer | Sample | Anisole (%Area) | Starting material (266) (%Area) | Amide (270) (%Area) | Acylurea (271) (%Area) |
|---|---|---|---|---|---|
| Flowplate | 1 | 13.7 | 0 | 68.9 | 3.9 |
| | 2 | 13.7 | 0 | 69.3 | 3.8 |
| | 3 | 13.4 | 0 | 70.4 | 3.9 |
| | 4 | 13.6 | 0 | 68.8 | 3.9 |
| | 5 | 13.8 | 0 | 68.5 | 3.9 |
| T-piece | 1 | 13.4 | 0 | 68.2 | 5.9 |
| | 2 | 13.5 | 0 | 68.8 | 5.8 |
| | 3 | 13.5 | 0 | 68.5 | 5.8 |
| | 4 | 13.3 | 0 | 69.0 | 5.8 |
| | 5 | 13.4 | 0 | 68.6 | 5.7 |

***N*-Benzyl-3-phenylpropanamide**

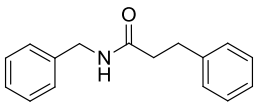

**270**

In an oven-dried round bottomed flask, a solution of (isocyanatomethyl)benzene (***concentration***) and anisole (***0.5*concentration***) was made up in dry THF, under nitrogen. In a separate oven-dried round bottomed flask, a solution of phenethylmagnesium chloride (***concentration***) was made up in dry THF under nitrogen, using a commercial bottle of the Grignard reagent (found to be 0.85 M concentration by **General method 1**).

Using a Harvard PHD Ultra syringe pump, equipped with 20 mL Normject disposable syringes, the solutions were mixed in a T-piece, at flow rates of 5 mL $min^{-1}$ each. After 14.6 s residence time, the reaction flow was quenched into dilute ammonium chloride solution.

An equilibration period of 3 residence times was allowed, then five samples were collected into vials containing 5 mL of dilute ammonium chloride solution and diethylamine (~1 %vol). Ethyl acetate (5 mL) was added to each sample, and the organic layer was sampled for HPLC analysis, with assay yields calculated against the internal standard (anisole). The values displayed in the main text were taken as the average yields of these five samples.

| Concentration (M) | Sample | Anisole (%Area) | Starting material (266) (%Area) | Amide (270) (%Area) | Acylurea (271) (%Area) |
|---|---|---|---|---|---|
| 0.25 | 1 | 11.8 | 0.7 | 54.9 | 10.6 |
| | 2 | 12.2 | 0.8 | 55.2 | 11.3 |
| | 3 | 12.2 | 0.9 | 54.8 | 11.7 |
| | 4 | 12.2 | 1.0 | 54.1 | 12.2 |
| | 5 | 12.4 | 1.1 | 53.3 | 12.7 |
| 0. 50 | 1 | 12.2 | 0 | 59.4 | 9.4 |
| | 2 | 11.8 | 0 | 58.6 | 9.5 |
| | 3 | 12.1 | 0 | 59.7 | 9.4 |
| | 4 | 11.9 | 0 | 58.6 | 9.3 |
| | 5 | 12.3 | 0 | 58.2 | 9.3 |
| 0.75 | 1 | 12.4 | 0 | 57.1 | 10.6 |
| | 2 | 12.6 | 0 | 56.5 | 10.7 |
| | 3 | 12.2 | 0 | 57.5 | 10.2 |
| | 4 | 12.7 | 0 | 55.0 | 10.7 |
| | 5 | 12.4 | 0 | 57.8 | 10.3 |

***N*-Benzyl-3-phenylpropanamide**

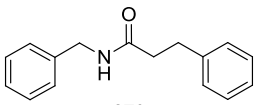

**270**

In an oven-dried round bottomed flask, a solution of (isocyanatomethyl)benzene (0.5 M) and anisole (0.25 M) was made up in dry THF, under nitrogen. In a separate oven-dried round bottomed flask, a solution of phenethylmagnesium chloride (***concentration***) was made up in dry THF under nitrogen, using a commercial bottle of the Grignard reagent (found to be 0.85 M concentration by **General method 1**).

Using a Harvard PHD Ultra syringe pump, equipped with 20 mL Normject disposable syringes, the solutions were mixed in a T-piece, at flow rates of 5 mL $min^{-1}$ each. After 14.6 s residence time, the reaction flow was quenched into dilute ammonium chloride solution.

An equilibration period of 3 residence times was allowed, then five samples were collected into vials containing 5 mL of dilute ammonium chloride solution and diethylamine (~1 %vol). Ethyl acetate (5 mL) was added to each sample, and the organic layer was sampled for HPLC analysis, with assay yields calculated against the internal standard (anisole). The values displayed in the main text were taken as the average yields of these five samples.

| Grignard concentration (M) | Grignard equivalents | Sample | Anisole (%Area) | Amide (270) (%Area) | Acylurea (271) (%Area) |
|---|---|---|---|---|---|
| 0.45 | 0.9 | 1 | 13.8 | 67.0 | 9.1 |
| | | 2 | 14.2 | 67.0 | 8.6 |
| | | 3 | 14.2 | 66.8 | 8.9 |
| | | 4 | 13.3 | 67.0 | 9.2 |
| | | 5 | 14.1 | 67.4 | 8.5 |
| 0.50 | 1.0 | 1 | 13.1 | 68.2 | 6.9 |
| | | 2 | 13.0 | 68.1 | 7.0 |
| | | 3 | 13.3 | 68.0 | 6.9 |
| | | 4 | 14.0 | 66.8 | 6.7 |
| | | 5 | 13.6 | 67.6 | 6.7 |
| 0.55 | 1.1 | 1 | 12.9 | 69.2 | 5.8 |
| | | 2 | 13.1 | 68.6 | 5.9 |
| | | 3 | 13.2 | 68.4 | 6.1 |
| | | 4 | 13.1 | 68.8 | 5.6 |
| | | 5 | Sample not collected | | |

***N*-Benzyl-3-phenylpropanamide**

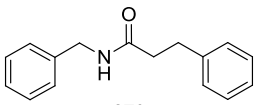

**270**

In an oven-dried round bottomed flask, a solution of (isocyanatomethyl)benzene (0.75 M) and anisole (0.375 M) was made up in dry THF, under nitrogen. In a separate oven-dried round bottomed flask, a solution of phenethylmagnesium chloride (0.75 M) was made up in dry THF under nitrogen, using a commercial bottle of the Grignard reagent (found to be 0.85 M concentration by **General method 1**).

Using a Harvard PHD Ultra syringe pump, equipped with 20 mL Normject disposable syringes, the solutions were pumped at flow rates of 5 mL $min^{-1}$ each.

The isocyanate stream was split by a T-piece. One stream (roughly 0.5 equivalents of isocyanate) was combined with the Grignard reagent, then after a 6.2 s residence time, the second stream (remaining 0.5 equivalents of isocyanate) was also introduced. After a further 6.6 s residence time, the reaction flow was quenched into dilute ammonium chloride solution.

An equilibration period of 3 residence times was allowed, then five samples were collected into vials containing 5 mL of dilute ammonium chloride solution and diethylamine (~1 %vol). Ethyl acetate (5 mL) was added to each sample, and the organic layer was sampled for HPLC analysis, with assay yields calculated against the internal standard (anisole).

This procedure was repeated two further times, to ensure reproducible results. The values displayed in the main text were taken as the average yields over all fourteen samples.

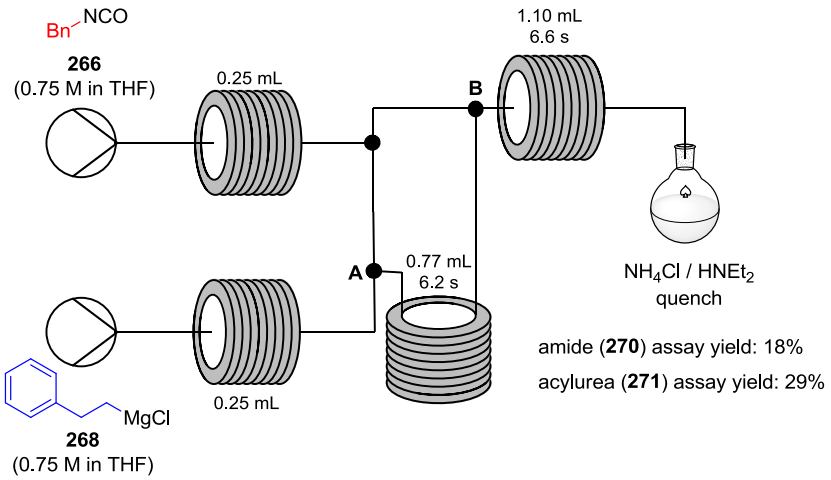

| Run | Sample | Anisole (%Area) | Starting material (266) (%Area) | Amide (270) (%Area) | Acylurea (271) (%Area) |
|---|---|---|---|---|---|
| **1** | 1 | 8.1 | 0 | 7.4 | 12.6 |
| | 2 | 7.4 | 0 | 6.5 | 12.1 |
| | 3 | 7.0 | 0 | 6.0 | 11.6 |
| | 4 | 7.0 | 0 | 5.9 | 11.8 |
| | 5 | Sample not collected | | | |
| **2** | 1 | 7.7 | 0 | 7.3 | 11.6 |
| | 2 | 6.9 | 0 | 6.4 | 10.7 |
| | 3 | 7.0 | 0 | 6.6 | 11.3 |
| | 4 | 6.8 | 0 | 6.1 | 10.9 |
| | 5 | 9.7 | 0 | 9.6 | 13.4 |
| **3** | 1 | 6.4 | 0 | 7.0 | 9.3 |
| | 2 | 7.0 | 0 | 7.6 | 9.8 |
| | 3 | 6.6 | 0 | 6.6 | 9.7 |
| | 4 | 6.8 | 0 | 7.0 | 10.1 |
| | 5 | 7.6 | 0 | 7.7 | 10.9 |

### 4.3.8. Additive screening

***N*-Benzyl-3-phenylpropanamide**

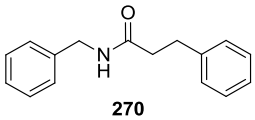

**270**

To a solution of (isocyanatomethyl)benzene (0.124 mL, 1 mmol), ***additive (1 mmol, 1 equivalent)***, and anisole (0.055 mL, 0.5 mmol) in dry THF (4 mL) at room temperature was added phenethylmagnesium chloride (0.85 M in THF, 1.29 mL, 1.1 mmol) as quickly as possible *via* syringe. The reaction was stirred for a further 30 minutes at room temperature. Saturated ammonium chloride solution (2 mL) was added in one portion, followed by water (2 mL) and ethyl acetate (2 mL). The organic layer was sampled for HPLC analysis, with assay yields calculated against the internal standard (anisole).

| Reaction Number | Additive (quantity) | Anisole (%Area) | Starting material (266) (%Area) | Amide (270) (%Area) | Acylurea (271) (%Area) |
|---|---|---|---|---|---|
| 1 | None | 12.6 | 0 | 49.2 | 6.5 |
| 2 | TMSCl (0.128 mL) | 14.3 | 0 | 56.3 | 1.2 |
| 3 | TBSCl (151 mg) | 13.5 | 0 | 41.5 | 8.4 |
| 4 | LiCl (42 mg) | 12.7 | 0 | 17.4 | 22.6 |
| 5 | LiBr (87 mg) | 14.7 | 0 | 14.9 | 22.1 |
| 6 | $MgCl_2$ (95 mg) | 12.8 | 0 | 45.5 | 8.7 |
| 7 | TMEDA (116 mg) | 12.7 | 0 | 41.5 | 9.2 |
| 8 | NMP (0.096 mL) | 14.9 | 0 | 35.8 | 5.9 |
| 9 | CuI (190 mg) | 12.2 | 0 | 56.7 | 3.0 |
| 10 | Bis[2-(*N*,*N*-dimethylamino)ethyl] ether (**280**, 0.191 mL) | 12.3 | 0 | 28.7 | 12.1 |

***N*-Benzyl-3-phenylpropanamide**

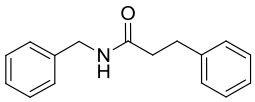

**270**

To a solution of (isocyanatomethyl)benzene (0.124 mL, 1 mmol), ***copper source (1 mmol, or 0.1 mmol)***, and anisole (0.055 mL, 0.5 mmol) in dry THF (4 mL) at room temperature was added phenethylmagnesium chloride (0.85 M in THF, 1.29 mL, 1.1 mmol) as quickly as possible *via* syringe. The reaction was stirred for a further 30 minutes at room temperature. Saturated ammonium chloride solution (2 mL) was added in one portion, followed by water (2 mL) and ethyl acetate (2 mL). The organic layer was sampled for HPLC analysis, with assay yields calculated against the internal standard (anisole).

| **Reaction Number** | **Additive (mmol, quantity)** | **Anisole (%Area)** | **Starting material (266) (%Area)** | **Amide (270) (%Area)** | **Acylurea (271) (%Area)** |
|---|---|---|---|---|---|
| 1 | CuCl (1, 99 mg) | 12.5 | 0 | 48.9 | 4.3 |
| 2 | CuBr (1, 143 mg) | 13.3 | 0 | 53.8 | 2.5 |
| 3 | $Cu(OAc)_2$ (1, 182 mg) | 16.4 | 0 | 23.7 | 17.6 |
| 4 | $Cu(acac)_2$ (1, 262 mg) | 16.0 | 0 | 28.4 | 13.9 |
| 5 | $Cu(OTf)_2$ (1, 362 mg) | 17.8 | 0 | 21.5 | 6.7 |
| 6 | $CuBr_2$ (1, 223 mg) | 13.6 | 0 | 51.7 | 4.6 |
| 7 | CuCl (0.1, 10 mg) | 13.0 | 0 | 51.8 | 4.1 |
| 8 | CuBr (0.1, 14 mg) | 13.4 | 0 | 48.1 | 3.4 |
| 9 | $Cu(OAc)_2$ (0.1, 18 mg) | 15.6 | 0 | 43.7 | 5.2 |
| 10 | $Cu(acac)_2$ (0.1, 26 mg) | 13.3 | 0 | 48.4 | 6.9 |
| 11 | $Cu(OTf)_2$ (0.1, 36 mg) | 13.5 | 0 | 50.1 | 3.8 |
| 12 | $CuBr_2$ (0.1, 22 mg) | 12.7 | 0 | 56.3 | 1.7 |
| 13 | CuI (0.1, 19 mg) | 14.0 | 0 | 48.6 | 3.9 |

***N*-Benzyl-3-phenylpropanamide**

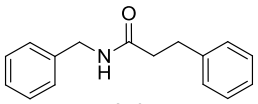

**270**

To a solution of (isocyanatomethyl)benzene (0.124 mL, 1 mmol), CuI (19 mg, 0.1 mmol), and anisole (0.055 mL, 0.5 mmol) in dry THF (4 mL) at room temperature was added phenethylmagnesium chloride (0.85 M in THF, 1.29 mL, 1.1 mmol) over 5 minutes *via* syringe pump. The reaction was stirred for a further 30 minutes at room temperature. Saturated ammonium chloride solution (2 mL) was added in one portion, followed by water (2 mL) and ethyl acetate (2 mL). The organic layer was sampled for HPLC analysis, with assay yields calculated against the internal standard (anisole).

| **Anisole (%Area)** | **Starting material (266) (%Area)** | **Amide (270) (%Area)** | **Acylurea (271) (%Area)** |
|---|---|---|---|
| 21.8 | 0 | 12.8 | 10.2 |

***N*-Benzyl-3-phenylpropanamide**

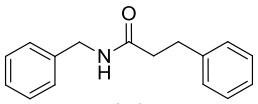

**270**

To a solution of (isocyanatomethyl)benzene (0.124 mL, 1 mmol), trimethylsilyl chloride (***quantity***) and anisole (0.055 mL, 0.5 mmol) in dry THF (4 mL) at room temperature was added phenethylmagnesium chloride (0.85 M in THF, 1.29 mL, 1.1 mmol) as quickly as possible *via* syringe. The reaction was stirred for a further 30 minutes at room temperature. Saturated ammonium chloride solution (2 mL) was added in one portion, followed by water (2 mL) and ethyl acetate (2 mL). The organic layer was sampled for HPLC analysis, with assay yields calculated against the internal standard (anisole).

| **Reaction Number** | **Eq. TMSCl** | **Anisole (%Area)** | **Starting material (266) (%Area)** | **Amide (270) (%Area)** | **Acylurea (271) (%Area)** |
|---|---|---|---|---|---|
| 1 | 0.1 | 15.9 | 0 | 42.4 | 7.8 |
| 2 | 0.5 | 14.4 | 0 | 60.8 | 4.0 |
| 3 | 1 | 15.6 | 0 | 64.6 | 2.4 |
| 4 | 2 | 17.8 | 0 | 58.5 | 3.0 |

***N*-Benzyl-3-phenylpropanamide**

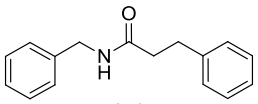

**270**

To a solution of (isocyanatomethyl)benzene (0.124 mL, 1 mmol), trimethylsilyl chloride (***quantity***), and anisole (0.055 mL, 0.5 mmol) in dry THF (4 mL) at room temperature was added phenethylmagnesium chloride (0.85 M in THF, 1.29 mL, 1.1 mmol) over 5 minutes *via* syringe pump. The reaction was stirred for a further 30 minutes at room temperature. Saturated ammonium chloride solution (2 mL) was added in one portion, followed by water (2 mL) and ethyl acetate (2 mL). The organic layer was sampled for HPLC analysis, with assay yields calculated against the internal standard (anisole).

| Reaction Number | TMSCl Equivalents | Anisole (%Area) | Starting material (266) (%Area) | Amide (270) (%Area) | Acylurea (271) (%Area) |
|---|---|---|---|---|---|
| 1 | 0.1 | 24.9 | 0 | 16.7 | 8.7 |
| 2 | 0.5 | 20.2 | 0 | 32.1 | 7.3 |
| 3 | 1 | 22.5 | 0 | 36.4 | 3.9 |
| 4 | 2 | 21.3 | 0 | 35.7 | 1.7 |

***N*-Benzyl-3-phenylpropanamide**

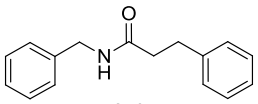

**270**

In an oven-dried round bottomed flask, a solution of (isocyanatomethyl)benzene (0.5 M), anisole (0.25 M) and ***additive*** was made up in dry THF, under nitrogen. The isocyanate solution was sonicated for 5 minutes, to ensure homogeneity as far as possible.

In a separate oven-dried round bottomed flask, a solution of phenethylmagnesium chloride (0.5 M) was made up in dry THF under nitrogen, using a commercial bottle of the Grignard reagent (found to be 0.85 M concentration by **General method 1**).

Using a Harvard PHD Ultra syringe pump, equipped with 20 mL Normject disposable syringes, the solutions were mixed in a T-piece, at flow rates of 5 mL $min^{-1}$ each. After a 14.6 s residence time, the reaction flow was quenched into dilute ammonium chloride solution.

An equilibration period of 3 residence times was allowed, then five samples were collected into vials containing 10 mL of dilute ammonium chloride solution and diethylamine (~1 %vol). Ethyl acetate (10 mL) was added to each sample, and the organic layer was sampled for HPLC analysis, with assay yields calculated against the internal standard (anisole). The values displayed in the main text were taken as the average yields of these five samples.

| Additive (eq.) | Sample | Anisole (%Area) | Amide (270) (%Area) | Acylurea (271) (%Area) |
|---|---|---|---|---|
| none | 1 | 13.2 | 64.0 | 7.5 |
| | 2 | 13.2 | 64.0 | 7.5 |
| | 3 | 13.2 | 64.4 | 7.3 |
| | 4 | 13.1 | 63.7 | 7.6 |
| | 5 | 13.2 | 64.0 | 7.4 |
| TMSCl (0.5) | 1 | 13.4 | 71.4 | 3.5 |
| | 2 | 13.3 | 70.5 | 3.5 |
| | 3 | 13.2 | 70.7 | 3.5 |
| | 4 | 13.1 | 70.9 | 3.4 |
| | 5 | 12.9 | 69.0 | 3.8 |
| $CuBr_2$ (0.1) | 1 | 13.4 | 74.0 | 2.5 |
| | 2 | 13.7 | 73.6 | 2.4 |
| | 3 | 13.6 | 74.0 | 2.5 |
| | 4 | 13.8 | 73.7 | 2.4 |
| | 5 | 13.6 | 74.3 | 2.1 |
| **$CuBr_2$ (0.01)** | 1 | 13.4 | 74.6 | 2.4 |
| | 2 | 13.5 | 74.7 | 2.3 |
| | 3 | 13.5 | 75.9 | 1.7 |
| | 4 | 13.3 | 75.3 | 1.9 |
| | 5 | 13.5 | 75.3 | 2.1 |
| $CuBr_2$ (0.001) | 1 | 13.7 | 65.7 | 7.4 |
| | 2 | 13.6 | 65.2 | 7.7 |
| | 3 | 13.6 | 65.6 | 7.4 |
| | 4 | 13.7 | 65.6 | 7.5 |
| | 5 | 13.2 | 62.7 | 7.9 |
| $CuBr_2$ (0.005) | 1 | 13.6 | 71.7 | 4.3 |
| | 2 | 13.5 | 71.7 | 3.0 |
| | 3 | 13.6 | 71.3 | 3.0 |
| | 4 | 13.6 | 71.7 | 2.9 |
| | 5 | 13.6 | 71.6 | 2.9 |

***N*-Benzyl-3-phenylpropanamide**[279]

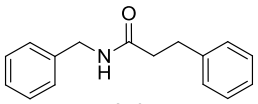

**270**

In round bottomed flasks, 0.5 M solutions of benzyl isocyanate (with 1 mol% $CuBr_2$) and phenethylmagnesium chloride were made up in dry THF. The isocyanate solution was sonicated for 5 minutes, to ensure homogeneity as far as possible.

Using a Harvard PHD Ultra syringe pump, equipped with 20 mL Normject disposable syringes, the solutions were mixed in a T-piece, at flow rates of 5 mL $min^{-1}$ each. After a 10.6 s residence time, the reaction flow was quenched into dilute ammonium chloride solution.

An equilibration period of 3 residence times was allowed, then a sample of **2.5 mmol** (10 mL combined flow volume) was collected into a flask containing 10 mL of dilute ammonium chloride solution and diethylamine (~1 %vol). Ethyl acetate (10 mL) was added to the sample, alongside water (10 mL) and saturated brine (10 mL), and the layers separated. The aqueous layer was extracted with further ethyl acetate (25 mL). The combined organics were dried over $MgSO_4$, and evaporated *in vacuo*. The crude product was washed with cold heptane (3 × 5 mL), to afford the desired product (**270**) (575 mg, 96% yield) as a white crystalline solid.

**Melting point:** 83-84 °C, literature value: 84.5-85.5 °C

**IR $\nu_{max}$:** 3276, 1630 $cm^{-1}$

**$^1$H NMR (400 MHz, $CDCl_3$):** δ = 8.32 (t, *J*=5.6 Hz, 1H), 7.31 - 7.24 (m, 4H), 7.24 - 7.16 (m, 4H), 7.13 (d, *J*=7.1 Hz, 2H), 4.25 (d, *J*=5.9 Hz, 2H), 2.85 (t, *J*=7.7 Hz, 2H), 2.45 (t, *J*=7.7 Hz, 2H)

**$^{13}$C NMR (101 MHz, $CDCl_3$):** δ = 171.2, 141.2, 139.5, 128.3, 128.23, 128.18, 127.1, 126.6, 125.9, 41.9, 36.9, 31.1

**LCMS (5 min high pH):** $t_R$ = 2.78 min, $[M+H^+]$ = 254.3 (96.2% purity)

**HRMS:** ($C_{16}H_{18}NO$) $[M+H^+]$ requires: 254.1539, $[M+H^+]$ found: 254.1534

### 4.3.9. Substrate scope

***N*-Butyl-3-phenylpropanamide**[280]

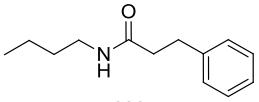

**282**

Prepared using **General method D**, by the reaction of 1-isocyanatobutane and phenethylmagnesium chloride.

The crude product was purified by chromatography on silica; elution gradient 0-50% ethyl acetate in heptane. The appropriate fractions were combined and evaporated *in vacuo* to afford the desired product (**282**) (201 mg, 98% yield) as a white crystalline solid.

**Melting point:** 32-35 °C

**IR $\nu_{max}$:** 3311, 2930, 1635, 1541, 1453 $cm^{-1}$

**$^{1}$H NMR (400 MHz, DMSO-$d_6$)** $\delta$ = 7.77 (br. s, 1H), 7.33 - 7.11 (m, 5H), 3.01 (q, *J*=6.6 Hz, 2H), 2.79 (t, *J*=7.7 Hz, 2H), 2.34 (t, *J*=7.7 Hz, 2H), 1.32 (s, 2H), 1.27 - 1.15 (m, 2H), 0.84 (t, *J*=7.3 Hz, 3H)

**$^{13}$C NMR (101 MHz, DMSO-$d_6$):** $\delta$ = 171.0, 141.4, 128.2, 128.2, 125.8, 38.0, 37.0, 31.2, 31.1, 19.5, 13.7

**LCMS (5 min high pH):** $t_R$ = 3.21 min, $[M+H^+]$ = 206.2 (100% purity)

**HRMS:** ($C_{13}H_{20}NO$) $[M+H^+]$ requires: 206.1539, $[M+H^+]$ found: 206.1528

**3-Phenyl-*N*-(4-phenylbutyl)propanamide**

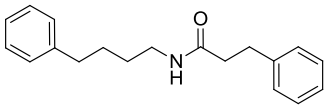

**283**

Prepared using **General method D**, by the reaction of (4-isocyanatobutyl)benzene and phenethylmagnesium chloride.

The crude product was purified by chromatography on silica; elution gradient 0-75% ethyl acetate in heptane. The appropriate fractions were combined and evaporated *in vacuo* to afford the desired product (**283**) (266 mg, 95% yield) as a white crystalline solid.

**Melting point:** 44-46 °C

**IR $\nu_{max}$:** 3309, 2937, 2861, 1634, 1495, 1541, 1453 $cm^{-1}$

**$^{1}$H NMR (400 MHz, DMSO-$d_6$)** $\delta$ = 7.76 (t, *J*=5.4 Hz, 1H), 7.30 - 7.21 (m, 4H), 7.20 - 7.12 (m, 6H), 3.04 (dt, *J*=5.4, 7.6 Hz, 2H), 2.79 (t, *J*=7.7 Hz, 2H), 2.54 (t, *J*=7.6 Hz, 2H), 2.34 (t, *J*=7.7 Hz, 2H), 1.50 (quin, *J*=7.6 Hz, 2H), 1.36 (quin, *J*=7.6 Hz, 2H)

**$^{13}$C NMR (101 MHz, DMSO-$d_6$):** $\delta$ = 171.0, 142.1, 141.3, 128.3, 128.2, 128.1, 125.8, 125.6, 38.1, 37.0, 34.8, 31.1, 28.8, 28.3 (Ar C signal at 128.2 is thought to consist of two overlapping signals)

**LCMS (5 min high pH):** $t_R$ = 3.03 min, $[M+H^+]$ = 282.4 (100% purity)

**HRMS:** ($C_{19}H_{24}NO$) $[M+H^+]$ requires: 282.1852, $[M+H^+]$ found: 282.1850

***N*-Isopropyl-3-phenylpropanamide**[279]

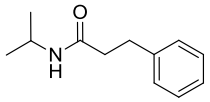

**284**

Prepared using **General method D**, by the reaction of 2-isocyanatopropane and phenethylmagnesium chloride.

The crude product required no further purification, and was identified as a pure sample of the desired product (**284**) (188 mg, 98% yield) as a white crystalline solid.

**Melting point:** 89-91 °C, literature value: 90-91 °C

**IR $\nu_{max}$:** 3297, 2968, 1637, 1540, 1453, 1364, 1230, 1171 $cm^{-1}$

**$^{1}$H NMR (400 MHz, DMSO-$d_6$)** $\delta$ = 7.66 (d, *J*=7.3 Hz, 1H), 7.30 - 7.23 (m, 2H), 7.21 - 7.13 (m, 3H), 3.81 (sptd, *J*=6.6, 7.3 Hz, 1H), 2.79 (t, *J*=7.8 Hz, 2H), 2.31 (t, *J*=7.8 Hz, 2H), 1.00 (d, *J*=6.6 Hz, 6H)

**$^{13}$C NMR (101 MHz, DMSO-$d_6$):** $\delta$ = 170.2, 141.4, 128.20, 128.18, 125.8, 40.1, 37.1, 31.2, 22.4

**LCMS (5 min high pH):** $t_R$ = 3.01 min, $[M+H^+]$ = 192.2 (96.5% purity)

**HRMS:** ($C_{12}H_{18}NO$) $[M+H^+]$ requires: 192.1383, $[M+H^+]$ found: 192.1374

***N*-(*tert*-Butyl)-3-phenylpropanamide**[279]

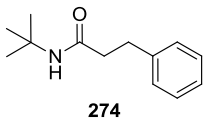

**274**

Prepared using **General method D**, by the reaction of 2-isocyanato-2-methylpropane and phenethylmagnesium chloride.

The crude product required no further purification, and was identified as the desired product (**274**) (190 mg, 93% yield) as a white crystalline solid.

**Melting point:** 88-89 °C, literature value: 88-89 °C

**IR $\nu_{max}$:** 3313, 2969, 1640, 1547, 1454, 1391, 1359, 1226 $cm^{-1}$

**$^{1}$H NMR (400 MHz, DMSO-$d_6$)** $\delta$ = 7.38 (br. s, 1H), 7.29 - 7.23 (m, 2H), 7.22 - 7.14 (m, 3H), 2.77 (t, *J*=7.7 Hz, 2H), 2.30 (t, *J*=7.7 Hz, 2H), 1.21 (s, 9H)

**$^{13}$C NMR (101 MHz, DMSO-$d_6$):** $\delta$ = 170.8, 141.5, 128.22, 128.15, 125.8, 49.8, 37.7, 31.2, 28.5

**LCMS (5 min high pH):** $t_R$ = 3.31 min, $[M+H^+]$ = 206.2 (100% purity)

**HRMS:** ($C_{13}H_{20}NO$) $[M+H^+]$ requires: 206.1539, $[M+H^+]$ found: 206.1535

***N*-(Benzo[*d*][1,3]dioxol-5-yl)-3-phenylpropanamide**

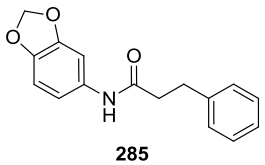

**285**

Prepared using **General method D**, by the reaction of 5-isocyanatobenzo[*d*][1,3]dioxole and phenethylmagnesium chloride.

The crude product was purified by chromatography on silica; elution gradient 0-50% ethyl acetate in heptane. The appropriate fractions were combined and evaporated *in vacuo* to afford the desired product (**285**) (227 mg, 84% yield) as a white crystalline solid.

**Melting point:** 116-118 °C

**IR $\nu_{max}$:** 3270, 2900, 1647, 1530, 1489, 1449, 1214 $cm^{-1}$

**$^{1}$H NMR (400 MHz, DMSO-$d_6$):** δ = 9.81 (br. s, 1H), 7.32 - 7.21 (m, 5H), 7.21 - 7.15 (m, 1H), 6.92 (dd, *J*=2.2, 8.3 Hz, 1H), 6.82 (d, *J*=8.3 Hz, 1H), 5.96 (s, 2H), 2.89 (t, *J*=7.7 Hz, 2H), 2.57 (t, *J*=7.7 Hz, 2H)

**$^{13}$C NMR (101 MHz, DMSO-$d_6$):** δ = 169.9, 147.0, 142.7, 141.1, 133.6, 128.3, 128.2, 125.9, 111.8, 108.0, 101.3, 100.9, 37.9, 30.8

**LCMS (5 min high pH):** $t_R$ = 3.38 min, $[M+H^+]$ = 270.2 (100% purity)

**HRMS:** ($C_{16}H_{16}NO_3$) $[M+H^+]$ requires: 270.1125, $[M+H^+]$ found: 270.1122

***N*-(Benzo[*d*][1,3]dioxol-5-yl)-3-phenylpropanamide**

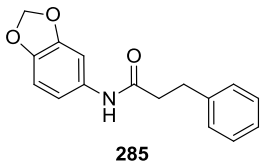

**285**

In round bottomed flasks, 0.5 M solutions of 5-isocyanatobenzo[*d*][1,3]dioxole (**with 5 mol% $CuBr_2$**) and phenethylmagnesium chloride were made up in dry THF. The isocyanate solution was sonicated for 5 minutes, to ensure homogeneity as far as possible.

Using a Harvard PHD Ultra syringe pump, equipped with 20 mL Normject disposable syringes, the solutions were mixed in a T-piece, at flow rates of 5 mL $min^{-1}$ each. After a 10.6 s residence time, the reaction flow was quenched into dilute ammonium chloride solution.

An equilibration period of 3 residence times was allowed, then samples of 1 mmol (4 mL combined flow volume) were collected into vials containing 10 mL of dilute ammonium chloride solution and diethylamine (~1 %vol). Ethyl acetate (10 mL) was added to each sample, alongside water (10 mL) and saturated brine (10 mL), and the layers separated. The aqueous layer was extracted with further ethyl acetate (25 mL). The combined organics were dried over $MgSO_4$, and evaporated *in vacuo*. The crude product was washed with heptane (2 × 5 mL), then recrystallised from DCM/heptane to afford the desired product (**285**) (242 mg, 90% yield) as an off-white solid.

**LCMS (5 min high pH):** $t_R$ = 3.38 min, $[M+H^+]$ = 270.2 (97.7% purity)

Full characterisation can be found above, on page 239.

***N*-(3,5-Bis(trifluoromethyl)phenyl)-3-phenylpropanamide**

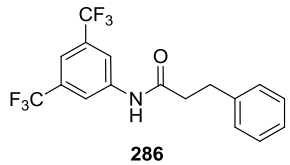

**286**

Prepared using **General method D**, by the reaction of 1-isocyanato-3,5-bis(trifluoromethyl)benzene and phenethylmagnesium chloride.

The crude product was purified by chromatography on silica; elution gradient 0-25% ethyl acetate in heptane. The appropriate fractions were combined and evaporated *in vacuo* to afford the desired product (**286**) (308 mg, 85% yield) as a white crystalline solid.

**Melting point:** 126-129 °C

**IR $\nu_{max}$:** 3274, 1674, 1572, 1382, 1277, 1174, 1130, 1112 $cm^{-1}$

**$^{1}$H NMR (400 MHz, DMSO-$d_6$):** δ = 10.57 (br. s, 1H), 8.24 (s, 2H), 7.73 (s, 1H), 7.32 - 7.22 (m, 4H), 7.21 - 7.16 (m, 1H), 2.94 (t, *J*=7.8 Hz, 2H), 2.70 (t, *J*=7.8 Hz, 2H)

**$^{13}$C NMR (101 MHz, DMSO-$d_6$):** δ = 171.5, 141.0, 140.8, 130.7 (q, *J*=32.8 Hz), 128.4, 128.2, 126.0, 123.2 (q, *J*=273.5 Hz), 118.7 - 118.5 (m), 115.8 (spt, *J*=3.8 Hz), 37.9, 30.4

**$^{19}$F NMR (377MHz, DMSO-$d_6$):** δ = −61.7 (s, 6F)

**LCMS (5 min high pH):** $t_R$ = 2.68 min, $[M+H^+]$ = 270.2 (96.8% purity)

**HRMS:** ($C_{17}H_{14}F_6NO$) $[M+H^+]$ requires: 362.0974, $[M+H^+]$ found: 362.0971

***N*-(4-Bromophenyl)-3-phenylpropanamide**[281]

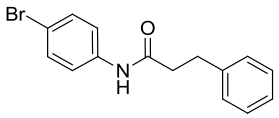


**287**

Prepared using **General method D**, by the reaction of 1-bromo-4-isocyanatobenzene and phenethylmagnesium chloride.

The crude product was purified by evaporative recrystallisation from acetone/heptane to afford the desired product (**287**) (283 mg, 93% yield) as a white crystalline solid.

**Melting point:** 148-151 °C

**IR $\nu_{max}$:** 3315, 3034, 2936, 1638, 1508, 1208, 1155, 1128 $cm^{-1}$

**$^{1}$H NMR (400 MHz, DMSO-$d_6$):** $\delta$ = 10.04 (br. s, 1H), 7.60 - 7.41 (m, 4H), 7.32 - 7.13 (m, 5H), 2.90 (t, *J*=7.5 Hz, 2H), 2.62 (t, *J*=7.5 Hz, 2H)

**$^{13}$C NMR (101 MHz, DMSO-$d_6$):** $\delta$ = 170.5, 141.1, 138.5, 131.5, 128.3, 128.2, 125.9, 120.9, 114.5, 37.9, 30.7

**LCMS (5 min high pH):** $t_R$ = 3.07 min, $[M+H^+]$ = 304.2, 306.2 (98.1% purity)

**HRMS:** ($C_{15}H_{15}[^{79}Br]NO$) $[M+H^+]$ requires: 304.0332, $[M+H^+]$ found: 304.0335

***N*-(3-chlorophenyl)-3-phenylpropanamide**

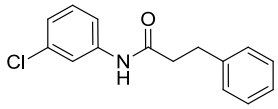

**288**

Prepared using **General method D**, by the reaction of 1-chloro-3-isocyanatobenzene and phenethylmagnesium chloride.

The crude product was purified by chromatography on silica; elution gradient 0-25% ethyl acetate in heptane. The appropriate fractions were combined and evaporated *in vacuo* to afford the desired product (**288**) (222 mg, 86% yield) as a white crystalline solid.

**Melting point:** 69-72 °C

**IR $\nu_{max}$:** 3291, 3026, 2932, 1656, 1591, 1525, 1453, 1208 $cm^{-1}$

**$^{1}$H NMR (400 MHz, DMSO-$d_6$):** δ = 10.08 (br. s, 1H), 7.81 (t, *J*=2.0 Hz, 1H), 7.46 - 7.38 (m, 1H), 7.34 - 7.22 (m, 5H), 7.21 - 7.15 (m, 1H), 7.11 - 7.05 (m, 1H), 2.91 (t, *J*=7.6 Hz, 2H), 2.64 (t, *J*=7.6 Hz, 2H)

**$^{13}$C NMR (101 MHz, DMSO-$d_6$):** δ = 170.7, 141.0, 140.6, 133.0, 130.3, 128.3, 128.2, 125.9, 122.7, 118.5, 117.3, 37.9, 30.6

**LCMS (2 min low pH):** $t_R$ = 1.19 min, $[M+H^+]$ = 260.0, 262.0 (100% purity)

**HRMS:** ($C_{15}H_{15}[^{35}Cl]NO$) $[M+H^+]$ requires: 260.0837, $[M+H^+]$ found: 260.0829

***N*,3-Diphenylpropanamide**[280]

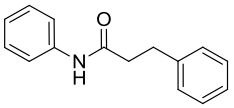

**289**

Prepared using **General method D**, by the reaction of isocyanatobenzene and phenethylmagnesium chloride.

The crude product was washed with cold heptane (5 mL) to afford the desired product (**289**) (203 mg, 90% yield) as a white crystalline solid.

**Melting point:** 88-90 °C, literature value: 92-94 °C

**IR $\nu_{max}$:** 3309, 1653, 1597, 1525, 1497, 1440, 1361, 1314, 1244 $cm^{-1}$

**$^{1}$H NMR (400 MHz, DMSO-$d_6$):** δ = 9.90 (s, 1H), 7.57 (d, *J*=7.8 Hz, 2H), 7.32 - 7.22 (m, 6H), 7.22 - 7.15 (m, 1H), 7.02 (t, *J*=7.3 Hz, 1H), 2.91 (t, *J*=7.7 Hz, 2H), 2.62 (t, *J*=7.7 Hz, 2H)

**$^{13}$C NMR (101 MHz, DMSO-$d_6$):** δ = 170.3, 141.2, 139.2, 128.7, 128.3, 128.2, 125.9, 123.0, 119.0, 37.9, 30.8

**LCMS (5 min high pH):** $t_R$ = 3.39 min, $[M+H^+]$ = 226.2 (98.6% purity)

**HRMS:** ($C_{15}H_{16}NO$) $[M+H^+]$ requires: 226.1226, $[M+H^+]$ found: 226.1222

***N*-(4-Chloro-3-(trifluoromethyl)phenyl)-3-phenylpropanamide**

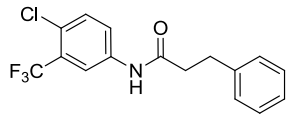

**290**

Prepared using **General method D**, by the reaction of 1-chloro-4-isocyanato-2-(trifluoromethyl)benzene and phenethylmagnesium chloride.

The crude product was purified by chromatography on silica; elution gradient 0-50% ethyl acetate in heptane. The appropriate fractions were combined and evaporated *in vacuo* to afford the desired product (**290**) (271 mg, 83% yield) as a white crystalline solid.

**Melting point:** 77-79 °C

**IR $\nu_{max}$:** 3265, 1659, 1535, 1320, 1129, 1111cm$^{-1}$

**$^{1}$H NMR (400 MHz, DMSO-d$_6$):** δ = 10.34 (br. s, 1H), 8.17 (d, *J*=2.5 Hz, 1H), 7.81 (dd, *J*=2.5, 8.7 Hz, 1H), 7.64 (d, *J*=8.7 Hz, 1H), 7.32 - 7.22 (m, 4H), 7.21 - 7.14 (m, 1H), 2.92 (t, *J*=7.7 Hz, 2H), 2.66 (t, *J*=7.7 Hz, 2H)

**$^{13}$C NMR (101 MHz, DMSO-d$_6$):** δ = 171.1, 140.9, 138.6, 132.1, 128.3, 128.2, 126.7 (q, *J*=30.7 Hz), 126.0, 123.7 - 123.5 (m), 122.7 (q, *J*=272.9 Hz), 117.6 (q, *J*=5.6 Hz), 37.9, 30.5

**$^{19}$F NMR (377MHz, DMSO-d$_6$):** δ = −61.5 (s, 3F)

**LCMS (2 min low pH):** $t_R$ = 1.32 min, [M+H$^+$] = 327.9, 329.8 (100% purity)

**HRMS:** ($C_{16}H_{14}[^{35}Cl]F_3NO$) [M+H$^+$] requires: 328.0711, [M+H$^+$] found: 328.0706

***N*-(4-Cyanophenyl)-3-phenylpropanamide**

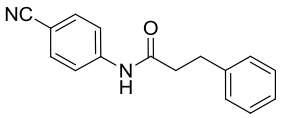

**291**

Prepared using **General method D**, by the reaction of 4-isocyanatobenzonitrile and phenethylmagnesium chloride.

The crude product was purified by chromatography on silica; elution gradient 0-50% ethyl acetate in heptane. The appropriate fractions were combined and evaporated *in vacuo* to afford the desired product (**291**) (170 mg, 68% yield) as an off white solid.

**Melting point:** 111-113 °C

**IR $\nu_{max}$:** 3258, 2219, 1672, 1595, 1532, 1316, 1265 $cm^{-1}$

**$^{1}$H NMR (400 MHz, DMSO-$d_6$):** δ = 10.35 (br. s, 1H), 7.75 (s, 4H), 7.31 - 7.22 (m, 4H), 7.21 - 7.15 (m, 1H), 2.91 (t, *J*=8.0 Hz, 2H), 2.68 (t, *J*=8.0 Hz, 2H)

**$^{13}$C NMR (101 MHz, DMSO-$d_6$):** δ = 171.3, 143.4, 140.9, 133.3, 128.3, 128.2, 126.0, 119.1, 119.0, 104.7, 38.0, 30.5

**LCMS (5 min high pH):** $t_R$ = 2.75 min, [M-$H^+$] 249.1 (96.8% purity)

**HRMS:** ($C_{16}H_{15}N_2O$) [M+$H^+$] requires: 251.1179, [M+$H^+$] found: 251.1171

**Ethyl 4-(3-phenylpropanamido)benzoate**

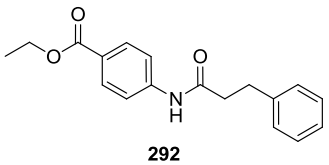

**292**

Prepared using **General method D**, by the reaction of ethyl 4-isocyanatobenzoate and phenethylmagnesium chloride.

The crude product was purified by chromatography on silica; elution gradient 0-100% ethyl acetate in heptane. The appropriate fractions were combined and evaporated *in vacuo* to afford the desired product (**292**) (255 mg, 86% yield) as an off white solid.

**Melting point:** 129-130 °C

**IR $\nu_{max}$:** 3315, 2994, 2941, 1707, 1669, 1521, 1407, 1271, 1174 $cm^{-1}$

**$^{1}$H NMR (400 MHz, DMSO-$d_6$):** $\delta$ = 10.24 (s, 1H), 7.93 - 7.86 (m, 2H), 7.76 - 7.68 (m, 2H), 7.32 - 7.23 (m, 4H), 7.22 - 7.15 (m, 1H), 4.28 (q, *J*=7.1 Hz, 2H), 2.92 (t, *J*=7.4 Hz, 2H), 2.67 (t, *J*=7.4 Hz, 2H), 1.30 (t, *J*=7.1 Hz, 3H)

**$^{13}$C NMR (101 MHz, DMSO-$d_6$):** $\delta$ = 171.0, 165.3, 143.5, 141.0, 130.2, 128.3, 128.2, 125.9, 124.0, 118.3, 60.3, 38.0, 30.6, 14.2

**LCMS (5 min high pH):** $t_R$ = 2.41 min, $[M+H^+]$ 298.2 (96.1% purity)

**HRMS:** ($C_{18}H_{20}NO_3$) $[M+H^+]$ requires: 298.1438, $[M+H^+]$ found: 298.1427

***N*-(4-Acetylphenyl)-3-phenylpropanamide**

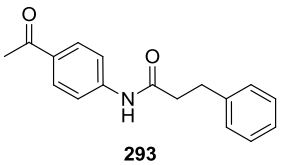

**293**

In round bottomed flasks, 0.5 M solutions of 1-(4-isocyanatophenyl)ethan-1-one (with 1 mol% $CuBr_2$) and phenethylmagnesium chloride were made up in dry THF. The isocyanate solution was sonicated for 5 minutes, to ensure homogeneity as far as possible. Using a Harvard PHD Ultra syringe pump, equipped with 20 mL Normject disposable syringes, the solutions were passed through a 50 cm pre-cooling loop, submerged in an ice bath at 0 °C, then mixed in a T-piece, at flow rates of 5 mL $min^{-1}$ each. After a 10.6 s residence time, where tubing was submerged in an ice bath at 0 °C, the reaction flow was quenched into dilute ammonium chloride solution.

An equilibration period of 3 residence times was allowed, then samples of 1 mmol (4 mL combined flow volume) were collected into vials containing 10 mL of dilute ammonium chloride solution and diethylamine (~1 %vol). Ethyl acetate (10 mL) was added to each sample, alongside water (10 mL) and saturated brine (10 mL), and the layers separated. The aqueous layer was extracted with further ethyl acetate (25 mL). The combined organics were dried over $MgSO_4$ and evaporated *in vacuo*. The crude product was purified by reverse phase chromatography, using a 120g C18 column; elution gradient 30-80% MeCN in $H_2O$, with a formic acid modifier. The appropriate fractions were combined and evaporated *in vacuo* to afford the desired product (**293**) (120 mg, 45 % yield) as a crystalline white solid.

**Melting point:** 135-137 °C

**IR $\nu_{max}$:** 3313, 1670, 1605, 1587, 1517, 1404, 1361, 1273, 1257 $cm^{-1}$

**$^1$H NMR (400 MHz, DMSO-$d_6$):** δ = 10.24 (br. s, 1H), 7.91 (d, *J*=8.7 Hz, 2H), 7.71 (d, *J*=8.7 Hz, 2H), 7.33 - 7.22 (m, 4H), 7.21 - 7.15 (m, 1H), 2.92 (t, *J*=7.9 Hz, 2H), 2.67 (t, *J*=7.9 Hz, 2H), 2.51 (s, 3H)

**$^{13}$C NMR (101 MHz, DMSO-$d_6$):** δ = 196.4, 171.0, 143.5, 141.0, 131.5, 129.4, 128.3, 128.2, 125.9, 118.2, 38.0, 30.6, 26.4

**LCMS (2 min low pH):** $t_R$ = 1.00 min, [M+H$^+$] 268.1 (100% purity)

**HRMS:** ($C_{17}H_{18}NO_2$) [M+H$^+$] requires: 268.1332, [M+H$^+$] found: 268.1328

***N*-(3,4-Dichlorobenzyl)-3-phenylpropanamide**

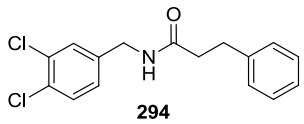

**294**

Prepared using **General method D**, by reaction of 1,2-dichloro-4-(isocyanatomethyl)benzene and phenethylmagnesium chloride.

The crude product was washed with cold heptane (3 × 5 mL) to afford the desired product (**294**) (277 mg, 90% yield) as a white crystalline solid.

**Melting point:** 95-97 °C

**IR $\nu_{max}$:** 3280, 1634, 1532, 1475, 1453, 1131 $cm^{-1}$

**$^{1}$H NMR (400 MHz, DMSO-$d_6$):** δ = 8.38 (t, *J*=5.8 Hz, 1H), 7.52 (d, *J*=8.2 Hz, 1H), 7.41 (d, *J*=2.0 Hz, 1H), 7.29 - 7.23 (m, 2H), 7.22 - 7.15 (m, 3H), 7.11 (dd, *J*=2.0, 8.2 Hz, 1H), 4.24 (d, *J*=5.8 Hz, 2H), 2.84 (t, *J*=7.6 Hz, 2H), 2.46 (t, *J*=7.6 Hz, 2H)

**$^{13}$C NMR (101 MHz, DMSO-$d_6$):** δ = 171.5, 141.1, 140.9, 130.8, 130.3, 129.1, 129.0, 128.2, 127.4, 125.9, 40.9, 36.8, 30.9 (Ar C signal at 128.2 is thought to consist of two overlapping signals)

**LCMS (2 min low pH):** $t_R$ = 1.19 min, [M+$H^+$] 307.9, 311.9 (96.5% purity)

**HRMS:** ($C_{16}H_{16}[^{35}Cl]_2NO$) [M+$H^+$] requires: 308.0604, [M+$H^+$] found: 308.0591

***N*-(2,4-Dimethoxybenzyl)-3-phenylpropanamide**

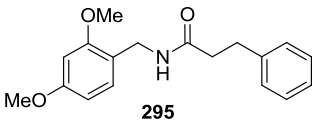


**295**

Prepared using **General method D**, by the reaction of 1-(isocyanatomethyl)-2,4-dimethoxybenzene with phenethylmagnesium chloride.

The crude product was washed with cold heptane (3 × 5 mL) to afford the desired product (**295**) (290 mg, 97% yield) as a white crystalline solid.

**Melting point:** 86-87 °C

**IR $\nu_{max}$:** 3312, 2935, 2833, 1638, 1540, 1207, 1154, 1127, 1029 $cm^{-1}$

**$^{1}$H NMR (400 MHz, DMSO-$d_6$):** δ = 8.02 (t, *J*=5.7 Hz, 1H), 7.31 - 7.23 (m, 2H), 7.23 - 7.15 (m, 3H), 6.90 (d, *J*=8.2 Hz, 1H), 6.52 (d, *J*=2.3 Hz, 1H), 6.41 (dd, *J*=2.4, 8.3 Hz, 1H), 4.13 (d, *J*=5.7 Hz, 2H), 3.76 (s, 3H), 3.73 (s, 3H), 2.83 (t, *J*=7.7 Hz, 2H), 2.43 (t, *J*=7.7 Hz, 2H)

**$^{13}$C NMR (101 MHz, DMSO-$d_6$):** δ = 171.2, 159.6, 157.6, 141.4, 128.6, 128.24, 128.21, 125.8, 119.0, 104.3, 98.1, 55.3, 55.2, 36.9, 36.7, 31.1

**LCMS (5 min high pH):** $t_R$ = 2.70 min, [M+$H^+$] 300.3 (95.7% purity)

**HRMS:** ($C_{18}H_{22}NO_3$) [M+$H^+$] requires: 300.1594, [M+$H^+$] found: 300.1586

***N*-(Furan-2-ylmethyl)-3-phenylpropanamide**[280]

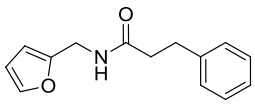

**296**

Prepared using **General method D**, by the reaction of 2-(isocyanatomethyl)furan and phenethylmagnesium chloride.

The crude product was washed with cold heptane (3 × 5 mL) to afford the desired product (**296**) (208 mg, 91% yield) as a pale yellow solid.

**Melting point:** 51-53 °C, literature value: 51-53 °C

**IR $\nu_{max}$:** 3308, 2926, 1636, 1531, 1444, 1148, 1078 $cm^{-1}$

**$^{1}$H NMR (400 MHz, DMSO-$d_6$):** δ = 8.28 (t, *J*=5.5 Hz, 1H), 7.55 (d, *J*=1.9 Hz, 1H), 7.30 - 7.23 (m, 2H), 7.22 - 7.13 (m, 3H), 6.37 (dd, *J*=1.9, 2.8 Hz, 1H), 6.15 (d, *J*=2.7 Hz, 1H), 4.24 (d, *J*=5.5 Hz, 2H), 2.82 (t, *J*=7.7 Hz, 2H), 2.41 (t, *J*=7.8 Hz, 2H)

**$^{13}$C NMR (101 MHz, DMSO-$d_6$):** δ = 171.1, 152.4, 142.0, 141.3, 128.21, 128.18, 125.8, 110.4, 106.6, 36.8, 35.4, 31.0

**LCMS (2 min low pH):** $t_R$ = 0.92 min, $[M+H^+]$ 230.1 (96.6% purity)

**HRMS:** ($C_{14}H_{16}NO_2$) $[M+H^+]$ requires: 230.1176, $[M+H^+]$ found: 230.1170

**3-Phenylpropanamide**[282]

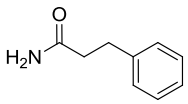

**297**

Prepared using **General method D**, by the reaction of isocyanatotrimethylsilane and phenethylmagnesium chloride.

The crude product was washed with cold heptane (3 × 5 mL), to afford the desired product (**297**) (67 mg, 45% yield) as a white crystalline solid.

**Melting point:** 97-100 °C, literature value: 96.1-97.6 °C

**IR $\nu_{max}$:** 3391, 3181, 1648, 1497, 1410 $cm^{-1}$

**$^{1}$H NMR (400 MHz, DMSO-$d_6$):** δ = 7.31 - 7.23 (m, 3H), 7.21 - 7.13 (m, 2H), 6.74 (br. s, 1H), 2.79 (t, *J*=7.8 Hz, 2H), 2.34 (t, *J*=7.8 Hz, 2H)

1 × NH not observed, assumed to be due to its exchangeable nature.

**$^{13}$C NMR (101 MHz, DMSO-$d_6$):** δ = 173.3, 141.4, 128.2, 128.1, 125.8, 36.6, 30.8

**LCMS (2 min low pH):** $t_R$ = 0.60 min, $[M+H^+]$ 150.0 (100% purity)

**HRMS:** ($C_9H_{12}NO$) $[M+H^+]$ requires: 150.0913, $[M+H^+]$ found: 150.0910

**(*R*)-3-Phenyl-*N*-(1-phenylethyl)propanamide**[283]

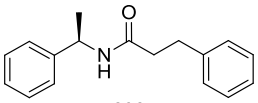

**298**

Prepared using **General method D**, by the reaction of (*R*)-(1-isocyanatoethyl)benzene and phenethylmagnesium chloride.

The crude product was purified by chromatography on silica; elution gradient 0-50% ethyl acetate in heptane. The appropriate fractions were combined and evaporated *in vacuo* to afford the desired product (**298**) (205 mg, 81% yield) as a white crystalline solid.

**Melting point:** 89-90 °C, literature value: 92 °C

**IR $\nu_{max}$:** 3305, 3062, 2984, 2928, 1636, 1538, 1453, 1227, 1126 $cm^{-1}$

**$^{1}$H NMR (400 MHz, DMSO-$d_6$):** δ = 8.23 (d, *J*=8.0 Hz, 1H), 7.31 - 7.15 (m, 10H), 4.91 (qd, *J*=7.1, 8.0 Hz, 1H), 2.81 (t, *J*=7.5 Hz, 2H), 2.42 (t, *J*=7.5 Hz, 2H), 1.30 (d, *J*=7.1 Hz, 3H)

**$^{13}$C NMR (101 MHz, DMSO-$d_6$):** δ = 170.3, 144.6, 141.3, 128.2, 128.2, 128.1, 126.4, 125.9, 125.8, 47.5, 36.9, 31.1, 22.4

**LCMS (5 min high pH):** $t_R$ = 2.75 min, [M+$H^+$] 254.3 (100% purity)

**HRMS:** ($C_{17}H_{20}NO$) [M+$H^+$] requires: 254.1539, [M+$H^+$] found: 254.1538

**Chiral purity:** 99:1 (*R*):(*S*), by chiral HPLC. Complete retention of chiral purity was observed during this reaction (see below for chiral HPLC traces of starting material and product).

The literature value for specific rotation of opposite enantiomer: $[\alpha]_D^{21}$ = −63.6 ° (*c*=1.03, EtOH) (quoted as 98% ee)

Measured specific rotation for this compound: $[\alpha]_D^{21}$ = +57.692 (*c*=1.04, EtOH)

## Chiral HPLC analysis of product 298

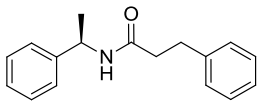

**298**

Sample of single enantiomer product:

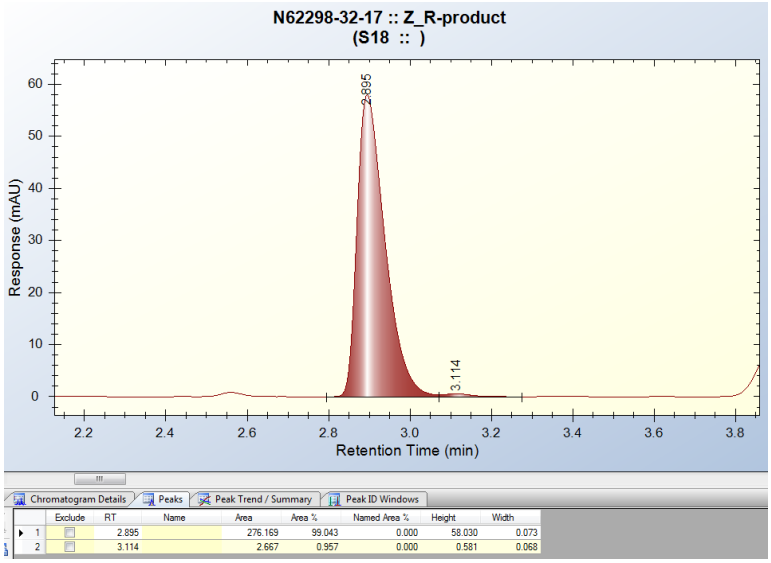


| | Exclude | RT | Name | Area | Area % | Named Area % | Height | Width |
|---|---|---|---|---|---|---|---|---|
| 1 | | 2.895 | | 276.169 | 99.043 | 0.000 | 58.030 | 0.073 |
| 2 | | 3.114 | | 2.667 | 0.957 | 0.000 | 0.581 | 0.068 |

**er = 99.0:1.0**

Mixture of enantiomers, as reference:

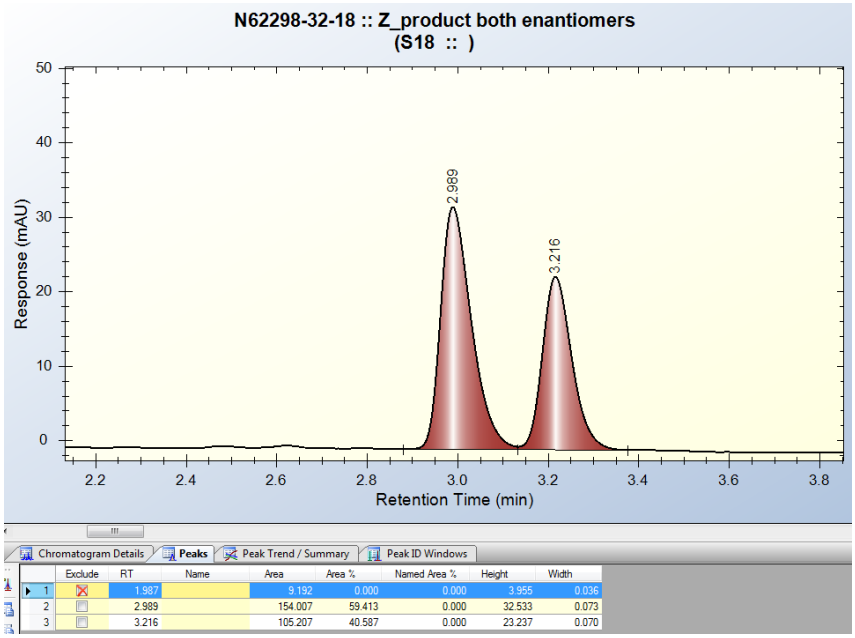


| | Exclude | RT | Name | Area | Area % | Named Area % | Height | Width |
|---|---|---|---|---|---|---|---|---|
| 1 | | 1.987 | | 9.192 | 0.000 | 0.000 | 3.955 | 0.036 |
| 2 | | 2.989 | | 154.007 | 59.413 | 0.000 | 32.533 | 0.073 |
| 3 | | 3.216 | | 105.207 | 40.587 | 0.000 | 23.237 | 0.070 |

Isocyanate starting material, single enantiomer:

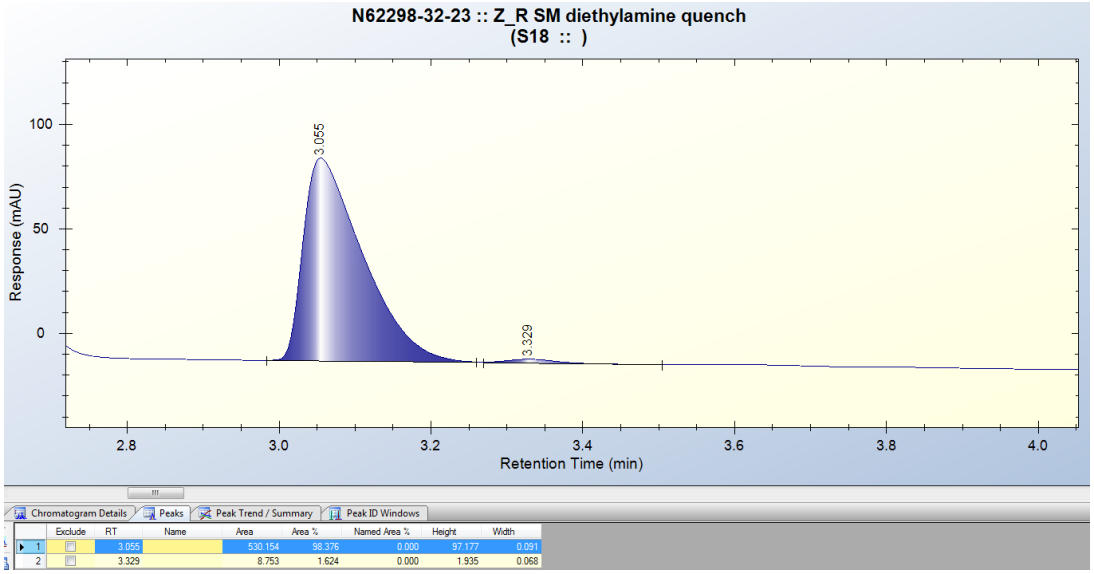


**er = 98.4:1.6**

Mixture of enantiomers, as reference:

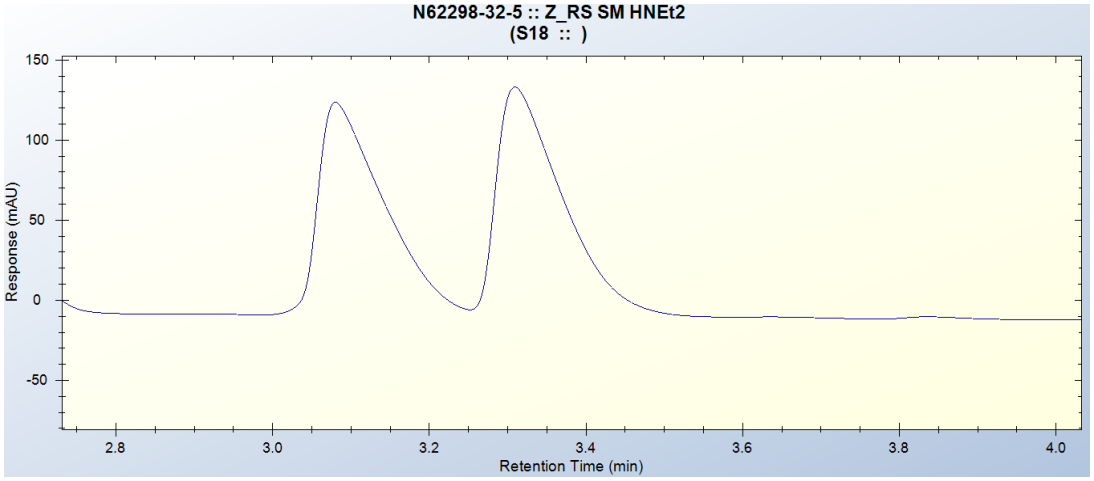


Chiral purity of product is slightly higher than that of the starting material, but within error. It can be assumed that there was no loss of stereochemical purity in this reaction.

**Both product and starting material were analysed by the same method:**

Column: Chiralpak ID-3, 150 × 4.6 mm, 3 micron

Flow rate: 1.2 mL $min^{-1}$

Mobile phase: Heptane/IPA/diethylamine 75/25/0.25 v/v/v

Column temperature: 30 °C

Detection method: UV @ 270 nm

Injection volume: 5 µL

Runtime: 25 min

**3-Phenyl-*N*-((1*S*,2*R*)-2-phenylcyclopropyl)propanamide**

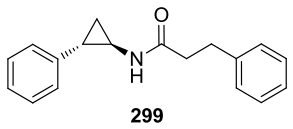

**299**

Prepared using **General method D**, by the reaction of ((1*S*,2*R*)-2-isocyanatocyclopropyl)benzene and phenethylmagnesium chloride.

The crude product was purified by chromatography on silica; elution gradient 0-50% ethyl acetate in heptane. The appropriate fractions were combined and evaporated *in vacuo* to afford the desired product (**299**) (215 mg, 81% yield) as a white crystalline solid.

**Melting point:** 95 °C

**IR $\nu_{max}$:** 3250, 3027, 1631, 1539, 1501, 1029 $cm^{-1}$

**$^{1}$H NMR (400 MHz, DMSO-$d_6$):** δ = 8.11 (d, *J*=4.1 Hz, 1H), 7.31 - 7.22 (m, 4H), 7.22 - 7.12 (m, 4H), 7.11 - 7.06 (m, 2H), 2.85 – 2.75 (m, 3H), 2.35 (t, *J*=7.8 Hz, 2H), 1.85 (ddd, *J*=3.4, 6.2, 9.3 Hz, 1H), 1.14 - 1.06 (m, 2H)

**$^{13}$C NMR (101 MHz, DMSO-$d_6$):** δ = 172.2, 141.4, 141.3, 128.21, 128.18, 128.1, 125.8, 125.7, 125.5, 36.8, 32.4, 31.0, 23.9, 15.2

**LCMS (5 min high pH):** $t_R$ = 2.83 min, [M+$H^+$] 266.3 (96.6% purity)

**HRMS:** ($C_{18}H_{20}NO$) [M+$H^+$] requires: 266.1539, [M+$H^+$] found: 266.1540

**1,3-Di(pyridin-3-yl)urea**[284]

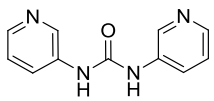

**303**

In a round bottomed flask, a 0.5 M solution of 3-isocyanatopyridine (with 1 mol% $CuBr_2$) was made up in dry NMP and sonicated for 5 minutes, to ensure homogeneity as far as possible. In a separate round bottomed flask, a 0.5 M solution of phenethylmagnesium chloride was made up in dry THF.

Using a Harvard PHD Ultra syringe pump, equipped with 20 mL Normject disposable syringes, the solutions were mixed in a T-piece, at flow rates of 5 mL $min^{-1}$ each. After a 10.6 s residence time, the reaction flow was quenched into dilute ammonium chloride solution.

An equilibration period of 3 residence times was allowed, then samples of 1 mmol (4 mL combined flow volume) were collected into vials containing 10 mL of dilute ammonium chloride solution and diethylamine (~1 %vol). Ethyl acetate (10 mL) was added to each sample, alongside water (10 mL) and saturated brine (10 mL), and the layers separated. The aqueous layer was extracted with further ethyl acetate (25 mL). The combined organics were dried over $MgSO_4$ and evaporated *in vacuo*.

The crude product was purified by chromatography on silica; elution gradient 0-10% methanol in dichloromethane. The appropriate fractions were combined and evaporated *in vacuo* to afford the urea (**303**), by-product of isocyanate decomposition (53 mg, 50% yield) as a beige crystalline solid.

**Melting point:** 219-223 °C, literature value: 220 °C

**IR $\nu_{max}$:** 3251, 3224, 3048, 2993, 1689, 1583, 1415, 1265, 1227 $cm^{-1}$

**$^1$H NMR (400 MHz, DMSO-$d_6$):** δ = 9.01 (s, 2H), 8.62 (d, *J*=2.5 Hz, 2H), 8.21 (dd, *J*=1.2, 4.7 Hz, 2H), 7.94 (ddd, *J*=1.2, 1.5, 8.2 Hz, 2H), 7.32 (dd, *J*=4.7, 8.2 Hz, 2H)

**$^{13}$C NMR (101 MHz, DMSO-$d_6$):** δ = 152.7, 143.1, 140.3, 136.2, 125.4, 123.6

**LCMS (2 min low pH):** $t_R$ = 0.58 min, $[M+H^+]$ 215.0 (100% purity)

**HRMS:** ($C_{11}H_{11}N_4O$) $[M+H^+]$ requires: 215.0927, $[M+H^+]$ found: 215.0927

**Benzyl 4-isocyanatopiperidine-1-carboxylate**

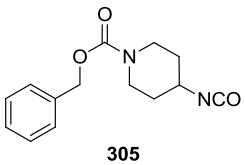


**305**

To a solution of 1-((benzyloxy)carbonyl)piperidine-4-carboxylic acid (1.32 g, 5 mmol) and triethylamine (1.3 mL, 9.3 mmol) in toluene (20 mL), under nitrogen, was added diphenylphosphinyl azide (1.24 mL, 6.5 mmol) slowly, at 95 °C. The resulting solution was stirred at 95 °C for 90 min, then heated to reflux for 2 h. The reaction mixture was allowed to cool to room temperature, then was transferred to a separating funnel, and washed with saturated aqueous $NaHCO_3$ solution (50 mL). The aqueous phase was back extracted with ethyl acetate (50 mL), then the organics were combined, dried over $MgSO_4$, filtered, and solvent removed *in vacuo*. The crude product was purified by silica chromatography; elution gradient 20-80% ethyl acetate in heptane. The appropriate fractions were combined evaporated *in vacuo* to afford the desired product (**305**) (488 mg, 38% yield) as a colourless oil.

**IR $\nu_{max}$:** 2952, 2864, 2253, 1694, 1425, 1272, 1222, 1018 $cm^{-1}$

**$^1$H NMR (400 MHz, DMSO-$d_6$):** δ = 7.43 - 7.26 (m, 5H), 5.07 (s, 2H), 3.83 (app. spt, *J*=4.1 Hz, 1H), 3.67 (td, *J*=4.7, 13.7 Hz, 2H), 3.18 (br. s, 2H), 1.90 - 1.81 (m, 2H), 1.57 - 1.45 (m, 2H)

**$^{13}$C NMR (101 MHz, DMSO-$d_6$):** δ = 154.3, 136.9, 128.4, 127.8, 127.5, 122.0, 66.2, 50.5, 41.0, 32.8

**LCMS (2 min low pH):** $t_R$ = 0.99 min, $[M+H^+]$ 333.0 (96.5% purity) This sample was quenched with diethylamine due to instability under LC conditions.

**Benzyl 4-(3-phenylpropanamido)piperidine-1-carboxylate**

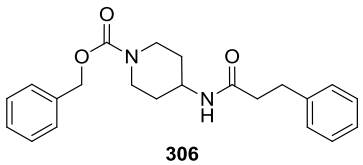

**306**

Prepared using **General method D**, by the reaction of benzyl 4-isocyanatopiperidine-1-carboxylate and phenethylmagnesium chloride.

The crude product was purified by chromatography on silica; elution gradient 0-100% ethyl acetate in heptane. The appropriate fractions were combined and evaporated *in vacuo* to afford the desired product (**306**) (325 mg, 89% yield) as a white crystalline solid.

**Melting point:** 122-125 °C

**IR $\nu_{max}$:** 3300, 1687, 1638, 1537, 1428, 1497, 1450, 1218, 1140 $cm^{-1}$

**$^{1}$H NMR (400 MHz, DMSO-$d_6$):** δ = 7.76 (d, *J*=7.6 Hz, 1H), 7.40 - 7.29 (m, 5H), 7.29 - 7.22 (m, 2H), 7.21 - 7.13 (m, 3H), 5.06 (s, 2H), 3.86 (app. td, *J*=3.4, 13.4 Hz, 2H), 3.79 - 3.68 (m, 1H), 2.94 (br. s, 2H), 2.80 (t, *J*=7.8 Hz, 2H), 2.34 (t, *J*=7.8 Hz, 2H), 1.68 (dd, *J*=3.4, 12.9 Hz, 2H), 1.20 (dq, *J*=3.4, 12.9 Hz, 2H)

**$^{13}$C NMR (101 MHz, DMSO-$d_6$):** δ = 170.5, 154.4, 141.2, 137.0, 128.4, 128.2, 127.8, 127.4, 125.8, 66.1, 45.3, 42.3, 37.0, 31.2, 31.1

**LCMS (2 min low pH):** $t_R$ = 1.08 min, $[M+H^+]$ 367.1 (95.9% purity)

**HRMS:** ($C_{22}H_{27}N_2O_3$) $[M+H^+]$ requires: 367.2016, $[M+H^+]$ found: 367.2010

***N*-Benzylbenzamide**[285]

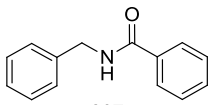

**307**

Prepared using **General method D**, by the reaction of (isocyanatomethyl)benzene and phenylmagnesium chloride.

The crude product was washed with cold heptane (3 × 2 mL) to afford the desired product (**307**) (208 mg, 98% yield) as a white crystalline solid.

**Melting point:** 102-105 °C, literature value: 104 °C

**IR $\nu_{max}$:** 3284, 1636, 1602, 1547, 1489, 1452, 1418 $cm^{-1}$

**$^{1}$H NMR (400 MHz, DMSO-$d_6$):** δ = 9.05 (t, *J*=6.1 Hz, 1H), 7.93 - 7.87 (m, 2H), 7.56 - 7.45 (m, 3H), 7.36 - 7.30 (m, 4H), 7.27 - 7.21 (m, 1H), 4.49 (d, *J*=6.1 Hz, 2H)

**$^{13}$C NMR (101 MHz, DMSO-$d_6$):** δ = 166.2, 139.7, 134.3, 131.2, 128.34, 128.31, 127.22, 127.18, 126.7, 42.6

**LCMS (5 min high pH):** $t_R$ = 2.46 min, $[M+H^+]$ 212.2 (98.9% purity)

**HRMS:** ($C_{14}H_{14}NO$) $[M+H^+]$ requires: 212.1070, $[M+H^+]$ found: 212.1065

***N*-Benzyl-2-phenylacetamide**[20]

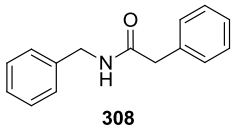

**308**

Prepared using **General method D**, by the reaction of (isocyanatomethyl)benzene and benzylmagnesium chloride.

The crude product was purified by chromatography on silica; elution gradient 0-75% ethyl acetate in heptane. The appropriate fractions were combined and evaporated *in vacuo* to afford the desired product (**308**) (204 mg, 91% yield) as a white crystalline solid.

**Melting point:** 118-120 °C, literature value: 118-119 °C

**IR $\nu_{max}$:** 3283, 1635, 1548, 1491, 1454 $cm^{-1}$

**$^{1}$H NMR (400 MHz, DMSO-$d_6$):** $\delta$ = 8.55 (t, *J*=5.9 Hz, 1H), 7.34 - 7.26 (m, 6H), 7.25 - 7.17 (m, 4H), 4.26 (d, *J*=5.9 Hz, 2H), 3.47 (s, 2H)

**$^{13}$C NMR (101 MHz, DMSO-$d_6$):** $\delta$ = 170.1, 139.4, 136.4, 129.0, 128.3, 128.2, 127.2, 126.8, 126.3, 42.3, 42.2

**LCMS (5 min high pH):** $t_R$ = 2.50 min, $[M+H^+]$ 226.2 (99.0% purity)

**HRMS:** ($C_{15}H_{16}NO$) $[M+H^+]$ requires: 226.1226, $[M+H^+]$ found: 226.1227

***N*-Benzylacrylamide**[286]

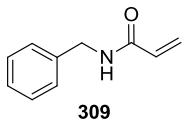

**309**

Prepared using **General method D**, by the reaction of (isocyanatomethyl)benzene and vinylmagnesium bromide.

The crude product was washed with cold heptane (3 × 2 mL) to afford the desired product (**309**) (159 mg, 99% yield) as a white crystalline solid.

**Melting point:** 60-64 °C, literature value: 58-59 °C

**IR $\nu_{max}$:** 3285, 1652, 1623, 1534, 1455, 1238 $cm^{-1}$

**$^{1}$H NMR (400 MHz, DMSO-$d_6$):** $\delta$ = 8.60 (br. s, 1H), 7.36 - 7.30 (m, 2H), 7.28 - 7.22 (m, 3H), 6.33 - 6.23 (m, 1H), 6.16 - 6.08 (m, 1H), 5.62 (dd, *J*=2.2, 10.0 Hz, 1H), 4.35 (d, *J*=5.9 Hz, 2H)

**$^{13}$C NMR (101 MHz, DMSO-$d_6$):** $\delta$ = 164.5, 139.3, 131.6, 128.3, 127.4, 126.8, 125.4, 42.1

**LCMS (5 min high pH):** $t_R$ = 1.89 min, $[M+H^+]$ 162.1 (97.3% purity)

**HRMS:** ($C_{10}H_{12}NO$) $[M+H^+]$ requires: 162.0913, $[M+H^+]$ found: 162.0909

***N*-Benzyl-2,4,6-trimethylbenzamide**

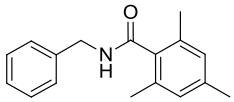

**272**

Prepared using **General method D**, by the reaction of (isocyanatomethyl)benzene and mesitylmagnesium bromide.

The crude product was purified by chromatography on silica; elution gradient 0-75% ethyl acetate in heptane. The appropriate fractions were combined and evaporated *in vacuo*, to afford the desired product (**272**) (232 mg, 92% yield) as a white crystalline solid.

**Melting point:** 135-137 °C

**IR $\nu_{max}$:** 3277, 1629, 1609, 1542, 1303, 1236 $cm^{-1}$

**$^{1}$H NMR (400 MHz, DMSO-$d_6$):** $\delta$ = 8.73 (t, *J*=6.1 Hz, 1H), 7.37 - 7.31 (m, 4H), 7.25 (app. dq, *J*=2.8, 5.9 Hz, 1H), 6.84 (s, 2H), 4.42 (d, *J*=6.1 Hz, 2H), 2.22 (s, 3H), 2.15 (s, 6H)

**$^{13}$C NMR (101 MHz, DMSO-$d_6$):** $\delta$ = 169.2, 139.6, 137.0, 135.7, 133.5, 128.2, 127.7, 127.5, 126.8, 42.3, 20.6, 18.8

**LCMS (5 min high pH):** $t_R$ = 2.85 min, $[M+H^+]$ 254.2 (98.2% purity)

**HRMS:** ($C_{17}H_{20}NO$) $[M+H^+]$ requires: 254.1539, $[M+H^+]$ found: 254.1531

***N*-Benzylcyclopropanecarboxamide**[287]

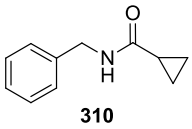

**310**

Prepared using **General method E**, by the reaction of (isocyanatomethyl)benzene with cyclopropylmagnesium bromide.

The crude product was washed with cold heptane (3 × 2 mL) to afford the desired product (**310**) (173 mg, 98% yield) as a white crystalline solid.

**Melting point:** 129-130 °C, literature value: 140-141 °C

**IR $\nu_{max}$:** 3290, 1633, 1547, 1495, 1453, 1238 $cm^{-1}$

**$^{1}$H NMR (400 MHz, DMSO-$d_6$):** δ = 8.53 (t, *J*=5.9 Hz, 1H), 7.36 - 7.29 (m, 2H), 7.27 - 7.19 (m, 3H), 4.28 (d, *J*=5.9 Hz, 2H), 1.60 (tt, *J*=4.9, 7.7 Hz, 1H), 0.74 - 0.62 (m, 4H)

**$^{13}$C NMR (101 MHz, DMSO-$d_6$):** δ = 172.5, 139.7, 128.2, 127.2, 126.7, 42.2, 13.5, 6.2

**LCMS (2 min low pH):** $t_R$ = 0.75 min, $[M+H^+]$ 176.0 (100% purity)

**HRMS:** ($C_{11}H_{14}NO$) $[M+H^+]$ requires: 176.1070, $[M+H^+]$ found: 176.1068

***N*-Benzyl-3-chlorobenzamide**[288]

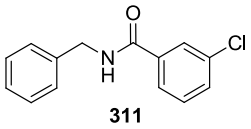


311

Prepared using **General method E**, by the reaction of (isocyanatomethyl)benzene and (3-chlorophenyl)magnesium bromide.

The crude product was purified by evaporative recrystallisation from heptane/acetone, to afford the desired product (**311**) (216 mg, 88% yield) as a pale yellow crystalline solid.

**Melting point:** 94-96 °C, literature value: 98-99 °C

**IR $\nu_{max}$:** 3283, 3062, 1633, 1536, 1316, 1296, 1236 $cm^{-1}$

**$^{1}$H NMR (400 MHz, DMSO-$d_6$):** δ = 9.16 (br. s, 1H), 7.94 (s, 1H), 7.86 (d, *J*=7.6 Hz, 1H), 7.61 (d, *J*=7.9 Hz, 1H), 7.55 - 7.49 (m, 1H), 7.32 (br. s, 4H), 7.25 (d, *J*=4.4 Hz, 1H), 4.48 (d, *J*=5.9 Hz, 2H)

**$^{13}$C NMR (101 MHz, DMSO-$d_6$):** δ = 164.7, 139.3, 136.3, 133.2, 131.1, 130.3, 128.3, 127.2, 127.0, 126.8, 126.0, 42.7

**LCMS (2 min low pH):** $t_R$ = 1.06 min, [M+H$^+$] 246.0, 248.0 (95.5% purity)

**HRMS:** ($C_{14}H_{13}[^{35}Cl]NO$) [M+H$^+$] requires: 246.0680, [M+H$^+$] found: 246.0673

***N*-Benzyl-4-((tetrahydro-2H-pyran-2-yl)oxy)benzamide**

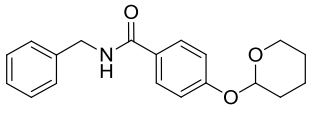

**312**

Prepared using **General method D**, by the reaction of (isocyanatomethyl)benzene and (4-((tetrahydro-2H-pyran-2-yl)oxy)phenyl)magnesium bromide.

The crude product was washed with cold heptane (3 × 2 mL) to afford the desired product (**312**) (292 mg, 94% yield) as a white crystalline solid.

**Melting point:** 115-157 °C

**IR $\nu_{max}$:** 3307, 2947, 1627, 1604, 1548, 1499, 1322, 1297, 1240, 1177 $cm^{-1}$

**$^{1}$H NMR (400 MHz, DMSO-$d_6$):** δ = 8.88 (t, *J*=5.9 Hz, 1H), 7.86 (d, *J*=8.6 Hz, 2H), 7.35 - 7.28 (m, 4H), 7.27 - 7.20 (m, 1H), 7.08 (d, *J*=8.6 Hz, 2H), 5.56 (br. s, 1H), 4.46 (d, *J*=5.9 Hz, 2H), 3.78 - 3.69 (m, 1H), 3.56 (td, *J*=3.9, 11.4 Hz, 1H), 1.92 - 1.70 (m, 3H), 1.67 - 1.49 (m, 3H)

**$^{13}$C NMR (101 MHz, DMSO-$d_6$):** δ = 165.6, 158.8, 139.8, 128.9, 128.2, 127.4, 127.1, 126.6, 115.7, 95.5, 61.5, 42.5, 29.7, 24.6, 18.4

**LCMS (2 min low pH):** $t_R$ = 1.10 min, [M+$H^+$] 312.0 (84.8% purity, 15.2% of deprotected material was observed, implying instability under LC conditions)

**HRMS:** ($C_{19}H_{22}NO_2$) [M+$H^+$] requires: 312.1594, [M+$H^+$] found: 312.1585

**3-Amino-*N*-benzylbenzamide**[289]

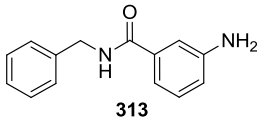

313

In round bottomed flasks, 0.5 M solutions of benzyl isocyanate (with 1 mol% $CuBr_2$) and (3-(bis(trimethylsilyl)amino)phenyl)magnesium chloride were made up in dry THF. The isocyanate solution was sonicated for 5 minutes, to ensure homogeneity as far as possible.

Using a Harvard PHD Ultra syringe pump, equipped with 20 mL Normject disposable syringes, the solutions were mixed in a T-piece, at flow rates of 5 mL $min^{-1}$ each. After a 10.6 s residence time, the reaction flow was quenched into an aqueous solution of HCl (0.5 M).

An equilibration period of 3 residence times was allowed, then samples of 1 mmol (4 mL combined flow volume) were collected into vials containing 5 mL of aqueous HCl (0.5 M) and diethylamine (~1 %vol). Ethyl acetate (10 mL) was added to each sample, and the protonated product was extracted with 0.5 M HCl (3 × 20 mL). The resulting aqueous solution was basified with saturated $K_2HCO_3$ solution (100 mL), then the desired product extracted again with ethyl acetate (3 × 20 mL). The combined organics were dried over $MgSO_4$, filtered and concentrated *in vacuo* to afford a brown oil. The crude product was triturated with cold $Et_2O$, to afford the desired product (**313**) (209 mg, 92% yield) as a pale brown solid.

**Melting point:** 79-83 °C, literature value: 83-84 °C

**IR $\nu_{max}$:** 3422, 3416, 3329, 1642, 1582, 1538, 1488, 1322 $cm^{-1}$

**$^1$H NMR (400 MHz, DMSO-$d_6$):** δ = 8.78 (t, *J*=6.0 Hz, 1H), 7.35 - 7.27 (m, 4H), 7.26 - 7.19 (m, 1H), 7.11 - 7.05 (m, 2H), 7.02 - 6.97 (m, 1H), 6.72 - 6.67 (m, 1H), 5.21 (br. s, 2H), 4.43 (d, *J*=6.0 Hz, 2H)

**$^{13}$C NMR (101 MHz, DMSO-$d_6$):** δ = 167.0, 148.7, 139.9, 135.3, 128.6, 128.2, 127.1, 126.6, 116.4, 114.3, 112.8, 42.4

**LCMS (2 min low pH):** $t_R$ = 0.63 min, [M+$H^+$] 227.1 (99.0% purity)

**HRMS:** ($C_{14}H_{15}N_2O$) [M+$H^+$] requires: 227.1179, [M+$H^+$] found: 227.1178

***N*-Benzylthiophene-2-carboxamide**[290]

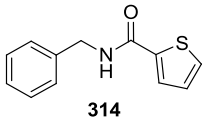

**314**

Prepared using **General method D**, by the reaction of (isocyanatomethyl)benzene and thiophen-2-ylmagnesium bromide.

The crude product was washed cold heptane (3 × 2 mL) to afford the desired product (**314**) (193 mg, 89% yield) as a light brown crystalline solid.

**Melting point:** 120-122 °C, literature value: 119 °C

**IR $\nu_{max}$:** 3350, 3091, 1619, 1541, 1422, 1301, 1247 $cm^{-1}$

**$^{1}$H NMR (400 MHz, DMSO-$d_6$):** δ = 9.03 (t, *J*=6.0 Hz, 1H), 7.80 (d, *J*=3.7 Hz, 1H), 7.76 (d, *J*=4.7 Hz, 1H), 7.37 - 7.29 (m, 4H), 7.28 - 7.21 (m, 1H), 7.15 (dd, *J*=3.7, 4.7 Hz, 1H), 4.45 (d, *J*=6.0 Hz, 2H)

**$^{13}$C NMR (101 MHz, DMSO-$d_6$):** δ = 161.1, 139.8, 139.5, 130.8, 128.3, 128.1, 127.9, 127.2, 126.8, 42.4

**LCMS (2 min low pH):** $t_R$ = 0.89 min, $[M+H^+]$ 218.0 (98.5% purity)

**HRMS:** ($C_{12}H_{12}NOS$) $[M+H^+]$ requires: 218.0634, $[M+H^+]$ found: 218.0627

***N*-Benzyl-2-methylbut-3-enamide**

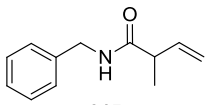

**315**

Prepared using **General method E**, by the reaction of (isocyanatomethyl)benzene and but-3-en-2-ylmagnesium chloride.

The crude product was purified by chromatography on silica; elution gradient 0-50% ethyl acetate in heptane. The appropriate fractions were combined and evaporated *in vacuo* to afford the desired product (**315**) (143 mg, 76% yield) as a colourless oil.

**IR $\nu_{max}$:** 3287, 1647, 1541, 1454, 1229 $cm^{-1}$

**$^{1}$H NMR (400 MHz, DMSO-$d_6$):** $\delta$ = 8.31 (br. s, 1H), 7.35 - 7.28 (m, 2H), 7.26 - 7.20 (m, 3H), 5.89 (ddd, *J*=7.2, 10.1, 17.2 Hz, 1H), 5.10 (td, *J*=1.5, 17.2 Hz, 1H), 5.05 - 5.00 (m, 1H), 4.32 - 4.19 (m, 2H), 3.07 (quin, *J*=7.0 Hz, 1H), 1.14 (d, *J*=7.0 Hz, 3H)

**$^{13}$C NMR (101 MHz, DMSO-$d_6$):** $\delta$ = 173.1, 139.6, 139.3, 128.2, 127.0, 126.6, 114.9, 44.0, 41.9, 17.1

**LCMS (2 min low pH):** $t_R$ = 0.86 min, $[M+H^+]$ 190.1 (100% purity)

**HRMS:** ($C_{12}H_{16}NO$) $[M+H^+]$ requires: 190.1226, $[M+H^+]$ found: 190.1222

Also isolated:

**(*E/Z*)-*N*-Benzylpent-3-enamide**

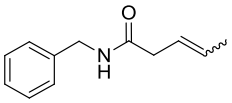

**315'**

The isomeric by-product (**315'**) (42 mg, 22% yield), as an off-white solid. This product was isolated as an inseparable mixture of *E*- and *Z*- isomers, in a ratio of roughly 1:0.6 (unknown which is the major isomer).

**Melting point:** 38-40 °C

**IR $\nu_{max}$:** 3285, 1636, 1543, 1454, 1236 $cm^{-1}$

**$^{1}$H NMR (400 MHz, DMSO-$d_6$):** $\delta$ = 8.35 - 8.23 (m, 2 × 1H), 7.35 - 7.27 (m, 4H), 7.27 - 7.19 (m, 6H), 5.60 - 5.44 (m, 4 × 1H), 4.28 - 4.22 (m, 2 × 2H), 2.95 (d, *J*=4.9 Hz, 2H), 2.86 (d, *J*=4.4 Hz, 2H), 1.64 (d, *J*=4.4 Hz, 3H), 1.60 (d, *J*=4.9 Hz, 3H)

Note: the majority of peaks in the $^{1}$H NMR overlap.

**$^{13}$C NMR (101 MHz, DMSO-$d_6$):** δ = 170.3, 170.2, 139.5, 128.2, 127.3, 127.2, 127.1, 126.7, 125.7, 125.3, 124.3, 42.02, 41.97, 34.1, 17.7, 12.8

4 signals are missing from the $^{13}$C NMR spectrum, and are assumed to be obscured by peaks from the other isomer.

**LCMS (2 min low pH):** $t_R$ = 0.86 and 0.87 min, [M+H$^+$] 190.1 (61.0% and 39.0%, 100% purity combined)

**HRMS:** ($C_{12}H_{16}NO$) [M+H$^+$] requires: 190.1226, [M+H$^+$] found: 190.1221

***N*-Benzyl-3-(1,3-dioxolan-2-yl)propanamide**

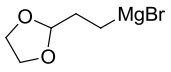


**320**

Magnesium granules (1.5 g) were stirred dry in a three-necked flask for 24 hours at 80 °C under vacuum (to remove oxide coating).

Dry THF (20 mL) was added to the solid magnesium at room temperature. 2-(2-Bromoethyl)-1,3-dioxolane (2 mL, 17 mmol) in dry THF (8 mL) was dropped in slowly, and the reaction heated briefly to 60 °C with a heat gun, in order to initiate reaction. Once the reaction had begun, the temperature maintained itself, and an ice bath was used to keep the temperature under 40 °C until the addition was complete and exotherm had ceased. The reaction was stirred at room temperature for 30 minutes, then transferred to another flask using a gas disperser as an in-line filter, then washed through with further dry THF (4 mL).

The resulting Grignard reagent (**320**) was titrated twice using **General method 1**, and was found to be of 0.49 M concentration.

***N*-Benzyl-3-(1,3-dioxolan-2-yl)propanamide**

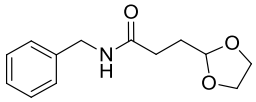

**316**

Prepared using **General method E**, by the reaction of (isocyanatomethyl)benzene, and the solution of *N*-benzyl-3-(1,3-dioxolan-2-yl)propenamide (**320**) generated in the previous experiment.

The crude product was purified by chromatography on silica; elution gradient 20-100% ethyl acetate in heptane. The appropriate fractions were combined and evaporated *in vacuo* to afford the desired product (**316**) (104 mg, 49% yield) as a white crystalline solid.

**Melting point:** 64-67 °C

**IR $\nu_{max}$:** 3302, 2942, 2890, 1634, 1531, 1455, 1207, 1148, 1028 $cm^{-1}$

**$^{1}$H NMR (400 MHz, DMSO-$d_6$):** δ = 8.33 (t, *J*=6.0 Hz, 1H), 7.34 - 7.28 (m, 2H), 7.26 - 7.20 (m, 3H), 4.80 (t, *J*=4.7 Hz, 1H), 4.25 (d, *J*=6.0 Hz, 2H), 3.91 - 3.71 (m, 4H), 2.23 (t, *J*=7.6 Hz, 2H), 1.82 (dt, *J*=4.7, 7.6 Hz, 2H)

**$^{13}$C NMR (101 MHz, DMSO-$d_6$):** δ = 171.4, 139.6, 128.2, 127.1, 126.7, 102.9, 64.3, 42.0, 29.7, 29.3

**LCMS (5 min high pH):** $t_R$ = 1.95 min, $[M+H^+]$ 236.3 (100% purity)

**HRMS:** ($C_{13}H_{18}NO_3$) $[M+H^+]$ requires: 236.1281, $[M+H^+]$ found: 236.1278

***N*-Benzylisobutyramide**[291]

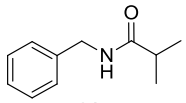

**317**

Prepared using **General method D**, by the reaction of (isocyanatomethyl)benzene and isopropylmagnesium chloride.

The crude product was purified by chromatography on silica; elution gradient 0-50% ethyl acetate in heptane. The appropriate fractions were combined and evaporated *in vacuo* to afford the desired product (**317**) (135 mg, 76% yield) as a white crystalline solid.

**Melting point:** 90-93 °C, literature value: 73-75 °C

**IR $\nu_{max}$:** 3285, 2972, 1639, 1539, 1455, 1240, 1103 $cm^{-1}$

**$^{1}$H NMR (400 MHz, DMSO-$d_6$):** δ = 8.25 (br. s, 1H), 7.36 - 7.28 (m, 2H), 7.26 - 7.18 (m, 3H), 4.25 (d, *J*=6.1 Hz, 2H), 2.42 (spt, *J*=6.8 Hz, 1H), 1.03 (d, *J*=6.8 Hz, 6H)

**$^{13}$C NMR (101 MHz, DMSO-$d_6$):** δ = 176.0, 139.8, 128.3, 127.0, 126.6, 41.8, 34.0, 19.6

**LCMS (5 min high pH):** $t_R$ = 2.13 min, $[M+H^+]$ 178.2 (100% purity)

**HRMS:** ($C_{11}H_{16}NO$) $[M+H^+]$ requires: 178.1226, $[M+H^+]$ found: 178.1224

Also isolated:

***N*-Benzylisobutyramide**

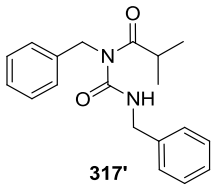


317'

The acylurea by-product (**317'**) (21 mg, 14% yield) as a colourless oil.

Note: yield calculated with respect to isocyanate

**IR $\nu_{max}$:** 3276, 2971, 1698, 1657, 1518, 1497, 1454, 1144 $cm^{-1}$

**$^{1}$H NMR (400 MHz, DMSO-$d_6$):** $\delta$ = 9.24 (br. s, 1H), 7.37 - 7.17 (m, 10H), 4.96 (s, 2H), 4.36 (d, *J*=5.9 Hz, 2H), 2.97 (spt, *J*=6.7 Hz, 1H), 0.99 (d, *J*=6.7 Hz, 6H)

**$^{13}$C NMR (101 MHz, DMSO-$d_6$):** $\delta$ = 155.2, 138.9, 138.1, 128.5, 128.3, 127.2, 127.0, 126.9, 126.4, 46.8, 43.7, 33.0, 19.6

Missing 1 × expected $^{13}$C NMR signal, assumed to be obscured by other peaks.

**LCMS (5 min high pH):** $t_R$ = 3.30 min, $[M+H^+]$ 311.3 (100% purity)

**HRMS:** ($C_{19}H_{23}N_2O_2$) $[M+H^+]$ requires: 311.1754, $[M+H^+]$ found: 311.1756

***N*-Benzyl-*N*-(benzylcarbamoyl)pivalamide**

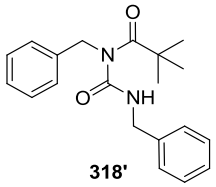


**318'**

Prepared using **General method D**, by the reaction of (isocyanatomethyl)benzene and *tert*-butylmagnesium chloride.

The crude product was purified by chromatography on silica; elution gradient 0-20% ethyl acetate in heptane. The appropriate fractions were combined and evaporated *in vacuo* to afford the by-product (**318'**) (72 mg, 44% yield) as a colourless oil. None of the desired product (**318**) could be isolated as a pure sample.

Note: yield calculated with respect to isocyanate.

**IR $\nu_{max}$:** 3393, 2965, 1685, 1646, 1508, 1503, 1451, 1349, 1205, 1179 $cm^{-1}$

**$^{1}$H NMR (400 MHz, DMSO-$d_6$):** $\delta$ = 8.71 (t, *J*=5.9 Hz, 1H), 7.33 - 7.18 (m, 8H), 7.16 - 7.11 (m, 2H), 4.76 (s, 2H), 4.24 (d, *J*=5.9 Hz, 2H), 1.21 (s, 9H)

**$^{13}$C NMR (101 MHz, DMSO-$d_6$):** $\delta$ = 180.8, 156.6, 138.6, 137.9, 128.19, 128.17, 127.3, 127.2, 126.9, 50.0, 43.8, 41.6, 28.0

Missing 1 × expected $^{13}$C NMR aromatic signal, assumed to be obscured by other peaks.

**LCMS (5 min high pH):** $t_R$ = 3.24 min, $[M+H^+]$ 325.3 (98.5% purity)

**HRMS:** ($C_{20}H_{25}N_2O_2$) $[M+H^+]$ requires: 325.1911, $[M+H^+]$ found: 325.1912

***N*-Benzyl-2,4,6-triisopropylbenzamide**

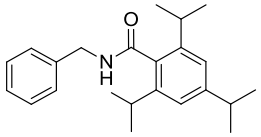

**319**

Prepared using **General method E**, by the reaction of (isocyanatomethyl)benzene and (2,4,6-triisopropylphenyl)magnesium bromide.

The crude product was washed cold heptane (3 × 2 mL) to afford the desired product (**319**) (298 mg, 88% yield) as a white crystalline solid.

**Melting point:** 189-190 °C

**IR $\nu_{max}$:** 3300, 2963, 1629, 1532, 1454, 1430, 1294 $cm^{-1}$

**$^{1}$H NMR (400 MHz, DMSO-$d_6$):** δ = 8.75 (t, *J*=6.2 Hz, 1H), 7.37 - 7.30 (m, 4H), 7.27 - 7.22 (m, 1H), 7.00 (s, 2H), 4.41 (d, *J*=6.2 Hz, 2H), 2.84 (spt, *J*=6.8 Hz, 3H), 1.18 (d, *J*=6.9 Hz, 6H), 1.17 (d, *J*=6.9 Hz, 6H), 1.10 (d, *J*=6.9 Hz, 6H)

1 × signal appears twice (2 × *i*-Pr $CH_3$), thought to be due to two separate rotamers.

**$^{13}$C NMR (101 MHz, DMSO-$d_6$):** δ = 169.3, 148.5, 144.2, 139.6, 134.5, 128.1, 127.4, 126.7, 120.2, 42.4, 33.7, 30.2, 24.3, 24.0, 23.9

1 × signal appears twice (2 × iPr $CH_3$), thought to be due to two separate rotamers.

**LCMS (2 min low pH):** $t_R$ = 1.42 min, [M+$H^+$] 338.2 (98.3% purity)

**HRMS:** ($C_{23}H_{32}NO$) [M+$H^+$] requires: 338.2478, [M+$H^+$] found: 338.2471

**5-Bromo-4-chloro-2,6-dimethoxypyrimidine**[292]

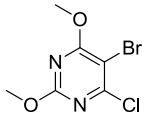

**322**

4-Chloro-2,6-dimethoxypyrimidine (1.75 g, 10 mmol) was dissolved in methanol (15 mL), then water (15 mL) and sodium bicarbonate (0.7 g, 8.33 mmol) were added. Bromine (0.9 mL, 17.47 mmol) was added dropwise (*via* dropping funnel) over 1 hour, to the resulting white suspension, maintaining good stirring. After 30 minutes of bromine addition, further sodium bicarbonate (0.7 g, 8.33 mmol) was added, and bromine addition continued. Once all of the bromine had been added, the yellow suspension was stirred for a further 30 minutes. Sodium thiosulfate (saturated aq. solution, 25 mL) was added slowly and the resulting white slurry was filtered, and the solids washed with water (3 × 20 mL). The sticky white solid was dried *in vacuo* to afford the desired brominated heterocycle (**322**) (2.49 g, 98 % yield) as a free flowing white solid.

**Melting point:** 98-99 °C, literature value: 97-98 °C

**IR $\nu_{max}$:** 1540, 1451, 1352, 1325, 1201, 1111, 1033 $cm^{-1}$

**$^{1}$H NMR (400 MHz, DMSO-d$_6$):** $\delta$ = 4.00 (s, 3H), 3.92 (s, 3H)

**$^{13}$C NMR (101 MHz, DMSO-d$_6$):** $\delta$ = 167.9, 162.5, 159.2, 96.3, 55.9, 55.5

**LCMS (2 min low pH):** $t_R$ = 1.10 min, [($^{81}$Br, $^{35}$Cl)M+H$^+$] 254.9 (99.1% purity)

**HRMS:** ($C_6H_7$[$^{79}$Br][$^{35}$Cl]$N_2O_2$) [M+H$^+$] requires: 252.9374, [M+H$^+$] found: 252.9376

***N*-Benzyl-4-chloro-2,6-dimethoxypyrimidine-5-carboxamide**

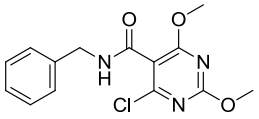

**324**

In a round bottomed flask, a 0.25 M solution of benzyl isocyanate (with 1 mol% $CuBr_2$) was made up in dry THF. The isocyanate solution was sonicated for 5 minutes, to ensure homogeneity as far as possible.

In a separate oven-dried and septum sealed volumetric flask, 5-bromo-4-chloro-2,6-dimethoxypyrimidine (700 mg, 2.76 mmol) was dissolved in dry THF, to a volume of 5 mL. This was transferred by syringe to an inert round bottomed flask, where further dry THF (2.9 mL) was added, in order to make up the correct final concentration. iPrMgCl.LiCl solution (0.93 M, 3.1 mL, 2.88 mmol) was added dropwise, and the resulting grey suspension stirred for 30 minutes. The Grignard exchange was observed to have completed by HPLC, resulting in a 0.25 M solution of the desired Grignard reagent.

Using a Harvard PHD Ultra syringe pump, equipped with 20 mL Normject disposable syringes, the solutions were mixed in a T-piece, at flow rates of 5 mL $min^{-1}$ each. After a 10.6 s residence time, the reaction flow was quenched into dilute ammonium chloride solution.

An equilibration period of 3 residence times was allowed, then a sample of 1 mmol (8 mL combined flow volume) were collected into vials containing 10 mL of dilute ammonium chloride solution and diethylamine (~1 %vol). Ethyl acetate (10 mL) was added to each sample, alongside water (10 mL) and saturated brine (10 mL), and the layers separated. The aqueous layer was extracted with further ethyl acetate (25 mL). The combined organics were dried over $MgSO_4$ and evaporated *in vacuo*. The crude product was purified by chromatography on silica; elution gradient 0-80% ethyl acetate in heptane. The appropriate fractions were combined and evaporated *in vacuo* to afford the desired product (**324**) (135 mg, 44% yield) as a white crystalline solid.

**Melting point:** 112-117°C

**IR $\nu_{max}$:** 3262, 1638, 1591, 1545, 1465, 1377, 1354, 1204, 1028 $cm^{-1}$

**$^1$H NMR (400 MHz, DMSO-d$_6$):** δ = 8.96 (t, *J*=6.0 Hz, 1H), 7.38 - 7.33 (m, 4H), 7.30 - 7.23 (m, 1H), 4.44 (d, *J*=6.0 Hz, 2H), 3.97 (s, 3H), 3.94 (s, 3H)

**$^{13}$C NMR (101 MHz, DMSO-d$_6$):** δ = 168.6, 163.1, 161.6, 156.8, 138.7, 128.3, 127.1, 126.9, 111.8, 55.3, 55.0, 42.3

**LCMS (2 min low pH):** $t_R$ = 0.90 min, [($^{35}$Cl)M+H$^+$] 307.9 (97.1% purity)

**HRMS:** ($C_{14}H_{15}[^{35}Cl]N_3O_3$) [M+H$^+$] requires: 308.0797, [M+H$^+$] found: 308.0798

Also isolated:

***N*-Benzyl-4-chloro-2,6-dimethoxypyrimidine-5-carboxamide**[293]

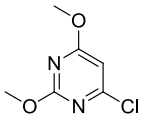

**321**

The quenched Grignard reagent (**321**) (14 mg, 8% yield) as a pale yellow crystalline solid.

**Melting point:** 68-71 °C, literature value: 73-74 °C

**IR $\nu_{max}$:** 1558, 1468, 1398, 1370, 1350, 1242 cm$^{-1}$

**$^1$H NMR (400 MHz, DMSO-$d_6$):** δ = 6.76 (s, 1H), 3.92 (s, 3H), 3.91 (s, 3H)

**$^{13}$C NMR (101 MHz, DMSO-$d_6$):** δ = 172.0, 164.4, 160.4, 100.4, 55.1, 54.6

**LCMS (2 min low pH):** $t_R$ = 0.90 min, [($^{35}$Cl)M+H$^+$] 174.9 (96.8% purity)

**HRMS:** ($C_6H_8[^{35}Cl]N_2O_2$) [M+H$^+$] requires: 175.0269, [M+H$^+$] found: 175.0263

Also isolated:

***N*-Benzyl-4-chloro-2,6-dimethoxypyrimidine-5-carboxamide**

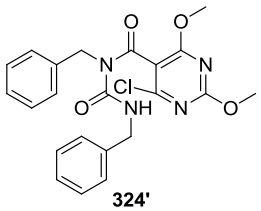

**324'**

The acylurea by-product (**324'**) (54 mg, 25% yield) was observed as a white crystalline solid.

Note: yield calculated with respect to isocyanate.

**Melting point:** 97-99 °C

**IR $\nu_{max}$:** 3300, 1701, 1651, 1587, 1521, 1492, 1365, 1214, 1032 cm$^{-1}$

**$^1$H NMR (400 MHz, $CDCl_3$):** δ = 9.52 (br. s, 1H), 7.41 - 7.31 (m, 5H), 7.25 - 7.20 (m, 3H), 7.00 - 6.94 (m, 2H), 5.25 (d, *J*=16.1 Hz, 1H), 4.63 (d, *J*=5.5 Hz, 2H), 4.58 (d, *J*=16.1 Hz, 1H), 4.02 (s, 3H), 3.64 (s, 3H)

**$^{13}$C NMR (101 MHz, $CDCl_3$):** δ = 168.2, 168.1, 164.22, 157.0, 154.6, 137.9, 137.0, 128.8, 128.4, 127.7, 127.54, 127.49, 127.1, 111.2, 55.8, 55.0, 48.9, 45.0

**LCMS (2 min low pH):** $t_R$ = 1.28 min, [($^{35}$Cl)M+H$^+$] 441.1 (98.3% purity)

**HRMS:** ($C_{22}H_{22}[^{35}Cl]N_4O_4$) [M+H$^+$] requires: 441.1324, [M+H$^+$] found: 441.1322

***N*-Benzyl-4-chloro-2,6-dimethoxypyrimidine-5-carboxamide**

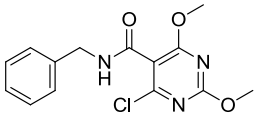

**324**

In a round bottomed flask, a 0.5 M solution of benzyl isocyanate (with 1 mol% $CuBr_2$) was made up in dry THF. The isocyanate solution was sonicated for 5 minutes, to ensure homogeneity as far as possible.

In a separate oven-dried and septum sealed volumetric flask, 5-bromo-4-chloro-2,6-dimethoxypyrimidine (875 mg, 3.45 mmol) was dissolved in dry THF, to a volume of 5 mL. This was transferred by syringe to an inerted round bottomed flask, where further dry THF (1.9 mL) was added, in order to make up the correct final concentration. iPrMgCl solution (1.89 M in THF, 1.9 mL, 3.59 mmol) was added dropwise, and the resulting grey suspension stirred for 30 minutes. The Grignard exchange was observed to have gone to completion by HPLC, resulting in a 0.5 M solution of the desired Grignard reagent.

Using a Harvard PHD Ultra syringe pump, equipped with 20 mL Normject disposable syringes, the solutions were mixed in a T-piece, at flow rates of 5 mL $min^{-1}$ each. After a 10.6 s residence time, the reaction flow was quenched into dilute ammonium chloride solution.

An equilibration period of 3 residence times was allowed, then two samples of 1 mmol (4 mL combined flow volume) were collected into vials containing 10 mL of dilute ammonium chloride solution and diethylamine (~1 %vol). Ethyl acetate (5 mL) was added to each sample, and the organic layer was sampled for HPLC analysis, which revealed a poorer profile than the previous reaction, so the samples were not worked up.

***N*-Benzyl-3-phenylpropanamide**

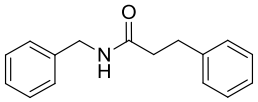

**270**

In round bottomed flasks, 0.5 M solutions of (isocyanatomethyl)benzene (with 1 mol% $CuBr_2$) and phenethylmagnesium chloride were made up in dry THF. The isocyanate solution was sonicated for 5 minutes, to ensure homogeneity as far as possible.

Using a Harvard PHD Ultra syringe pump, equipped with 2 × 60 mL Normject disposable syringes, the solutions were mixed in a T-piece, at flow rates of 5 mL $min^{-1}$ each. After a 10.6 s residence time, the reaction flow was quenched into dilute ammonium chloride solution (225 mL).

The entire volume of the two syringes was collected, then ethyl acetate (100 mL) and saturated brine (50 mL) were added. The layers were separated and the organics extracted with further ethyl acetate (100 mL). The combined organics were dried over $MgSO_4$, filtered, and solvent removed *in vacuo*. The crude solid was washed with cold heptane (3 × 25 mL) to afford the desired product (**270**) (6.64 g, 95% yield) as a white crystalline solid.

Note: the 1.77 mL reactor "dead volume" was subtracted from the total processed volume, in order to calculate the yield.

**LCMS (2 min low pH):** $t_R$ = 1.04 min, $[M+H^+]$ 240.1 (96.1% purity)

Full characterisation can be found above, on page 234.

### 4.3.10. QCL-IR experiments

**Flow setup**

In oven-dried round bottomed flasks, solutions of (isocyanatomethyl)benzene (with $CuBr_2$) and phenethylmagnesium chloride were made up in dry THF. The isocyanate solution was sonicated for 5 minutes, to ensure homogeneity as far as possible.

Using a precision syringe pump (Pump 11 Elite, Harvard Apparatus) equipped with 2 × 10 mL Normject disposable syringes, the solutions were introduced to a microfluidic device *via* two inlets. The syringe pump was calibrated to deliver flow rates of 0.5 mL $min^{-1}$, resulting in a combined flow rate of 1 mL $min^{-1}$.

**QCL based mid-IR Imaging**

QCL based mid-IR imaging was performed in transmission mode using a Spero (Daylight Solutions Inc., CA, US) microscope that was equipped with four individual QCLs, facilitating continuous coverage of the 900−1800 $cm^{-1}$ wavenumber range with four wavenumbers spectral and a 4.25 × 4.25 $\mu m^2$ lateral pixel size within a 2 × 2 $mm^2$ field of view, using a 4.0 × (0.15 NA) magnification IR objective, coupled with a 480 × 480 bolometer detector. A laser calibration curve was collected through an 8 mm thick $CaF_2$ window material (supplied by Crystan Ltd., UK) in order to normalise laser intensity across the aforementioned mid-IR collection range for all intensities.

A new laser calibration curve was collected before each of the experiments reported, in order to minimize the effect of laser drift. After the laser calibration, hyperspectral images were collected in transmission mode and the solvent subtracted, using a pre-collected solvent background spectrum. The obtained spectral images were analysed using a toolkit developed in MatLab (R2016a). Within this toolkit, the absorption was averaged within 9 × 9 pixel squares along the reaction pathway, to give a single absorption value at each residence time, as per the example below (**Figure 33**)

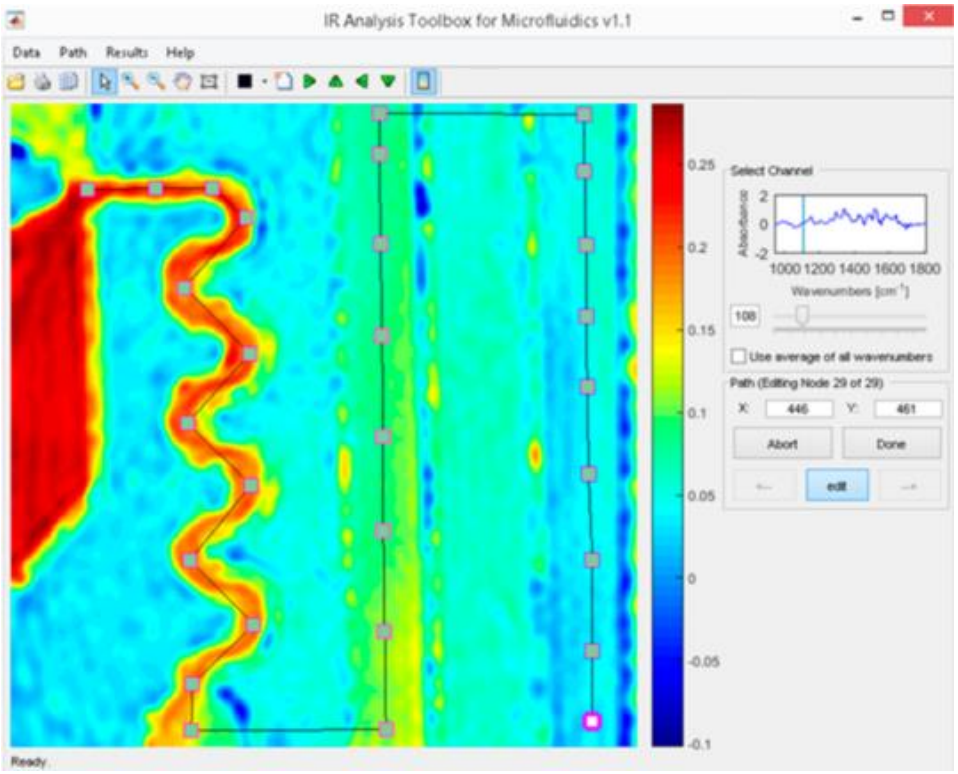


**Figure 33** - Depiction of the MatLab toolkit used to obtain absorption data along the QCL-IR reaction pathway.

Further analysis of data was carried out using Microsoft Excel 2016, with additional manipulation attempted using DynoChem v4.1.0.0, published by Scale-Up Systems (www.scale-up.com).

**Concentration calibration**

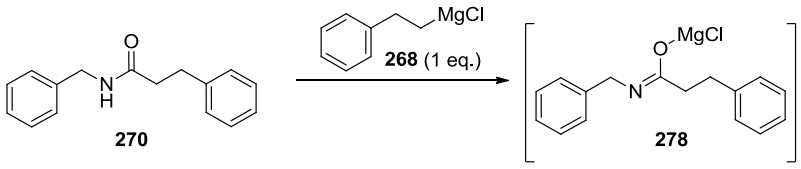


In oven-dried round bottomed flasks, equimolar solutions of and *N*-benzyl-3-phenylpropanamide and phenethylmagnesium chloride were made up in dry THF.

Using a precision syringe pump (Pump 11 Elite, Harvard Apparatus) equipped with 2 × 10 mL Normject disposable syringes, the solutions were introduced to a microfluidic device *via* two inlets. The syringe pump was calibrated to deliver flow rates of 0.5 mL $min^{-1}$, resulting in a combined flow rate of 1 mL $min^{-1}$.

Quantitative deprotonation was observed to occur within the mixing section of the microfluidic device. The IR response at 1572 $cm^{-1}$ was taken in six distinct areas (45 × 75 pixels each) towards the end of the channel, for each concentration. The average response was taken from these, and plotted.

The following concentrations were examined, giving the responses indicated:

| Concentration (M) | Area 1 | Area 2 | Area 3 | Area 4 | Area 5 | Area 6 | Average | Standard deviation |
|---|---|---|---|---|---|---|---|---|
| **0** | 0.0029 | 0.0036 | 0.0022 | 0.0029 | 0.0002 | 0.0011 | 0.0022 | 0.0013 |
| **0.05** | 0.2422 | 0.2408 | 0.2713 | 0.2752 | 0.2959 | 0.2904 | 0.2693 | 0.0234 |
| **0.1** | 0.5350 | 0.5215 | 0.6003 | 0.6070 | 0.6652 | 0.6392 | 0.5947 | 0.0567 |
| **0.15** | 0.8318 | 0.7968 | 0.9214 | 0.8981 | 0.9883 | 0.9346 | 0.8952 | 0.0702 |
| **0.2** | 1.0585 | 0.9922 | 1.1500 | 1.0993 | 1.2186 | 1.3907 | 1.1516 | 0.1403 |
| **0.25** | 1.2937 | 1.1925 | 1.3853 | 1.3359 | 1.5062 | 1.3924 | 1.3510 | 0.1055 |
| **0.3** | 1.5260 | 1.3864 | 1.5657 | 1.4988 | 1.6755 | 1.5622 | 1.5358 | 0.0947 |

These values were plotted to form **Figure 29** in the main text, where the error bars represent the range of values for each concentration, found across the six areas examined.

***N*-Benzyl-3-phenylpropanamide**

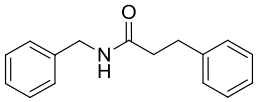

**270**

In oven-dried round bottomed flasks, an ***X*** M solution of (isocyanatomethyl)benzene (with ***Z*** M $CuBr_2$) and a ***Y*** M phenethylmagnesium chloride were made up in dry THF. The isocyanate solution was sonicated for 5 minutes, to ensure homogeneity as far as possible.

Both solutions were taken up into 10 mL disposable syringes, and pumped through the microfluidic device at 0.5 mL $min^{-1}$ per stream. The resulting metalated intermediate (**278**) concentrations were observed by QCL-IR, using the calibration value previously calculated (**Figure 29**).

Scenarios 1, 2 and 5 were used to make up the graph used within the main text (**Figure 30**).

| **Scenario number** | **Concentration (266), *X* (M)** | **Concentration (268), *Y* (M)** | **Concentration $CuBr_2$, *Z* (M)** |
|---|---|---|---|
| **1** | 0.25 | 0.375 | 0.0025 |
| **2** | 0.25 | 0.375 | 0.0075 |
| **3** | 0.2 | 0.375 | 0.0025 |
| **4** | 0.25 | 0.25 | 0.0025 |
| **5** | 0.25 | 0.25 | 0 |

| Calculated residence time (ms) | Calculated yield of metalated intermediate (278) for each scenario (%) | | | | |
|---|---|---|---|---|---|
| | 1 | 2 | 3 | 4 | 5 |
| 0 | 2.69 | 1.55 | 2.42 | 5.07 | 3.85 |
| 0.19 | 3.75 | 4.39 | 3.94 | 4.66 | 2.42 |
| 0.36 | 6.12 | 7.57 | 5.79 | 5.44 | 2.47 |
| 0.54 | 5.70 | 8.16 | 5.17 | 5.03 | 1.39 |
| 0.70 | 6.84 | 12.83 | 5.92 | 7.59 | 3.57 |
| 0.89 | 7.46 | 9.75 | 6.02 | 4.19 | 0.00 |
| 1.06 | 8.84 | 14.18 | 7.41 | 8.00 | 2.95 |
| 1.22 | 11.35 | 18.94 | 11.27 | 7.12 | 1.46 |
| 1.31 | 14.05 | 18.79 | 15.36 | 8.67 | 2.29 |
| 4.01 | 18.89 | 37.35 | 21.37 | 16.78 | 4.46 |
| 4.47 | 20.54 | 41.84 | 23.37 | 18.04 | 4.36 |
| 4.94 | 21.93 | 47.83 | 25.02 | 20.82 | 6.03 |
| 5.44 | 22.50 | 47.48 | 25.80 | 19.71 | 3.07 |
| 5.78 | 24.56 | 50.38 | 28.74 | 21.02 | 3.22 |
| 6.12 | 28.07 | 53.16 | 33.32 | 22.87 | 4.65 |
| 6.46 | 30.53 | 55.40 | 36.43 | 24.77 | 6.68 |
| 6.77 | 32.20 | 60.01 | 38.67 | 28.21 | 9.97 |
| 7.22 | 34.83 | 60.95 | 42.56 | 28.36 | 7.92 |
| 7.49 | 38.40 | 60.33 | 47.98 | 27.97 | 7.73 |
| 10.55 | 41.08 | 65.28 | 51.87 | 33.55 | 8.16 |
| 10.79 | 41.15 | 64.75 | 51.88 | 34.37 | 8.76 |
| 11.03 | 42.51 | 63.87 | 53.36 | 34.21 | 8.48 |
| 11.31 | 45.41 | 63.67 | 56.95 | 35.66 | 7.24 |
| 11.61 | 49.12 | 69.10 | 61.75 | 40.17 | 10.27 |
| 11.97 | 51.37 | 71.79 | 64.56 | 42.14 | 13.10 |
| 12.33 | 51.82 | 73.56 | 64.89 | 43.64 | 14.90 |
| 12.63 | 50.42 | 73.78 | 62.97 | 44.64 | 14.75 |
| 12.81 | 49.93 | 72.02 | 62.24 | 45.06 | 13.83 |
| 13.02 | 50.19 | 67.98 | 62.49 | 43.20 | 11.74 |
| 13.39 | 51.41 | 67.81 | 64.03 | 44.91 | 14.71 |
| 13.58 | 51.93 | 69.14 | 64.50 | 46.34 | 14.15 |
| 13.83 | 51.59 | 68.76 | 63.98 | 45.73 | 14.31 |
| 14.05 | 51.57 | 68.01 | 63.05 | 47.64 | 15.58 |

## References


1. S. D. Roughley, A. M. Jordan, *J. Med. Chem.* **2011**, *54*, 3451–3479.
2. A. El-Faham, F. Albericio, *Chem. Rev.* **2011**, *111*, 6557–6602.
3. I. Mohammed, I. R. Kummetha, G. Singh, N. Sharova, G. Lichinchi, J. Dang, M. Stevenson, T. M. Rana, *J. Med. Chem.* **2016**, *59*, 7677–7682.
4. A. Greenberg, *The Amide Linkage: Structural Significance in Chemistry, Biochemistry, and Materials Science*, John Wiley & Sons, Hoboken, NJ, USA, **2003**.
5. D. J. C. Constable, P. J. Dunn, J. D. Hayler, G. R. Humphrey, J. L. Leazer, Jr., R. J. Linderman, K. Lorenz, J. Manley, B. A. Pearlman, A. Wells, A. Zaks, T. Y. Zhang, *Green Chem.* **2007**, *9*, 411–420.
6. K. D. Wehrstedt, P. A. Wandrey, D. Heitkamp, *J. Hazard. Mater.* **2005**, *126*, 1–7.
7. E. Valeur, M. Bradley, *Chem. Soc. Rev.* **2009**, *38*, 606.
8. R. M. de Figueiredo, J.-S. Suppo, J.-M. Campagne, *Chem. Rev.* **2016**, *116*, 12029–12122.
9. H. Charville, D. Jackson, G. Hodges, A. Whiting, *Chem. Commun.* **2010**, *46*, 1813–23.
10. K. Arnold, A. S. Batsanov, B. Davies, A. Whiting, *Green Chem.* **2008**, *10*, 124–134.
11. K. Ishihara, S. Ohara, H. Yamamoto, *J. Org. Chem.* **1996**, *61*, 4196–4197.
12. N. Gernigon, R. M. Al-Zoubi, D. G. Hall, *J. Org. Chem.* **2012**, *77*, 8386–8400.
13. S. Fatemi, N. Gernigon, D. G. Hall, *Green Chem.* **2015**, *17*, 4016–4028.
14. H. Noda, M. Furutachi, Y. Asada, M. Shibasaki, N. Kumagai, *Nat. Chem.* **2017**, *9*, 571–577.
15. Z. Liu, H. Noda, M. Shibasaki, N. Kumagai, *Org. Lett.* **2018**, *20*, 612–615.
16. J. S. Carey, D. Laffan, C. Thomson, M. T. Williams, *Org. Biomol. Chem.* **2006**, *4*, 2337–2347.
17. C. Gunanathan, Y. Ben-David, D. Milstein, *Science* **2007**, *317*, 790–2.
18. C. Song, S. Qu, Y. Tao, Y. Dang, Z. Wang, *ACS Catal.* **2014**, *4*, 2854–2865.
19. F. Hasanayn, H. Harb, *Inorg. Chem.* **2014**, *53*, 8334–8349.
20. L. U. Nordstrøm, H. Vogt, R. Madsen, *J. Am. Chem. Soc.* **2008**, *130*, 17672–17673.
21. E. Sindhuja, R. Ramesh, S. Balaji, Y. Liu, *Organometallics* **2014**, *33*, 4269–4278.
22. A. J. A. Watson, R. J. Wakeham, A. C. Maxwell, J. M. J. Williams, *Tetrahedron* **2014**, *70*, 3683–3690.
23. Y. Zhang, C. Chen, S. C. Ghosh, Y. Li, S. H. Hong, *Organometallics* **2010**, *29*, 1374–

1378.

24. Q. Han, X. Xiong, S. Li, *Catal. Commun.* **2015**, *58*, 85–88.
25. B. Kang, Z. Fu, S. Hong, *J. Am. Chem. Soc.* **2013**, *135*, 11704–11707.
26. R. J. Griffiths, G. A. Burley, E. P. A. Talbot, *Org. Lett.* **2017**, *19*, 870–873.
27. X. Yan, K. Fang, H. Liu, C. Xi, *Chem. Commun.* **2013**, *49*, 10650.
28. J. R. Khusnutdinova, Y. Ben-David, D. Milstein, *J. Am. Chem. Soc.* **2014**, *136*, 2998–3001.
29. A. Brennführer, H. Neumann, M. Beller, *Angew. Chem. Int. Ed.* **2009**, *48*, 4114–4133.
30. C. F. J. Barnard, *Organometallics* **2008**, *27*, 5402–5422.
31. R. Jana, T. P. Pathak, M. S. Sigman, *Chem. Rev.* **2011**, *111*, 1417–1492.
32. S. D. Friis, T. Skrydstrup, S. L. Buchwald, *Org. Lett.* **2014**, *16*, 4269–4299.
33. D. Seebach, *Angew. Chem. Int. Ed.* **1979**, *18*, 239–336.
34. Y. Wiesel, R. Suchi, M. Michman, S. Patai, *Tetrahedron Lett.* **1973**, *14*, 3907–3910.
35. A. Latorre, S. Rodríguez, J. Izquierdo, F. V. González, *Tetrahedron Lett.* **2009**, *50*, 2653–2655.
36. A. Nagaki, Y. Takahashi, J. Yoshida, *Angew. Chem. Int. Ed.* **2016**, *55*, 5327–5331.
37. M. A. Ganiek, M. R. Becker, G. Berionni, H. Zipse, P. Knochel, *Chem. Eur. J.* **2017**, *23*, 10280–20284.
38. C. Chatgilialoglu, D. Crich, M. Komatsu, I. Ryu, *Chem. Rev.* **1999**, *99*, 1991–2070.
39. R. S. Grainger, P. Innocenti, *Heteroat. Chem.* **2007**, *18*, 568–571.
40. J. C. Walton, *Acc. Chem. Res.* **2014**, *47*, 1406–1416.
41. M. T. Reetz, *J. Am. Chem. Soc.* **2013**, *135*, 12480–12496.
42. M. Yan, Y. Kawamata, P. S. Baran, *Chem. Rev.* **2017**, *117*, 13230–13319.
43. M. H. Shaw, J. Twilton, D. W. C. MacMillan, *J. Org. Chem.* **2016**, *81*, 6898–6926.
44. M. B. Plutschack, B. Pieber, K. Gilmore, P. H. Seeberger, *Chem. Rev.* **2017**, *117*, 11796–11893.
45. N. Hoffmann, *Chem. Rev.* **2008**, *108*, 1052–1103.
46. F. Lovering, J. Bikker, C. Humblet, *J. Med. Chem.* **2009**, *52*, 6752–6756.
47. P. J. Koovits, J. P. Knowles, K. I. Booker-Milburn, *Org. Lett.* **2016**, *18*, 5608–5611.
48. L. D. Elliott, M. Berry, B. Harji, D. Klauber, J. Leonard, K. I. Booker-Milburn, *Org. Process Res. Dev.* **2016**, *20*, 1806–1811.
49. T. P. Yoon, M. A. Ischay, J. Du, *Nat. Chem.* **2010**, *2*, 527–532.
50. Y. Xi, H. Yi, A. Lei, *Org. Biomol. Chem.* **2013**, *11*, 2387–2403.

51. B. Quiclet-Sire, S. Z. Zard, *Pure Appl. Chem.* **2011**, *83*, 519–551.
52. E. L. Tyson, Z. L. Niemeyer, T. P. Yoon, *J. Org. Chem.* **2014**, *79*, 1427–1436.
53. M. N. Hopkinson, B. Sahoo, J.-L. Li, F. Glorius, *Chem. Eur. J.* **2014**, *20*, 3874–3886.
54. I. Ghosh, T. Ghosh, J. I. Bardagi, B. König, *Science* **2014**, *346*, 725–728.
55. I. Ghosh, B. König, *Angew. Chem. Int. Ed.* **2016**, *55*, 7676–7679.
56. L. Marzo, I. Ghosh, F. Esteban, B. König, *ACS Catal.* **2016**, *6*, 6780–6784.
57. N. A. Romero, D. A. Nicewicz, *Chem. Rev.* **2016**, *116*, 10075–10166.
58. C. K. Prier, D. A. Rankic, D. W. C. Macmillan, *Chem. Rev.* **2013**, *113*, 5322–5363.
59. C. B. Larsen, O. S. Wenger, *Chem. Eur. J.* **2018**, *24*, 2039–2058.
60. H. G. Roth, N. A. Romero, D. A. Nicewicz, *Synlett* **2016**, *27*, 714–723.
61. A. Joshi-Pangu, F. Lévesque, H. G. Roth, S. F. Oliver, L. C. Campeau, D. Nicewicz, D. A. DiRocco, *J. Org. Chem.* **2016**, *81*, 7244–7249.
62. D. M. Arias-Rotondo, J. K. McCusker, *Chem. Soc. Rev.* **2016**, *45*, 5803–5820.
63. K. Jähnisch, V. Hessel, H. Löwe, M. Baerns, *Angew. Chem. Int. Ed.* **2004**, *43*, 406–446.
64. Y. Mo, K. F. Jensen, *React. Chem. Eng.* **2016**, *1*, 501–507.
65. J. Britton, T. F. Jamison, *Nat. Protoc.* **2017**, *12*, 2423–2446.
66. C. F. Carter, H. Lange, S. V Ley, I. R. Baxendale, B. Wittkamp, J. G. Goode, N. L. Gaunt, *Org. Process Res. Dev.* **2010**, *14*, 393–404.
67. J. M. Reckamp, A. Bindels, S. Duffield, Y. C. Liu, E. Bradford, E. Ricci, F. Susanne, A. Rutter, *Org. Process Res. Dev.* **2017**, *21*, 816–820.
68. A. Nagaki, K. Imai, S. Ishiuchi, J. Yoshida, *Angew. Chem. Int. Ed.* **2015**, *54*, 1914–1918.
69. A. Hafner, P. Filipponi, L. Piccioni, M. Meisenbach, B. Schenkel, F. Venturoni, J. Sedelmeier, *Org. Process Res. Dev.* **2016**, *20*, 1833–1837.
70. B. Gutmann, D. Cantillo, C. O. Kappe, *Angew. Chem. Int. Ed.* **2015**, *54*, 6688–6728.
71. L. Benati, G. Bencivenni, R. Leardini, M. Minozzi, D. Nanni, R. Scialpi, P. Spagnolo, G. Zanardi, *J. Org. Chem.* **2006**, *71*, 3192–3197.
72. S. Fujiwara, Y. Shimizu, T. Shin-ike, N. Kambe, *Org. Lett.* **2001**, *3*, 2085–2088.
73. J. H. Rigby, D. M. Danca, J. H. Homer, *Tetrahedron Lett.* **1998**, *39*, 8413–8416.
74. F. Minisci, *Tetrahedron Lett.* **1971**, 59–62.
75. F. Minisci, *Synthesis* **1973**, *1*, 1–24.
76. D. T. Sawyer, A. Sobkowiak, T. Matsushita, *Acc. Chem. Res.* **1996**, *29*, 409–416.
77. A. Agosti, G. Bertolini, G. Bruno, C. Lautz, T. Glarner, W. Deichtmann, *Org. Process Res. Dev.* **2017**, *21*, 451–459.

78. D. Elad, J. Rokach, *J. Org. Chem.* **1964**, *29*, 1855–1859.
79. P. Wender, S. K. Singh, *Tetrahedron Lett.* **1990**, *31*, 2517–2520.
80. E. M. Scanlan, J. C. Walton, *Chem. Commun.* **2002**, 2086–2087.
81. E. M. Scanlan, A. M. Z. Slawin, J. C. Walton, *Org. Biomol. Chem.* **2004**, *2*, 716–724.
82. G. A. DiLabio, E. M. Scanlan, J. C. Walton, *Org. Lett.* **2005**, *7*, 155–158.
83. G. López-Valdez, S. Olguín-Uribe, L. D. Miranda, *Tetrahedron Lett.* **2007**, *48*, 8285–8289.
84. R. S. Grainger, P. Innocenti, *Angew. Chem. Int. Ed.* **2004**, *43*, 3445–3448.
85. G. López-Valdez, S. Olguín-Uribe, A. Millan-Ortíz, R. Gamez-Montaño, L. D. Miranda, *Tetrahedron* **2011**, *67*, 2693–2701.
86. A. Millan-Ortiz, G. Lopez-Valdez, F. Cortez-Guzman, L. D. Miranda, *Chem. Commun.* **2015**, *51*, 8345–8348.
87. N. Rodríguez, L. J. Goossen, *Chem. Soc. Rev.* **2011**, *40*, 5030–5048.
88. J. Cornella, I. Larrosa, *Synthesis* **2012**, *44*, 653–676.
89. A. J. J. Straathof, *Chem. Rev.* **2014**, *114*, 1871–1908.
90. P. Gallezot, *Chem. Soc. Rev.* **2012**, *41*, 1538–1558.
91. F. Minisci, A. Cetterio, C. Giordano, *Acc. Chem. Res.* **1983**, *16*, 27–32.
92. Z. Duan, S. Ranjit, P. Zhang, X. Liu, *Chem. Eur. J.* **2009**, *15*, 3666–3669.
93. S. Ranjit, Z. Duan, P. Zhang, X. Liu, *Org. Lett.* **2010**, *12*, 4134–4136.
94. W. Jia, N. Jiao, *Org. Lett.* **2010**, *12*, 2000–2003.
95. Y. Zhu, X. Li, X. Wang, X. Huang, T. Shen, Y. Zhang, X. Sun, M. Zou, S. Song, N. Jiao, *Org. Lett.* **2015**, *17*, 4702–4705.
96. Z. Wang, L. Zhu, F. Yin, Z. Su, Z. Li, C. Li, *J. Am. Chem. Soc.* **2012**, *134*, 4258–4263.
97. X. Liu, Z. Wang, X. Cheng, C. Li, *J. Am. Chem. Soc.* **2012**, *134*, 14330–14333.
98. J. M. Neely, T. Rovis, *J. Am. Chem. Soc.* **2014**, *136*, 2735–2738.
99. F. Fontana, F. Minisci, M. C. N. Barbosa, E. Vismara, *J. Org. Chem.* **1991**, *56*, 2866–2869.
100. J. Miao, H. Ge, *Synlett* **2014**, *25*, 911–919.
101. M. Li, C. Wang, H. Ge, *Org. Lett.* **2011**, *13*, 2062–2064.
102. P. Y. Lee, P. Liang, W. Y. Yu, *Org. Lett.* **2017**, *19*, 2082–2085.
103. M. Li, C. Wang, P. Fang, H. Ge, *Chem. Commun.* **2011**, *47*, 6587–9.
104. M. Reckenthäler, A. G. Griesbeck, *Adv. Synth. Catal.* **2013**, *355*, 2727–2744.
105. Y. Jin, H. Fu, *Asian J. Org. Chem.* **2017**, 368–385.

106. K. Okada, K. Okamoto, M. Oda, *J. Am. Chem. Soc.* **1988**, *110*, 8736–8738.
107. K. Okada, K. Okamoto, N. Morita, K. Okubo, M. Oda, *J. Am. Chem. Soc.* **1991**, *113*, 9401–9402.
108. W. Cheng, R. Shang, M. Fu, Y. Fu, *Chem. Eur. J.* **2017**, *23*, 2537–2541.
109. J. Schwarz, B. König, *Green Chem.* **2016**, *18*, 4743–4749.
110. G. L. Lackner, K. W. Quasdorf, G. Pratsch, L. E. Overman, *J. Org. Chem.* **2015**, *80*, 6012–6024.
111. G. L. Lackner, K. W. Quasdorf, L. E. Overman, *J. Am. Chem. Soc.* **2013**, *135*, 15342–15345.
112. Y. Slutskyy, L. E. Overman, *Org. Lett.* **2016**, *18*, 2564–2567.
113. K. Xu, Z. Tan, H. Zhang, J. Liu, S. Zhang, Z. Wang, *Chem. Commun.* **2017**, *53*, 10719–10722.
114. S. Z. Zard, *Chem. Soc. Rev.* **2008**, *37*, 1603–1618.
115. S. Hammes-Schiffer, A. A. Stuchebrukhov, *Chem. Rev.* **2010**, *110*, 6939–6960.
116. D. R. Weinberg, C. J. Gagliardi, J. F. Hull, C. F. Murphy, C. A. Kent, B. C. Westlake, A. Paul, D. H. Ess, D. G. McCafferty, T. J. Meyer, *Chem. Rev.* **2012**, *112*, 4016–4093.
117. O. S. Wenger, *Acc. Chem. Res.* **2013**, *46*, 1517–1526.
118. G. J. Choi, R. R. Knowles, *J. Am. Chem. Soc.* **2015**, *137*, 9226–9229.
119. D. C. Miller, G. J. Choi, H. S. Orbe, R. R. Knowles, *J. Am. Chem. Soc.* **2015**, *137*, 13492–13495.
120. J. Davies, T. D. Svejstrup, D. Fernandez Reina, N. S. Sheikh, D. Leonori, *J. Am. Chem. Soc.* **2016**, *138*, 8092–8095.
121. D. F. Reina, E. M. Dauncey, S. P. Morcillo, T. D. Svejstrup, M. V. Popescu, J. J. Douglas, N. S. Sheikh, D. Leonori, *Eur. J. Org. Chem.* **2017**, 2108–2111.
122. K. Wu, Y. Du, T. Wang, *Org. Lett.* **2017**, *19*, 5669–5672.
123. Y. Li, R. Mao, J. Wu, *Org. Lett.* **2017**, *19*, 4472–4475.
124. J. Davies, N. S. Sheikh, D. Leonori, *Angew. Chem. Int. Ed.* **2017**, *56*, 13361–13365.
125. T. D. Svejstrup, W. Zawodny, J. J. Douglas, D. Bidgeli, N. S. Sheikh, D. Leonori, *Chem. Commun.* **2016**, *52*, 12302–12305.
126. M. D. Kärkäs, *ACS Catal.* **2017**, *7*, 4999–5022.
127. L. J. Allen, P. J. Cabrera, M. Lee, M. S. Sanford, *J. Am. Chem. Soc.* **2014**, *136*, 5607–5610.
128. E. B. Corcoran, M. T. Pirnot, S. Lin, S. D. Dreher, D. A. DiRocco, I. W. Davies, S. L.

Buchwald, D. W. C. MacMillan, *Science* **2016**, *353*, 279–283.
129. P. Ruiz-Castillo, S. L. Buchwald, *Chem. Rev.* **2016**, *116*, 12564–12649.
130. E. B. Corcoran, M. T. Pirnot, S. Lin, S. D. Dreher, D. A. Dirocco, I. W. Davies, S. L. Buchwald, D. W. C. Macmillan, *Science* **2016**, *353*, 279–283.
131. E. Brachet, T. Ghosh, I. Ghosh, B. König, *Chem. Sci.* **2015**, *6*, 987–992.
132. L.-C. Yu, J.-W. Gu, S. Zhang, X. Zhang, *J. Org. Chem.* **2017**, *82*, 3943–3949.
133. J. Liu, Q. Liu, H. Yi, C. Qin, R. Bai, X. Qi, Y. Lan, A. Lei, *Angew. Chem. Int. Ed.* **2014**, *53*, 502–506.
134. T. Kamon, Y. Irifune, T. Tanaka, T. Yoshimitsu, *Org. Lett.* **2011**, *13*, 2674–2677.
135. H. Zhou, P. Lu, X. Gu, P. Li, *Org. Lett.* **2013**, *15*, 5646–5649.
136. T. Yoshimitsu, K. Matsuda, H. Nagaoka, K. Tsukamoto, T. Tanaka, *Org. Lett.* **2007**, *9*, 5115–5118.
137. S. Zheng, D. N. Primer, G. A. Molander, *ACS Catal.* **2017**, *7*, 7957–7961.
138. V. Corcé, L. M. Chamoreau, E. Derat, J. P. Goddard, C. Ollivier, L. Fensterbank, *Angew. Chem. Int. Ed.* **2015**, *54*, 11414–11418.
139. M. Jouffroy, D. N. Primer, G. A. Molander, *J. Am. Chem. Soc.* **2016**, *138*, 475–478.
140. T. K. Grimsrud, A. Andersen, *J. Occup. Med. Toxicol.* **2010**, *5*, 1–6.
141. W. M. Cheng, R. Shang, H. Z. Yu, Y. Fu, *Chem. Eur. J.* **2015**, *21*, 13191–13195.
142. J. Zhang, A. Bellomo, N. Trongsiriwat, T. Jia, P. J. Carroll, S. D. Dreher, M. T. Tudge, H. Yin, J. R. Robinson, E. J. Schelter, P. J. Walsh, *J. Am. Chem. Soc.* **2014**, *136*, 6276–6287.
143. W. F. Petersen, R. J. K. Taylor, J. R. Donald, *Org. Lett.* **2017**, *19*, 874–877.
144. W. F. Petersen, R. J. K. Taylor, J. R. Donald, *Org. Biomol. Chem.* **2017**, *15*, 5831–5845.
145. G. Z. Wang, R. Shang, W. M. Cheng, Y. Fu, *Org. Lett.* **2015**, *17*, 4830–4833.
146. C. C. Nawrat, C. R. Jamison, Y. Slutskyy, D. W. C. MacMillan, L. E. Overman, *J. Am. Chem. Soc.* **2015**, *137*, 11270–11273.
147. Y. Su, N. J. W. Straathof, V. Hessel, T. Noël, *Chem. Eur. J.* **2014**, *20*, 10562–10589.
148. M. Betou, L. Male, J. W. Steed, R. S. Grainger, *Chem. Eur. J.* **2014**, *20*, 6505–6517.
149. T. J. Smith, K. J. Stevenson, *Handbook of Electrochemistry*, Elsevier, Radarweg, **2007**.
150. M. Martiny, E. Steckhan, T. Esch, *Chem. Ber.* **1993**, *126*, 1671–1682.
151. C. Le, M. K. Wismer, Z.-C. Shi, R. Zhang, D. V. Conway, G. Li, P. Vachal, I. W. Davies, D. W. C. MacMillan, *ACS Cent. Sci.* **2017**, *3*, 647–653.
152. D. F. Swinehart, *J. Chem. Educ.* **1962**, *39*, 333–335.

153. D. Cambié, C. Bottecchia, N. J. W. Straathof, V. Hessel, T. Noël, *Chem. Rev.* **2016**, *116*, 10276–10341.
154. R. S. Andrews, J. J. Becker, M. R. Gagné, *Angew. Chem. Int. Ed.* **2012**, *51*, 4140–4143.
155. M. Obst, R. Shaikh, B. König, *React. Chem. Eng.* **2017**, *2*, 472–478.
156. "Sigma-Aldrich Catalogue," can be found under www.sigmaaldrich.com, **Accessed 25th February 2018**.
157. S. Fukuzumi, H. Kotani, K. Ohkubo, S. Ogo, N. V. Tkachenko, H. Lemmetyinen, *J. Am. Chem. Soc.* **2004**, *126*, 1600–1601.
158. Y. Wang, O. Haze, J. P. Dinnocenzo, S. Farid, R. S. Farid, I. R. Gould, *J. Org. Chem.* **2007**, *72*, 6970–6981.
159. M. A. Haga, E. S. Dodsworth, G. Eryavec, P. Seymour, A. B. P. Lever, *Inorg. Chem.* **1985**, *24*, 1901–1906.
160. J. Luo, J. Zhang, *ACS Catal.* **2016**, *6*, 873–877.
161. H. Huang, C. Yu, Y. Zhang, Y. Zhang, P. S. Mariano, W. Wang, *J. Am. Chem. Soc.* **2017**, *139*, 9799–9802.
162. N. R. Patel, C. B. Kelly, A. P. Siegenfeld, G. A. Molander, *ACS Catal.* **2017**, *7*, 1766–1770.
163. J. K. Matsui, G. A. Molander, *Org. Lett.* **2017**, *19*, 436–439.
164. Á. Gutiérrez-Bonet, J. C. Tellis, J. K. Matsui, B. A. Vara, G. A. Molander, *ACS Catal.* **2016**, *6*, 8004–8008.
165. D. Prat, A. Wells, J. Hayler, H. F. Sneddon, C. R. McElroy, S. Abou-Shehada, P. J. Dunn, *Green Chem.* **2016**, *18*, 288–296.
166. R. Bro, A. K. Smilde, *Anal. Methods* **2014**, *6*, 2812–2831.
167. R. Carlson, J. E. Carlson, *Org. Process Res. Dev.* **2005**, *9*, 680–689.
168. T. Marino, F. Russo, A. Criscuoli, A. Figoli, *J. Memb. Sci.* **2017**, *542*, 418–429.
169. H. L. Parker, J. Sherwood, A. J. Hunt, J. H. Clark, *ACS Sustain. Chem. Eng.* **2014**, *2*, 1739–1742.
170. M. Torrent, M. Solá, G. Frenking, *Chem. Rev.* **2000**, *100*, 439–493.
171. T. B. Demissie, K. Ruud, J. H. Hansen, *Organometallics* **2015**, *34*, 4218–4228.
172. T. B. Demissie, J. H. Hansen, *Dalt. Trans.* **2016**, *45*, 10878–10882.
173. "British Geological Survey 'Risk List,'" can be found under http://www.bgs.ac.uk/mineralsuk/statistics/riskList.html, **Accessed 25th February 2018**.

174. N. A. Romero, K. A. Margrey, N. E. Tay, D. A. Nicewicz, *Science* **2015**, *349*, 1326–1330.
175. S. Caron, N. M. Thomson, *J. Org. Chem.* **2015**, *80*, 2943–2958.
176. H. Babad, A. G. Zeiler, *Chem. Rev.* **1973**, *73*, 75–91.
177. D. Liu, Z. Tian, Z. Yan, L. Wu, Y. Ma, Q. Wang, W. Liu, H. Zhou, C. Yang, *Bioorg. Med. Chem.* **2013**, *21*, 2960–2967.
178. S. Lang, J. A. Murphy, *Chem. Soc. Rev.* **2006**, *35*, 146–156.
179. S. Ozaki, *Chem. Rev.* **1972**, *72*, 457–496.
180. E. F. V. Scriven, K. Turnbull, *Chem. Rev.* **1988**, *88*, 298–368.
181. J. Wiss, C. Fleury, C. Heuberger, U. Onken, M. Glor, *Org. Process Res. Dev.* **2007**, *11*, 1096–1103.
182. L. Kürti, B. Czakó, *Strategic Applications of Named Reactions in Organic Synthesis*, Elsevier, Burlington, **2005**.
183. H. Lebel, O. Leogane, *Org. Lett.* **2005**, *7*, 4107–4110.
184. T. Shioiri, K. Ninomiya, S. Yamada, *J. Am. Chem. Soc.* **1972**, *94*, 6203–6205.
185. J. W. Keillor, X. Huang, *Org. Synth.* **2004**, *10*, 549–551.
186. P. Dubé, N. F. Fine, M. Vetelino, M. Couturier, C. L. Aboussafy, S. Pichette, M. L. Jorgensen, M. Hardink, *Org. Lett.* **2009**, *11*, 5622–5625.
187. G. Schäfer, C. Matthey, J. W. Bode, *Angew. Chem. Int. Ed.* **2012**, *51*, 9173–9175.
188. K. A. Parker, E. G. Gibbons, *Tetrahedron Lett.* **1975**, 981–984.
189. Y. Zhang, J. Jiang, Y. Chen, *Tetrahedron Lett.* **1987**, *28*, 3815–3816.
190. E. Chorell, P. Das, F. Almqvist, *J. Org. Chem.* **2007**, *72*, 4917–4924.
191. C. Christophersen, M. Begtrup, S. Ebdrup, H. Petersen, P. Vedsø, *J. Org. Chem.* **2003**, *68*, 9513–9516.
192. A. V Lygin, A. de Meijere, *Org. Lett.* **2009**, *11*, 389–392.
193. V. Pace, L. Castoldi, W. Holzer, *Chem. Commun.* **2013**, *49*, 8383–8385.
194. H. Yang, D. Huang, K. H. Wang, C. Xu, T. Niu, Y. Hu, *Tetrahedron* **2013**, *69*, 2588–2593.
195. K. Sasaki, D. Crich, *Org. Lett.* **2011**, *13*, 2256–2259.
196. B. Zhou, W. Hou, Y. Yang, Y. Li, *Chem. Eur. J.* **2013**, *19*, 4701–4706.
197. K. D. Hesp, R. G. Bergman, J. A. Ellman, *J. Am. Chem. Soc.* **2011**, *133*, 11430–11433.
198. X. Geng, C. Wang, *Org. Biomol. Chem.* **2015**, *13*, 7619–7623.
199. W. Liu, J. Bang, Y. Zhang, L. Ackermann, *Angew. Chem. Int. Ed.* **2015**, *54*, 14137–

14140.

200. J. Li, L. Ackermann, *Angew. Chem. Int. Ed.* **2015**, *54*, 8551–8554.
201. J. R. Hummel, J. A. Ellman, *Org. Lett.* **2015**, *17*, 2400–2403.
202. E. Kianmehr, A. Rajabi, M. Ghanbari, *Tetrahedron Lett.* **2009**, *50*, 1687–1688.
203. T. Miura, Y. Takahashi, M. Murakami, *Chem. Commun.* **2007**, 3577–3579.
204. T. T. S. Lew, D. S. W. Lim, Y. Zhang, *Green Chem.* **2015**, *17*, 5140–5143.
205. E. Serrano, R. Martin, *Angew. Chem. Int. Ed.* **2016**, *55*, 11207–11211.
206. A. Correa, R. Martin, *J. Am. Chem. Soc.* **2014**, *136*, 7253–7256.
207. P. Anastas, N. Eghbali, *Chem. Soc. Rev.* **2010**, *39*, 301–312.
208. S. Y. Tang, R. A. Bourne, R. L. Smith, M. Poliakoff, *Green Chem.* **2008**, *10*, 268–269.
209. R. W. Taft, *J. Am. Chem. Soc.* **1952**, *74*, 3120–3128.
210. X. Li, I. Coldham, *J. Am. Chem. Soc.* **2014**, *136*, 5551–5554.
211. A. Chanda, A. M. Daly, D. A. Foley, M. A. LaPack, S. Mukherjee, J. D. Orr, G. L. Reid, D. R. Thompson, H. W. Ward, *Org. Process Res. Dev.* **2015**, *19*, 63–83.
212. S. A. Eisenbeis, R. Chen, M. Kang, M. Barrila, R. Buzon, *Org. Process Res. Dev.* **2015**, *19*, 244–248.
213. P. B. Palde, T. F. Jamison, *Angew. Chem. Int. Ed.* **2011**, *50*, 3525–3528.
214. D. M. Roberge, N. Bieler, M. Mathier, M. Eyholzer, B. Zimmermann, P. Barthe, C. Guermeur, O. Lobet, M. Moreno, P. Woehl, *Chem. Eng. Technol.* **2008**, *31*, 1155–1161.
215. V. Hessel, *Chem. Eng. Technol.* **2009**, *32*, 1655–1681.
216. J. M. Commenge, L. Falk, *Chem. Eng. Process.* **2011**, *50*, 979–990.
217. R. L.-Y. Bao, R. Zhao, L. Shi, *Chem. Commun.* **2015**, *51*, 6884–6900.
218. Y. Liu, C. S. Da, S. L. Yu, X. G. Yin, J. R. Wang, X. Y. Fan, W. P. Li, R. Wang, *J. Org. Chem.* **2010**, *75*, 6869–6878.
219. S. Hardy, S. F. Martin, *Org. Lett.* **2011**, *13*, 3102–3105.
220. D. A. Horton, G. T. Bourne, M. L. Smythe, *Chem. Rev.* **2003**, *103*, 893–930.
221. C. Zhou, L. Guo, G. Morriello, A. Pasternak, Y. Pan, S. P. Rohrer, E. T. Birzin, S. E. W. Huskey, T. Jacks, K. D. Schleim, K. Cheng, J. M. Schaeffer, A. A. Patchett, L. Yang, *Bioorg. Med. Chem. Lett.* **2001**, *11*, 415–417.
222. P. R. Markies, G. Schat, S. Griffioen, A. Villena, O. S. Akkerman, F. Bickelhaupt, *Organometallics* **1991**, *10*, 1531–1546.
223. A. Krasovskiy, P. Knochel, *Angew. Chem. Int. Ed.* **2004**, *43*, 3333–3336.
224. P. Knochel, W. Dohle, N. Gommermann, F. F. Kneisel, F. Kopp, T. Korn, I. Sapountzis,

V. A. Vu, *Angew. Chem. Int. Ed.* **2003**, *42*, 4302–20.

225. A. Krasovskiy, B. F. Straub, P. Knochel, *Angew. Chem. Int. Ed.* **2005**, *45*, 159–162.
226. N. Boudet, P. Knochel, *Org. Lett.* **2006**, *8*, 3737–3740.
227. M. R. Kole, R. K. Reddy, M. V Schulmerich, M. K. Gelber, R. Bhargava, *Anal. Chem.* **2012**, *84*, 10366–10372.
228. K. Yeh, S. Kenkel, J. Liu, R. Bhargava, *Anal. Chem.* **2015**, *87*, 485–493.
229. H. Keles, F. Susanne, H. Livingstone, S. Hunter, C. Wade, R. E. Bourdon, A. Rutter, *Org. Process Res. Dev.* **2017**, *21*, 1761–1768.
230. P. R. D. Murray, D. L. Browne, J. C. Pastre, C. Butters, D. Guthrie, S. V Ley, *Org. Process Res. Dev.* **2013**, *17*, 1192–1208.
231. R. L. Hartman, J. R. Naber, N. Zaborenko, S. L. Buchwald, K. F. Jensen, *Org. Process Res. Dev.* **2010**, *14*, 1347–1357.
232. R. C. Betori, J. M. Kallemeyn, D. S. Welch, *Org. Process Res. Dev.* **2015**, *19*, 1517–1523.
233. N. Likhite, T. Lakshminarasimhan, M. H. V. R. Rao, V. Shekarappa, S. Sidar, V. Subramanian, K. J. Fraunhoffer, S. Leung, R. Vaidyanathan, *Org. Process Res. Dev.* **2016**, *20*, 1328–13358.
234. C. Nunn, A. DiPietro, N. Hodnett, P. Sun, K. M. Wells, *Org. Process Res. Dev.* **2018**, *22*, 54–61.
235. D. G. Blackmond, *Angew. Chem. Int. Ed.* **2005**, *44*, 4302–4320.
236. D. G. Blackmond, *J. Am. Chem. Soc.* **2015**, *137*, 10852–10866.
237. J. Burés, *Angew. Chem. Int. Ed.* **2016**, *55*, 2028–2031.
238. J. Burés, *Angew. Chem. Int. Ed.* **2016**, *55*, 16084–16087.
239. X. Yang, Y. Zhang, D. Ma, *Adv. Synth. Catal.* **2012**, *354*, 2443–2446.
240. E. Kianmehr, M. H. Baghersadi, *Adv. Synth. Catal.* **2011**, *353*, 2599–2603.
241. E. V Vinogradova, N. H. Park, B. P. Fors, S. L. Buchwald, *Org. Lett.* **2013**, *15*, 1394–1397.
242. E. V Vinogradova, B. P. Fors, S. L. Buchwald, *J. Am. Chem. Soc.* **2012**, *134*, 11132–11135.
243. T. Brodmann, P. Koos, A. Metzger, P. Knochel, S. V. Ley, *Org. Process Res. Dev.* **2012**, *16*, 1102–1113.
244. L. Shi, Y. Chu, P. Knochel, H. Mayr, *Org. Lett.* **2012**, *14*, 2602–2605.
245. R. L.-Y. Bao, R. Zhao, L. Shi, *Chem. Commun.* **2015**, *51*, 6884–6900.

246. T. P. Petersen, M. R. Becker, P. Knochel, *Angew. Chem. Int. Ed.* **2014**, *53*, 7933–7937.
247. T. Cernak, K. D. Dykstra, S. Tyagarajan, P. Vachal, S. W. Krska, *Chem. Soc. Rev.* **2016**, *45*, 546–576.
248. M. Ketels, M. A. Ganiek, N. Weidmann, P. Knochel, *Angew. Chem. Int. Ed.* **2017**, *56*, 12770–12773.
249. C. E. Tucker, T. N. Majid, P. Knochel, *J. Am. Chem. Soc.* **1992**, *114*, 3983–3985.
250. D. Ma, Q. Cai, *Acc. Chem. Res.* **2008**, *41*, 1450–1460.
251. D. S. Surry, S. L. Buchwald, *Chem. Sci.* **2011**, *2*, 27–50.
252. M. R. Becker, P. Knochel, *Angew. Chem. Int. Ed.* **2015**, *54*, 12501–12505.
253. A. Frischmuth, M. Fernández, N. M. Barl, F. Achrainer, H. Zipse, G. Berionni, H. Mayr, K. Karaghiosoff, P. Knochel, *Angew. Chem. Int. Ed.* **2014**, *53*, 7928–7932.
254. D. Haas, J. M. Hammann, R. Greiner, P. Knochel, *ACS Catal.* **2016**, *6*, 1540–1552.
255. P. Knochel, M. C. P. Yeh, S. C. Berk, J. Talbert, *J. Org. Chem.* **1988**, *53*, 2390–2392.
256. H. Sierotzki, G. Scalliet, *Phytopathology* **2013**, *103*, 880–887.
257. C. Torborg, M. Beller, *Adv. Synth. Catal.* **2009**, 3027–3043.
258. T. N. Glasnov, C. O. Kappe, *Adv. Synth. Catal.* **2010**, *352*, 3089–3097.
259. S. Jeanmart, A. J. F. Edmunds, C. Lamberth, M. Pouliot, *Bioorg. Med. Chem.* **2016**, *24*, 317–341.
260. H. Wang, X. Gao, X. Zhang, H. Jin, K. Tao, T. Hou, *Bioorg. Med. Chem. Lett.* **2017**, *27*, 90–93.
261. D. K. Inaoka, T. Shiba, D. Sato, E. O. Balogun, T. Sasaki, M. Nagahama, M. Oda, S. Matsuoka, J. Ohmori, T. Honma, M. Inoue, K. Kita, S. Harada, *Int. J. Mol. Sci.* **2015**, *16*, 15287–15308.
262. "Kessil A160WE Tuna Blue 40W LED lamp specifications," can be found under http://www.kessil.com/aquarium/Saltwater_A160_Tuna_Blue.php, **Accessed 25th February 2018**.
263. "Hepatochem PhotoredOx Box," can be found under http://www.hepatochem.com/photochemistry/photoredox-box/, **Accessed 25th February 2018**.
264. "Hepatochem PhotoredOx Duo," can be found under http://www.hepatochem.com/photochemistry/photoredox-duo/, **Accessed 25th February 2018**.
265. L. A. Paquette, H.-S. Lin, *Synth. Commun.* **1994**, *24*, 2503–2506.

266. A. Krasovskiy, P. Knochel, *Synthesis* **2006**, 890–891.
267. S. T. Gadge, B. M. Bhanage, *J. Org. Chem.* **2013**, *78*, 6793–6797.
268. M. Gerard, L. Gerard, *Derives d'oxamates comportant un heterocycle azote diversement substitue* **2003**, FR2829766 A1.
269. D. M. Schultz, J. W. Sawicki, T. P. Yoon, *Beilstein J. Org. Chem.* **2015**, *11*, 61–65.
270. I. M. Downie, M. J. Earle, H. Heaney, K. F. Shuhaibar, *Tetrahedron* **1993**, *49*, 4015–4034.
271. D. A. Klumpp, R. Rendy, Y. Zhang, A. Gomez, A. McElrea, *Org. Lett.* **2004**, *6*, 1789–1792.
272. W. Koch, M. C. Holthausen, *A Chemist's Guide to Density Functional Theory*, Wiley, Weinheim, **2001**.
273. M. J. Frisch, G. W. Trucks, H. B. Schlegel, G. E. Scuseria, M. A. Robb, J. R. Cheeseman, G. Scalmani, V. Barone, B. Mennucci, G. A. Petersson, et al., **2013**.
274. A. D. Becke, *J. Chem. Phys.* **1993**, *98*, 5648–5652.
275. P. Brandt, C. Hedberg, P. G. Andersson, *Chem. Eur. J.* **2003**, *9*, 339–347.
276. M. Cossi, N. Rega, G. Scalmani, V. Barone, *J. Comput. Chem.* **2003**, *24*, 669–681.
277. K. Fukui, *Acc. Chem. Res.* **1981**, *14*, 363–368.
278. R. G. Kadesch, *J. Am. Chem. Soc.* **1941**, *64*, 726–726.
279. S. Hanada, E. Tsutsumi, Y. Motoyama, H. Nagashima, *J. Am. Chem. Soc.* **2009**, *131*, 15032–15040.
280. Z. Wu, K. L. Hull, *Chem. Sci.* **2016**, *7*, 969–975.
281. K. Ishihara, Y. Lu, *Chem. Sci.* **2016**, *7*, 1276–1280.
282. R. Ohmura, M. Takahata, H. Togo, *Tetrahedron Lett.* **2010**, *51*, 4378–4381.
283. I. Shiina, H. Ushiyama, Y. K. Yamada, Y. I. Kawakita, K. Nakata, *Chem. Asian J.* **2008**, *3*, 454–461.
284. D. K. Kumar, D. A. Jose, A. Das, P. Dastidar, *Chem. Commun.* **2005**, 4059–4061.
285. T. Maki, K. Ishihara, H. Yamamoto, *Org. Lett.* **2006**, *8*, 1431–1434.
286. S.-R. Sheng, X.-C. Wang, X.-L. Liu, C.-S. Song, *Synth. Commun.* **2003**, *33*, 2867–2872.
287. Y. H. Yang, M. Shi, *J. Org. Chem.* **2005**, *70*, 8645–8648.
288. B. Roberts, D. Liptrot, L. Alcaraz, T. Luker, M. J. Stocks, *Org. Lett.* **2010**, *12*, 4280–4283.
289. V. C. Agwada, *J. Chem. Eng. Data* **1982**, *27*, 479–481.
290. X. Cui, Y. Zhang, F. Shi, Y. Deng, *Chem. Eur. J.* **2011**, *17*, 1021–1028.

291. I. R. Morgan, A. Yazici, S. G. Pyne, B. W. Skelton, *J. Org. Chem.* **2008**, *73*, 2943–2946.
292. C. O. Okafor, *J. Org. Chem.* **1973**, *38*, 4386–4390.
293. S. B. Greenbaum, *J. Am. Chem. Soc.* **1954**, *76*, 6052–6054.

# Appendix: DFT Calculations

## Structures

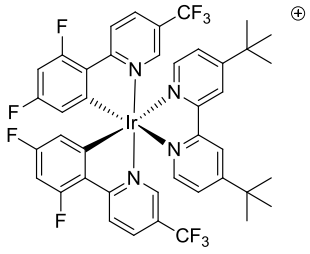


**156**

Iridium(III) catalyst

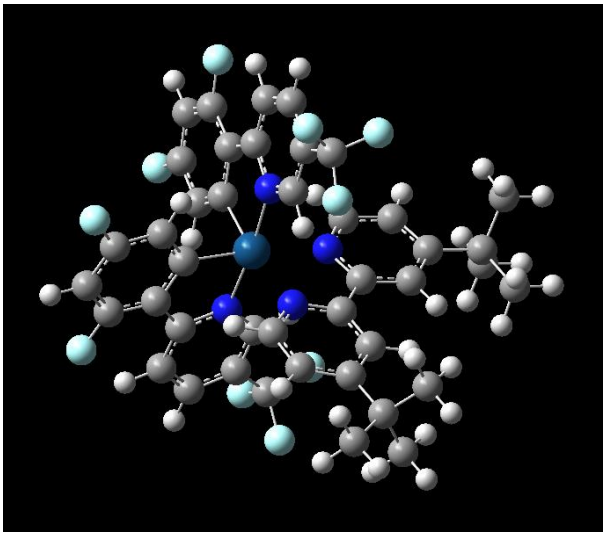

| | |
|---|---|
| Route | UB3LYP/GEN Pseudo=read FormCheck Opt Freq scrf=(cpcm,solvent=acetone) |
| Smiles | FC1=C(C2=[N]3C=C(C(F)(F)F)C=C2)C([Ir]435(C6=CC(F)=CC(F)=C6C7=[N]5C=C(C(F)(F)F)C=C7)[N]8=CC=C(C(C)(C)C)C=C8C9=[N]4C=CC(C(C)(C)C)=C9)=CC(F)=C1 |
| Formula | $C_{42}H_{34}F_{10}IrN_4^+$ |
| Charge | 1 |
| Multiplicity | 1 |
| Dipole (Debye) | 10.0250 |
| Gibbs energy (a.u.) | −2942.641912 |
| # Imaginary frequencies | 0 |

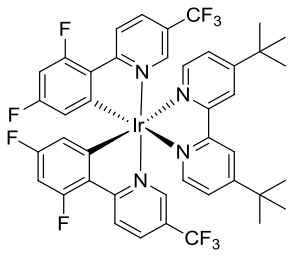


**156'**

Iridium(II) catalyst

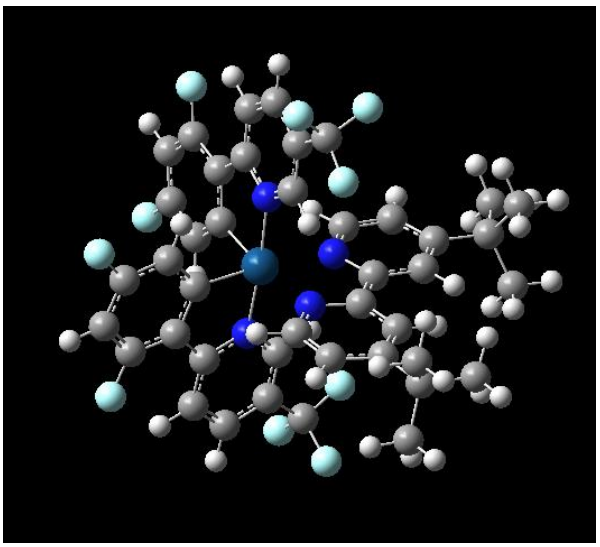

| | |
|---|---|
| Route | UB3LYP/GEN Pseudo=read FormCheck Opt(MaxCyc=50) Freq scrf=(cpcm,solvent=acetone) |
| Smiles | FC1=C(C2=[N]3C=C(C(F)(F)F)C=C2)C([Ir]435(C6=CC(F)=CC(F)=C6C7=[N]5C=C(C(F)(F)F)C=C7)[N]8=CC=C(C(C)(C)C)C=C8C9=[N]4C=CC(C(C)(C)C)=C9)=CC(F)=C1 |
| Formula | $C_{42}H_{34}F_{10}IrN_4$ |
| Charge | 0 |
| Multiplicity | 2 |
| Dipole (Debye) | 1.7807 |
| Gibbs energy (a.u.) | −2942.755601 |
| # Imaginary frequencies | 0 |

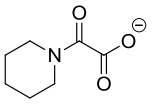

171

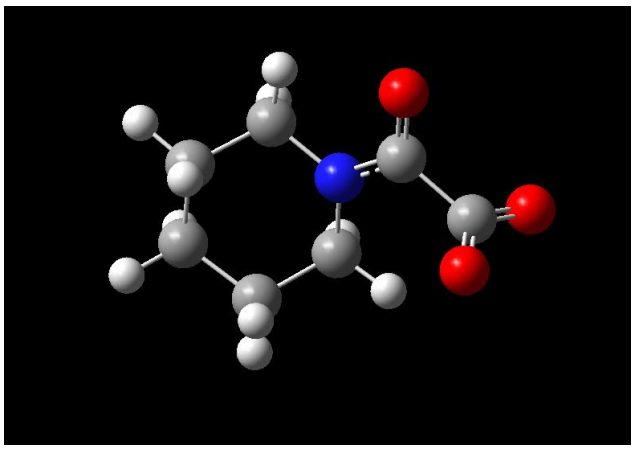

| | |
|---|---|
| Route | UB3LYP/6-31+G(d,p) FormCheck opt(MaxCyc=1000) freq scrf=(cpcm,solvent=acetone) |
| Smiles | O=C(C([O-])=O)N1CCCCC1 |
| Formula | $C_7H_{10}NO_3^-$ |
| Charge | −1 |
| Multiplicity | 1 |
| Dipole (Debye) | 16.5508 |
| Gibbs energy (a.u.) | −553.280058 |
| # Imaginary frequencies | 0 |

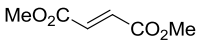


**155**

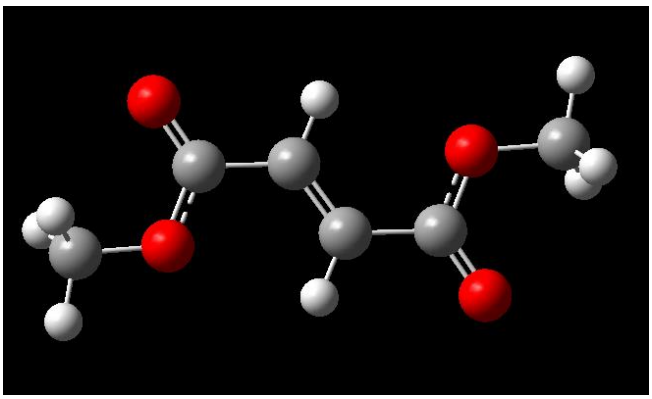

| | |
|---|---|
| Route | UB3LYP/6-31+G(d,p) FormCheck opt(MaxCyc=1000) freq scrf=(cpcm,solvent=acetone) |
| Smiles | O=C(OC)/C=C/C(OC)=O |
| Formula | $C_6H_8O_4$ |
| Charge | 0 |
| Multiplicity | 1 |
| Dipole (Debye) | 0 |
| Gibbs energy (a.u.) | −534.288989 |
| # Imaginary frequencies | 0 |

$CO_2$

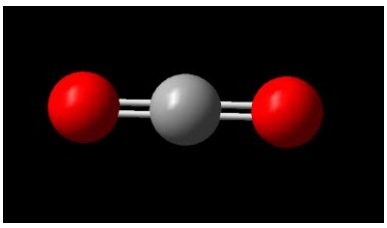

| | |
|---|---|
| Route | UB3LYP/6-31+G(d,p) FormCheck opt(MaxCyc=1000) freq scrf=(cpcm,solvent=acetone) |
| Smiles | O=C=O |
| Formula | $CO_2$ |
| Charge | 0 |
| Multiplicity | 1 |
| Dipole (Debye) | 0 |
| Gibbs energy (a.u.) | −188.602442 |
| # Imaginary frequencies | 0 |

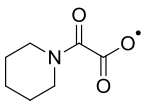

172

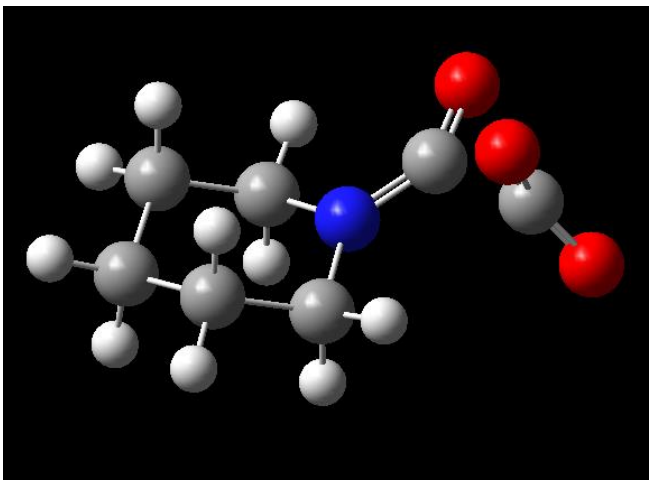

| | |
|---|---|
| Route | UB3LYP/6-31+G(d,p) FormCheck opt(MaxCyc=1000) freq scrf=(cpcm,solvent=acetone) |
| Smiles | O=C(C([O])=O)N1CCCCC1 |
| Formula | $C_7H_{10}NO_3$• |
| Charge | 0 |
| Multiplicity | 2 |
| Dipole (Debye) | 8.6220 |
| Gibbs energy (a.u.) | −553.079468 |
| # Imaginary frequencies | 0 |

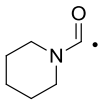


173

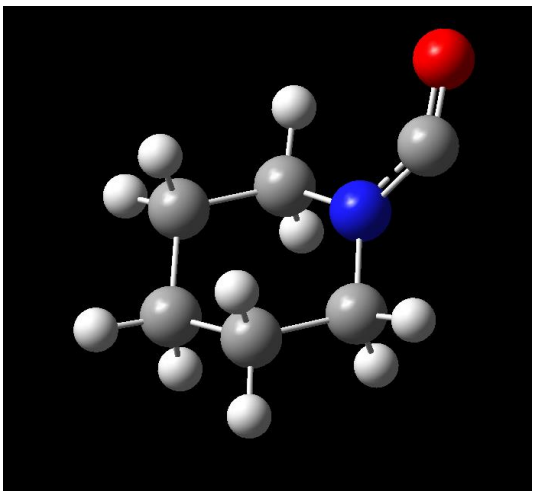

| | |
|---|---|
| Route | UB3LYP/6-31+G(d,p) FormCheck opt(MaxCyc=1000) freq scrf=(cpcm,solvent=acetone) |
| Smiles | O=[C]N1CCCCC1 |
| Formula | $C_6H_{10}NO$• |
| Charge | 0 |
| Multiplicity | 2 |
| Dipole (Debye) | 5.9455 |
| Gibbs energy (a.u.) | −364.508489 |
| # Imaginary frequencies | 0 |

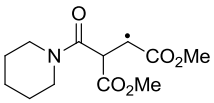


174

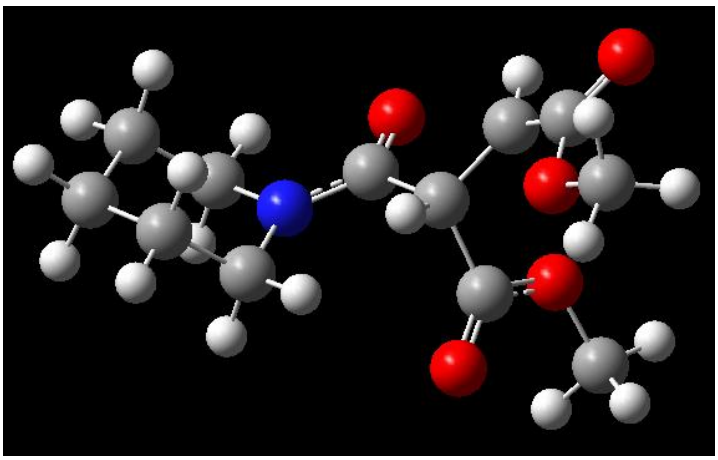

| | |
|---|---|
| Route | UB3LYP/6-31+G(d,p) FormCheck opt=(Loose, MaxCyc=1000) freq scrf=(cpcm,solvent=acetone) |
| Smiles | O=C(C(C(OC)=O)[C]C(OC)=O)N1CCCCC1 |
| Formula | $C_{12}H_{18}NO_5$• |
| Charge | 0 |
| Multiplicity | 2 |
| Dipole (Debye) | 6.2363 |
| Gibbs energy (a.u.) | −898.797993 |
| # Imaginary frequencies | 0 |

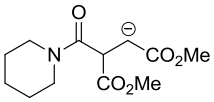


**175**

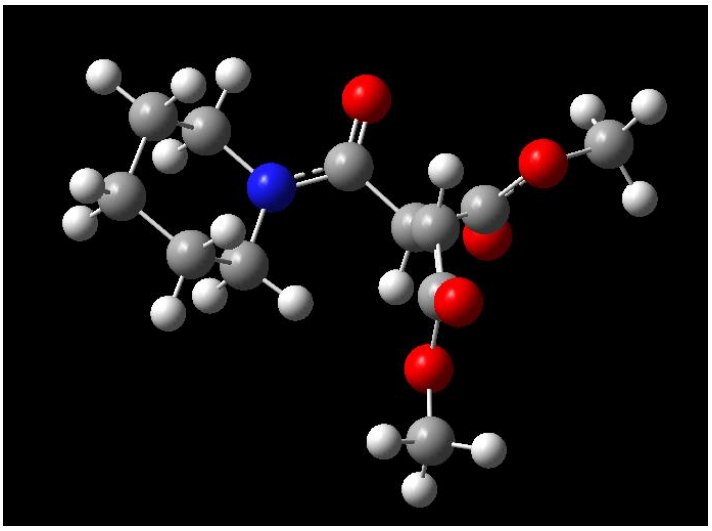

| | |
|---|---|
| Route | UB3LYP/6-31+G(d,p) FormCheck opt=(Loose, MaxCyc=1000) freq scrf=(cpcm,solvent=acetone) |
| Smiles | O=C(C(C(OC)=O)[CH-]C(OC)=O)N1CCCCC1 |
| Formula | $C_{12}H_{18}NO_5^-$ |
| Charge | −1 |
| Multiplicity | 1 |
| Dipole (Debye) | 9.4163 |
| Gibbs energy (a.u.) | −898.943215 |
| # Imaginary frequencies | 0 |

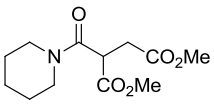


**157**

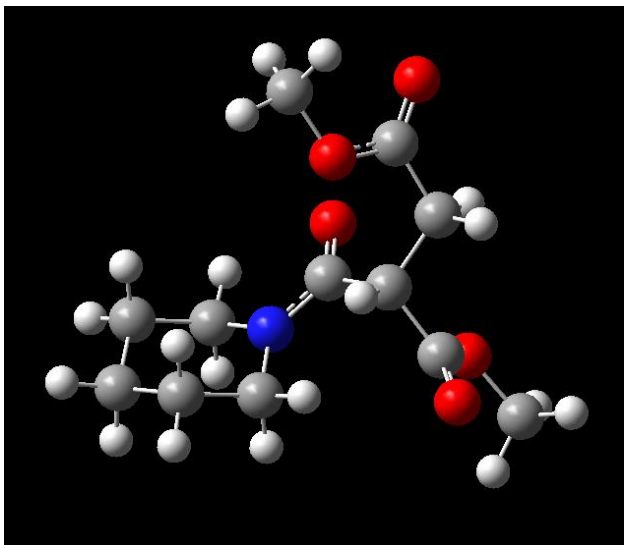

| | |
|---|---|
| Route | UB3LYP/6-31+G(d,p) FormCheck opt=(Loose, MaxCyc=1000) freq scrf=(cpcm,solvent=acetone) |
| Smiles | O=C(C(C(OC)=O)CC(OC)=O)N1CCCCC1 |
| Formula | $C_{12}H_{19}NO_5$ |
| Charge | 0 |
| Multiplicity | 1 |
| Dipole (Debye) | 6.5661 |
| Gibbs energy (a.u.) | −899.441512 |
| # Imaginary frequencies | 0 |

176

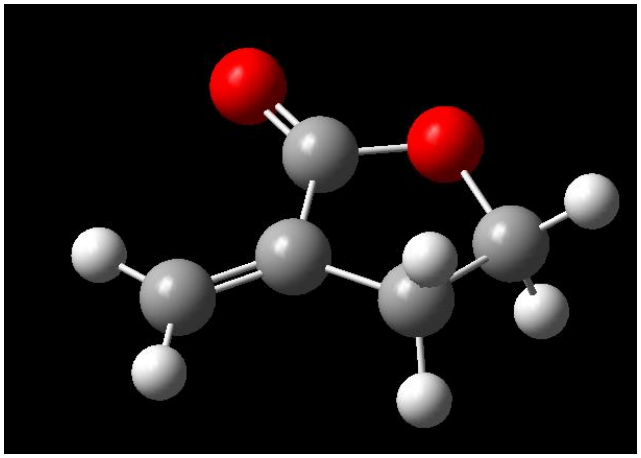

| | |
|---|---|
| Route | UB3LYP/6-31+G(d,p) FormCheck Opt=(Tight, MaxCyc=100) freq scrf=(cpcm,solvent=acetone) |
| Smiles | C=C1CCOC1=O |
| Formula | $C_5H_6O_2$ |
| Charge | 1 |
| Multiplicity | 1 |
| Dipole (Debye) | 6.6588 |
| Gibbs energy (a.u.) | −344.537709 |
| # Imaginary frequencies | 0 |

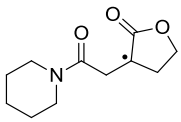


177

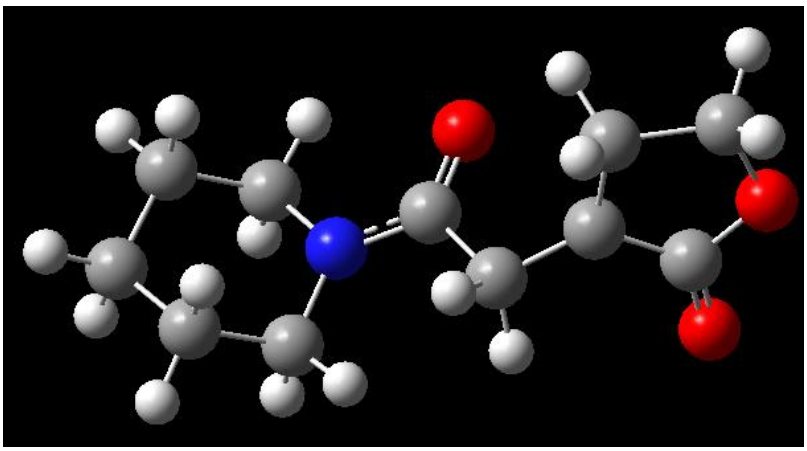

| | |
|---|---|
| Route | UB3LYP/6-31+G(d,p) FormCheck opt(Tight, MaxCyc=1000) freq scrf=(cpcm,solvent=acetone) |
| Smiles | O=C(C[C]1CCOC1=O)N2CCCCC2 |
| Formula | $C_{11}H_{16}NO_3$• |
| Charge | 0 |
| Multiplicity | 2 |
| Dipole (Debye) | 9.3175 |
| Gibbs energy (a.u.) | −709.062690 |
| # Imaginary frequencies | 0 |

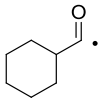

178

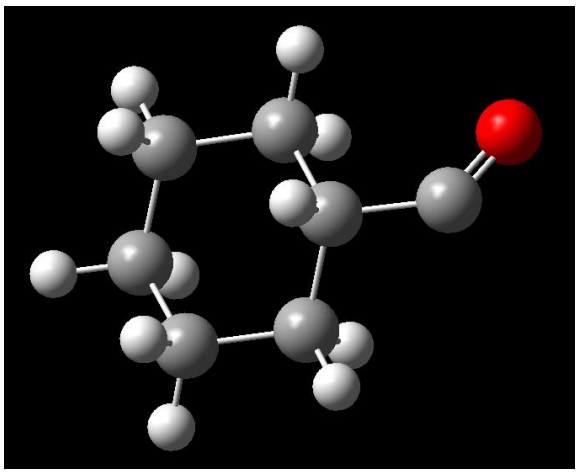

| | |
|---|---|
| Route | UB3LYP/6-31+G(d,p) FormCheck Opt=(Tight, MaxCyc=1000) Freq scrf=(cpcm,solvent=acetone) |
| Smiles | O=[C]C1CCCCC1 |
| Formula | $C_7H_{11}O$• |
| Charge | 0 |
| Multiplicity | 2 |
| Dipole (Debye) | 3.8441 |
| Gibbs energy (a.u.) | −348.445826 |
| # Imaginary frequencies | 0 |

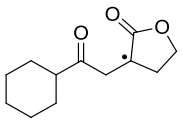

179

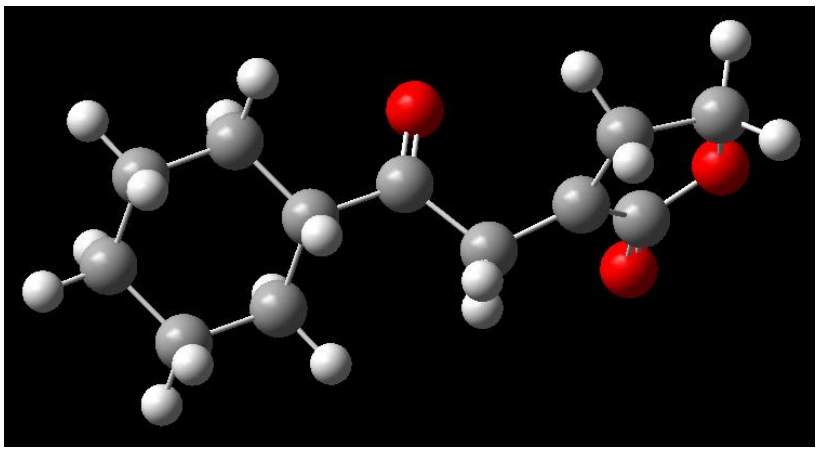

| | |
|---|---|
| Route | UB3LYP/6-31+G(d,p) FormCheck Opt=(Tight, MaxCyc=1000) freq scrf=(cpcm,solvent=acetone) |
| Smiles | O=C(C[C]1CCOC1=O)C2CCCCC2 |
| Formula | $C_{12}H_{17}O_3$• |
| Charge | 0 |
| Multiplicity | 2 |
| Dipole (Debye) | 8.4007 |
| Gibbs energy (a.u.) | −692.998956 |
| # Imaginary frequencies | 0 |

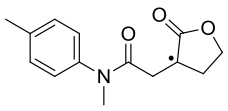

203

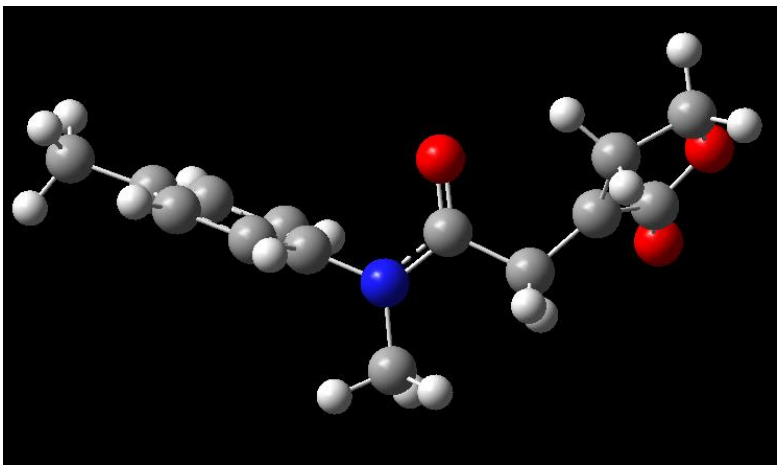

| | |
|---|---|
| Route | UB3LYP/6-31+G(d,p) FormCheck Opt=(Tight, MaxCyc=1000) freq scrf=(cpcm,solvent=acetone) |
| Smiles | O=C(C[C]1CCOC1=O)N(C)C2=CC=C(C)C=C2 |
| Formula | $C_{14}H_{16}NO_3$• |
| Charge | 0 |
| Multiplicity | 2 |
| Dipole (Debye) | 7.9745 |
| Gibbs energy (a.u.) | −823.374738 |
| # Imaginary frequencies | 0 |

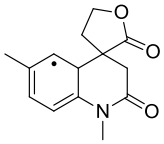


204

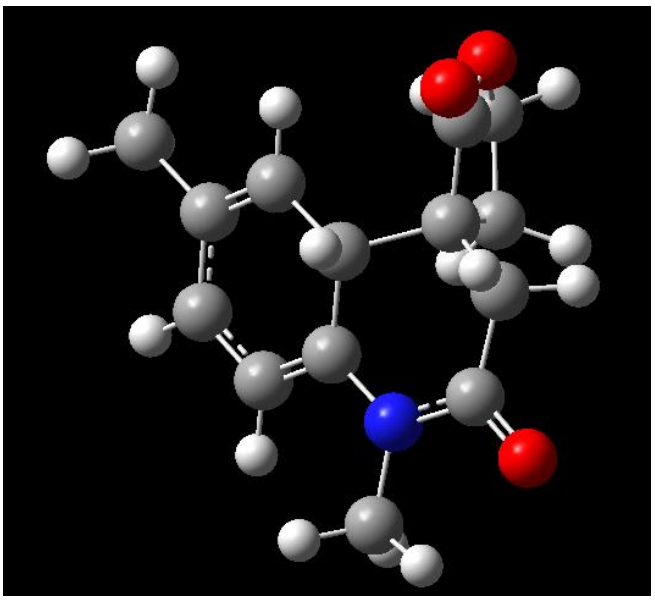

| | |
|---|---|
| Route | UB3LYP/6-31+G(d,p) FormCheck Opt=(Tight, MaxCyc=1000) Freq scrf=(cpcm,solvent=acetone) |
| Smiles | CN1C2=CC=C(C)[C]C2C3(C(OCC3)=O)CC1=O |
| Formula | $C_{14}H_{16}NO_3$• |
| Charge | 0 |
| Multiplicity | 2 |
| Dipole (Debye) | 7.9256 |
| Gibbs energy (a.u.) | −823.365051 |
| # Imaginary frequencies | 0 |

206

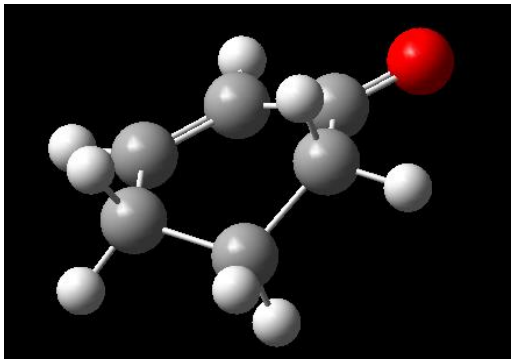

| | |
|---|---|
| Route | UB3LYP/6-31+G(d,p) FormCheck opt(Tight, MaxCyc=1000) freq scrf=(cpcm,solvent=acetone) |
| Smiles | O=C1CCCC=C1 |
| Formula | $C_6H_8O$ |
| Charge | 0 |
| Multiplicity | 1 |
| Dipole (Debye) | 5.7989 |
| Gibbs energy (a.u.) | −308.602408 |
| # Imaginary frequencies | 0 |

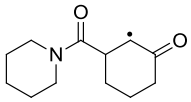


**207**

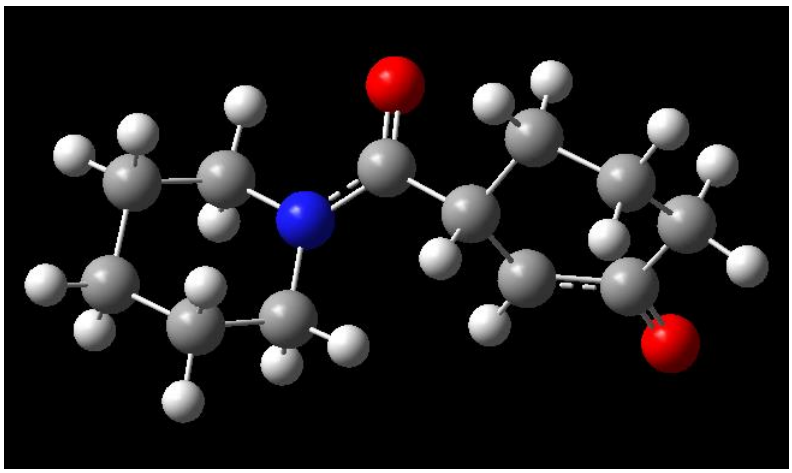

| | |
|---|---|
| Route | UB3LYP/6-31+G(d,p) FormCheck opt(Tight, MaxCyc=1000) freq scrf=(cpcm,solvent=acetone) |
| Smiles | O=C(C1CCCC([C]1)=O)N2CCCCC2 |
| Formula | $C_{12}H_{18}NO_2$• |
| Charge | 0 |
| Multiplicity | 2 |
| Dipole (Debye) | 7.0525 |
| Gibbs energy (a.u.) | −673.112990 |
| # Imaginary frequencies | 0 |

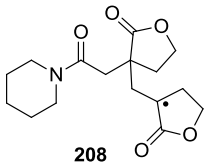


208

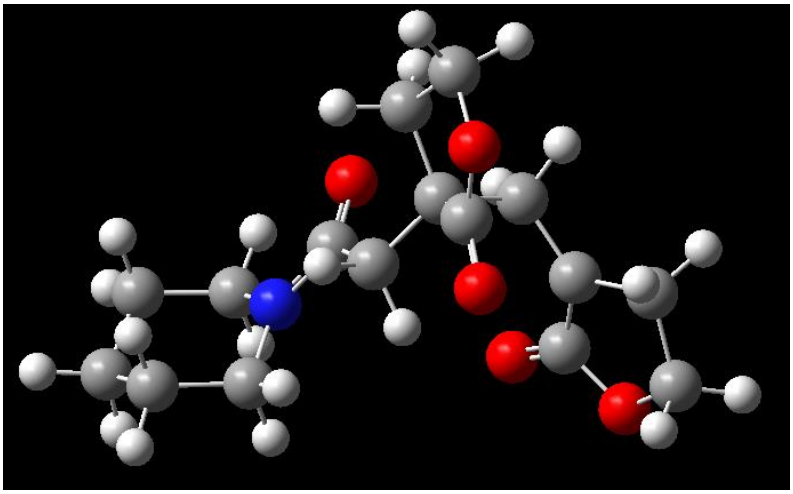

| | |
|---|---|
| Route | UB3LYP/6-31+G(d,p) FormCheck Opt=(Tight, MaxCyc=1000) Freq scrf=(cpcm,solvent=acetone) |
| Smiles | O=C(CC1(C[C]2C(OCC2)=O)CCOC1=O)N3CCCCC3 |
| Formula | $C_{16}H_{22}NO_5^{\bullet}$ |
| Charge | 0 |
| Multiplicity | 2 |
| Dipole (Debye) | 4.1672 |
| Gibbs energy (a.u.) | −1053.591813 |
| # Imaginary frequencies | 0 |

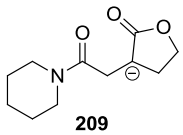


**209**

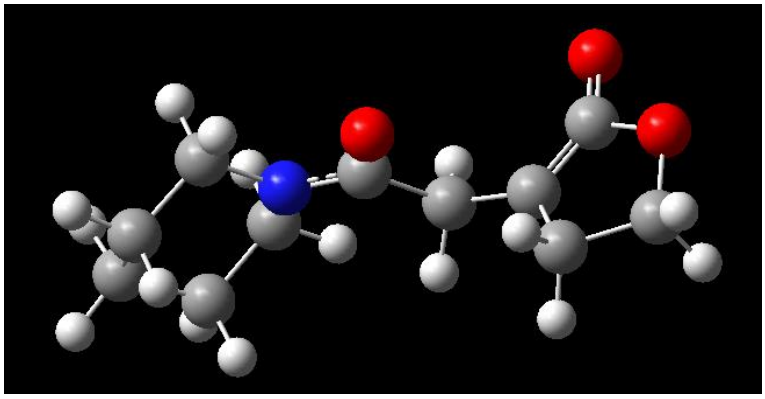

| | |
|---|---|
| Route | UB3LYP/6-31+G(d,p) FormCheck opt(Tight, MaxCyc=1000) freq scrf=(cpcm,solvent=acetone) |
| Smiles | O=C(C[C-]1CCOC1=O)N2CCCCC2 |
| Formula | $C_{11}H_{16}NO_3^-$ |
| Charge | −1 |
| Multiplicity | 1 |
| Dipole (Debye) | 19.3946 |
| Gibbs energy (a.u.) | −709.195396 |
| # Imaginary frequencies | 0 |

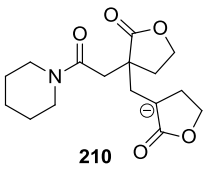


210

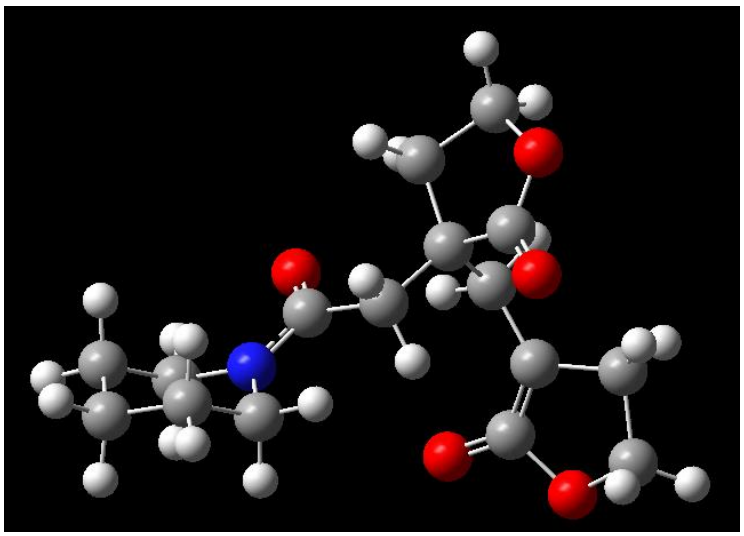

| | |
|---|---|
| Route | UB3LYP/6-31+G(d,p) FormCheck Opt=(Tight, MaxCyc=1000) Freq scrf=(cpcm,solvent=acetone) |
| Smiles | O=C(CC1(C[C-]2C(OCC2)=O)CCOC1=O)N3CCCCC3 |
| Formula | $C_{16}H_{22}NO_5^-$ |
| Charge | −1 |
| Multiplicity | 1 |
| Dipole (Debye) | 15.1696 |
| Gibbs energy (a.u.) | −1053.726981 |
| # Imaginary frequencies | 0 |

## Transition states

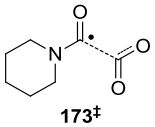


173‡

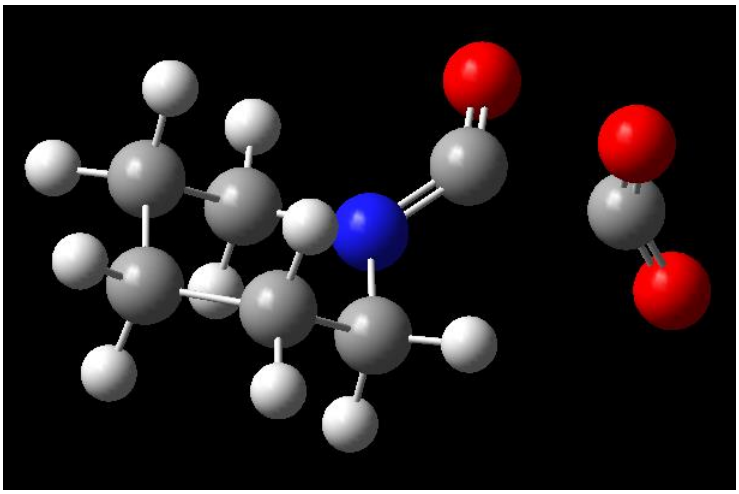

| | |
|---|---|
| Route | UB3LYP/6-31+G(d,p) FormCheck Opt=(QST3, maxcyc=200, CalcFC, Tight) Freq scrf=(cpcm,solvent=acetone) |
| Smiles | O=[C](c(o)=O)N1CCCCC1 |
| Formula | $C_7H_{10}NO_3^{\bullet}$ |
| Charge | 0 |
| Multiplicity | 2 |
| Dipole (Debye) | 8.5509 |
| Gibbs energy (a.u.) | −553.078702 |
| # Imaginary frequencies | 1 |

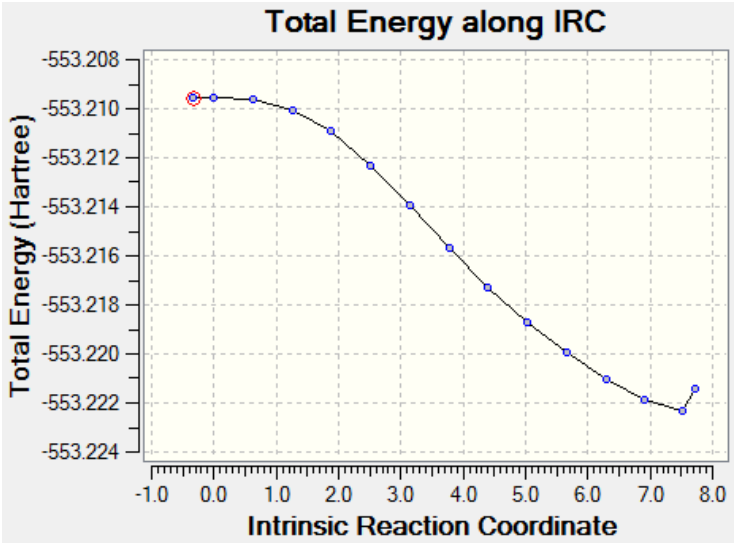

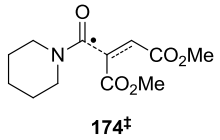


**174‡**

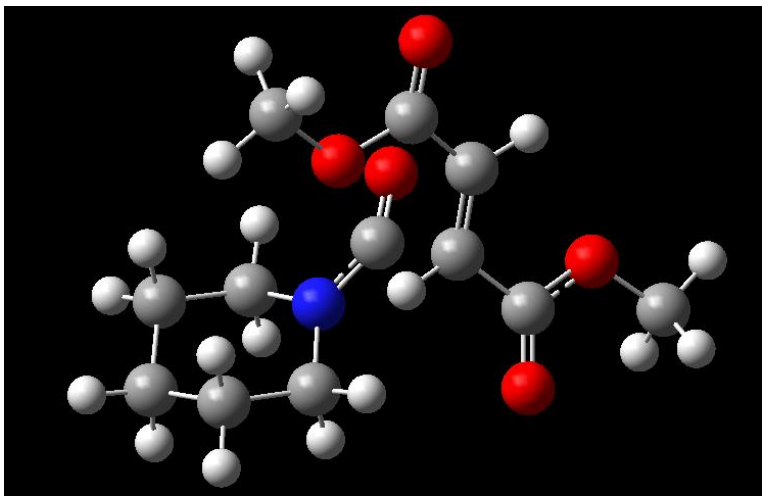

| | |
|---|---|
| Route | UB3LYP/6-31+G(d,p) FormCheck Opt=(QST3, maxcyc=200, CalcFC, Tight) Freq scrf=(cpcm,solvent=acetone) |
| Smiles | O=[C](c(C(OC)=O)cC(OC)=O)N1CCCCC1 |
| Formula | $C_{12}H_{17}NO_5^{\bullet}$ |
| Charge | 0 |
| Multiplicity | 2 |
| Dipole (Debye) | 6.4062 |
| Gibbs energy (a.u.) | −898.768608 |
| # Imaginary frequencies | 1 |

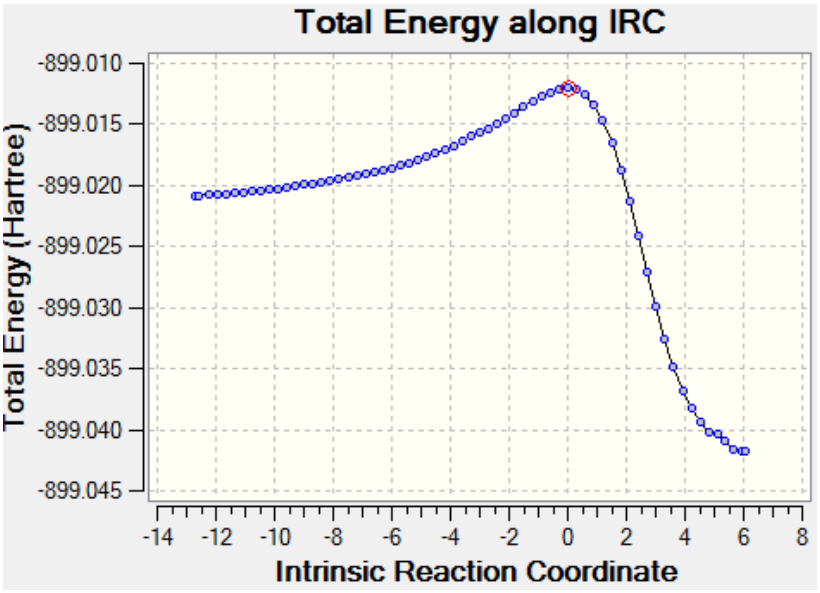

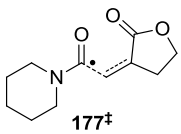


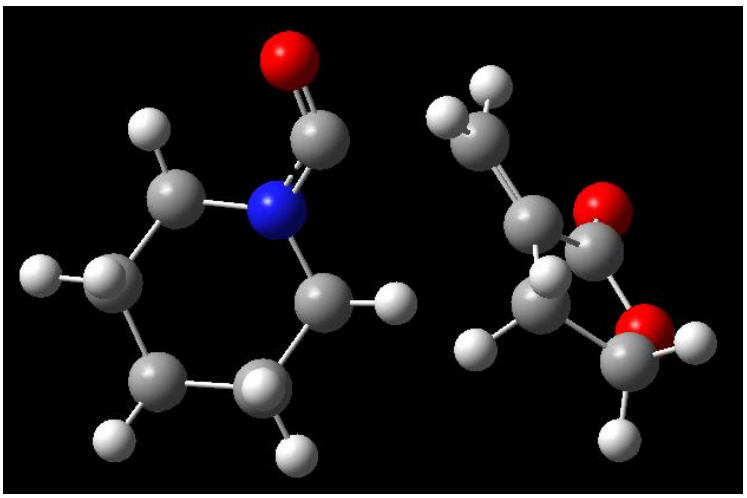

| | |
|---|---|
| Route | UB3LYP/6-31+G(d,p) FormCheck Opt=(QST3, maxcyc=200, CalcFC, Tight) Freq scrf=(cpcm,solvent=acetone) |
| Smiles | O=[C](cc1CCOC1=O)N2CCCCC2 |
| Formula | $C_{11}H_{15}NO_3^{\bullet}$ |
| Charge | 0 |
| Multiplicity | 2 |
| Dipole (Debye) | 8.1756 |
| Gibbs energy (a.u.) | −709.019504 |
| # Imaginary frequencies | 1 |

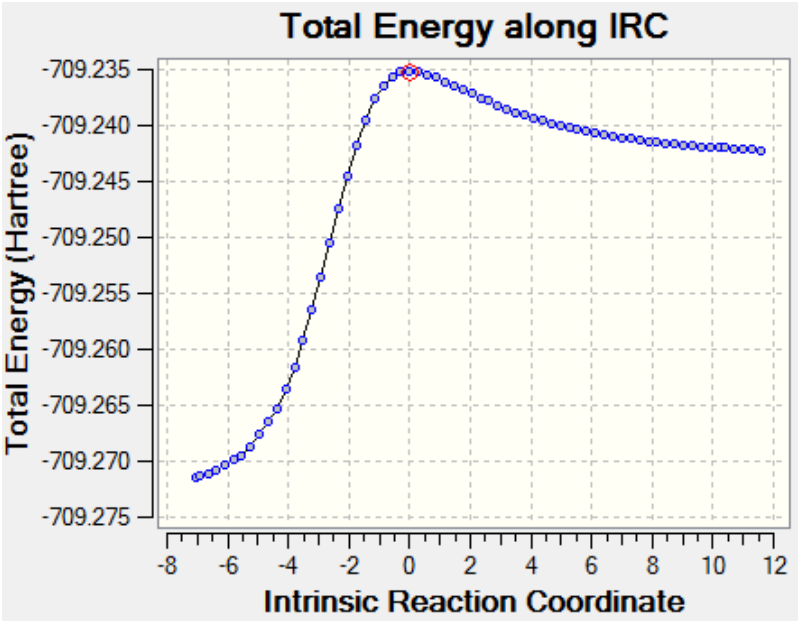

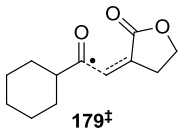


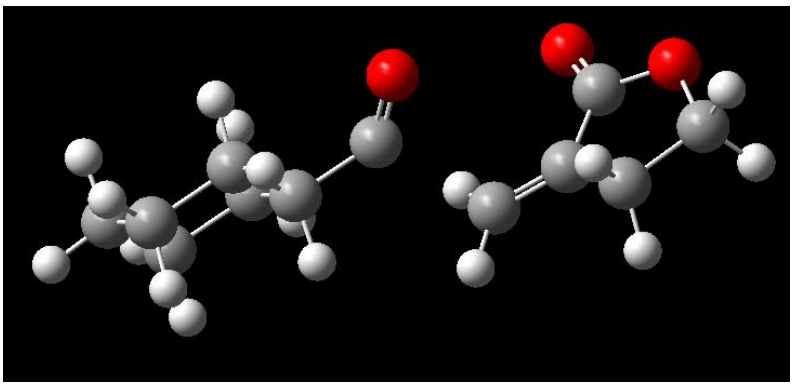

| | |
|---|---|
| Route | UB3LYP/6-31+G(d,p) FormCheck Opt=(QST3, maxcyc=200, CalcFC, Tight) Freq scrf=(cpcm,solvent=acetone) |
| Smiles | O=[C](cc1CCOC1=O)C2CCCCC2 |
| Formula | $C_{12}H_{16}O_3^{\bullet}$ |
| Charge | 0 |
| Multiplicity | 2 |
| Dipole (Debye) | 9.4237 |
| Gibbs energy (a.u.) | −692.961605 |
| # Imaginary frequencies | 1 |

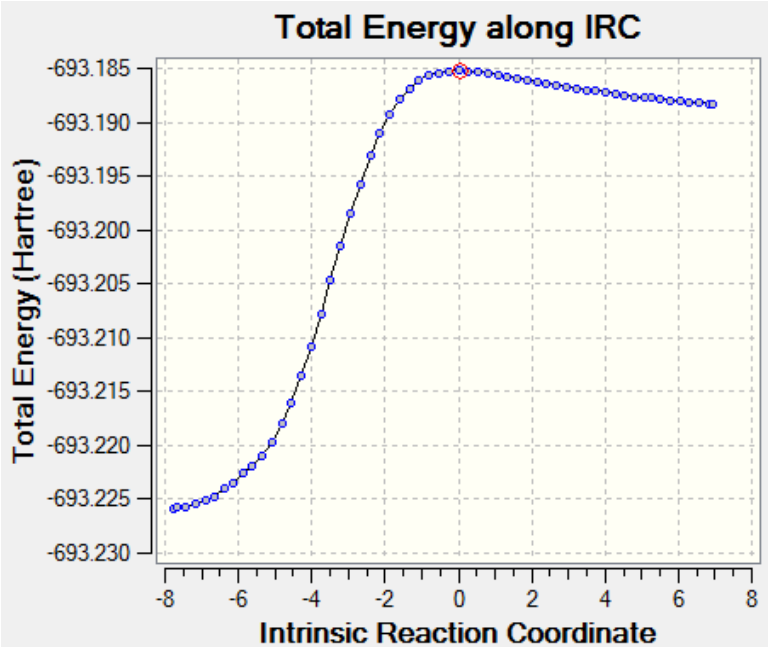

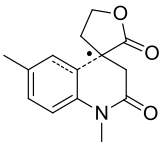

**204‡**

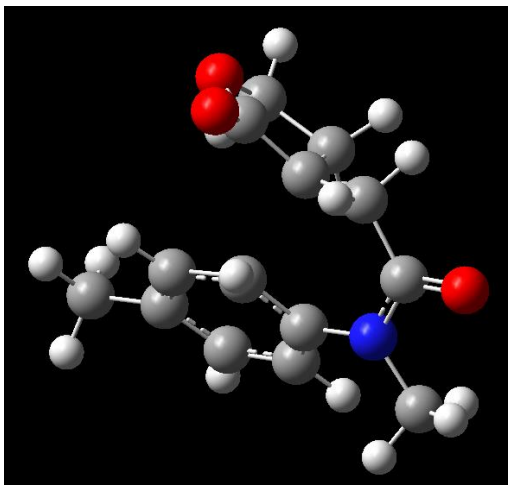

| | |
|---|---|
| Route | UB3LYP/6-31+G(d,p) FormCheck Opt=(QST3, maxcyc=200, CalcFC, Tight) Freq scrf=(cpcm,solvent=acetone) |
| Smiles | CN1C2=CC=C(C)cc2[C@]3(C(OCC3)=O)CC1=O |
| Formula | $C_{14}H_{15}NO_3^{\bullet}$ |
| Charge | 0 |
| Multiplicity | 2 |
| Dipole (Debye) | 9.2978 |
| Gibbs energy (a.u.) | −823.348429 |
| # Imaginary frequencies | 1 |

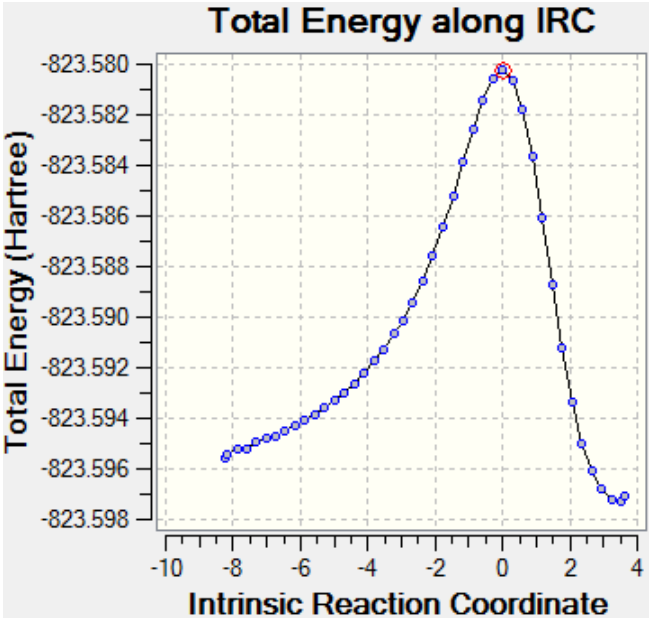

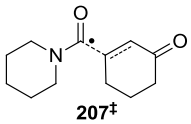


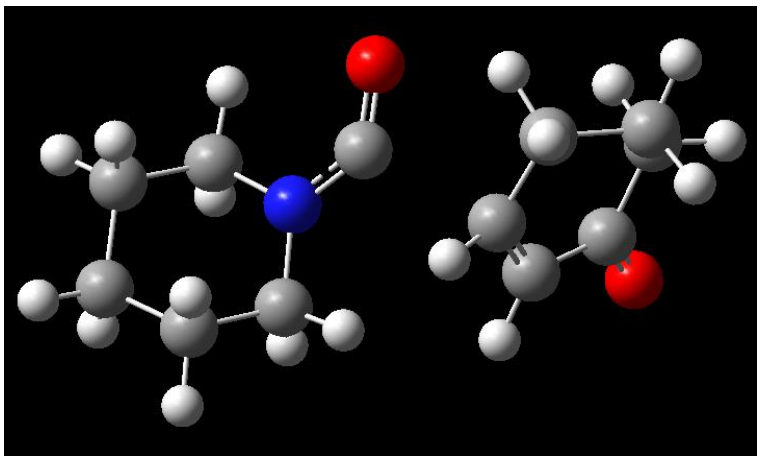

| | |
|---|---|
| Route | UB3LYP/6-31+G(d,p) FormCheck Opt=(QST3, maxcyc=200, CalcFC, Tight) Freq scrf=(cpcm,solvent=acetone) |
| Smiles | O=[C](c(CCC1)cC1=O)N2CCCCC2 |
| Formula | $C_{12}H_{17}NO_2^{\bullet}$ |
| Charge | 0 |
| Multiplicity | 2 |
| Dipole (Debye) | 8.0039 |
| Gibbs energy (a.u.) | −673.078693 |
| # Imaginary frequencies | 1 |

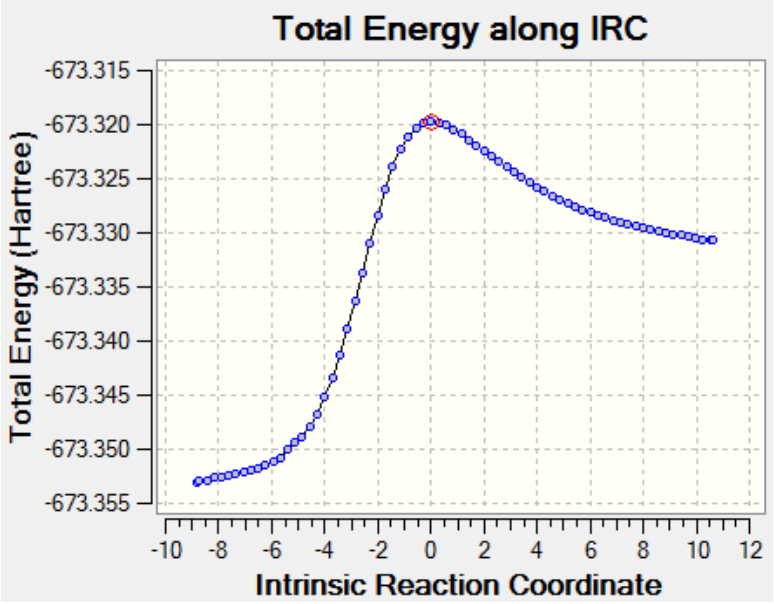

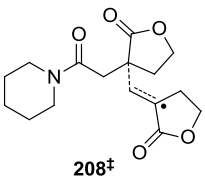


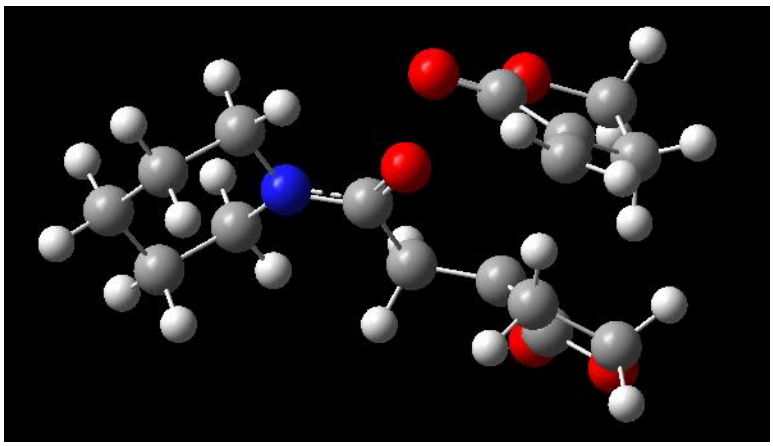

| | |
|---|---|
| Route | UB3LYP/6-31+G(d,p) FormCheck Opt=(QST3, maxcyc=200, CalcFC, Tight) Freq scrf=(cpcm,solvent=acetone) |
| Smiles | O=C(C[C@]1(c[c]2C(OCC2)=O)CCOC1=O)N3CCCCC3 |
| Formula | $C_{16}H_{21}NO_5^{\bullet}$ |
| Charge | 0 |
| Multiplicity | 2 |
| Dipole (Debye) | 4.1827 |
| Gibbs energy (a.u.) | −1053.563162 |
| # Imaginary frequencies | 1 |

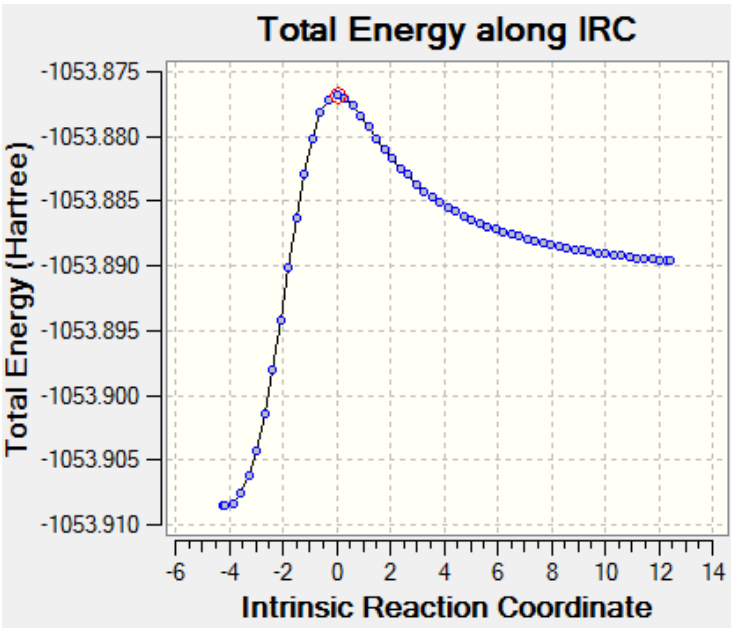

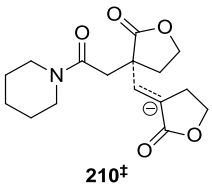


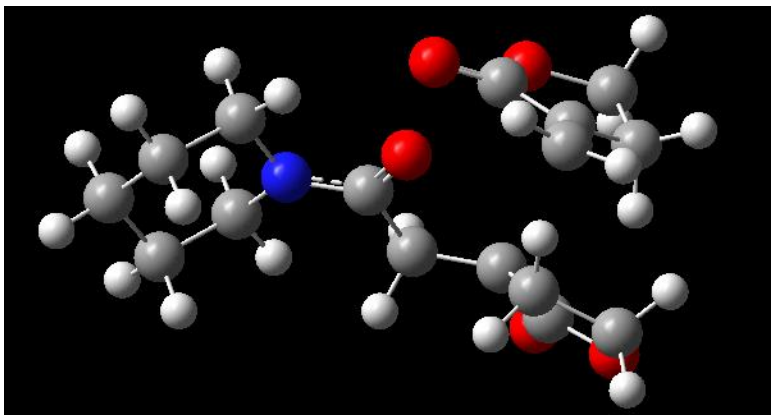

| | |
|---|---|
| Route | UB3LYP/6-31+G(d,p) FormCheck Opt=(QST3, maxcyc=200, CalcFC, Tight) Freq scrf=(cpcm,solvent=acetone) |
| Smiles | O=C(C[C@]1(c[c-]2C(OCC2)=O)CCOC1=O) N3CCCCC3 |
| Formula | $C_{16}H_{21}NO_5^-$ |
| Charge | −1 |
| Multiplicity | 1 |
| Dipole (Debye) | 10.0524 |
| Gibbs energy (a.u.) | −1053.705008 |
| # Imaginary frequencies | 1 |